An investigation into the replication biology of *Helicoverpa armigera* stunt virus

Thesis

Submitted in the fulfilment of the requirements for the degree of

Doctor of Philosophy
(Microbiology)

In the

FACULTY OF SCIENCE
RHODES UNIVERSITY

By

JAMES ROSWELL SHORT

July 2010

ABSTRACT

Tetraviruses are a family of small non-enveloped positive sense RNA viruses that exclusively infect members of the order Lepidoptera. Their replication biology is poorly studied because, with the exception of Providence virus (PrV), tetraviruses are unable to replicate in tissue culture cells. The overall aim of the research described in this thesis was to develop a fundamental understanding of the replication of tetraviruses, focussing on the site of replication within host cells and in particular, the subcellular localisation of the viral replicase. *Helicoverpa armigera* stunt virus (HaSV, Genus: *Omegatetravirus*) was chosen for this study because it is the only tetravirus for which the cDNAs have been shown to be infectious.

In the absence of tissue culture cell lines susceptible to HaSV infection, the approach was to use confocal fluorescence microscopy to examine the subcellular localisation of the HaSV replicase fused to enhanced green fluorescent protein (EGFP) in mammalian and insect tissue culture cells. The replicase (with EGFP fused at its C-terminus) localised to punctate structures throughout the cytoplasm of transfected HeLa and Sf9 cells. These structures were then shown – using live cell imaging and time lapse photography – to behave similarly to cellular endocytic organelles and fluorescence partially overlapped with membranes containing the late endosomal marker protein CD63. Biochemical fractionation of Sf9 cells expressing the replicase via a recombinant baculovirus (as well as transfected HeLa and Sf9 cells expressing EGFP-replicase fusion proteins) demonstrated that the replicase was strongly associated with detergent-resistant membranes (DRMs) in these cells. Deletion analysis of the replicase coding sequence revealed two regions involved in the generation of the punctuate structures. Firstly, the C-terminal half of the replicase RNA-dependant RNA polymerase domain was found to be essential for targeting

and the tight association with DRMs while the second region, within the N-terminal 44 amino acids, enhanced localisation through a combination of secondary structural elements and sequence-specific functions. A comparative immunofluorescence study on PrV, which replicates as a persistent infection in an insect midgut cell line, showed that the PrV replicase also localised to punctate structures in the cytoplasm. Biochemical fractionation showed that the replicase was also strongly associated with DRMs. This thesis describes the development of new experimental systems for the study of tetravirus replication biology and the data lead to the conclusion that the HaSV replicase associates with DRMs derived from alternate endocytic pathway organelles.

TABLE OF CONTENTS

Supplementary Data CD

Video 1a

Video 1b

Video 2

Digital copies of figures

- Chapter 3, Figures 3.3, 3.4 and 3.5
- Chapter 5, Figures 5.6, 5.7 and 5.11

Manuscript: Short *et al.*, 2010

DISCLAIMER

The financial assistance of the National Research Foundation (NRF), the German Academic Exchange Service (DAAD) and the Andrew Mellon Foundation is hereby acknowledged. The opinions expressed and conclusions arrived at are those of the author and are not necessarily those of the NRF, DAAD or the Andrew Mellon Foundation.

ACKNOWLEDGEMENTS

The last 4 and a half years have been an amazing journey. This project has taught me so much about myself and life in general. Being one of those people who trusts that all things will work out for my good in the end, I sort of stumbled into this whole thing without any expectations. That being said, it has proved to be one of the most life-giving experiences I could have hoped for.

Of course, as always, behind every thesis is a nation of people to thank. Firstly, Prof. Dorrington, my supervisor since I entered this world of discovery just over 5 years ago. You always seem to bring the best out in me and have certainly helped to mould me into the researcher I am today through your wisdom and advice as well as the amazing opportunities you have provided. Mrs Val Hodgson: Thank you so much for everything, the list is too long to include here but thank you specifically for your help in proofreading this thesis, making this research possible through your hard work in the lab and, possibly most importantly, for making fun of me whenever I try to tell other people what to do. The past and present members of Lab 417, you have all had to deal with my rubbish sense of humour; that alone deserves thanks. Dr. Michele Tomassichio, Dr. Mez Jiwaji, Dr. Cheryl Walter and Jo-Anne de le Mare: you all helped me settle into this game and get on my feet, for which I am very thankful. Dr. Petra Gentz, your help with the bioinformatics in this thesis was invaluable. Thank you for the huge amount I have learnt from you about lab work in general, you are an amazing teacher. Michele and Ariano Mendes, for helping me dilute the X chromosomes slightly. Dr. Gwynneth Matcher and Ritah Nakayinga for always having a smile and a hello, even when things aren't going as well as we would like. Marli Vlok for making "tonsil" jokes so much fun. Jane Charlton for resurrecting the "Zambezi awards" and knowing more about computers than me. Dr. Caroline Knox and Prof. Greg Blatch, for always being positive and acting as referees for so many applications. Prof Albi van Dijk and Rencia van der Sluis for help in constructing the recombinant baculoviruses used in this study.

Beyond that I owe special thanks to a group of friends and family who have all contributed to this work in some way. Firstly, my wonderful fiancée, Miss Derralyn Martin, aka love of my life. Thank you for loving me when I wake up at 5pm as if it's normal and handling my stress even though you have plenty of your own. Beyond your help with organising the references in this thesis, you have been an absolutely amazing support and I am truly blessed by you. Jade Fernley, thank you for proof reading my lit review, I hope it provided some entertainment at least. Theo te water Naude and Neels Strijdom for putting up with my nocturnal habits and squeaky door and to Theo for keeping me entertained with games and many cups of tea. Mom and Tam, thank you for being supportive and interested throughout this process. To my friends who have watched, supported and encouraged me through this process, especially Sean and Sarah Bennets, Fred Otten, Ryan and Tara Walmsley, Tarryn Wilmer, Louise Groenewald, Ryan Brear, Jordan Rainer, Lester and Melissa Bhana, Dean Flanagan and Craig Bailie. To the funding agencies that made this work possible through the funding they provided: Ernst and Ethel Eriksen Trust, German Academic Exchange Service (DAAD), National Research Foundation, Mellon Foundation and Rhodes University. Finally, thanks to my Father who led me to this point. You have always been my peace in the storm, my greatest joy, my greatest supporter and my greatest source of inspiration. You made me who I am and gave me the ultimate when I could never have earned or deserved it. May this work make you famous.

LIST OF ABBREVIATIONS AND VIRUS NAMES

GENERAL ABBREVIATIONS

6xHis - 6xhistidine/hexahistidine

(+ve) - positive-sense

(-ve) - negative-sense

CDS - coding sequence

DAPI - 4',6-diamidino-2-phenylindole

DMEM - Dulbecco's modified Eagle medium

DNA - deoxyribonucleic acid

ds - double-stranded

DRM - detergent-resistant membranes

EEA1 - early endosomal autoantigen 1

EGFP - enhanced green fluorescent protein

ER - endoplasmic reticulum

ExPASy - Expert Protein Analysis System

GEEC - GPI-AP-enriched early endosomal compartment

GPI - glycosylphosphatidylinositol

GPI-AP - glycosylphosphatidylinositol-anchored protein

GST - glutathione S-transferase

HEL - helicase

Ig - immunoglobulin

IPTG - isopropyl β-D-1-thiogalactopyranoside

kb - kilobase(s)

LB - Luria-Bertani

LDL - low density lipoprotein

MOI - multiplicity of infection

MT - methyltransferase

MVB - multivesicular body
nt(s) - nucleotide(s)
ORF - open reading frame
PBS - phosphate buffered sailne
PCR - polymerase chain reaction
pfu - plaque-forming units
PNS - post nuclear supernatant
RBS - ribosome binding site
RdRp - RNA-dependant RNA polymerase
RNA - ribonucleic acid
RPCR - reverse PCR
SDS - sodium dodecyl sulphate
SDS-PAGE - sodium dodecyl sulphate polyacrylamide gel electrophoresis
ss - single-stranded
TDPPs - template-dependant polynucleotide polymerases
VDAC - voltage-dependant anion channel
VLP - virus-like particle
VPg - genome-linked virus protein
vRNA - viral RNA

VIRUS NAME ABBREVIATIONS

AcMNPV - *Autographa californica multiple nuclearpolyhedrovirus*
BMV - *Brome mosaic virus*
CMV - *Human cytomegalovirus*
DpTV - *Dendrolimus punctatus tetravirus*
EeV - *Euprosterna elaeasa virus*
ERAV - *Equine rhinitis A virus*
FHV - *Flock House virus*
FMDV - *Foot-and-mouth disease virus*
HaSV - *Helicoverpa armigera stunt virus*

HSV - *Herpes simplex virus*

IBDV - *Infectious bursal disease virus*

IPNV - *Infectious pancreatic necrosis virus*

NβV - *Nudaurelia capensis beta-virus*

NωV - *Nudaurelia capensis omega-virus*

PrV - *Providence virus*

PV - *Polivirus*

RV - *Rubella virus*

SFV - *Semliki Forest virus*

SIN - *Sindbis virus*

SV40 - *Simian virus 40*

TaV - *Thosea asigna virus*

TnV - *Trichoplusia ni virus*

LIST OF TABLES AND FIGURES

List of figures:

List of tables:

CHAPTER 1
LITERATURE REVIEW

1.1 INTRODUCTION

The major obstacle faced by all RNA viruses is that of genome replication. This requires RNA-dependent RNA replication in host cells that have DNA genomes and use DNA-dependent RNA polymerases for the production of RNA. Thus no cellular machinery capable of genomic viral RNA (vRNA) replication is present in host cells. Over fifteen years ago reports of RNA-dependent RNA polymerase (RdRp) activity in plant cells began to emerge (Schiebel *et al.*, 1993) and there is now evidence of non-viral RdRps in many eukaryotic cell types, some of which have a fidelity comparable to that of their viral equivalents. It appears that these RdRps are involved in cellular processes such as RNA silencing and are unable to replicate the genomes of RNA viruses (Schiebel *et al.*, 1998; Sijen *et al.*, 2001; Ahlquist, 2002; Vaistij *et al.*, 2002; Alder *et al.*, 2003). Thus RNA viruses carry their own RNA replication proteins, which in many cases function together with specific host and viral-encoded proteins to produce infectious vRNAs (Ahlquist 2002; Ortín and Parra, 2006). Since this function is one of the fundamental differences between the virus and host cells, vRNA replication remains a key target for the development of antiviral therapies for treatment of diseases caused by RNA viruses (Ferrer-Orta *et al.*, 2006).

1.2 REPLICASES OF POSITIVE SENSE RNA VIRUSES

Template-dependent polynucleotide polymerases (TDPPs) are responsible for the replication of cellular and viral genomes as well as cellular transcription. Normal cellular functions in DNA repair or replication and RNA production are carried out by DNA-dependent DNA polymerases and DNA-dependent RNA polymerases respectively. However, the absence of host

cellular processes that can be exploited for genome-wide RNA replication has meant that all RNA viruses must carry their own RNA replication machinery, broadly referred to as viral replicases. These replicases form RNA replication complexes in the host cell that may also contain host factors. Although there is some diversity in the number of replication proteins a particular virus produces and the additional functions that they perform, all positive sense (+ve) RNA viruses studied thus far have two characteristics in common: they encode a highly conserved RdRp domain (Koonin, 1991; Ahlquist, 2002) and all are associated with host cellular membranes (Ortín and Parra, 2006).

1.2.1. Structure and functional domains of RNA replicases

The replication complexes produced by RNA viruses are multi-functional enzymes designed for the mass production of vRNA and range in complexity from a single protein encoding a single RdRp domain to an intricate assembly of viral and host encoded factors. Many replicases carry other functional domains such as methyl- or guanyl-transferase (MT) domains responsible for attachment of 5' RNA caps, and helicase (HEL) domains that aid in the unwinding of double-stranded (ds) RNA replication intermediates (Van der Heijden and Bol, 2002). In addition to the fundamental role they play in RNA replication, many also function in the recruitment of host factors required for viral replication and all replicases of (+ve) RNA viruses investigated to date have been shown to interact with host membranes .

At the core of viral replication complexes is the RdRp domain, which has a high degree of structural conservation, not only among viral replicases, but also among all TDPPs, including cellular DNA and RNA replication proteins and reverse transcriptases (Ahlquist, 2002). All TDPPs form a common tertiary structure that is often likened to a cupped right hand arranged with three distinct regions called the palm, thumb and fingers subdomains (Figure 1.1) (Ollis *et al.*, 1985). A conserved region of between 120 and 210

amino acids lies within the palm subdomain of all the RNA-dependent polymerases of retroviruses, retrotransposons, (+ve) and negative sense (-ve) single stranded (ss) RNA viruses, as well as some ds RNA viruses (Poch *et al.*, 1989).

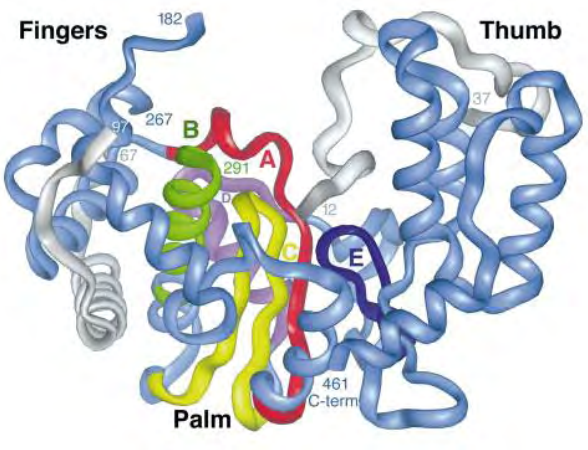

Figure 1.1: Crystal structure of the Poliovirus replicase, $3D^{pol}$, showing the thumb, fingers and palm subdomains. A ribbon representation with the fingers (top left), palm (bottom) and thumb (top right) subdomains as indicated. Motifs A to E are colour-coded as follows: A – red, B – green, C – yellow, D – violet and E – dark blue. Reproduced from Hansen *et al.* (1997).

The palm subdomain contains four highly conserved motifs named A, B, C and D (also known as motifs I, II, III and IV, Figure 1.1) that occur in an identical linear arrangement and which together contain 4 invariant and 18 conserved amino acids (Poch *et al*., 1989). These are assembled around motif C, which is the core catalytic domain containing the signature GDD box (Kamer and Argos, 1984; Argos, 1988). Poch *et al.* (1989) hypothesised that the four motifs, separated by comparable numbers of amino acids, comprised a “polymerase module” or polymerase domain that is essential in template placement and nucleotide polymerisation. A subsequent study identified a total of eight conserved motifs in RNA replicases even though only three, corresponding to motifs A, B and C, are universally conserved (Koonin, 1991). As there can be a large degree of variation over the full length of viral

replicase sequences, even among closely related viruses (Johnson *et al.*, 2001), these three motifs within the palm subdomain provide a useful means of comparison.

As the catalytic core of the RdRp domain, motifs A to C are centred around the active site (Figure 1.1). Motifs A ($DX_{4-5}D$, where X is a non-conserved amino acid) and C (GDD) are spatially arranged with aspartic acid residues positioned for the binding of the divalent ions (Mn^{2+} or Mg^{2+}) that are essential for the catalysis of the polynucleotide polymerisation reaction, while motif B ($(S/T)GX_3TX_3N(S/T)$) contains an essential asparagine residue that determines whether DNA or RNA is synthesised by discriminating between dNTPs and NTPs (Poch *et al.*, 1989; Hansen *et al.*, 1997). Although these three motifs are typically present in a canonical A-B-C arrangement, Gorbalenya *et al.* (2002) identified an isolated group of replicases that carried a unique C-A-B permutation. Originally this permutation was only identified in two ds RNA birnaviruses, Infectious pancreatic necrosis virus (IPNV) and Infectious bursal disease virus (IBDV), and two tetraviruses, *Thosea asigna* virus (TaV) and *Euprosterna elaeasa* virus (EeV) (Gorbalenya *et al.*, 2002). However, more recently the permuted palm subdomain has also been observed in Drosophila A virus and Grapevine virus Q (Ambrose *et al.*, 2009; Sabanadzovic *et al.*, 2009). Computational remodelling of the permutations into the three-dimensional structure of the Poliovirus (PV) replicase showed that this arrangement is compatible with the major secondary structural elements and would be capable of maintaining structural integrity (Gorbalenya *et al.*, 2002).

1.2.2. Classification of RNA-dependent RNA polymerases from positive sense RNA viruses

Replicases provide a useful means of identification and classification of RNA viruses (Gorbalenya *et al.*, 2002). Phylogenetic analysis of the replicase sequences of (+ve) ss RNA viruses has enabled the classification of three

supergroups (I, II and III) of viral replicases based on differences in RdRp sequences, which is usually accompanied by the presence or absence of other associated domains and functions (Koonin, 1991; Van der Heijden and Bol, 2002). This classification system takes into account three RdRp, three HEL, two MT and two proteinase domains and separates viruses into supergroup I (picorna-like), supergroup II (divided into the carmo-like and flavi-like lineages) or supergroup III (alpha-like) replicases (Table 1.1) (Gorbalenya *et al.*, 1988, 1989, 1990; Koonin, 1991; Rozanov *et al.*, 1992; Kadre and Haenni, 1997, Van der Heijden and Bol, 2002).

Table 1.1: The conserved domains encoded by the replicases of each of the (+) RNA virus supergroups. Adapted from Van der Heijden and Bol (2002).

Supergroup	Type of domain			
	RdRp	**HEL**	**MT**	**Proteinase**
I: Picorna-like viruses	I	1, 2 or 3	-	Cys or Ser
II: Carmo-like viruses*	II	-	-	-
II: Flavi-like viruses*	II	2	2	Ser
III: Alpha-like viruses	III	1	1	Cys or Papain-like

*: The carmo-like and flavi-like viruses are two lineages within the supergroup II replicases.

Picorna-like replicases (supergroup I) encode a type I RdRp domain and a conserved cysteine proteinase motif required for post-translational processing of the replicase. In addition, they may encode a type 1, 2 or 3 HEL domain, but MT domains are absent because the majority of these viruses make use of VPgs (genome-linked virus proteins) to prime (+ve) and (-ve) RNA synthesis and stabilise vRNA (Table 1.1) (Wimmer *et al.*, 1993). Supergroup II replicases are divided into two major lineages. The first is the carmo-like replicases that carry a type II RdRp domain but lack HEL, MT and proteinase domains, while the second lineage, the flavi-like replicases, also utilise a type II RdRp domain but encode HEL (type 2), MT (type 2) and serine proteinase domains (Table 1.1). Finally, supergroup III replicases comprise the alpha-like virus replicases named after the *Alphavirus* genus of

the *Togaviridae*. Type III RdRp, type 1 MT and type 1 HEL domains as well as cysteine or papain-like proteinase domains are characteristic of this group (Table 1.1) (reviewed in Van der Heijden and Bol, 2002). The replicase encoded by *Helicoverpa armigera* stunt virus (HaSV), which is the subject of this study, falls within this last group (Gordon *et al.*, 1995).

The MT, HEL and RdRp domains conserved within the alpha-like superfamily are found in a linear arrangement with the MT domain closest to the N-terminus followed by the HEL and the RdRp domains towards the C-terminus (Figure 1.2) (Rozanov *et al.*, 1992). In their study of alpha-like replicases, Rozanov *et al.* (1992) showed that the MT domain was unique among replicase proteins and identified a series of four motifs (I to IV) that contained four invariant amino acids. Similar bioinformatic analysis of the HEL domains from various proteins involved in DNA and RNA unwinding revealed seven signature motifs, five of which are unique to the type 1 HEL domain found in alpha-like replicases (Gorbalenya *et al.*, 1988, 1989; Kadre and Haenni, 1997). Motif B of the RdRp domain of alpha-like viruses contains a unique S/T pairing separated by nine amino acids (Koonin, 1991). An additional "X" or macro domain of unknown function is found in alpha-like viruses infecting animals and cystein or papain-like proteases may be present and are involved in autoproteolytic cleavage (Table 1.1, Figure 1.2) (Van der Heijden and Bol, 2002).

1.3 THE *TETRAVIRIDAE*

The first tetravirus was isolated more than forty years ago from a South African population of pine emperor moth (*Nudaurelia cytherea capensis*) larvae (Hendry *et al.*, 1968). *Nudaurelia capensis* β virus (NβV) was among five small RNA viruses present in diseased larvae (Jukes, 1970) and analysis of virion structure revealed the characteristic $T = 4$ icosahedral capsid structure for which the family is now named (Finch *et al.*, 1974; Sehnke *et al.*, 1988; Rossmann and Johnson, 1989; Olson *et al.*, 1990). The relative

abundance of NβV in infected insects ultimately resulted in it becoming the type member of a new group of viruses called the *Nudaurelia* β-like viruses (Reinganum *et al.*, 1978; Mathews, 1982).

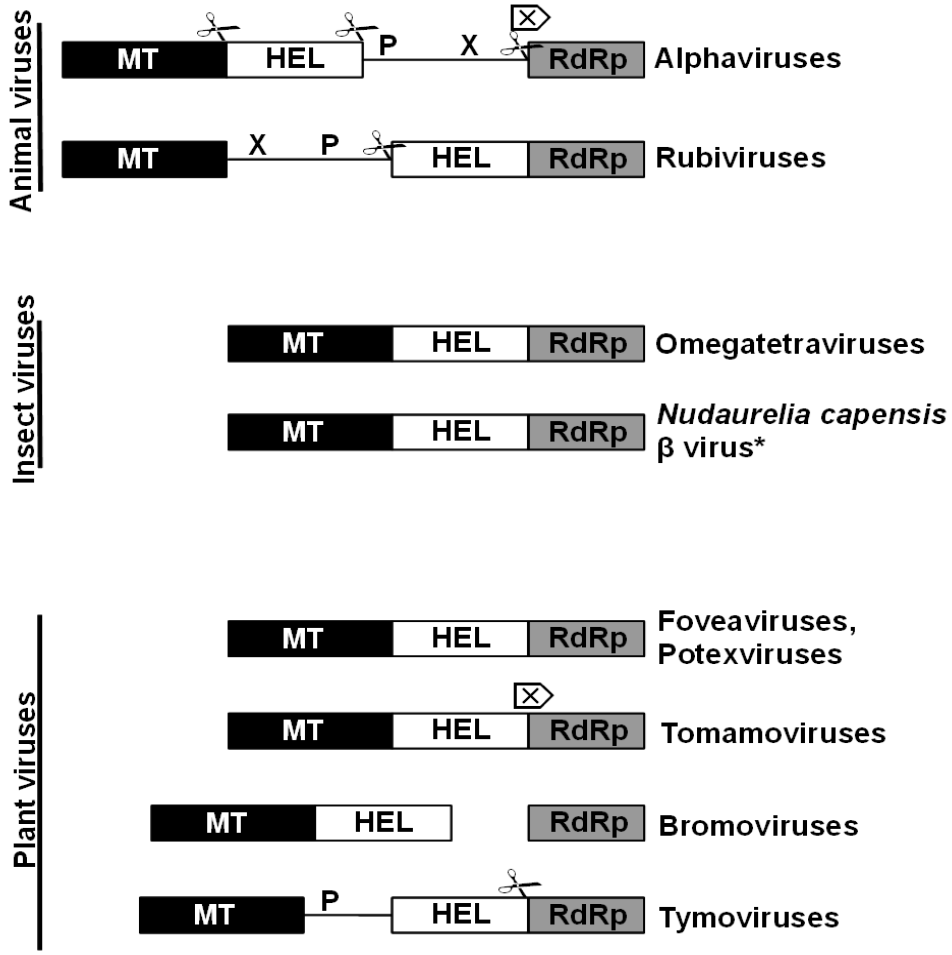

Figure 1.2: Schematic representation of the organisation of conserved functional domains of replicases within the alpha-like virus supergroup. Some of the genera (right) of viruses carrying alpha-like virus replicases, divided into animal, insect or plant viruses (left). *: *Nudaurelia capensis* β virus is the only betatetravirus with an alpha-like replicase, MT: Guanyl/methyltransferase, HEL: Helicase, P: Papain-like protease, X: "X" or macro domain, RdRp: RNA-dependent RNA polymerase, ✂: Known cleavage sites, ⊠: Read-through stop codons. Adapted from Van der Heijden and Bol (2002).

In 1985, Hendry *et al.* isolated another small, non-occluded RNA virus co-infecting diseased *N. capensis* larvae, which was designated *Nudaurelia capensis* ω virus (NωV). While NωV had a number of biophysical

characteristics in common with NβV, there were differences in surface morphology and the two viruses were serologically unrelated (Hendry *et al.*, 1985). Furthermore, NωV virions contained a bipartite ss RNA genome in contrast to the monopartite genome of NβV. NωV became the first member of a second genus within the *Tetraviridae* called the ω-like tetraviruses, where it remained the sole member until the discovery of HaSV in a collapsed *Helicoverpa armigera* (cotton bollworm) colony (Hanzlik *et al.*, 1993).

To date there are eleven assigned members of the *Tetraviridae* in addition to the fourteen members that remain as yet unassigned (Hanzlik *et al.*, 2005; Walter *et al.*, 2008). All tetraviruses have capsids displaying the distinctive *T* = 4 icosahedral symmetry with an average diameter of approximately 40 nm encapsidating (+ve) RNA genomes. The family is divided into two genera according to genomic organisation with NωV and NβV remaining the prototype viruses for what are now known as the bipartite *Omegatetravirus* and the monopartite *Betatetravirus* genera respectively (Dorrington and Short, 2010).

1.3.1. Host range, pathology and virus-host interactions

Tetraviruses are distinguishable from other insect viruses by their characteristic *T* = 4 icosahedral symmetry and their unusually narrow host range. All tetraviruses are thought to infect the midgut cells of insects within the Order Lepidoptera with the host range of each virus generally being limited to one or a small group of species within a single family (Hanzlik *et al.*, 2005). In some instances, most notably that of *N. capensis*, a number of tetraviruses can infect a single species (Jukes, 1979; Walter *et al.*, 2008). With the exception of Providence virus (PrV), no tetraviruses have been found able to replicate in tissue culture cell lines (Bawden *et al.*, 1999; Pringle *et al.*, 2003). In an effort to establish an infectious tissue culture system for HaSV, Bawden *et al.* (1999) attempted to induce HaSV replication

by infection of fourteen tissue culture cell lines with HaSV particles or transfection with genomic RNA. None of the thirteen insect cell lines nor the one mammalian tissue culture cell line were found to be permissive for replication. The authors suggested that this was most likely due to a lack of cell surface receptors suitable for the entry of HaSV particles and the absence of host factors essential for the replication of HaSV RNA.

During infection, HaSV particles have been observed in the cytoplasm of columnar, goblet and basal regenerative cells, but not in endocrine cells (Brooks *et al.*, 2002), indicating some degree of specificity even within the larval midgut. Furthermore, Brooks *et al.* (2002) noted significant changes in the subcellular architecture of HaSV-infected cells, including an accumulation of lysosomes, increased cytosolic vacuolation and a concurrent increase in cell shedding to the midgut lumen. Cell shedding was correlated with an increase in apoptosis (programmed cell death) in infected cells. Subsequent studies have shown that there may be a correlation between the cytosolic acidification that occurs as a precursor of programmed cell death and the maturation of virus particles (discussed in detail below) (Matsuyama and Reed, 2000; Nilsson *et al.*, 2006; Tomasicchio *et al.*, 2007; Kirkegaard and Jäättelä, 2009).

1.3.2. Capsid structure, assembly and maturation

Three-dimensional reconstructions of electron micrographs of NβV particles revealed a novel $T = 4$ icosahedral symmetry and the presence of Y-shaped trimers on the capsid surface (Finch *et al.*, 1974). This was later confirmed when the structure of NβV virions was reconstructed to 32 Å by cryo-electron microscopy (Olson *et al.*, 1990). Since then the availability of a crystal structure for NωV at 2.8 Å resolution revealed similar core structures that are distinguishable by the presence of deeper grooves between Y-shaped trimers and prominent pits on each triangular face of NβV (Figure 1.3) (Finch *et al.*, 1974; Olson *et al.*, 1990; Johnson *et al.*, 1994; Munshi *et al.*, 1996). Cryo-

electron microscopy structures are now available for HaSV and PrV (Figure 1.3) (Speir and Johnson, 2008) and the crystal structure of PrV has recently been solved at a resolution of 3.8 Å (Speir *et al.*, 2010).

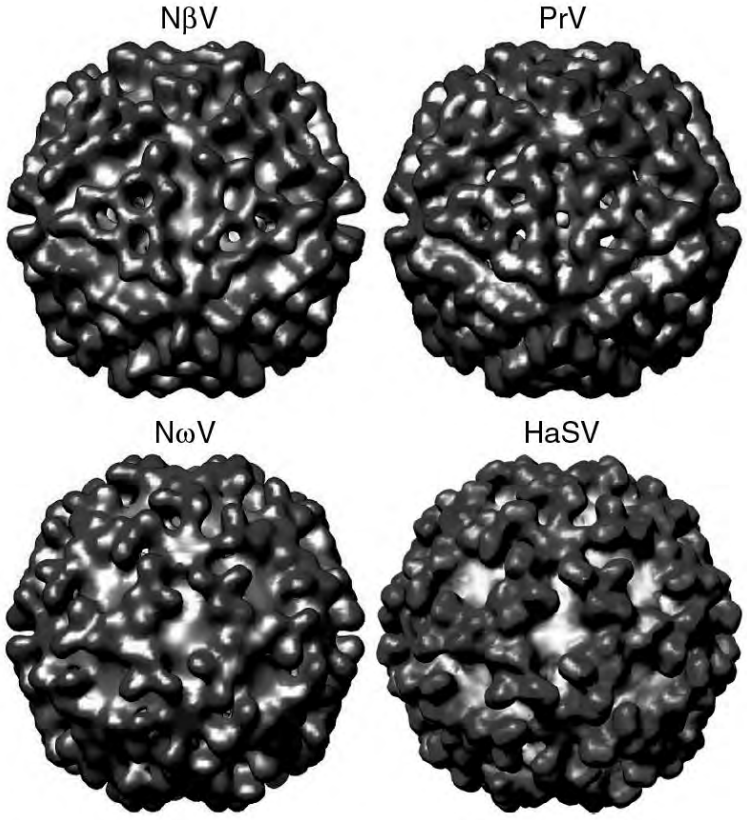

Figure 1.3: Three-dimensional representations of cryo-electron microscopy reconstructions of NβV, PrV, NωV and HaSV. All four reconstructions are resolved to below 30 Å and are viewed down their two-fold icosahedral axis. Reproduced from Speir and Johnson (2008).

Capsids are assembled from 240 identical capsid protein precursors (VCAP), each with an internal helical domain, a core β-barrel domain and an external Ig-like domain (Figure 1.4, Panel A), the former two regions displaying significant structural similarity to the $T = 3$ nodaviruses (Finch *et al.*, 1974; Fisher and Johnson, 1993; Munshi *et al.*, 1996; Speir *et al.*, 2010). The Ig-like domain, unique among non-enveloped viruses, is inserted between the E and F strands of the β-barrel domain and is the dominant structure on the exterior of the virus capsid (Munshi *et al.*, 1996; Speir and Johnson, 2008; Speir *et al.*, 2010). Furthermore, it is the least conserved region of VCAP

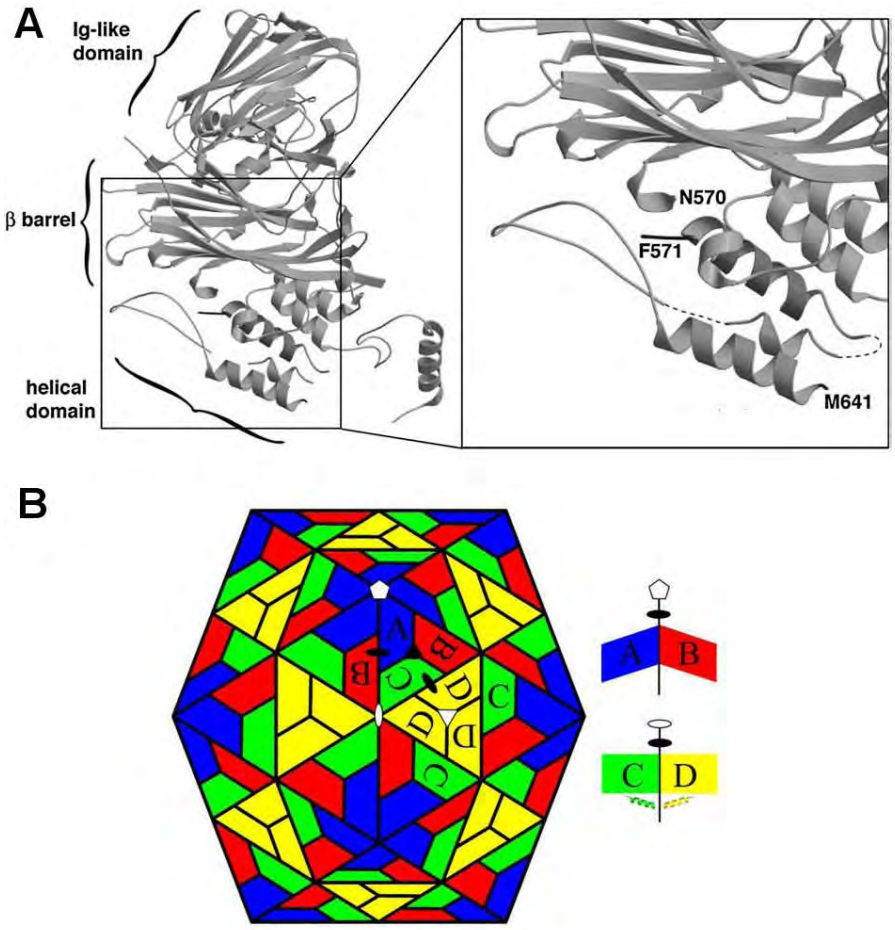

Figure 1.4: The tertiary structure and quasi-equivalence of the NωV capsid displaying the three distinct capsid protein domains. Panel A shows a ribbon diagram of the C subunit of NωV with the positions of the three structural domains. The internal helical domain with N^{570}/F^{571} autoproteolytic cleavage site is enlarged. Panel B shows a schematic diagram of the positions of the four quasi-equivalent capsid subunits in $T = 4$ viruses: A (blue), B (red), C (green) and D (yellow). White pentagons, ellipses and triangles represent 5-fold, 2-fold and 3-fold icosahedral axes, while black ellipses and triangles represent quasi-2-fold and quasi-3-fold axes. The flat conformation at quasi-2-fold axes is stabilised by ordered C-terminal helices. Taken from Speir and Johnson (2008).

and, along with the different orientation of the Ig-like domain that creates the distinct surface morphologies of ω- and β-like viruses, is thought to enable virus-specific interactions with different hosts (Munshi *et al.*, 1996; Helgstrand *et al.*, 2004; Speir *et al.*, 2010). As in all icosahedral viruses, the β-barrel domain is the core around which the capsid assembles (Munshi *et al*., 1996; Helgstrand *et al.*, 2004; Speir *et al.*, 2010). The internal helical domain, formed by the N- and C-termini of VCAP, has been implicated in capsid

assembly, RNA binding and stabilisation during encapsidation, as well as the translocation of vRNA into the cell during infection (Sehnke *et al.*, 1988; Munshi *et al*., 1996; Helgstrand *et al.*, 2004; Speir *et al.*, 2010).

Assembly of the tetravirus capsid is proposed to start with the self-association of structurally equivalent trimers, each subunit assuming one of the four slightly different quasi-equivalent conformations, A, B, C and D, after the assembly into procapsids (Figure 1.4, Panel B) (Finch *et al.*, 1974; Olson *et al.*, 1990; Johnson *et al.*, 1994). NωV procapsids (48 to 49 nm in diameter) are larger and more rounded in shape than mature virus-like particles (VLPs) (42 nm in diameter) (Figure 1.5) and are thought to mature as the result of conformational changes driven by electrostatic interactions (Canady *et al.*, 2000, 2001). The rearrangements occur rapidly (in the sub-second range) and are reversible until approximately 15 % of the capsid protein precursors have undergone autoproteolytic cleavage at their C-termini (Canady *et al.*, 2001; Tang *et al.*, 2009).

Cleavage of VCAP produces the large (β) (56 to 64 kDa) and small (γ) (6 to 8 kDa) capsid proteins observed in all tetravirus particles studied so far (Hanzlik *et al*., 2005; Yi *et al.*, 2005; Zeddam *et al.*, 2010), with the γ polypeptide of NωV acting as a molecular switch determining the quasi-symmetry of each subunit (Munshi *et al.*, 1996). In the C and D subunits, the γ polypeptide is ordered and, through interactions between the ABC and DDD morphological units, creates a flat contact, preventing excess curvature (Figure 1.4, Panel B) (Munshi *et al.*, 1996). In PrV, however, the N-terminal helices of the β polypeptide fulfil this function, with the γ polypeptide possibly bracing the N-terminal helices in their position in an arrangement similar to that observed in nodaviruses (Fisher and Johnson, 1993; Speir *et al.*, 2010). Autoproteolytic cleavage occurs between a conserved asparagine/phenylalanine pair (N^{570} and F^{571} in NωV, N^{575} and F^{576} in HaSV and N^{556} and F^{557} in PrV) in a reaction that is inhibited by N570T, E103Q and E103S mutations in NωV (Taylor *et al.*, 2002; Taylor and Johnson, 2005;

Speir *et al.*, 2010). Little is known about what promotes the conformational changes leading to particle maturation *in vivo*, but exposing procapsids to a pH below 5.8 has been shown to induce maturation (Canady *et al.*, 2000, 2001; Taylor *et al.*, 2002). This observation, along with the correlation between VLP maturation and apoptosis has led to the hypothesis that cytosolic acidification may play a role in virus maturation *in vivo* (Tomasicchio *et al.*, 2007).

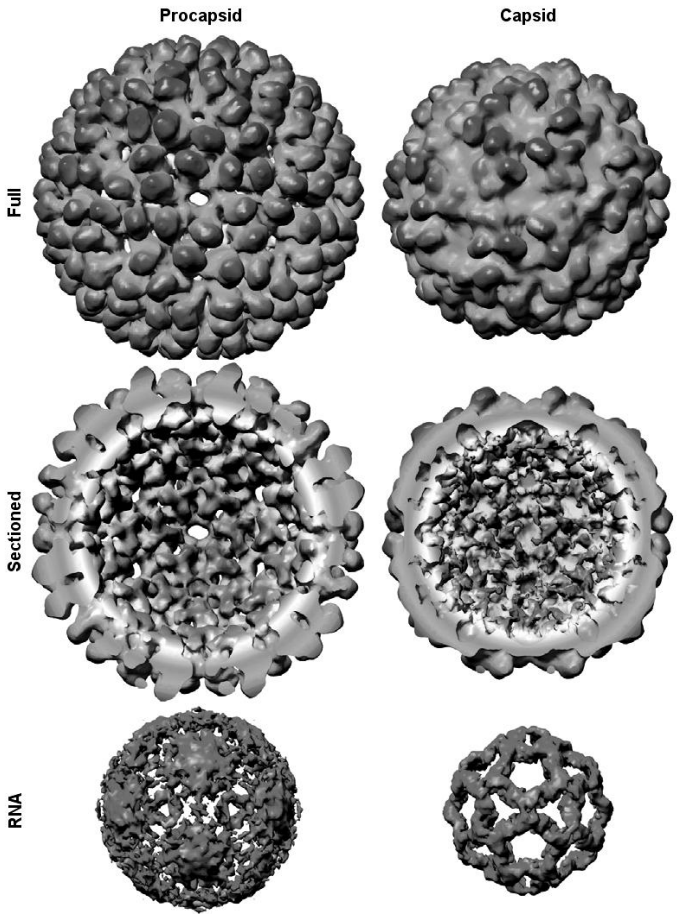

Figure 1.5: Three-dimensional reconstructions of full and sectioned HaSV procapsid and capsid structures including their packaged RNA. Sectioned particles in are sectioned down the 2-fold axis of symmetry. Reproduced from Speir and Johnson (2008).

1.3.3. Genomic organisation

Tetraviruses are classified according to their respective genome organisation with the betatetraviruses being monopartite and the omegatetraviruses bipartite (Hanzlik *et al.*, 2005). At present, the full genome sequences of six tetraviruses have been determined, including four betatetraviruses (NβV, TaV, EeV and PrV) and two omegatetraviruses (HaSV and *Dendrolimus punctatus* tetravirus (DpTV)) (Table 1.2). The cDNA sequence of NωV RNA2 has also been reported (Du Plessis *et al.*, 2005).

Table 1.2: Members of the *Tetraviridae* for which nucleotide sequences are available. Modified from Dorrington and Short (2010).

Virus	Acronym	GenBank Acc. No.	References
Genus: Betatetravirus			
Euprosterna elaeasa virus	EeV	AF461742	Gorbalenya *et al.* (2002)
Nudaurelia capensis β virus	NβV	AF102884	Gordon *et al.* (1999)
Providence virus	PrV	NC014126	Pringle *et al.* (2003)
Thosea asigna virus	TaV	AF282930 AF062037	Pringle *et al.* (1999)
Genus: Omegatetravirus			
Helicoverpa armigera stunt virus	HaSV	U18246 EU345431 L37299	Gordon *et al.* (1995) Hanzlik *et al.* (1995)
Nudaurelia capensis ω virus	NωV	DQ054400	Du Plessis *et al.* (2005)
Dendrolimus punctatus tetravirus	DpTV	AY594352 AY594353	Yi *et al.* (2005)

The betatetraviruses encode both the replicase and VCAP on a single genomic RNA that ranges from 5714 and 5698 nucleotides (nts) (TaV and EeV respectively) to 6625 nts (NβV) in length (Figure 1.6) (Gordon *et al.*, 1999; Pringle *et al.*, 2003; Zeddam *et al.*, 2010). In NβV, the two open reading frames (ORFs) overlap substantially with the replicase ORF proximal to the 5' end and *VCAP* at the 3' end (Gordon *et al.*, 1999; Pringle *et al.*, 1999, 2003; Zeddam *et al.*, 2010). *VCAP* is translated from a subgenomic RNA that, in NβV and TaV, originates just upstream of the *VCAP* ORF (Gordon *et al.*, 1999; Pringle *et al.*, 1999). Both TaV and EeV encode

N-terminal extensions to VCAP that are processed from the nascent protein via the action of a 2A-like cleavage site to generate an additional 17 kDa polypeptide (p17) of unknown function (Pringle *et al.*, 1999; Zeddam, *et al.*, 2010). As opposed to the tRNA-like structure at the 3' end of NβV RNA (Gordon *et al.*, 1999), both the genomic and subgenomic TaV and EeV RNAs are thought to terminate in 3' pseudoknots and the TaV and EeV replicase sequences suggest that the genomic RNAs may carry a 5' VPg (Zeddam *et al.*, 2010).

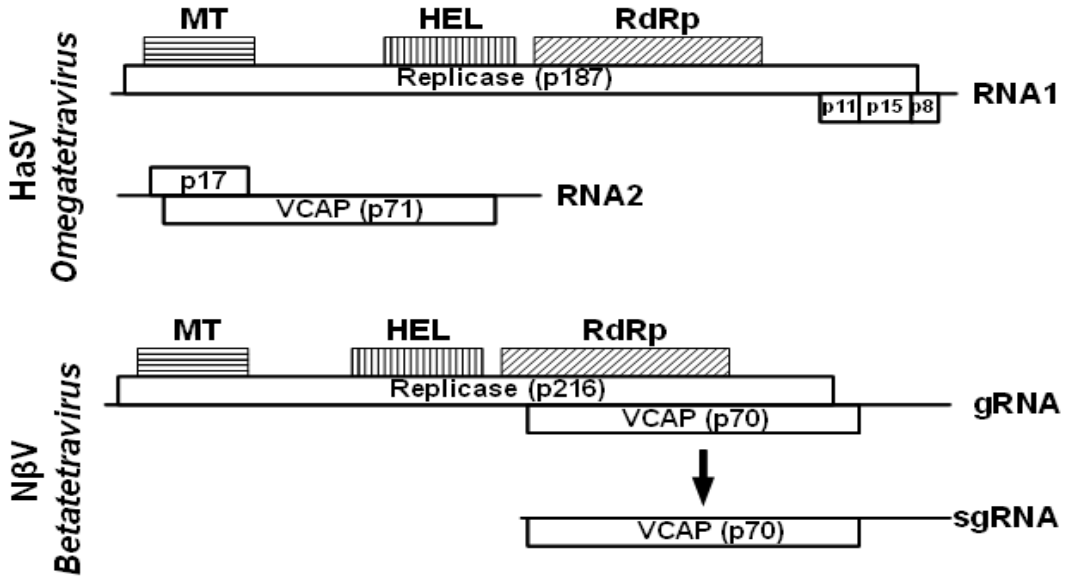

Figure 1.6: The genomic organisation of the tetraviruses. The top panel shows the genomic organisation of HaSV, a typical omegatetravirus, while the bottom panel shows the genomic organisation of the *Betatetravirus* type member NβV. The name of the protein translated from each ORF is indicated inside the open blocks. Molecular masses for each protein is indicated in kDa by the value following the p. Conserved replicase domains are indicated by hatched blocks above the respective replicase ORFs in HaSV. MT: Guanyl/methyltransferase domain, HEL: Helicase domain, RdRp: RNA-dependent RNA polymerase domain, gRNA: genomic RNA, sgRNA: subgenomic RNA.

PrV has an atypical genomic organisation encoding an additional 5'-proximal ORF of unknown function (*p130*) that encodes a 2A-like processing site predicted to generate 17 and 113 kDa polypeptides (p17 and p113 respectively) (Walter *et al.*, 2010). The replicase ORF is unique among tetraviruses in that it generates two overlapping replication proteins through the function of a read-through stop signal, the N-terminal region of the larger

replication protein, p104, corresponding directly to the early termination product (p40) (Walter *et al.*, 2010). Finally, two 2A-like processing sites are present upstream of the *VCAP* ORF and are predicted to generate polypeptides of 7 and 8 kDa (Walter *et al.*, 2010).

Both the omegatetraviruses sequenced to date encode *VCAP* on a distinct genomic RNA (RNA2, approximately 2500 nts) (Figure 1.6). The larger RNA (RNA1, 5312nts in HaSV and 5492 nts in DpTV) encodes the replicase (189 and 180 kDa in HaSV and DpTV respectively), in addition to three small ORFs for proteins of 8, 11 and 15 kDa at the 3' end (Gordon *et al.*, 1995; Yi *et al.*, 2005). It is unknown whether the three small proteins are expressed (Gordon *et al.*, 1995; Yi *et al.*, 2005). The smaller of the RNAs carries two ORFs, with *VCAP* overlapping with the 5' proximal ORF that encodes a 17 kDa non-structural protein thought to be an RNA binding protein (Hanzlik *et al.*, 1995; Du Plessis *et al.*, 2005; Yi *et al.*, 2005; Zhou *et al.*, 2008). Both HaSV genomic RNAs are capped at their 5' ends and terminate in 3' tRNA-like structures that can be charged with valine *in vitro* (unpublished data cited in Gordon *et al.*, 1999).

1.3.4. Tetravirus replication

The replication of tetraviruses is thought to occur in the midgut cells of the insects they infect (Moore *et al.*, 1985; Bawden *et al.*, 1999; Brooks *et al.*, 2002). The only tetravirus that has been shown to replicate in tissue culture is PrV, which exists as a persistent infection of a *Helicoverpa zea* midgut-derived cell line (MG8) although it is also able to infect *H. zea* FB33 and *Spodoptera exigua* Se-1 cells (Pringle *et al.*, 2003). In the first study on tetravirus replication, particles of the betatetravirus, *Trichoplusia ni* virus (TnV), were detected in midgut cells of *Trichoplusia ni* larvae during the early stages of infection and later during development in immature sex bodies (Greenwood and Moore, 1984). Transmission electron microscopy analysis of cells infected with PrV and TnV showed virions organised in crystalline

arrays associated with cytoplasmic vesicles (Greenwood and Moore, 1984; Pringle *et al.*, 2003). Bawden *et al.* (1999) analysed HaSV-infected *H. armigera* larvae for the presence of vRNAs over time following infection with wild-type virus. RNA1 was first detected three days after infection with RNA2 appearing two days later. This suggested that RNA1, encoding the viral replicase, was preferentially replicated early during the infection cycle. No subgenomic RNA was detected in the infected larvae (Bawden *et al.*, 1999). A similar observation has been made for PrV where replication of the genomic RNA precedes that of the subgenomic RNA (Pringle *et al.*, 2003). In general it is held that the betatetravirus subgenomic RNA is not replicated (Hanzlik *et al.*, 2005), although Pringle *et al.* (2003) observed negative sense vRNA corresponding in size to the subgenomic RNA.

1.3.5. The tetravirus replicase

Tetravirus replicases can be clustered into three distinct groups, with each bearing similarities to a different superfamily of virus replicases (Section 1.2.2) (Gordon *et al.*, 1995; Walter *et al.*, 2010; Zeddam *et al.*, 2010). The first group contains the replicases encoded by NβV, HaSV and DpTV, all of which have replicases related to those of the alpha-like superfamily of replicases (Gordon *et al.*, 1995; Gordon *et al.*, 1999; Yi *et al.*, 2005). Each replicase contains the characteristic modular N- to C-terminal arrangement of the conserved MT, HEL and RdRp domains (reviewed in Van der Heijden and Bol, 2002). Over these three regions, HaSV and DpTV show a high degree of sequence similarity with 67 %, 63 % and 76 % amino acid sequence identity over the three domains respectively (Gordon *et al.*, 1995; Yi *et al.*, 2005). Although this is significantly higher than the sequence similarity observed between NβV and either HaSV or DpTV, more than one third of the amino acids over each of the domains that have been compared are identical between all three viruses (Gordon *et al.*, 1995; Gordon *et al.*, 1999; Yi *et al.*, 2005). The DpTV RdRp domain, expressed as a recombinant polypeptide in *Escherichia coli*, is capable of primer-independent initiation of vRNA

synthesis *in vitro* (Zhou *et al.*, 2006). Interestingly, the tetraviruses are the only insect-specific alpha-like viruses, although there are a number of insect borne animal (alphaviruses) and plant (marafiviruses) viruses within the group (Van der Hiejden and Bol, 2002). HaSV, DpTV and NβV replicases lack any signs of co- or post-translational processing (Gordon *et al.*, 1995; Gordon *et al.*, 1999; Yi *et al.*, 2005), a characteristic shared with only a small group of plant viruses that includes the unclassified *Foveavirus* and *Potexvirus* genera (Van der Heijden and Bol, 2002).

A second group of tetravirus replicases comprises those encoded by TaV and EeV. Over the full length of their replicase sequences they share 68 % identity and together with the ds RNA birnaviruses, IPNV and IBDV, and *Drosophila* A virus, form a cluster distantly related to members of the picorna-like virus superfamily of viral replicases and are distinct from other (+ve) ss RNA viruses (Gorbalenya *et al.*, 2002; Ambrose *et al.*, 2009; Zeddam *et al.*, 2010). Characteristic of this cluster is the unique internally permuted C-A-B arrangement of the canonical A, B and C motifs conserved in the palm subdomain of all TDPPs (Section 1.2.1) (Poch *et al.*, 1989; Gorbalenya *et al.*, 2002; Ambrose *et al.*, 2009; Zeddam *et al.*, 2010). Another unusual feature of these replicases is the lack of discernible MT and HEL domains, unlike other picorna-like viruses which typically encode a HEL domain (Gorbalenya *et al.*, 2002; Van der Heijden and Bol, 2002). Both TaV and EeV replicases encode conserved sequences that, in birnaviruses, are responsible for the addition of 5’ VPgs to genomic RNAs, leading Zeddam *et al.* (2010) to suggest a similar function in these two tetraviruses. The significant differences in replicase sequence and genomic organisation has led to the proposal that TaV and EeV be classified in a separate family called the *Permutotetraviridae* (Zeddam *et al.*, 2010).

The final group contains PrV as the sole member, with a replicase that is significantly different from the other tetraviruses. Phylogenetic analysis using the PrV sequence groups it along with (+ve) RNA plant viruses like the

tombus- and umbraviruses, which belong to the carmo-like virus lineage of supergroup II (Walter *et al.*, 2010). The absence of MT and HEL domains in the PrV replicase is consistent with other carmo-like replicases (Walter *et al.*, 2010). The PrV replicase is unique among the tetravirus replicases in that it undergoes co-translational modification via the action of a read-through stop codon that results in the production of a major (p40) and minor (p104) replication protein, with p104 carrying the RdRp domain (Walter *et al.*, 2010).

1.4 SUBCELLULAR REPLICASE-HOST INTERACTIONS

1.4.1. Replicase-host interactions and viral replication complexes

The RdRp activity of many replicases is dependent on the assembly of vRNA replication complexes that often require specific interactions with cellular proteins and/or self-association of viral proteins (Buck, 1996; O'Reilly *et al.*, 1998; Dye *et al.*, 2005; Wileman, 2006). Three of the best studied (+ve) ss RNA replicases in terms of replicase-host interactions are protein A of Flock House virus (FHV) (*Nodaviridae*), $3D^{pol}$ from PV and Foot-and-mouth disease virus (FMDV) (*Picornaviridae*) and proteins 1a and 1b from the alpha-like virus Brome mosaic virus (BMV) (*Bromoviridae*), all of which have been shown to self-associate and/or interact with host proteins.

Protein A of FHV is the sole viral protein required for replicase activity (Ball, 1995) and has been shown to self-associate through the function of several non-overlapping internal sequences (Dye *et al.*, 2005). The importance of this self-interaction is demonstrated in that protein A deletion mutants with diminished self-interaction also show reduced RNA replication ability, indicating that multimerisation of protein A is essential for the efficient replication of FHV RNA (Dye *et al.*, 2005). Efficient RNA replication is also dependent on virus-encoded factors such as *cis*-acting elements within vRNA (Ball and Li, 1993) and host factors such as glycerophospholipids (Wu *et al.*,

1992) and heat shock protein 90, which is essential for the accumulation of FHV replication complexes in mitochondria of infected *Drosophila melanogaster* cells (Miller *et al.*, 2001; Kampmueller and Miller, 2005).

Analysis of the crystal structure of $3D^{pol}$ from PV revealed several protein-protein interactions that produce higher order structures, which Hansen *et al.* (1997) suggested were important for RdRp activity. This was in agreement with previous observations of $3D^{pol}$ self-interaction using glutaraldehyde cross-linking and the observation that the binding of a single synthetic template requires replicase multimers (Pata *et al.*, 1995). In terms of interactions with host proteins, the formation of FMDV replication complexes has recently been shown to occur in the presence of viral encoded 2C and 3A proteins as well as the host poly(A) binding protein and RNA helicase A (Lawrence and Reider, 2009).

Self-association of the BMV replication protein 1a, containing MT and HEL domains, is important for the recruitment of the RdRp domain (encoded by protein 2a) and the development of the replication complex (O'Reilly *et al.*, 1998). A comprehensive study of BMV-infected yeast cells by Kushner *et al.* (2003) showed that there were approximately 100 genes that, when deleted, increased or decreased BMV replication by more than 3-fold, demonstrating the complexity of virus-host interactions during RNA replication. The genes identified included those involved in membrane and chromatin remodelling, endocytosis, osmoregulation and ubiquitination. Although the exact functions of these genes in viral replication remain to be identified, the large number of host factors affecting vRNA production underscores the importance of host factors in the BMV life cycle in yeast cells. Other sources have identified further examples of host protein requirements for BMV replication including the yeast decapping activator complex Lsm1p-7p/Pat1p/Dhh1p, which is required for recruitment of vRNA for replication (Díez *et al.*, 2000; Mas *et al.*, 2006). Mas *et al.* (2006) suggested that this cellular function may be a key

regulator of the switch between translation and replication of BMV RNA, which is also dependent on specific cellular fatty acids (Lee *et al.*, 2001).

1.4.2. Subcellular localisation of replicases and anchoring to specific membranes

The various viral and host protein components involved in the formation of virus replication complexes have been shown to be associated with host-derived membranes in all (+ve) RNA viruses studied thus far, which is thought to concentrate the required viral and host factors and to create a localised site of replication (Netherton *et al.*, 2007). Additional functions such as avoidance of host anti-viral defence systems like proteolytic degradation of the viral replicase and/or RNAi-mediated degradation of ds RNA intermediates, have also been suggested (Jonczyk *et al.*, 2007).

RNA viruses have been shown to replicate their RNA in association with a wide variety of cellular membranes and are directed to their cellular location by various signals located within the replicase sequence. For example, FHV protein A is targeted to the mitochondria in infected *Drosophila* DL-1 and yeast cells by a target sequence within the N-terminal 46 amino acids (Miller *et al.*, 2001; Miller and Ahlquist, 2002). A similar localisation is seen in the type member of the alphanodaviruses, Nodamura virus, in both the greater wax moth (*Galleria mellonella*) and suckling mice (Garzon *et al.*, 1990). In the betanodavirus, Atlantic halibut nodavirus, protein A carries two mitochondrial localisation signals, one in the N-terminal 40 amino acids and another a further 225 amino acids downstream, either of which are capable of targeting enhanced green fluorescent protein (EGFP) to the mitochondria (Mézeth *et al.*, 2007). Interestingly, in FHV, vRNA replication is not dependent on mitochondrial localisation (Miller *et al.*, 2003). Retargeting of FHV protein A to the endoplasmic reticulum (ER) results in replicase activity, implying that specific membranes are not required for vRNA production (Miller *et al.*, 2003). In the first study on the three-dimensional structure of

replicase-membrane associations, Kopek *et al.* (2007) showed that approximately 100 copies of FHV protein A reside in invaginations of the outer mitochondrial membranes, approximately 50 nm in diameter and located in the inter-membrane space. These spherules also contained on average, three RNA replication intermediates and had a necked channel of approximately 10 nm, allowing for the export of vRNA and the import of nucleotides.

In contrast to FHV, the Tomato ringspot virus replication complex is anchored to the ER by a C-terminal transmembrane helix and an N-terminal amphipathic helix present in the nucleoside triphosphate-binding protein (NTB) as well as by a multipass transmembrane protein called X2 (Han and Sanfaçon, 2003; Wang *et al.*, 2004; Zhang *et al.*, 2005; Zhang and Sanfaçon, 2006). Immunofluorescence analysis of the BMV replication proteins 1a and 2a in infected barley protoplasts has shown that 1a is capable of localisation to the ER independent of other viral proteins (Restrepo-Hartwig and Ahlquist, 1996; Restrepo-Hartwig and Ahlquist, 1999). This localisation is directed via a peripheral membrane association within the N-terminal MT domain of 1a (Den Boom *et al.*, 2001).

PV-induced vesicles have been shown by electron microscopy to be formed from ER membranes and contain the COPII protein complex (Bienz *et al.*, 1987; Rust *et al.*, 2001). Later in the infectious cycle, PV proteins colocalise with Golgi marker proteins, consistent with the function of COPII in ER-Golgi transport (Bolten *et al.*, 1998). The same is true for FMDV, with the non-structural proteins 2B and 2C associating with the ER and Golgi when expressed alone in cells (Moffat *et al.*, 2005). However, in FMDV-infected cells replication complexes do not overlap with markers of the ER or Golgi leading Knox *et al.* (2005) to hypothesise that it may exclude host proteins from the membranes it sequesters. Although the studies on PV and FMDV indicate a stringent localisation, biochemical studies conducted by Schlegel

et al. (1996) indicated that membranes may be derived from the lysosomes in addition to the Golgi and the ER.

The togaviruses Semliki Forest virus (SFV), Sindbis virus (SIN) (both in the genus *Alphavirus*) and Rubella virus (RV) (Genus: *Rubivirus*) replicate their RNA in association with cytopathic vacuoles that are derived from endosomes and lysosomes (Grimley *et al.*, 1968; Froshauer *et al.*, 1988; Magliano *et al.*, 1998; Kujala *et al.*, 1999, 2001; Matthews *et al.*, 2009). In both SFV and SIN, the replicase complexes are also associated with fibrous structures that appear to form bonds between the cytopathic vesicles and the rough ER (Froshauer *et al.*, 1988). In a recent study by Matthews *et al.* (2009) the N-terminus of the RV replication protein P150 and its precursor P200 was shown to be essential for fibre formation and the subcellular location of replication complexes, which replicate vRNA at cellular sites that partially overlap with endocytic and lysosomal membranes (Matthews *et al.*, 2009).

To date, no studies have been conducted regarding the subcellular interactions of tetravirus replicases. Tomasicchio *et al.* (2007) demonstrated that the induction of apoptosis in yeast cells expressing VCAP resulted in the spontaneous maturation of VLPs. This, coupled with the acid maturation of VLPs and the cytosolic acidification caused during apoptosis, led Tomasicchio *et al.* to hypothesise that the viral replicase could associate with either the mitochondria or lysosomes due to their role in the induction of apoptosis (Matsuyama and Reed, 2000; Nilsson *et al.*, 2006). This was further supported by experiments demonstrating an increased incidence of apoptosis in HaSV-infected cells, suggesting that virus replication may induce apoptosis *in vivo* (Brooks *et al.*, 2002). Capsid maturation through cytosolic acidification could therefore be the result of the replicase-dependent induction of apoptosis (Tomasicchio *et al.*, 2007). Tetraviruses preferentially infect highly endocytic midgut cells and the observation that HaSV infection results in the accumulation of lysosomes (Brooks *et al.*, 2002) suggests a

possible association of replication and endocytic organelles in host cells. The potential association of tetraviral replication, and the viral life cycle, with endocytic organelles warrants a discussion of cellular endocytosis, which will enable the comparison of the data obtained during the course of this study with the various organelles of cellular endocytic pathways. A significant proportion of the data discussed in this thesis is suggestive of interactions between these organelles and the HaSV replicase. Therefore, a full understanding of the cellular processes involved will greatly aid in the interpretation of these data.

1.5 CLASSICAL AND ALTERNATE ENDOCYTIC PATHWAYS

The endocytic pathway comprises a series of morphologically heterogeneous compartments designed for uptake of extracellular components. These are largely destined for lysosomes, where they are degraded and the constituents (amino acids, nucleotides, lipids, cholesterol, etc.) made available for metabolism elsewhere in the cell (Gruenberg and Maxfield, 1995; Fielding and Fielding, 1997; Gu and Gruenberg, 1999; Mullins and Bonifacino, 2001). Since many viruses and a number of plant and toxic bacterial proteins exploit normal endocytic pathways to gain entry into their host cells, much of what we now know about the cellular processes involved in endocytosis is the direct result of studies aimed at understanding specific virus- and toxin-host interactions (reviewed in Johannes and Goud, 1998; Lord and Roberts, 1998; Pelkmans and Helenius, 2003). Ultimately, the progression of the extracellular cargo through the endocytic pathway is achieved through a combination of vesicular transport and maturation that is further complicated by the continuous retrograde recycling of components to the plasma membrane and *trans* Golgi network, as well as the infrequent removal of undigested material from the cell upon fusion of lysosomes with the plasma membrane.

There is evidence that there may be a number of different endocytic pathways that a given cell may utilise and that different cells (and viruses) may utilise them to different extents and for different functions (Pelkmans and Helenius, 2003). In addition, some proteins, such as glycosylphosphatidylinositol (GPI)-anchored proteins (GPI-APs) and (under certain conditions) tetraspannins cluster within distinct but overlapping regions of the plasma membrane and are endocytosed and trafficked along with detergent-resistant membranes (DRMs), the function of which is still largely unclear (Berditchevski, 2001; Claas *et al.*, 2001; Levy and Shoham, 2005; Hein *et al.*, 2009; Zheng and Foster, 2009).

1.5.1. Classical or clathrin-dependent endocytosis

The uptake of extracellular macromolecules at the plasma membrane occurs primarily through receptor mediated endocytosis, allowing the cell to selectively bind and internalise components from the surrounding environment (summarised in Figure 1.7, Centre) (Gruenberg and Maxfield, 1995). For this purpose, transmembrane receptor proteins are displayed on the outer surface of the plasma membrane where they bind to their respective ligands. After binding between the receptor and an appropriate ligand (or virus particle) has occurred, the receptor associates with transient invaginations of the plasma membrane caused by clathrin polymerisation, where it interacts with clathrin-associated sorting proteins and adaptor proteins, such as AP-2 (adaptor protein complex 2) and arrestin (Zaremba and Keen, 1983; Matsui and Kirchhausen, 1990; Trowbridge *el al.*, 1993; Shih *et al.*, 1995; reviewed in Robinson 1994; Mousavi *et al.*, 2004; Traub 2009). This results in the stabilisation and formation of a clathrin-coated pit and the specific accumulation of virus- and/or ligand-bound receptors. The clathrin-coated pit is then closed and pinched off to form a clathrin-coated vesicle by dynamin and its associated proteins (reviewed in Schmid *et al.*, 1998) and will transport the virus particle through the endocytic pathway until a virus-specific acidic pH triggers the next stage of infection (Helenius *et al.*,

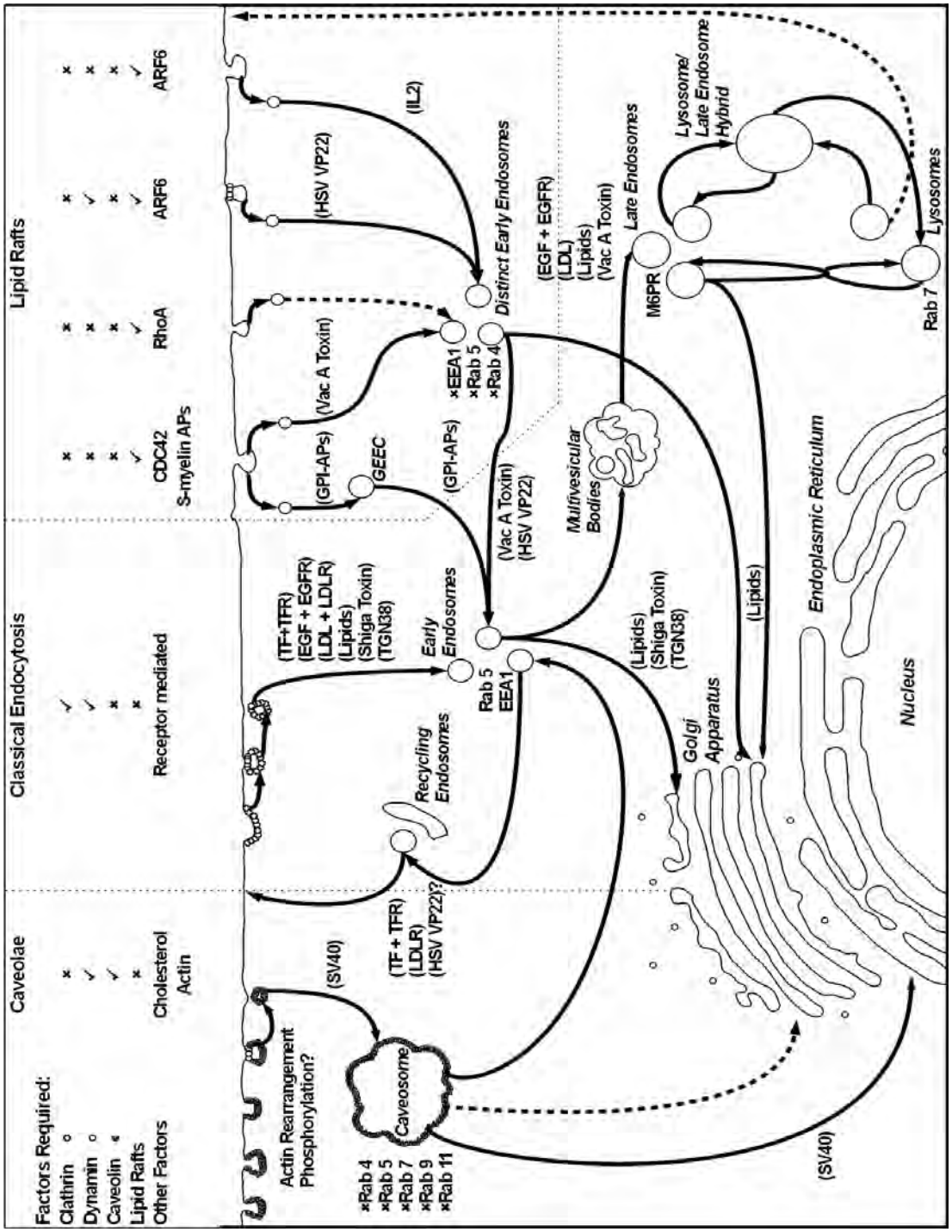

Figure 1.7: Cellular endocytic pathways. Schematic representations of caveolae (left), classical clathrin-dependent (centre) and lipid raft-dependent (right) endocytosis as described in text. The table (top) indicates which major factors are required for each endocytic pathway. Organelle names are in italics and examples of cargo carried by specific organelles are in brackets. Normal text indicates selected factors present as organelle-specific markers. In the distinct early endosomes and caveosomes, notable markers that are absent are indicated with a cross before the marker name.

1980). Since the lumen of the clathrin-coated vesicle contains fluid from outside the cell, it will also contain unbound extracellular components, which are taken up via fluid-phase endocytosis. These vesicles are short-lived (approximately 1 minute) and shed their coat within seconds of being formed, rendering them competent for fusion with the early endosomes (Aniento *et al.*, 1993).

Within a few minutes endocytosed material is found in early endosomes, which are characteristically small (0.3 to 0.4 μm in diameter), tubulo-vesicular organelles with an internal pH of approximately 6.0 (Dunn and Maxfield, 1992; Thilo *et al.*, 1995; reviewed in Gruenberg and Maxfield, 1995). These then undergo fusion events with newly endocytosed material from the plasma membrane at a rate that declines with age (Ajioka and Kaplan, 1986; Ward *et al.*, 1990; Dunn and Maxfield, 1992). The fusion events require the activity of protein phosphatases as well as the small GTPase Rab5, Syntaxin 13 and the tethering factor, early endosomal autoantigen 1 (EEA1) (Gorvel *et al.*, 1991; Bucci *et al.*, 1992; Woodman *et al.*, 1992; Clauge, 1999; McBride *et al.*, 1999; Luzio *et al.*, 2000). Rab5 functions as an important kinetic regulator of the transport of newly endocytosed material from the plasma membrane to the early endosomes, specifically with regard to vesicle fusion (Bucci *et al.*, 1992).

The accumulation of lysosome-targeted constituents is further facilitated by the recycling of the receptors to the plasma membrane by recycling endosomes that bud from early endosomes, which at this point can be termed sorting endosomes (Dunn *et al.*, 1989). This sorting process allows for receptors to follow a number of different paths from the early endosomes. For example, transferrin is recycled back to the plasma membrane along with its receptor via recycling endosomes (Dautry-Varsat *et al.*, 1983; Klausner *et al.*, 1983), while EGF (epidermal growth factor) is routed through the endocytic pathway to the lysosomes where it is degraded along with its receptor (Carpenter and Cohen, 1979). LDL (low density lipoprotein) is

transported for degradation, as opposed to the receptor which is recycled back to the plasma membrane (Goldstein *et al.*, 1979). Furthermore, studies showing that lipids (Puri *et al*., 2001) and proteins, such as Shiga toxin produced by *Shigella dysenteriae* and TGN38 (Ghosh *et al*., 1998; Mallard *et al.*. 1998), were sorted from this point to the Golgi, revealed the presence of a retrograde post-Golgi pathway for the recovery of secretory/biosynthetic pathway constituents (Mallard *et al.*, 2002). In some cases toxins, and probably host proteins, are further transported to the ER (reviewed in Johannes and Goud, 1998; Lord and Roberts, 1998). Hence, the early endosome forms the major point for the sorting of proteins to be recycled or degraded (Gruenberg *et al.*, 1989). It appears that the recycling pathway is regulated by another small GTPase, Rab4, which plays a similar role to that of Rab5 in the early endosomes (Van Der Sluijs *et al.*, 1992). In addition to the functions relating to the movement of receptors, a number of lipids have been shown to follow the endocytic pathway to the lysosomes where they are further shuttled to the Golgi apparatus (Koval and Pagano, 1990; Chen *et al.*, 1998; Pagano *et al.*, 1999; Pagano, 2003).

With time, early endosomes become resistant to fusion with newly endocytosed material as they mature to form late endosomes via multivesicular bodies (MVBs) (reviewed in Gruenberg and Maxfield, 1995; Piper and Luzio, 2001). Although dependent on cell type, maturation typically takes between 4 and 30 minutes in mammalian cells (Dunn and Maxfield, 1992; Thilo *et al.*, 1995). This process proceeds in the absence of homotypic fusion *in vitro*, which is in contrast to both the early and late endosomes (Gruenberg *et al.*, 1989; Bomsel *et al.*, 1990; Aniento *et al.*, 1993). MVBs function as a means of transport and maturation from early to late endosomes, which is demonstrated by the observation that although the protein composition of the early and late endosomes are distinct, there is a large degree of overlap between the protein content of both endosomal compartments and MVB's (Aniento *et al.*, 1993; Emans *et al.*, 1993).

As MVBs mature, they are transported towards the late endosomes by an active process requiring intact microtubules and the motor proteins dynein and kinesin (Gruenberg *et al.*, 1989; Bomsel *et al.*, 1990; Aniento *et al.*, 1993, Bananis *et al.*, 2004). This maturation into late endosomes coincides with an increase in the ability of these vesicles to fuse with traffic from the Golgi apparatus, which contain lysosomal enzymes targeted to the late endosomes by the mannose-6-phosphate receptor (Griffiths *et al.*, 1988; Geuze *et al.*, 1988). As is the case with early endosomes, a retrograde post-Golgi recovery pathway retrieves secretory pathway components from the late endosomes in a Rab9-dependent manner (Lombardi *et al.*, 1993; Itin *et al.*, 1997; Carrol *et al.*, 2001).

Experimental evidence suggests that late endosomes then transfer their cargo to lysosomes in a combination of “fusion-fission” and “kiss-and-run” events (Bright *et al.*, 2005; reviewed in Mullins and Bonifacino, 2001). Bright *et al.* (2005) found that the majority of content-mixing in live rat kidney cells was the result of “kiss-and-run” or “kiss-and-linger” events where the content in the late endosome is delivered to the lysosome through brief contact that does not result in fusion. This allows for the mixing of the contents of the two organelles without direct fusion, although a late endosome may subsequently fuse with a different lysosome (Bright *et al.*, 2005). It has also been observed that microtubule-dependent tubules may form over relatively large distances to facilitate content-mixing as well. Bright *et al.* (2005) describe one such tubule that protruded from a lysosome and connected with a late endosome at a distance of over 13 μm.

Fusion events also occur as late endosomes fuse with lysosomes to form late endosome-lysosome hybrid organelles that contain marker proteins from both organelles and are less electron dense than lysosomes. The mechanism is not dependent on phosphorylation or microtubules (as is the case with early and late endosomal fusion events respectively), but is reliant on the activity of a Rab protein (Mullock *et al.*, 1994, 1998; Bright *et al.*, 2005;

reviewed in Luzio *et al.*, 2000). This late endosome-lysosome hybrid organelle then matures to reform a lysosomal compartment, apparently due to a combination of digestive processes and a membrane and late endosome-specific protein recovery system to remove late endosomal components (Bright *et al.*, 1997; Mullock *et al.*, 1998; Luzio *et al.*, 2000; Bright *et al.*, 2005).

Maturation of the late endosome-lysosome hybrid therefore reforms the lysosome by a combination of degradation and membrane recycling processes. At the end of the maturation process, the lysosomes are characterised by their acidic pH (approximately 4.5), the presence of acid hydrolases and specific integral membrane glycoproteins, an absence of mannose 6-phosphate receptors and recycling cell surface receptors and a perinuclear distribution that is dependent on Rab7 (Mellman *et al.*, 1986; Feng *et al.*, 1995; Bucci *et al.*, 2000; Luzio *et al.*, 2002).

1.5.2. Detergent-resistant membranes, lipid rafts, caveolae and clathrin-independent endocytosis

The membrane compartmentalisation model states that membrane microdomains are areas of biological membranes with different protein and/or lipid composition to the regions surrounding them, which are able to function in biosynthetic processes and endocytic transport or as specialised reaction centres and enzyme, substrate and/or adaptor concentration sites (Simons and Ikonen, 1997). DRMs represent a subset of membrane fractions that are insoluble in cold, non-ionic detergents and have a low buoyant density, which is largely due to their association with high concentrations of cholesterol, sphingomyelin and glycolipids (reviewed in Anderson and Jacobson, 2002; Zheng and Foster, 2009). Although they have often been associated with specific membrane microdomains, it has been argued that DRMs more accurately represent the incomplete solubilisation of membranes under the specified conditions and only exist as a result of the detergent treatments

(Lichtenberg *et al.*, 2005). Nevertheless, differential solubility in various detergents remains an important means of studying lipid-protein interactions, especially those associated with genuine *in vivo* lipid microdomains.

In a number of cases, DRM isolation has been important for the isolation and characterisation of previously unidentified components of both the secretory and endocytic pathways in the cell, including the recently discovered clathrin-independent endocytic components (Figure 1.7, Left and Right). For example, Lamaze *et al.* (2001) showed that interleukin 2 receptors, ultimately destined for the lysosomes, associate with DRMs on the cell surface and internally after dynamin-dependent and clathrin-independent endocytosis. In Madin Darby Canine Kidney (MDCK) cells, the GPI anchor of membrane dipeptidase is important for maturation in the Golgi apparatus (Hein *et al.*, 2009) and Triton X-100-insoluble monocyte lipid rafts contain proteins from the ER and the endocytic pathway as well as proteins involved in vesicular fusion and actin-based vesicular transport (Li *et al.*, 2003). Interestingly, these non-classical pathways seem to be able to deliver their cargo to a number of different cellular destinations including lysosomes, the ER and the Golgi apparatus (Nichols and Lippincott-Schwartz, 2001).

A number of viruses and bacterial toxins make use of these pathways to enter cells (Figure 1.7) including Simian virus 40 (SV40), targeted to the ER via caveosomes, and Cholera toxin, which is taken up by numerous cellular processes but requires clathrin-independent endocytosis to gain access to the Golgi apparatus for it to be toxic (Tran *et al.*, 1987; Norkin, 1999). These non-classical pathways also appear to play an important role in the regulation and transport of intracellular cholesterol (Fielding and Fielding, 1997) and are thought to play a role in *Plasmodium falciparum* infection of human erythrocytes (Murphy *et al.*, 2004). Studies such as these are revealing that the inner complexity of both the secretory and endocytic pathways goes beyond the well-defined classical pathways and are identifying a number of

previously unacknowledged pathways (reviewed in Nichols and Lippincott-Schwartz, 2001; Johannes and Lamaze, 2002; Pelkmans and Helenius, 2003; Mayor and Pagano, 2007).

Although there are several clathrin-independent endocytic pathways, unambiguous classification of these pathways is somewhat difficult. In broad terms, these alternative pathways are generally dependent on dynamin, caveolin or lipid rafts with the classical endocytic pathway dependent on clathrin and dynamin (Section 1.5.1). The caveolae pathway is dependent on caveolin-1 and dynamin, while lipid-raft dependent endocytosis may or may not be dynamin dependent (Figure 1.7) (Pelkmans and Helenius, 2003; Mayor and Pagano, 2007). Since there appears to be some plasticity in terms of function and the uptake of different cargo in different cells, this survey will discuss lipid rafts and caveolae in terms of what is known in general and will attempt to avoid cell- or tissue-specific functions.

Lipid rafts

Lipid rafts have been defined as “dynamic assemblies of cholesterol and glycosphingolipids that are present in the lateral plane of membranes” (Johannes and Lamaze, 2002) with sphingolipids acting as spacers due to their relatively large head groups (Simons and Ikonen, 1997). This cholesterol-lipid interaction results in a tightly packed structure that differs significantly from the surrounding membrane. The structure and function is maintained by lipid-lipid interactions, associations of lipids and proteins that are recruited through their high affinity for lipid rafts (such as GPI-APs) and protein-protein interactions, which can result in large protein complexes. The concentration and partition of specific proteins onto the distinct lipid rafts produces membrane reaction centres that are especially active in cellular signalling and trafficking (Simons and Ikonen, 1997; Foster *et al.*, 2003; Li *et al.*, 2003; Botto *et al.*, 2004).

In addition to functions in signal transduction, a number of vesicular transport pathways are associated with lipid rafts. For example, it has been hypothesised that they are involved in post-Golgi retrograde secretory pathway transport that runs parallel to that observed in the classical endocytic pathway (Simons and Ikonen, 1997). This pathway provides an alternative route for the recovery of ER and Golgi proteins mis-transported towards the cell surface along the secretory pathway. While low levels of EGF stimulate receptor-mediated endocytosis almost exclusively via the classical pathway, higher concentrations of EGF result in the ubiquitination of the EGF receptor, which is sufficient to stimulate internalisation by a lipid raft-dependent route (Sigismund *et al.*, 2005). In addition there are dynamin-independent pathways that appear to require the small GTPases CDC42, ARF6 or RhoA (Mayor and Pagano, 2007), both the CDC42- and ARF6-dependent pathways require sphingomyelin-associated proteins but not glycosphingolipids (Cheng *et al.*, 2006). The CDC42 pathway is also reported to be involved in the uptake of a large proportion of GPI-APs (Kalia *et al.*, 2006). In contrast, the Herpes simplex virus (HSV) protein VP22 is internalised via an ARF6-dependent pathway that is also dynamin-dependent (Nishi and Saigo, 2007). The complexity in terms of the small GTPases that are required and the observation of dynamin-dependent and -independent pathways for many of them means that it is difficult to know what differences are the result of cell type as opposed to changes in experimental methods. However, what is clear is that there are a rapidly increasing number of reports of endocytosis by lipid raft-associated mechanisms that are both clathrin- and caveolin-independent.

Caveolae

Many cell types have flask-shaped, stable invaginations on the plasma membrane called plasmalemmal vesicles or caveolae (in reference to their cave-like appearance when viewed by electron microscopy) (reviewed in Stan, 2005). These invaginations typically have an outer diameter of approximately 70 nm and can occur in a number of distributions across the

cell surface. Although discovered by electron microscopy over half a century ago, the first protein component, caveolin (now caveolin-1), was only discovered in 1992 (Palade, 1953; Rothberg *et al.*, 1992). Since then further caveolins (caveolin-2 and caveolin-3) and a number of other lipid and protein components such as sphingolipids, glycosphingolipids, fatty acids, cholesterol, signalling proteins and GPI-APs have been shown to be involved in the formation of caveolae – although protein-protein interactions are the determining factor for formation (Simons and Ikonen, 1997; Aboulaich *et al.*, 2004; Sprenger *et al.*, 2004; Cheng *et al.*, 2006; Zheng and Foster, 2009).

Caveolae are multi-functional membrane domains utilised in the up- or down-regulation of enzyme activity through the compartmentalisation of enzymes, endocytosis, cholesterol transport and homeostasis, signal transduction and cell signalling (Fielding and Fielding, 1997; Henley *et al.*, 1998; Kurzchalia and Parton, 1999; Sowa *et al.*, 2001; Sandvig *et al.*, 2008). Although caveolae have been thought of as specialised lipid rafts and the majority of data available appears to confirm this, their association with cholesterol has been questioned (Foster *et al.*, 2003). However, in contrast to lipid rafts there are a number of distinct molecules associated with caveolae, most notably the caveolins (Rothberg *et al.*, 1992; Liu *et al.*, 1997; Sowa *et al.*, 2001). Additionally, cholesterol and an association with intact actin cytoskeletal elements are required for their formation while internalisation is dynamin-dependent and is a triggered event (Parton *et al.*, 1994; Thomsen *et al.*, 2002). Internalisation via caveolae is also very slow with only around 2 % of caveolin-1-positive vesicles budding from the plasma membrane per minute in mouse embryonic fibroblasts (Kirkham *et al.*, 2005). In SV40-infected cells, phosphorylation of caveolae-associated proteins is required for the extensive actin rearrangements necessary for internalisation (Pelkmans *et al.*, 2001). In contrast to the other endocytic pathways described above, internalisation by caveolae does not appear to be involved in constitutive or fluid-phase endocytosis (Pelkmans *et al.*, 2001).

Destinations of material internalised by clathrin-independent endocytosis

Although there are a number of different mechanisms available to cells for internalisation, it appears that the majority of endocytosed material is ultimately transported into Rab5- and EEA1-positive early endosomes, where normal sorting processes direct cargo to the degradative pathway, the secretory pathway or back to the plasma membrane (Figure 1.7) (Hansen *et al.*, 1993; Mayor and Pagano, 2007). However, there are alternate routes and intermediate compartments associated with each of the pathways that are different from those observed in the classical pathway (Figure 1.7).

Endocytosis by lipid raft-dependent pathways usually bud into distinct early endosome-like compartments. Clathrin-, caveolin-1- and dynamin-independent carrier vesicles bud directly from tubular invaginations of the plasma membrane containing GPI-APs (Kirkham *et al.*, 2005). Naslavsky *et al.* (2003) reported that the interleukin 2 receptor, internalised by AFR6-associated endocytosis, enters endosomes distinct from those containing cargo from the classical pathway. The same has been observed for GPI-APs from a CDC42-dependent, dynamin-, AFR6- and RhoA-independent pathway (Sabharanjak *et al.*, 2002; Kalia *et al.*, 2006) and the VacA cytotoxin produced by *Helicobacter pylori* (Gauthier *et al.*, 2005). These endosomes are acidic structures devoid of EEA1, Rab4 and Rab5 (Kalia *et al.*, 2006). Later they acquire EEA1 and Rab5 and undergo homotypic fusion with other ARF6-associated GPI-AP-enriched early endosomal compartments (GEECs) and heterotypic fusion with early endosomes from the classical pathway, ultimately resulting in an overlap with typical endocytic cargo like LDL (Radhakrishna and Donaldson, 1997; Naslavsky *et al.*, 2003; Kalia *et al.*, 2006). Following convergence, cargo from both the lipid raft-associated and classical pathways are transported together to the lysosomes in a Rab7-dependent manner (Naslavsky *et al.*, 2003) or sorted by normal cellular processes to the Golgi or the plasma membrane.

Caveolae deliver their cargo to caveosomes (Pelkmans *et al.*, 2001), which are pre-existing, static, stable and cholesterol-enriched structures that have neutral luminal pH and are devoid of Rab4, Rab5, Rab7, Rab9 and Rab11 (Thomsen *et al.*, 2002; Pelkmans and Helenius, 2003). From here cargo can be transported to early endosomes (Gagescu *et al.*, 2000) or the smooth ER (Kartenbeck *et al.*, 1989). However, caveosomes appear to function in specific sorting of only the cargo derived from caveolae-associated endocytosis since they do not seem to receive cargo from the classical endocytic pathway, as demonstrated by the absence of classical markers or ligands (Pelkmans *et al.*, 2001). This is further substantiated by the observation that they do not accumulate fluid-phase markers such as fluorescent-labelled dextran, even in the presence of cargo known to be internalised via caveolae (Pelkmans *et al.*, 2001).

In addition to alphaviruses (SFV and SIN) and RV, all of which form replication complexes that associate at least in part with classical endocytic organelles (Froshauer *et al.*, 1988; Matthews *et al.*, 2009), alternate endocytic pathways are involved in the life cycles of viruses such as SV40 and HSV (Norkin, 1999; Nishi and Saigo, 2007). Since all the tetraviruses studied thus far have been shown to infect the midgut cells of their hosts, it is possible that the well developed endocytic systems present in these cells are important in one or more stages in the tetravirus life cycle.

1.6 PROBLEM STATEMENT

Very little is known about tetravirus replication biology and to date there is no literature available on the subcellular site of tetravirus replication. Their unusually narrow host range and tissue tropism as well as the absence of an *in vitro* cell culture system has hampered the study of the replication and expression strategies of the *Tetraviridae* (Bawden *et al.*, 1999). Thus, the broad aim of the research described in this thesis was to develop new

experimental systems for studying tetravirus replication, focusing on the subcellular localisation of the HaSV replicase.

1.7 SIGNIFICANCE OF UNDERSTANDING HaSV REPLICATION BIOLOGY

Besides contributing to knowledge about tetravirus replication, studies on the replication biology of the replicase from HaSV has the potential to impact the understanding of RNA replication in other viruses. HaSV relies on a single virus encoded protein for vRNA replication and, as a result, represents one of the simplest viruses known. This simplicity means that auxiliary functions, encoded by additional viral proteins in more complex viruses, must, in the case of HaSV, be supplied by host proteins. As a result, understanding gained from the analysis of the replication biology of HaSV could shed light on host functions essential for virus replication and thus identify auxiliary processes supplied by the host cell. In addition, the results obtained from this "basic" viral unit could be extrapolated to larger viruses with more complicated genomes and protein production strategies, enabling an increased understanding of the reasons behind the greater complexity and the ways in which different replication strategies are suited to particular cellular environments.

1.8 OBJECTIVES

1. To develop experimental systems for studying tetravirus replication
2. Analysis of the cellular distribution and subcellular localisation of the HaSV replicase in tissue culture cell lines
3. Identification and characterisation of HaSV replicase membrane targeting domains

CHAPTER 2

PRODUCTION OF ANTISERUM FOR THE DETECTION OF THE HaSV REPLICASE

2.1 INTRODUCTION

The discovery of HaSV by Hanzlik *et al.* in 1993 resulted in significant advances in the knowledge of the *Tetraviridae*. This was because, unlike many tetravirus hosts, *H. armigera* can be reared in laboratory colonies, and as a result HaSV has proven to be an important tool in understanding some of the common features found in the broader virus family. However, at the outset of the research described in this thesis, the replication biology of HaSV was essentially unknown. This was due to the absence of a replication-competent tissue culture system, as well as the inability to detect HaSV replicase in infected cells because of the unavailability of replicase-specific antiserum. Thus the first objective of this study was to identify potential antigenic regions of the HaSV replicase, to overexpress them in *E. coli* and to use purified protein to raise polyclonal anti-replicase antiserum.

2.2 MATERIALS AND METHODS

Unless otherwise indicated, recombinant DNA methods were generally as described in Sambrook *et al.* (1989). The *E. coli* strain DH5α (*F- endA1 glnV44 thi-1 recA1 relA1 gyrA96 deoR nupG Φ80dlacZΔM15 Δ(lacZYA-argF)U169, hsdR17(rK⁻ mK⁺), λ–*) (Hanahan, 1983) was used to propagate recombinant plasmids and *E. coli* BL21 (DE3) (*B F- dcm ompT hsdS(r_B- m_B-) gal λ(DE3)*) (Studier and Moffatt, 1986; Studier *et al.*, 1990) was used for the overexpression of polypeptide fragments.

2.2.1. Bioinformatic analysis of the HaSV replicase and selection of fragments for bacterial expression

Potentially hydrophilic domains of the HaSV replicase were identified by bioinformatic analysis according to Kyte and Doolittle (1982), generated by online submission of the HaSV replicase amino acid sequence (cDNA GenBank accession number EU345431) to the ProtScale program (Gasteiger *et al.*, 2005) hosted by the Expert Protein Analysis System (ExPASy) (ProtScale last accessed at http://au.expasy.org/tools/protscale.html on 29/03/2010).

2.2.2. Recombinant plasmids for the overexpression of HaSV replicase protein fragments in *E. coli*

Basic restriction maps of the recombinant expression vectors used in the experiments described in this chapter are shown in Figure 2.1 and their construction is described in detail in Appendix A. The bacterial expression vector pT7-7_6xHis –*Xba* I (referred to as pT7-7_6xHis) contains the T7 RNA polymerase promoter, ribosome binding site (RBS) and a hexa-histidine (6xHis) sequence following the methionine residue which is directly upstream of a multiple cloning cassette (Figure 2.1). Both pJRS17 and pJRS19 were derived from pT7-7_6xHis and contain the 5' fragments of the HaSV replicase CDS corresponding to the N-terminal 150 or 218 amino acids respectively, fused in frame with the 3' end of the 6xHis CDS for the production of His-REP_{1-150} and His-REP_{1-218}. A recombinant plasmid for the expression of a glutathione S-transferase (GST)-tagged HaSV replicase fragment, pJRS23, was also constructed. Derived from the commercially available pGEX-4T-2 (GE Healthcare), pJRS23 contains the sequence coding for the carboxy-terminal 564 amino acids of the HaSV replicase fused at its N-terminus to the C-terminus of GST, with expression under the control of an inducible *tac* promoter.

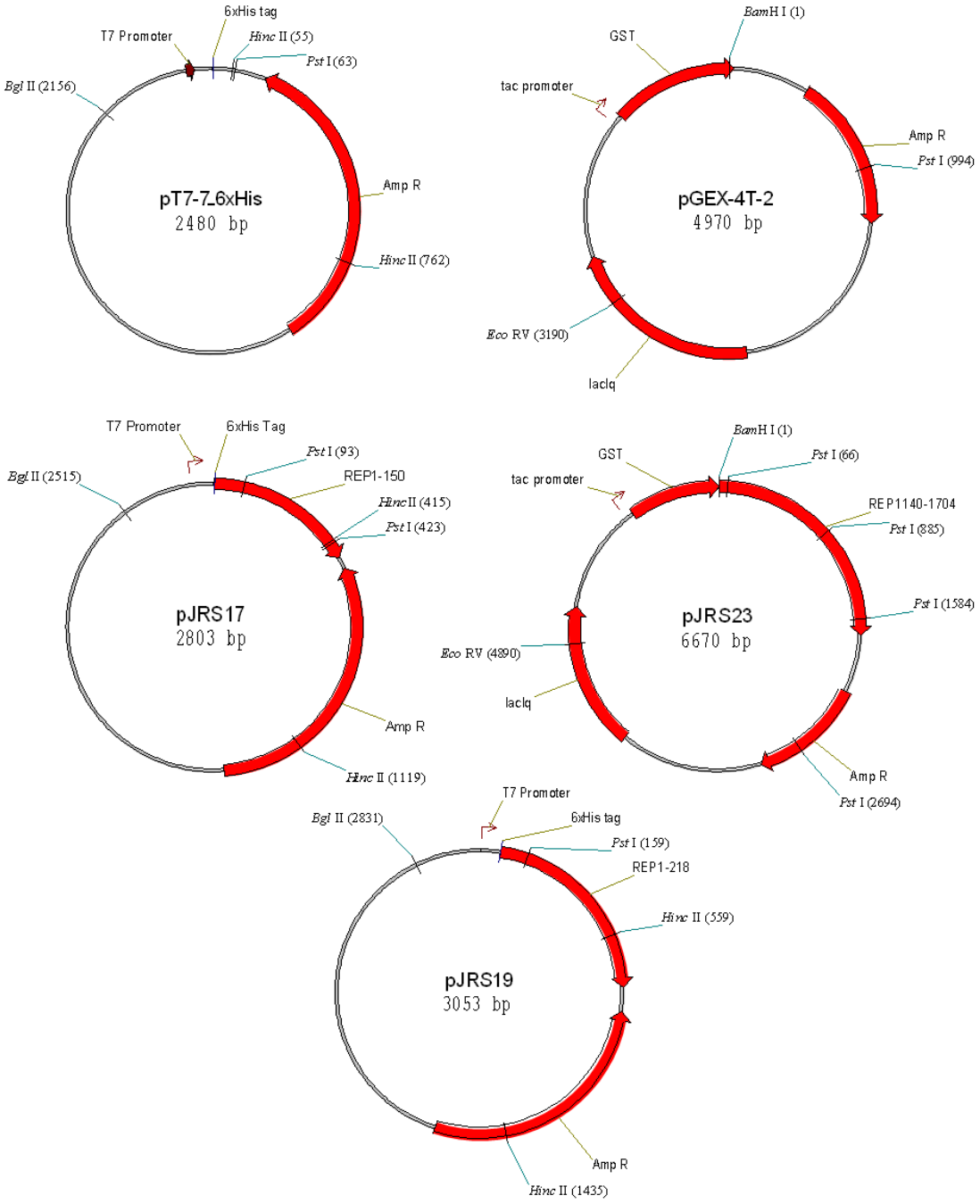

Figure 2.1: Restriction maps of the recombinant bacterial expression vectors used in the overproduction of HaSV replicase fragments in *E. coli* cells. Amp R: *β*-lactamase, GST: glutathione S-transferase, laclq: *lac* operon repressor protein, T7 Promoter: T7 bacteriophage RNA polymerase promoter, tac Promoter: hybrid bacterial promoter. The cloning strategy used to generate these plasmids can be found in Appendix A.

2.2.3. Overexpression of HaSV replicase fragments in *E. coli* BL21 (DE3) cells

Recombinant constructs pJRS17, pJRS19 or pJRS23 were transformed into competent *E. coli* BL21 (DE3) cells, with 1 ml of an overnight culture inoculated into 100 ml Luria-Bertani (LB) broth (containing 125 µg/ml ampicillin) and grown at 37 °C with shaking until the cultures reached an $OD_{600\ nm}$ of between 0.4 and 0.6. Protein expression was induced by adding isopropyl β-D-1-thiogalactopyranoside (IPTG) to a final concentration of 1 µM and cultures were then grown further until cultures had reached an $OD_{600\ nm}$ of between 0.8 and 1.0. Cells were harvested by centrifugation at 10 000 x *g* at 4 °C for 10 minutes and samples analysed by sodium dodecyl sulphate (SDS) polyacrylamide gel electrophoresis (SDS-PAGE) (Laemmli, 1970). SDS-PAGE was conducted using discontinuous glycine/polyacrylamide gels with 4 % stacking and 7.5 % or 15 % resolving gels for GST-$REP_{1140-1704}$ and the His-tagged replicase fragments (His-REP_{1-150} and His-REP_{1-218}) respectively. *E. coli* cell-free extracts were generated by centrifuging 1 ml of an overnight culture at 16 000 x *g* for 1 minute in a bench-top microfuge and resuspending the resulting pellet in 100 µl of 1 x sample buffer (10 % glycerol, 125 mM Tris-Cl pH 6.8, 4 % SDS, 10 % β-mercaptoethanol, 0.01 % bromophenol blue) per 1 $OD_{600\ nm}$ unit followed by boiling for 5 minutes.

2.2.4. Solubility of HaSV replicase fragments

Cells expressing HaSV replicase fragments were harvested as in Section 2.2.3 and resuspended in 2 ml lysis buffer (50 mM NaH_2PO_4 (pH 8.0), 300 mM NaCl, 10 mM imidazole) in the case of pJRS17 and pJRS19, or 2 ml phosphate buffered saline (PBS) (140 mM NaCl, 2.7 mM KCl, 10 mM Na_2PO_4, 1.8 mM KH_2PO_4, pH 7.4) for pJRS23, after which 20 µg lysozyme was added to each sample. Cells were incubated on ice for 30 minutes before being sonicated using a hand-held 3 mm probe (Vibra Cell™) at 40 % power for ten 10 second cycles. Soluble and insoluble fractions were

separated by centrifugation of sonicated extracts at 10 000 x *g* at 4 °C for 30 minutes. Proteins were resolved by SDS-PAGE and detected using coomassie staining.

2.2.5. Purification of recombinant replicase polypeptides and antiserum production

Gel-purification of HaSV replicase polypeptides

Insoluble replicase polypeptides were purified by gel-purification from SDS-polyacrylamide gels (Method provided by Dr. Sharon Braunagel, Department of Biochemistry and Biophysics, Texas A and M University, College Station, Texas, USA). Following SDS-PAGE using a 15 % polyacrylamide resolving gel, the resolving gel was incubated in 100 ml ice-cold 100 mM KCl for 5 minutes to visualise protein bands. The appropriate protein band (visible as an opaque white band) was then excised from the resolving gel and finely diced into small pieces before incubation at 4 °C in PBS (pH 7.4) overnight. The extracts were then passed through a glass wool plug placed at the bottom of a disposable 2 ml plastic syringe to remove the acrylamide gel and the eluted protein concentrated by ethanol precipitation by adding 1.6 x volume ice cold 95 % ethanol. Samples were incubated on ice for 1 hour with occasional inversion before centrifugation at 10 000 x *g* for 5 minutes at room temperature. Pellets were dried and then incubated in 100 µl PBS per gel on ice for 2.5 hours. Finally, the resuspended protein was resolved using SDS-PAGE and detected by coomassie staining.

Denaturing nickel-affinity purification of His-REP$_{1-218}$

Cells expressing His-REP$_{1-218}$ (pJRS19) were harvested as described in Section 2.2.3 before being resuspended in buffer B (8 M urea, 0.1 M NaH_2PO_4, 0.01 M Tris-Cl, pH 8). The 25 kDa 6xHis-tagged polypeptide was purified using the denaturing nickel-affinity protocol for Ni-NTA spin columns (Qiagen) according to the manufacturer's directions. The resulting fractions were analysed by SDS-PAGE using a 12 % resolving polyacrylamide gel.

Elution fractions were pooled, concentrated and exchanged into buffer B without urea by dialysis using Amicon Ultra-15 centrifugal filter units (10 kDa cut-off) (Millipore).

Expression and solubility of GST-REP$_{1140-1704}$

The expression of GST-REP$_{1140-1704}$ was induced in cells transformed with pJRS23 by the addition of 1 µM IPTG once the cells had reached an $OD_{600\ nm}$ of between 0.4 and 0.6. They were grown further with shaking at 37 °C and harvested in PBS (pH 7.4) as described in Section 2.2.3. Crude extracts were obtained by sonication of the cells on ice as described in Section 2.2.4. Soluble and insoluble fractions were obtained by centrifugation of the crude extracts at 10 000 x *g* for 30 minutes at 4 °C, analysed by SDS-PAGE and the proteins visualised using coomassie staining.

Production of rabbit polyclonal antiserum directed against His-REP$_{1-218}$

Approximately 1 mg of purified protein was used to raise a rabbit polyclonal antiserum against different regions of the HaSV replicase (produced by Prof. D. U. Bellstedt, Department of Biochemistry, University of Stellenbosch, Stellenbosch, South Africa). The specificity and optimal concentration of the antiserum generated against the His-REP$_{1-218}$ polypeptide were tested using crude extracts of *E. coli* BL21 (DE3) cells transformed with pT7-7_6xHis, pJRS17 or pJRS19 and/or mock- and HaSV-infected *H. armigera* larvae. *H. armigera* midgut cell-free extracts were produced by homogenising a single mock- or HaSV-infected larva in 1.5 ml centrifuge tubes using a glass rod in a small volume of PBS. The homogenate was then diluted with an equal volume of 2 x sample buffer and boiled for 5 minutes. Proteins in the cell-free extracts were resolved using 12 % or 15 % polyacrylamide resolving gels and transferred to Hybond™-C extra nitrocellulose membrane (GE Healthcare) using the Biorad® Mini Trans-blot electrophoretic transfer cell system as recommended by the manufacturer. Antibodies were diluted in Tris-buffered saline (150 mM NaCl, 50 mM Tris-Cl, pH 7.6) containing 0.1 % Tween-20 and 1 % BSA, fraction V (Roche Applied Biosciences) for western analyses.

2.3 RESULTS

Hydropathy plots (Kyte and Doolittle, 1982) were used to identify regions of the HaSV replicase with relatively high levels of predicted hydrophilicity (Figure 2.2). Two regions that might serve as antigens for antibody production were selected for expression in heterologous expression systems because they represented the regions with the highest probability of being soluble. The first region included the N-terminal 150 amino acids of the replicase (REP_{1-150}). As this fragment ended within the replicase MT domain, a second fragment including the entire MT domain (REP_{1-218}) was also selected. Secondly, the C-terminal 564 amino acids were chosen ($REP_{1140-1704}$) based on the high proportion of predicted hydrophilic regions (Figure 2.2).

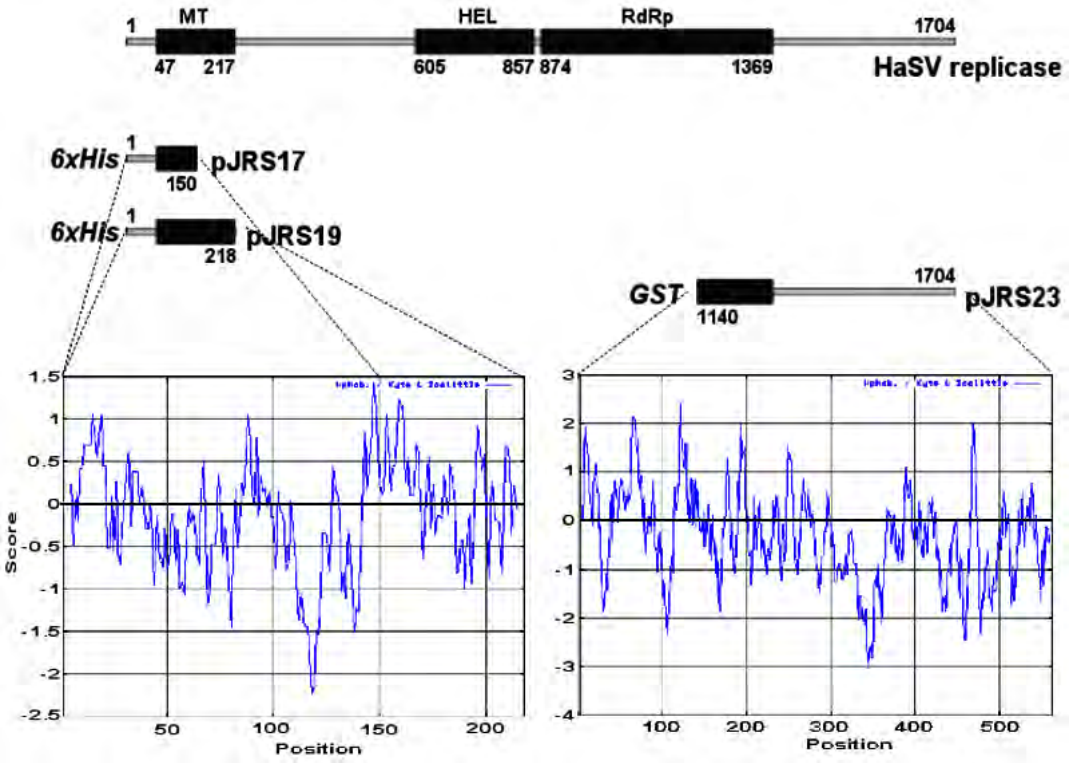

Figure 2.2: Schematic representation of the regions of the HaSV replicase selected for overexpression in bacterial cells and their corresponding hydropathy plots. The expression plasmids pJRS17, pJRS19 and pJRS23 encode His-REP_{1-150}, His-REP_{1-218} and GST-$REP_{1140-1704}$ respectively. The native replicase is shown with the methyltransferase (MT), helicase (HEL) and RNA-dependent RNA polymerase (RdRp) domains indicated by black boxes. Kyte and Doolittle hydropathy plots (Kyte and Doolittle, 1982) are shown below the N- and C-terminal fragments.

2.3.1. Expression and purification of replicase polypeptides His-REP$_{1-150}$ and His-REP$_{1-218}$

The first HaSV replicase fragment to be expressed in *E. coli* cells was His-REP$_{1-150}$. Crude extracts derived from *E. coli* cells transformed with pJRS17 and pT7-7_6xHis were compared using SDS-PAGE analysis, showing the expression of a polypeptide of approximately 17.5 kDa, corresponding to the predicted size of His-REP$_{1-150}$ (Figure 2.3, Panel A, Lanes 7 to 10), which was not present in cells transformed with the control vector plasmid, pT7-7_6xHis (Figure 2.3, Panel A, Lane 6). This 17.5 kDa polypeptide appeared to be largely insoluble since it was not detected in the supernatant fractions of solubility experiments but was only visible in pellet fractions following SDS-PAGE (Figure 2.3, Panel B, Lane 6 vs Lane 8). Attempts to gel-purify the polypeptide from the insoluble fraction using the acrylamide gel purification protocol (Section 2.2.5) were unsuccessful (data not shown). It was concluded that His-REP$_{1-150}$ was insoluble when expressed in *E. coli* cells and could not be solubilised for use in antiserum production.

Next the N-terminal replicase polypeptide was extended to include the entire MT domain. It was thought that the presence of the full MT sequence would aid in the proper folding of the polypeptide since this domain constitutes a functionally distinct portion of the full length HaSV replicase. Initial SDS-PAGE analysis of crude extracts of *E. coli* cells transformed with pJRS19 indicated that a protein of approximately 25 kDa was overexpressed in cells cultured in the presence of IPTG (Figure 2.4, Lane 4). This polypeptide was absent in cells transformed with pT7-7_6xHis (Figure 2.4, Lane 2). As was the case with His-REP$_{1-150}$, the 25 kDa polypeptide was largely insoluble, with the majority of the polypeptide being detected in pellet fractions while remaining undetectable in supernatant fractions of solubility experiments (Figure 2.4, Lane 5 vs Lane 6). However, in contrast His-REP$_{1-150}$, it was possible to gel-purify His-REP$_{1-218}$ (Figure 2.4, Lane 7).

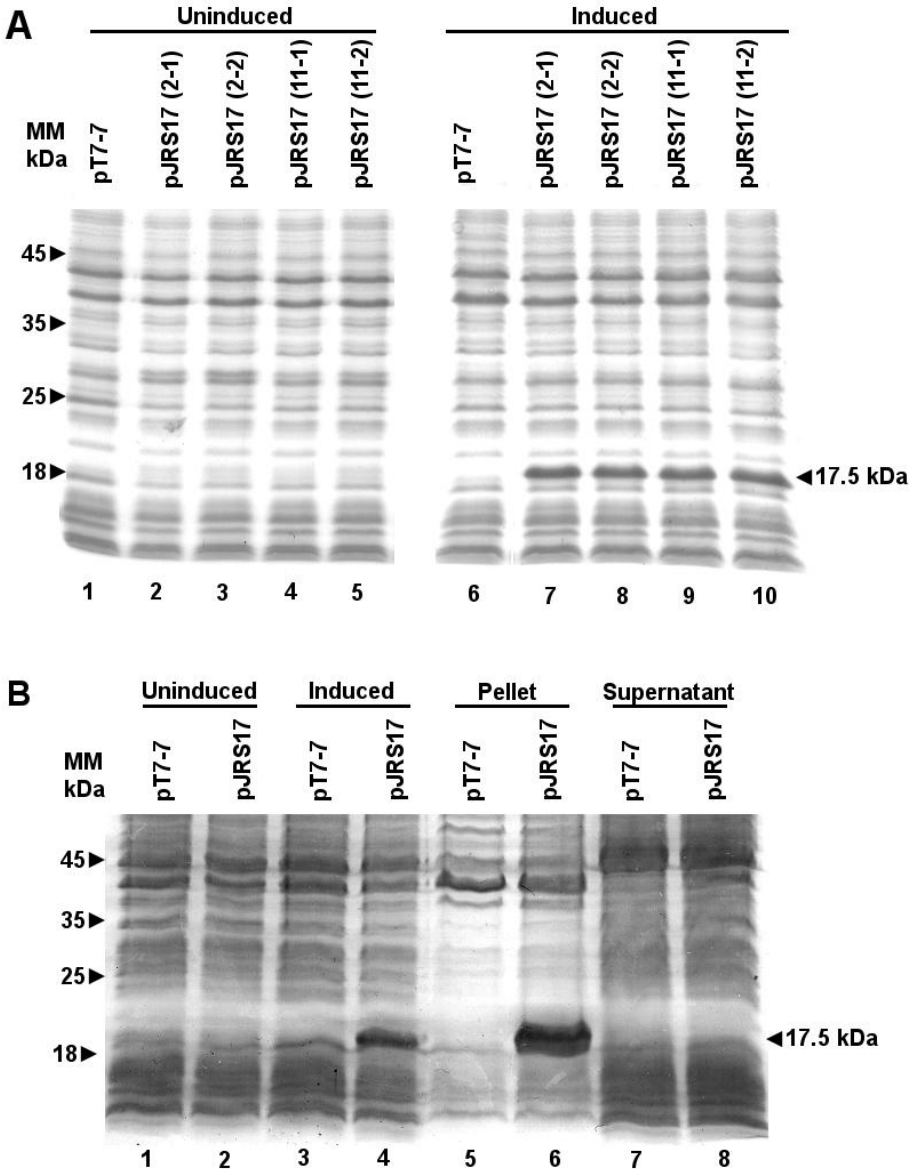

Figure 2.3: Overexpression and solubility of His-REP$_{1\text{-}150}$ in *E. coli* BL21 (DE3) cells. A: SDS-PAGE analysis of cell-free extracts of *E. coli* BL21 (DE3) cells transformed with pT7-7_6xHis or pJRS17 plasmid isolates showing uninduced cells (Lanes 1 to 5) or cells induced with IPTG (Lanes 6 to 10). B: SDS-PAGE analysis showing IPTG-induction and solubility of His-REP$_{1\text{-}150}$ expression. Crude extracts of uninduced (Lanes 1 and 2) and induced (Lanes 3 and 4) *E. coli* BL21 (DE3) cells transformed with pT7-7_6xHis or pJRS17 are shown. Pellet (Lanes 5 and 6) and supernatant (Lanes 7 and 8) fractions, representing insoluble and soluble protein fractions respectively, were derived from the IPTG-induced cells. Molecular mass standards are indicated in kDa on the left of each image and the arrows on the right indicate the recombinant 17.5 kDa His-REP$_{1\text{-}150}$ polypeptide.

Approximately 1.2 mg of His-REP$_{1\text{-}218}$ was purified, concentrated and dialysed for use in raising rabbit polyclonal anti-replicase antiserum designated anti-REP$_{1\text{-}128}$(a).

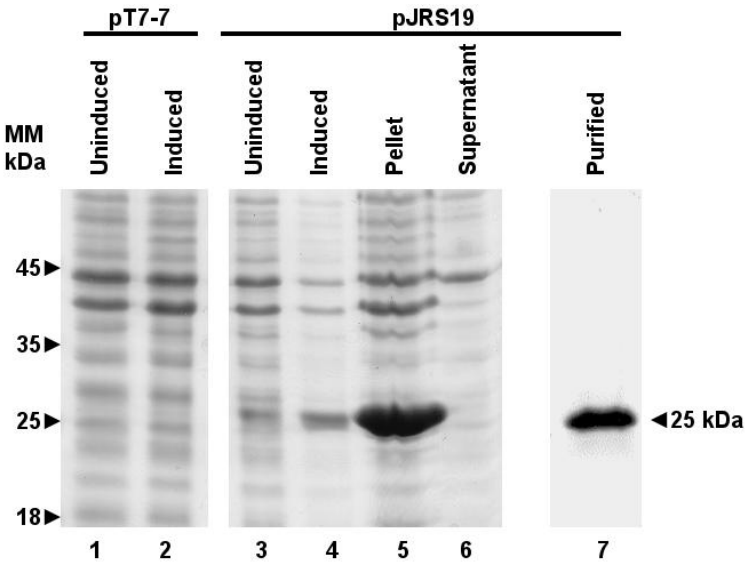

Figure 2.4: Overexpression, solubility and gel-purification of His-REP$_{1-218}$. SDS-PAGE analysis of crude extracts of *E. coli* cells transformed with pT7-7_6xHis and pJRS19 showing uninduced cells (Lanes 1 and 3) and cells induced with IPTG (Lanes 2 and 4). Pellet (Lane 5) and supernatant (Lane 6) fractions, representing insoluble and soluble protein fractions respectively, were derived from the induced cells transformed with pJRS19. His-REP$_{1-218}$ following gel-purification, concentration and dialysis is shown in lane 7. Molecular mass standards are indicated on the left in kDa and the 25 kDa His-REP$_{1-218}$ polypeptide is indicated on the right.

2.3.2. Validation of anti-REP$_{1-218}$(a) polyclonal antiserum

The suitability of the anti-REP$_{1-218}$(a) antiserum for western analysis was determined using varying amounts of *E. coli* cell-free extracts expressing N-terminal HaSV replicase fragments and homogenised HaSV-infected *H. armigera* larvae. The antiserum was able to detect His-REP$_{1-218}$ in crude protein extracts derived from *E. coli* cells transformed with pJRS19, even when these protein extracts were diluted 100-fold (Figure 2.5, Lanes 3 and 5). This band was not detected in crude extracts derived from cells transformed with the control vector plasmid, pT7-7_6xHis (Figure 2.5, Lane 1). Detection of His-REP$_{1-150}$ was far less sensitive. The 17.5 kDa protein was only weakly detected at a dilution of 1:10 (Figure 2.5, Lane 2). Longer exposure of the X-ray film resulted in the detection of a stronger signal that was also absent from cells transformed with pT7-7_6xHis (data

not shown). Non-specific proteins of approximately 60, 36 and 27 kDa were detected in all three *E. coli* extracts (Figure 2.5, Lanes 1 to 3). No HaSV-specific proteins were detected by this antiserum in crude extracts derived from infected *H. armigera* larvae (Figure 2.5, Lanes 8 and 9).

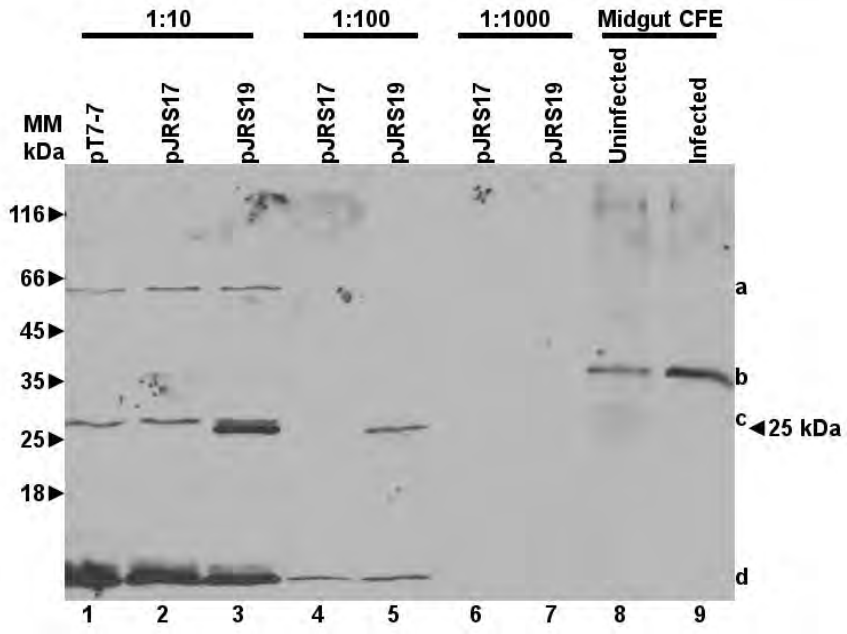

Figure 2.5: The affinity of anti-REP$_{1\text{-}128}$(a) antiserum tested against crude extracts of *E. coli* cells transformed with pT7-7_6xHis, pJRS17 and pJRS19. Western analysis of varying dilutions of cell free extracts of *E. coli* BL21 (DE3) cells transfected with pT7-7_6xHis (Lane 1), pJRS17 (Lanes 2, 4 and 6) or pJRS19 (Lanes 3, 5 and 7) as well as undiluted crude extracts derived from uninfected (Lane 8) and HaSV-infected (Lane 9) *H. armigera* larvae using anti-REP$_{1\text{-}218}$(a) antiserum at a dilution of 1:12 000. The ratios 1:10, 1:100 and 1:1000 represent 10-fold serial dilutions of the transformed *E. coli* cell free extracts. Molecular mass standards are indicated on the left in kDa. Asterisks ("*") represent distinct *E. coli* and *H. armigera* proteins detected by the REP$_{1\text{-}218}$(a) antiserum and are indicated on the right in addition to His-REP$_{1\text{-}218}$ (25 kDa) and His-REP$_{1\text{-}150}$ (17.5 kDa) polypeptides. His-REP$_{1\text{-}150}$ was only detectable as a faint band in lane 2.

2.3.3. Denaturing nickel affinity purification of His-REP$_{1\text{-}218}$

The poor specificity and low sensitivity of the anti-REP$_{1\text{-}218}$(a) antiserum meant that the antibodies would be unsuitable for use in western analysis and further biochemical analysis of the HaSV replicase. As a result, it was

decided to purify the REP_{1-218} polypeptide, which carries an N-terminal 6xHis tag, using nickel affinity chromatography to generate a polypeptide of higher purity, less likely to produce an antiserum that would cross react with *E. coli* proteins. Native nickel affinity purification was unsuccessful (data not shown), so His-REP_{1-218} was purified using a denaturing nickel affinity purification protocol. This proved to be more efficient than the gel purification and approximately 1.6 mg of His-REP_{1-218} was purified, with 1.3 mg being used to generate anti-REP_{1-218}(b) antiserum. SDS-PAGE analysis showed that His-REP_{1-218} was successfully purified using the Ni-NTA matrix (Figure 2.6, Lanes 9 to 11). Although the purified polypeptide (Figure 2.6, Lane 12) contained a small amount of contaminating *E. coli* protein detected between 40 and 50 kDa (also faintly visible in Figure 2.6, Lanes 9 to 11), it was used to raise rabbit polyclonal antibodies.

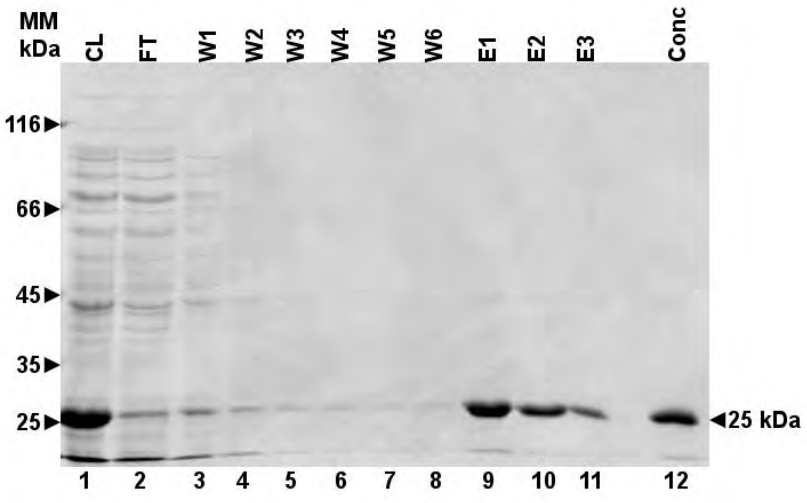

Figure 2.6: Denaturing nickel affinity purification of His-REP_{1-218}. SDS-PAGE analysis of fractions collected during the nickel affinity purification of His-REP_{1-218} from *E. coli* BL21 (DE3) cells transformed with pJRS19 under denaturing conditions. The cleared lysate ("CL", Lane 1), flow-through ("FT", Lane 2), wash (Lanes 3 to 8), elution (Lanes 9 to 11) and final, purified, dialysed and concentrated ("Conc", Lane 12) fractions are shown. Molecular mass standards are indicated on the left of the gel in kDa and the arrowhead on the right indicates the 25 kDa His-REP_{1-218}.

2.3.4. Validation of rabbit anti-REP$_{1-218}$(b) polyclonal antiserum

The specificity and sensitivity of the antiserum raised against His-REP$_{1-218}$ was tested using various dilutions of *E. coli* cells transformed with pJRS19 and purified His-REP$_{1-218}$. In contrast to the antiserum raised against gel-purified antigen, the anti-REP$_{1-218}$(b) antiserum (raised against affinity-purified REP$_{1-218}$) appeared to be both more sensitive and more selective for the detection of His-REP$_{1-218}$. The 25 kDa recombinant polypeptide was detected in cells transformed with pJRS19 and not in cells transformed with pT7-7_6xHis (Figure 2.7, Lane 2 vs Lane 1). A number of cross-reacting proteins were detected in the undiluted *E. coli* extracts (Figure 2.7, Lanes 1 and 2) but were only weakly detected at a dilution of 1:10 (Figure 2.7, Lane 3). Purified His-REP$_{1-218}$ was detectable at below 50 ng (Figure 2.7, Lane 6).

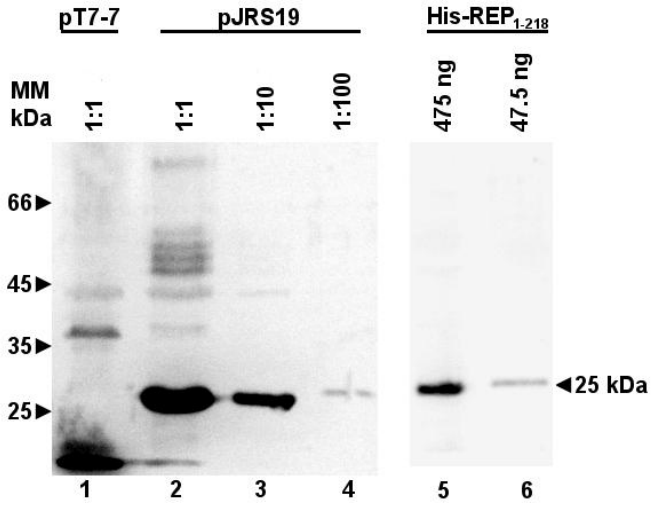

Figure 2.7: The affinity of anti-REP$_{1-218}$(b) antiserum tested using *E. coli* crude extracts and purified His-REP$_{1-218}$. Western analysis of varying dilutions of cell free extracts of cells transformed with pT7-7_6xHis (Lane 1) and pJRS19 (Lanes 2 to 4) purified His-REP$_{1-218}$ (Lanes 5 and 6) using anti-REP$_{1-218}$(b) antiserum at a dilution of 1:15 000. The ratios 1:1, 1:10 and 1:100 represent 10-fold serial dilutions of the *E. coli* crude extracts and the mass of purified His-REP$_{1-218}$ loaded is indicated in lanes 5 and 6. Molecular mass standards are indicated on the left of each blot in kDa and His-REP$_{1-218}$ (25 kDa) is indicated on the right of the blot.

2.3.5. Expression and purification of GST-REP$_{1140-1704}$

In order to generate an antiserum directed against the C-terminus of the replicase for use in co-immunoprecipitation experiments, it was decided to use the second hydrophilic replicase fragment (amino acid residues 1120 to 1704) with a GST tag that might facilitate solubility of the fusion protein. The expression of GST-REP$_{1140-1704}$ in *E. coli* cells transformed with pJRS23 resulted in the overproduction of a protein with an estimated molecular mass of 87 kDa upon induction of expression with IPTG that was absent in uninduced cells (Figure 2.8, Lane 1 vs Lane 2). However, the fusion protein was not soluble, consistently appearing in the pellet fraction during solubility experiments (Figure 2.8, Lane 3 vs Lane 4). Attempts to increase the solubility of GST-REP$_{1140-1704}$ using detergents such as Triton X-100 and *N*-lauroylsarcosine were unsuccessful (data not shown), precluding the use of the fusion polypeptide for antibody production.

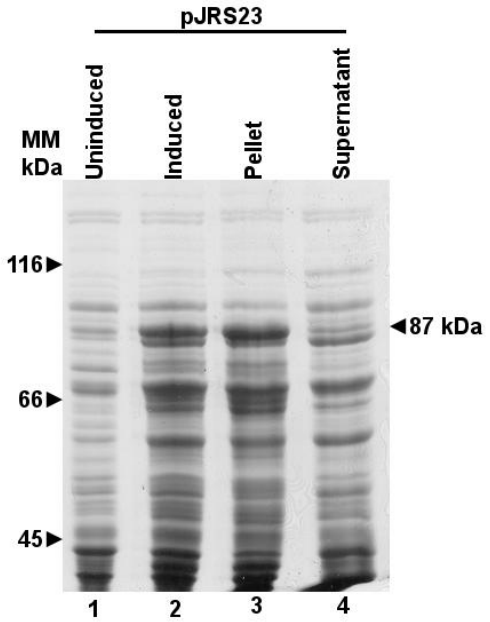

Figure 2.8: Overexpression and solubility of GST-REP$_{1140-1704}$ expressed in *E. coli* cells. SDS-PAGE analysis of cell free extracts of *E. coli* BL21 (DE3) cells transformed with pJRS23 showing uninduced cells (Lane 1) and cells induced with IPTG (Lane 2). Pellet (Lane 3) and supernatant (Lane 4) fractions were obtained from IPTG-induced cells expressing GST-REP$_{1140-1704}$. Molecular mass standards are indicated on the left in kDa and the arrowhead on the right indicates the 87 kDa GST-REP$_{1140-1704}$.

2.4 DISCUSSION

The absence of suitable antibodies for the detection of the HaSV replicase by western analysis and immunofluorescence microscopy has prevented the biochemical characterisation and *in vivo* detection of the viral replicase. During the course of this study, four attempts were made to express HaSV replicase fragments in *E. coli* cells using three different polypeptides identified as REP_{1-150}, REP_{1-218} and $REP_{1140-1704}$. Ultimately two anti-replicase antisera were produced, both of which were raised against 6xHis tagged polypeptide consisting of the N-terminal 218 amino acids (His-REP_{1-218}), including the entire MT domain of the replicase. Validation of the antibodies raised against His-REP_{1-218} showed that both anti-REP_{1-218}(a) and anti-REP_{1--218}(b) were able to detect similar amounts of *E. coli*-expressed polypeptide fragments, but that the anti-REP_{1-218}(b) antiserum was somewhat more sensitive and selective. Although the full-length wild-type HaSV replicase was not detected, the anti-REP_{1-218}(b) antiserum might be suitable for the detection of the HaSV replicase by western blot, provided that sufficient replicase could be produced.

CHAPTER 3

SUBCELLULAR LOCALISATION OF THE HaSV REPLICASE IN MAMMALIAN AND INSECT TISSUE CULTURE CELLS

3.1 INTRODUCTION

Replication complexes of (+ve) RNA viruses have thus far all been found to associate with host-derived membranes. The specific site of virus replication is often determined as a result of the trafficking of the viral replicase, a process that is usually sufficient for the generation of vRNA replication factories. Localisation of the viral replicase, and the concurrent formation of replication complexes, typically results in the modification of host-derived membranes in order to concentrate viral and host factors into a localised replication site and to avoid host defence mechanisms (Jonczyk *et al.*, 2007; Netherton *et al.*, 2007).

The subcellular location of vRNA replication is important since there is often a coupling of the location of the viral replicase and other stages in the viral life cycle. One such example is that of the alphaviruses, which make use of the mildly acidic environment of the early endosomes during virus entry and uncoating before targeting vRNA replication to endocytic and lysosomal membranes (Schlesinger and Schlesinger, 2001). The location of viral replication within host cells may play additional roles in virus replication beyond multiplication of vRNA. Thus, identifying the location of the HaSV replicase in cells represents the first step towards understanding the most fundamental aspects of tetravirus replication biology and may shed light on other aspects of the virus life cycle.

At present, very little is known about the cellular location of tetravirus replication, largely due to the absence of experimental systems for the study

of their replication biology. Other than PrV, none of the tetraviruses have been found to replicate in tissue culture cell lines and no replication-competent *ex vivo* experimental system for HaSV exists (Bawden *et al.*, 1999; Pringle *et al.*, 2003). This study of HaSV replication *in vivo* was hampered by both the absence of suitable antiserum directed against the HaSV replicase and a lack of antibodies against insect cellular markers. As a result a novel experimental system for the study of HaSV replication biology needed to be developed.

This chapter describes the use of fluorescence microscopy to examine the subcellular localisation of HaSV replicase fused to EGFP (REP_{1-1704}-EGFP) in mammalian (HeLa) and *Spodoptera frugiperda* pupal ovarian (Sf9) cells. The distribution of EGFP fluorescence was compared to that of known organelle markers in mammalian cells and live cell imaging techniques were used to characterise the dynamics of replicase-associated structures. Selected data presented here has been published (Short *et al.*, 2010) and are reproduced with permission from the publisher.

3.2 MATERIALS AND METHODS

Unless otherwise stated, tissue culture cell lines were maintained as described in Appendix C.

3.2.1. Recombinant plasmids used for expression of replicase-EGFP fusion proteins

Restriction maps of recombinant plasmids used in the experiments described in this chapter are shown in Figure 3.1 and their construction outlined in Appendix A. The mammalian expression construct pJRS7 (Appendix A.4) contains a full length copy of the HaSV replicase CDS, with a mutated stop codon cloned into the *Bam*HI site of pEGFP-N1, such that the replicase ORF

Figure 3.1: Plasmid maps of the recombinant expression vectors used in the expression of HaSV replicase-EGFP fusion proteins in tissue culture cells. Amp R: *β*-lactamase, CMV Promoter: Human cytomegalovirus immediate early promoter, EGFP: enhanced green fluorescent protein, hr/AcMNPV Promoter: hybrid insect promoter, Kan/Neo R: neomycin phosphotransferase. The cloning strategy used to generate these plasmids can be found in Appendix A.

is fused at its C-terminal end with the N-terminus of EGFP (REP_{1-1704}-EGFP). Expression of REP_{1-1704}-EGFP is controlled by a human cytomegalovirus (CMV) immediate early promoter. The plasmid pJRS8 (Appendix A.5) carries the full length replicase ORF fused at its N-terminus to the C-terminus of EGFP (EGFP-REP_{1-1704}) expressed from the same CMV promoter. Finally, pJRS26 (Appendix A.6) encodes the same REP_{1-1704}-EGFP CDS as pJRS7, under the control of a hybrid hr/AcMNPV promoter consisting of the *Autographa californica* multiple nuclearpolyhedrovirus (AcMNPV) hr5 enhancer fused to the AcMNPV immediate early promoter (obtained from Prof. Vernon Ward, University of Otago, New Zealand).

3.2.2. Transfection of tissue culture cells

Monolayers of HeLa cells were transfected in 24 well plates on 13 mm glass cover slips for immunofluorescence, or in glass bottomed 35 mm Petri dishes (Asahi Techno Glass Corporation) for live cell imaging using Fugene® HD (Roche) according to an optimised protocol based on the manufacturer's instructions. Cells were seeded to approximately 60 % confluence and incubated in complete Dulbecco's modified Eagle medium (DMEM) overnight before transfection. Monolayers were transfected at about 80 % confluence as follows (quantities indicated are those for a single well in a 24 well plate, this to be multiplied by a factor of five for 35 mm Petri dishes). For small plasmids (such as the 4.7 kilobase (kb) pEGFP-N1 control plasmid, lacking the HaSV replicase sequence), 100 ng of plasmid DNA (purified using QIAprep Spin Miniprep Kit (Qiagen)) was added to 19 µl serum-free DMEM followed by 0.5 µl of Fugene® HD transfection reagent to produce the Fugene:DNA complex. For larger plasmids (such as the 9.8 kb pJRS7 containing the full length HaSV replicase CDS), 300 ng of DNA and 3 µl Fugene® HD were diluted to a total of 20 µl with serum-free DMEM as above. The Fugene:DNA complex was briefly mixed and complex formation was allowed to proceed at room temperature for 30 minutes. The medium was

aspirated from each well and the complex added directly to cells in a drop-wise manner, before the addition of a further 80 µl of serum free DMEM. Cells were incubated as normal for three hours followed by the addition of 900 µl complete DMEM. Thereafter the cells were incubated at 37 °C with 10 % CO_2 for between 16 and 24 hours depending on the experiment. Sf9 cells were transfected as for HeLa cells with the exception that cells were initially seeded at approximately 70 % and transfected at 85 % confluence.

3.2.3. Immunofluorescence staining of HeLa cells

Following transfection, cells intended for immunofluorescence staining were briefly rinsed three times in PBS (pH 7.5) before being fixed with 4 % paraformaldehyde in PBS for 15 minutes. Cells were again rinsed twice in PBS and then subjected to immunofluorescence microscopy according to one of the following protocols depending on the primary antibody used.

Triton X-100-based permeabilisation protocol

Immunofluorescence detection of the ER and Golgi apparatus (method provided by Dr. Caroline Knox, Department of Biochemistry, Microbiology and Biotechnology, Rhodes University, Grahamstown, South Africa) was done using polyclonal rabbit antibodies directed against ERp60 and β-COP (both obtained from Prof. Tom Wileman, University of East Anglia, Norwich, UK) as follows. After fixing, cells were incubated in 400 µl permeablisation buffer (5 % normal goat serum, 1 % Triton X-100, 10 % sucrose in PBS, pH 7.5) for 20 minutes with gentle shaking. Primary antibody was then added to cells at a dilution of 1:400 for β-COP or 1:8 000 for ERp60 in permeabilisation buffer with gentle shaking for one hour. Cells were then briefly rinsed three times in PBS-Tween (1 % Tween 20 in PBS, pH 7.5) before the addition of secondary antibody (Alexa Fluor 546-conjugated goat anti-rabbit, Invitrogen) diluted 1:500 in permeablisation buffer. Following a 30 minute incubation, cells were briefly rinsed three times in PBS-Tween followed by three 10 minute washes,

also in PBS-Tween. DAPI (4',6-diamidino-2-phenylindole) (500 µg.ml^{-1}) was added to the second wash to visualise nuclei. Coverslips were mounted on glass slides using Fluorescent Mounting Medium (DakoCytomation).

Saponin-based permeabilisation protocol

Immunofluorescence detection of the early and late endosomes (method provided by Dr. Kristine Schauer, Molecular Mechanisms of Intracellular Transport group, Institut Curie, Paris, France) was done using goat anti-EEA1 (Santa Cruz Biotechnology, Inc., sc-6415) and mouse anti-CD63 (Invitrogen, 187300) antibodies as follows. After fixing, cells were quenched for 10 minutes in 50 mM NH_4Cl in PBS (pH 7.5) before being permeabilised in saponin buffer (0.2 % BSA, 0.05 % saponin in PBS, pH 7.5) for 15 minutes. Coverslips were then inverted into 25 µl droplets of saponin buffer containing primary antibodies (anti-EEA1 (1:200) or anti-CD63 (1:35)) on parafilm. After 30 minutes cells were briefly rinsed three times in saponin buffer before being incubated in 400 µl saponin buffer containing a 1:500 dilution of secondary antibody (Alexa Fluor 546-conjugated donkey anti-goat or Alexa Fluor 546-conjugated goat anti-mouse, both from Invitrogen) for 30 minutes in the 24 well plate. Cells were then rinsed and mounted as for Triton X-100-permeabilised cells.

3.2.4. Organelle specific staining of live HeLa and Sf9 cells

Both HeLa and Sf9 cells were grown and transfected (Section 3.2.2) in glass bottomed 35 mm Petri dishes (Asahi Techno Glass Corporation). Cells were incubated in the presence of 200 nM MitoTracker® Red 580, 50 nM LysoTracker® Red DND-99 or 100 nM ER-Tracker™ Blue-White DPX (Invitrogen) for 30 minutes prior to imaging according to an optimised protocol derived from the manufacturer's instructions. Both LysoTracker® and MitoTracker® have been used in previous studies to visualise lysosomes (Kawar and Jarvis, 2001, Kawar *et al.,* 2001, Aumiller *et al.*, 2006) and

mitochondria (Chow *et al.*, 2009) in Sf9 cells and, as a result, both were used to stain Sf9 cells. However, ER-Tracker™ does not stain the ER in insect cells and could therefore not be used in Sf9 cells. Cascade Blue®-conjugated dextran (10,000 Da) (Invitrogen) was added to complete growth medium at the time of transfection in order to allow for maximal loading of the endocytic pathway prior to imaging. Cells were incubated for up to 24 hours according to manufacturer's instructions before being rinsed and incubated in complete growth medium prior to imaging (mammalian cells were incubated in complete DMEM without phenol red for live cell imaging).

3.2.5. Confocal laser scanning microscopy, image analysis and image editing

All images were obtained using a Zeiss LSM 510-META confocal microscope with a live cell imaging facility. Unless otherwise indicated all images represent 0.8 µm thick optical slices that were scanned at optimal x,y resolution, as determined by the proprietary Zeiss Scanning Microscope LSM 510 software (release version 4.2), using 63x oil immersion objective lenses. Sequential time-lapse images of live cells (t-stacks) each represent 1 µm optical slices. Blue diode (405 nm), argon (488 nm) and helium/neon (543 nm) laser lines were used to image the respective fluorophores using standard filter sets with laser attenuation modified for each sample to obtain maxium light intensity resolution. Images were viewed and/or analysed using the Zeiss LSM 5 Image Browser (v 4.2.0), ZEN 2008 Light Edition (both Carl Zeiss), ImageJ 1.42o (http://rsb.info.nih.gov/ij/) or GIMP 2.6.6 (www.gimp.org). Time-lapse imaging was performed on cells from 16 hours after transfection for 6 to 8 hours and the image series analysed using ImageJ 1.42o and a manual particle tracking plug-in (Sbalzarini and Koumoutsakos, 2005) for the analysis of particle movements.

3.3 RESULTS

3.3.1. Subcellular distribution of HaSV replicase-EGFP fusion proteins in fixed and live tissue culture cells

The transfection protocols for HeLa and Sf9 cells were optimised using control plasmids expressing EGFP (pEGFP-N1 or pCW56 in HeLa and Sf9 cells respectively) and experimental plasmids expressing REP_{1-1704}-EGFP (pJRS7 and pJRS26 in HeLa and Sf9 cells respectively) (Figure 3.1). Using the optimised protocol, transfection frequencies of 8 % (for pJRS7) and between 40 % and 50 % (for pEGFP-N1, pCW56 and pJRS26) were reproducibly achieved as evidenced by EGFP fluorescence.

Plasmids expressing REP_{1-1704}-EGFP (pJRS7 or pJRS26), EGFP-REP_{1-1704} (pJRS8) and EGFP (pEGFP-N1 or pCW56) were transfected into HeLa and Sf9 cells and the subcellular distribution of the proteins determined by fluorescence microscopy. Native EGFP fluorescence was observed throughout the cytoplasm of transfected cells with some accumulation of fluorescence in the nucleus (Figure 3.2, Panel B, Images a and e). EGFP-REP_{1-1704}-associated fluorescence was also present throughout the cytoplasm of transfected cells but, in contrast to native EGFP the fusion protein was excluded from the nucleus (Figure 3.2, Panel B, Image d) either due to its large size or because the replicase carries a nuclear export signal. Fluorescence associated with REP_{1-1704}-EGFP was concentrated in small cytoplasmic structures in both cell lines (Figure 3.2, Panel B, Images b and f). The same punctate distribution was also observed in live cells eliminating the possibility that the punctate structures were experimental artefacts produced by the fixation process (Figure 3.2, Panel B, Images c and g). The difference in distribution between REP_{1-1704}-EGFP and EGFP-REP_{1-1704} suggested that the N-terminus of the replicase may be important in targeting of the protein to the punctate structures. Although the size, shape and location of the

punctate structures do not share definitive characteristics with any major cellular organelles, the structures were clearly excluded from the nucleus. The characteristic perinuclear distributions associated with the ER and Golgi apparatus were not observed. The mitochondria typically form reticular structures that are spread throughout the cytoplasm of cells and could have accounted for the structures observed, as could the organelles of either the endocytic or secretory pathways. Another possibility was that the morphology could be caused by the modification of host organelles.

3.3.2. Subcellular localisation of REP_{1-1704}-EGFP by immunofluorescence

Following the observation that the full length HaSV replicase fused to the N-terminus of EGFP was located in small punctate structures within the cytosol of both Sf9 and HeLa cells, further investigation into the origin of those structures was necessary. Firstly, REP_{1-1704}-EGFP-associated fluorescence in HeLa cells was compared with that of marker proteins for the major organelles by immunofluorescence microscopy. The paucity of appropriate antibodies directed against marker proteins in insect cells precluded similar immunofluorescence studies in the Sf9 cells. In HeLa cells, the punctate structures were examined in relation to the peripheral Golgi, ER, early endosomes and late endosomes. HeLa cells transfected with pJRS7 (REP_{1-1704}-EGFP) were incubated for 16 to 24 hours before being fixed and stained with antibodies directed against *β*-COP (Golgi), ERp60 (ER), EEA1 (early endosomes) or CD63 (late endosomes) respectively. Cells were then examined by confocal fluorescence microscopy to determine the extent of co-localisation.

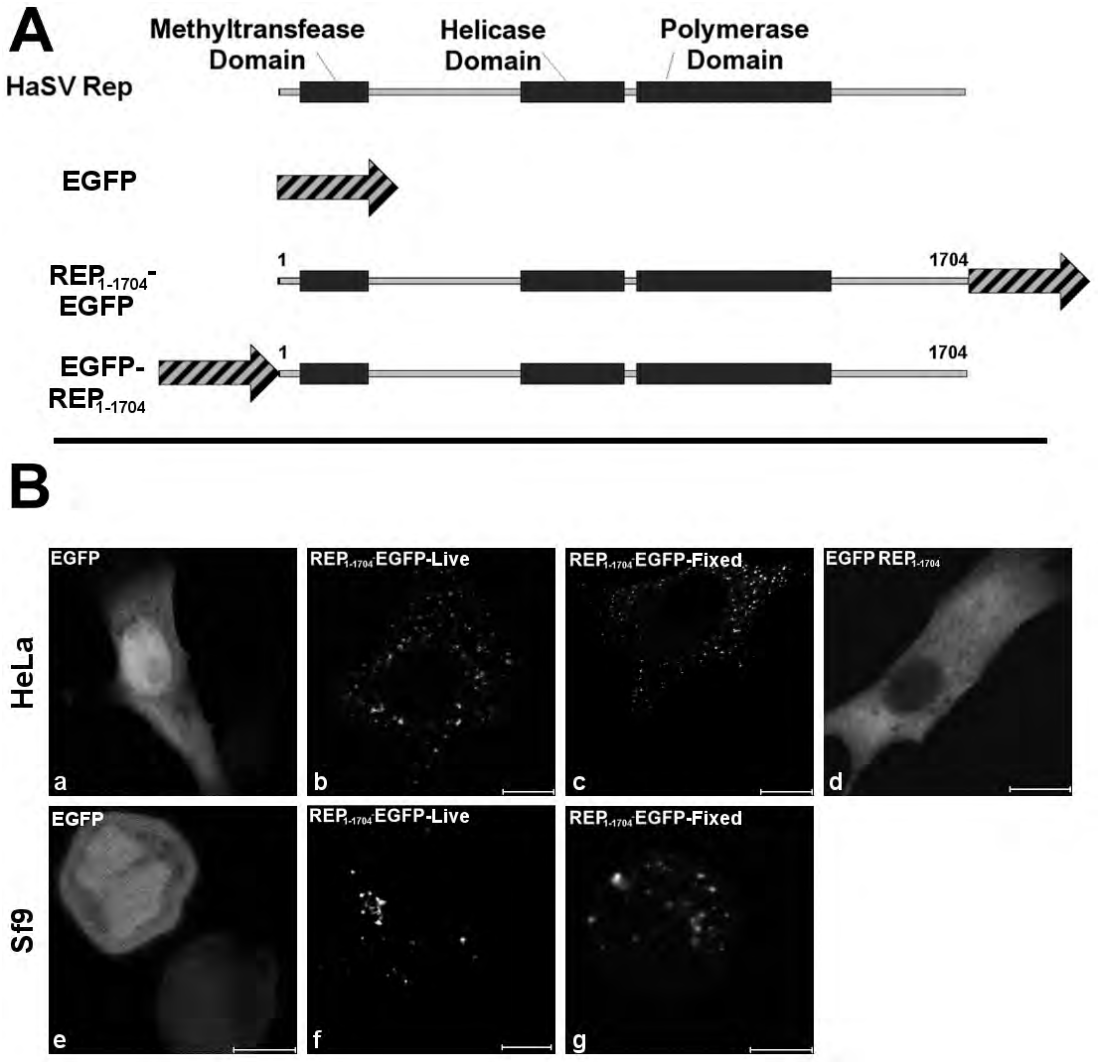

Figure 3.2: The distribution of EGFP and full-length HaSV replicase-EGFP fusion proteins in fixed and live HeLa and Sf9 cells. Panel A shows schematic representations of EGFP and N- or C-terminal fusions of EGFP to the HaSV replicase and Panel B contains images of the typical distribution of EGFP fluorescence observed in cells expressing each protein. Fixed cells expressing EGFP (a and e), REP_{1-1704}-EGFP (c and g) or EGFP-REP_{1-1704} (d) as well as live cells expressing REP_{1-1704}-EGFP (b and f) were imaged using confocal fluorescence microscopy. Scale bars represent 10 µm.

As expected, staining of HeLa cells with *β*-COP produced the distinctive perinuclear staining pattern of the peripheral Golgi, with the majority of the signal being detected in a defined location to one side of the nucleus (Figure 3.3, Image a). ERp60-associated signal was observed in a typical reticular pattern throughout the cytosol with characteristic fluorescence visualisation of the nuclear envelope (Figure 3.3, Image d). Both EEA1

(Figure 3.3, Image g) and CD63 (Figure 3.3, Images j and m) were observed in punctate structures distributed throughout the cytosol. Importantly, no significant differences in morphology or distribution of any of these organelles was observed in cells transfected with pJRS7 as compared with untransfected cells, indicating that substantial remodelling of these membranes by the replicase-EGFP fusion protein was unlikely.

Comparison of the distribution of the Golgi- and ER-specific marker proteins with the EGFP fluorescence associated with REP_{1-1704}-EGFP revealed a marked difference in the distribution of the two signals indicating that neither the Golgi apparatus nor the ER were the site of REP_{1-1704}-EGFP localisation (Figure 3.3, Images a to c and d to f respectively). There was significant similarity between the subcellular distribution patterns of REP_{1-1704}-EGFP and both CD63 and EEA1 suggesting that endocytic organelles might be candidate sites to which the HaSV replicase is targeted in HeLa cells. Initial experiments involving both marker proteins with cells fixed 20 to 24 hours after transfection showed no overlap between EGFP fluorescence and the markers of either organelle (Figure 3.3, Images g to i and m to o). However, when cells were fixed and stained 16 hours post-transfection, some overlap was observed with the late endosomes (Figure 3.3, Images j to l). There was approximately 20 % overlap between the REP_{1-1704}-EGFP-derived punctate structures and late endosomes defined by the CD63 marker in 10 % of the transfected cells imaged on each cover slip. These data suggested that the HaSV replicase may be associated with the late endosomes during the early stages of subcellular localisation in HeLa cells. The lack of complete overlap could indicate that REP_{1-1704}-EGFP is later moved to a different cellular location or that accumulation of the protein results in late endosome modification to the extent that CD63, and probably other host proteins, are no longer present. Alternatively, the replicase-EGFP fusion protein could be present in cytosolic aggregates, though the cytosolic distribution of EGFP-REP_{1-1704} suggests that this is less likely.

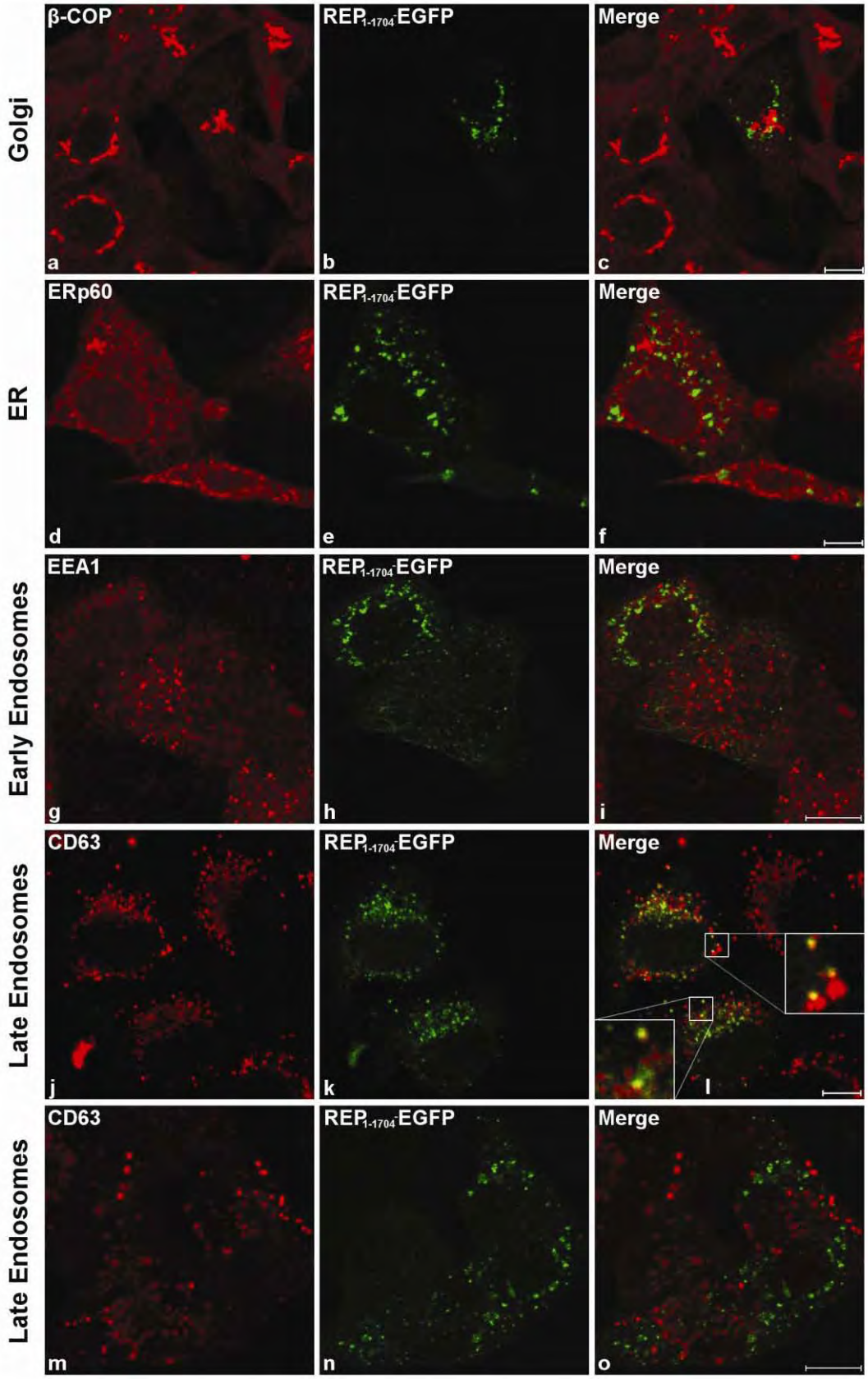
Golgi
β-COP
REP1-1704-EGFP
Merge
a
b
c
ER
ERp60
REP1-1704-EGFP
Merge
d
e
f
Early Endosomes
EEA1
REP1-1704-EGFP
Merge
g
h
i
Late Endosomes
CD63
REP1-1704-EGFP
Merge
j
k
l
Late Endosomes
CD63
REP1-1704-EGFP
Merge
m
n
o

Figure 3.3 (page 64): Comparison of the distribution of REP_{1-1704}-EGFP with that of cellular organelles in HeLa cells by confocal immunoflourecence microscopy. HeLa cells expressing REP_{1-1704}-EGFP were stained with antiserum against the specific organelle marker proteins β-COP (Golgi) (a – c), ERp60 (ER) (d – f), EEA1 (early endosomes) (g – i) and CD63 (late endosomes) after 16 (j – l) or 24 (m – o) hours. Primary antibodies were detected using species specific secondary antibodies conjugated to Alexa Fluor 546. Areas of partial overlap (l) are magnified approximately 3-fold. Scale bars represent 10 µm.

3.3.3. Subcellular localisation of REP_{1-1704}-EGFP in live cells

Tomasicchio *et al.* (2007) hypothesised that the destabilisation of acidic subcellular organelles (lysosomes or mitochondria) and subsequent acidification of the cytoplasm may be involved in the tetravirus lifecycle. The results of co-localisation experiments in this study suggested that the endocytic compartment might be the site for targeting of the viral replicase. To further investigate the role of acidic organelles in the localisation of the HaSV replicase, live HeLa and Sf9 cells expressing REP_{1-1704}-EGFP were stained with commercially available stains which label the lumens of lysosomes, mitochondria and fluid-phase endocytic organelles. Cells were also stained with ER-Tracker™, which specifically labels the ER membranes of mammalian cells, to further exclude the organelles of the secretory pathway.

Validation of the staining protocols showed that the mitochondrion-specific MitoTracker® Red 580 displayed a typical mitochondrial staining pattern in both HeLa and Sf9 cells (Figure 3.4, Panel A, Left Column). Similarly, LysoTracker® Red DND-99 produced the normal punctate cytosolic distribution, comparable to that of the late endosomal marker protein CD63, in both cell types (Figure 3.4, Panel B, Left Column). The incubation of cells in the presence of Cascade Blue®-conjugated dextran (10 000 Da) also resulted in punctate cytosolic structures associated with the dextran (Figure 3.4, Panel C, Left Column. While the use of these stains in insect cells had previously been described (Entchev *et al.*, 2000; Kawar and Jarvis,

2001; Kawar *et al.,* 2001; Kurisu *et al.*, 2003; Aumiller *et al.*, 2006; Sasamura *et al.*, 2007; Chow *et al.*, 2009), ER-Tracker™ Blue-White DPX concentrates in the ER of mammalian cells via a lipid-based transport mechanism that does not have the same effect in insect cells, preventing the use of ER-Tracker™ in Sf9 cells. HeLa cells stained with ER-Tracker™ did however result in the visualisation of the nuclear envelope along with a reticular morphology in the cytoplasm of HeLa cells, as expected (Figure 3.4, Panel D, Left Column). As was the case for cells subjected to immunofluorescence, no significant differences were observed between transfected and untransfected cells, supporting the suggestion that REP_{1-1704}-EGFP does not cause significant remodelling of the organelles tested.

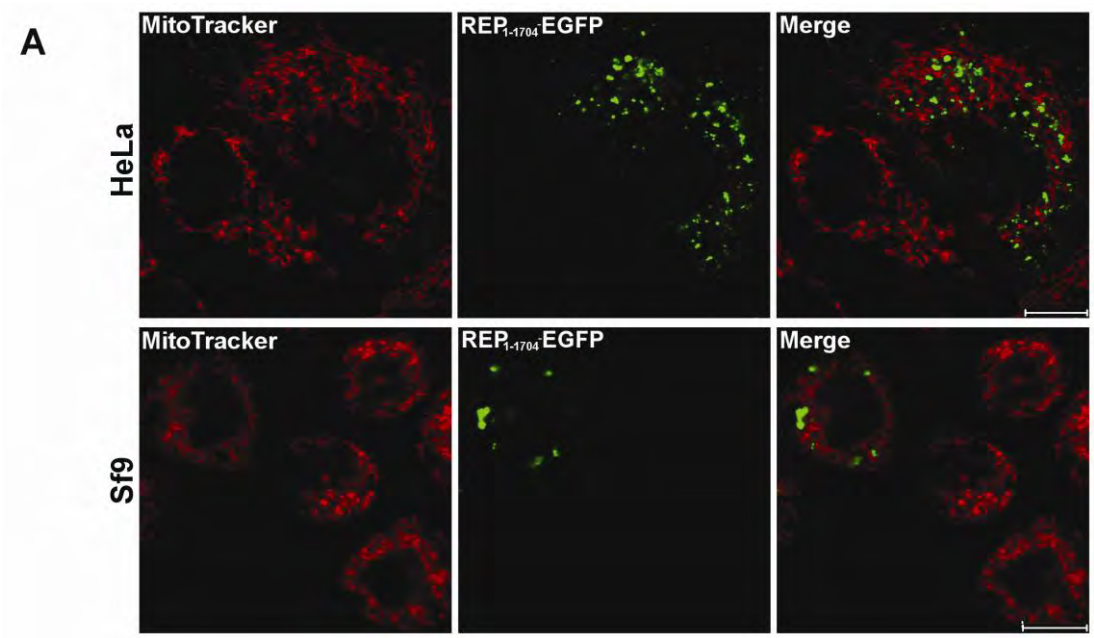

Figure 3.4 (Here and page 67): Comparison of the distribution of REP_{1-1704}-EGFP with that of organelle-specific stains in live HeLa and Sf9 cells by confocal fluorescence microscopy. Cells expressing REP_{1-1704}-EGFP were stained with MitoTracker® Red 580 (mitochondria) (Panel A), Lysotracker® Red DND-99 (lysosomes) (Panel B), Cascade Blue-conjugated dextran (classical endocytic pathway) (Panel C) or ET-Tracker™ Blue-White DPX (ER) (Panel D). HeLa cells are shown in the top row of each panel and Sf9 cells are displayed in the bottom row, except in panel D, which shows only HeLa cells since the ER of Sf9 cells cannot be stained using ER-Tracker™. Scale bars represent 10 µm.

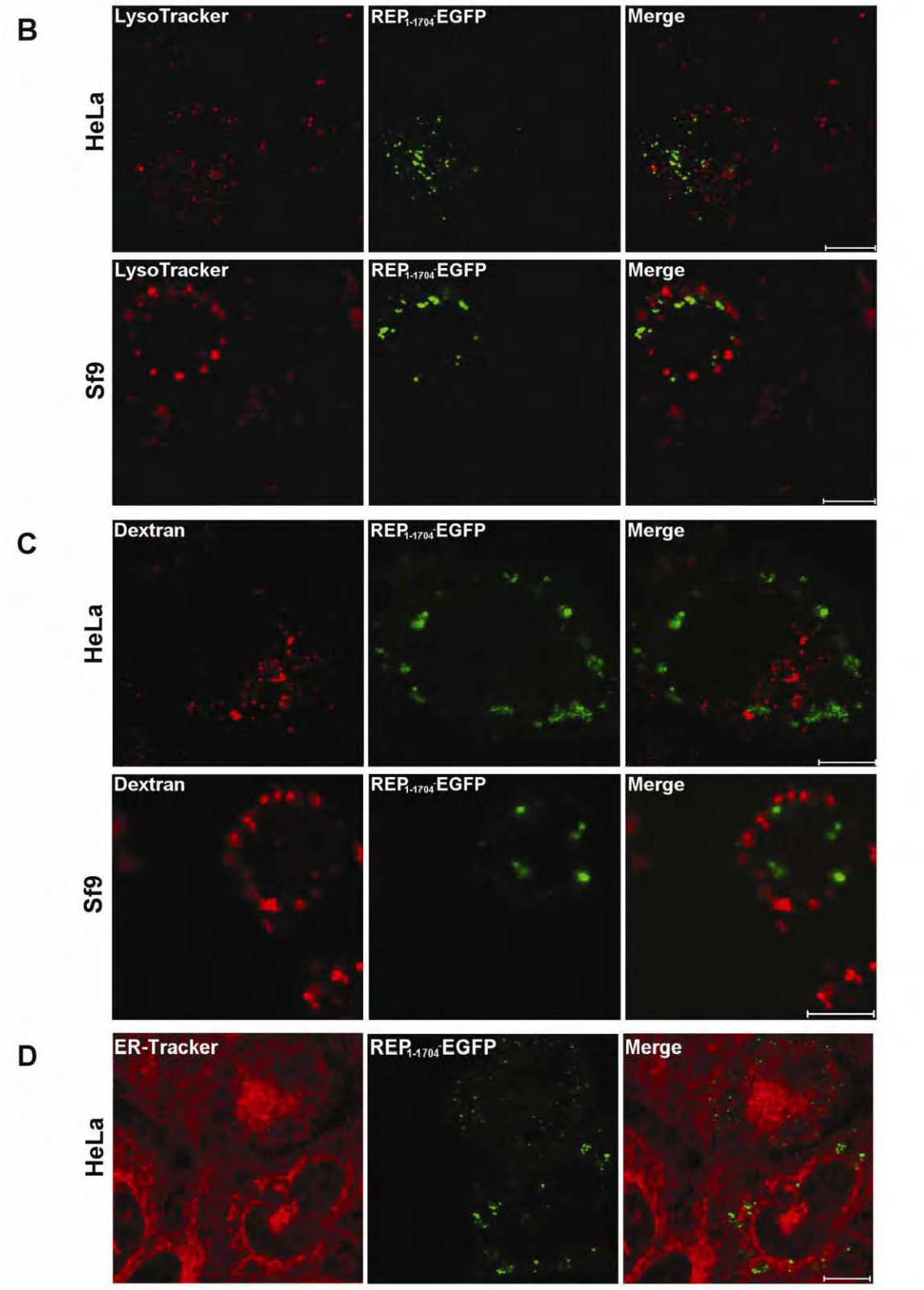

Figure 3.4: Figure legend on page 66.

Following validation of the live cell stains, co-localisation experiments were conducted to determine the site of REP_{1-1704}-EGFP localisation in both the HeLa and Sf9 cells. Comparisons with the MitoTracker® signal showed no overlap with REP_{1-1704}-EGFP fluorescence in either cell type, excluding the mitochondria as a potential site of replicase localisation (Figure 3.4, Panel A). The same was true for cells stained with ER-Tracker™ (Figure 3.4, Panel D), confirming previous immunofluorescence data obtained using ERp60 that excluded the ER as the site of REP_{1-1704}-EGFP-association.

No significant overlap was seen with either LysoTracker®, specific for lysosomes and acidic organelles, or endocytosed dextran (Figure 3.4, Panels B and C). This was the case even when dextran uptake was allowed proceed throughout the endocytic pathway to the point of delivery to the lysosomes, as shown by the overlap of the two signals after approximately 24 hours (Figure 3.5). These results indicated that, while there was some interaction between REP_{1-1704}-EGFP and endocytic organelles, this interaction did not occur through, nor migrate along, the classical endocytic pathway. Rather this interaction might proceed via an alternate pathway that intersects with the clathrin-dependent pathway at the late endosomes, as is the case for some of clathrin-independent endocytic pathways. Alternatively, the data could indicate a replicase-dependent means of excluding the organelle marker proteins that were used in the immunofluorescence studies and the fluorescence-conjugated dextran, possibly through membrane permeabilisation or destabilisation. The latter explanation is less likely since no evidence for the large-scale remodelling of endocytic membranes was observed in transfected cells.

3.3.4. Time-lapse imaging of REP_{1-1704} EGFP in live cells

In order to clarify the location of REP_{1-1704}-EGFP-containing structures, time-lapse imaging was employed to analyse the sub-cellular dynamics of the

punctate structures. Since the subcellular movements of major organelles have been described in some detail, the data obtained from time-lapse imaging were compared to the flux of replicase-associated structures. Live cells, expressing $REP_{1\text{-}1704}$-EGFP, were imaged over time with successive images being taken at various intervals over a 6 to 8 hour period starting at 16 hours after transfection. Consecutive images were analysed as "t-stacks" to follow general movements and dynamics.

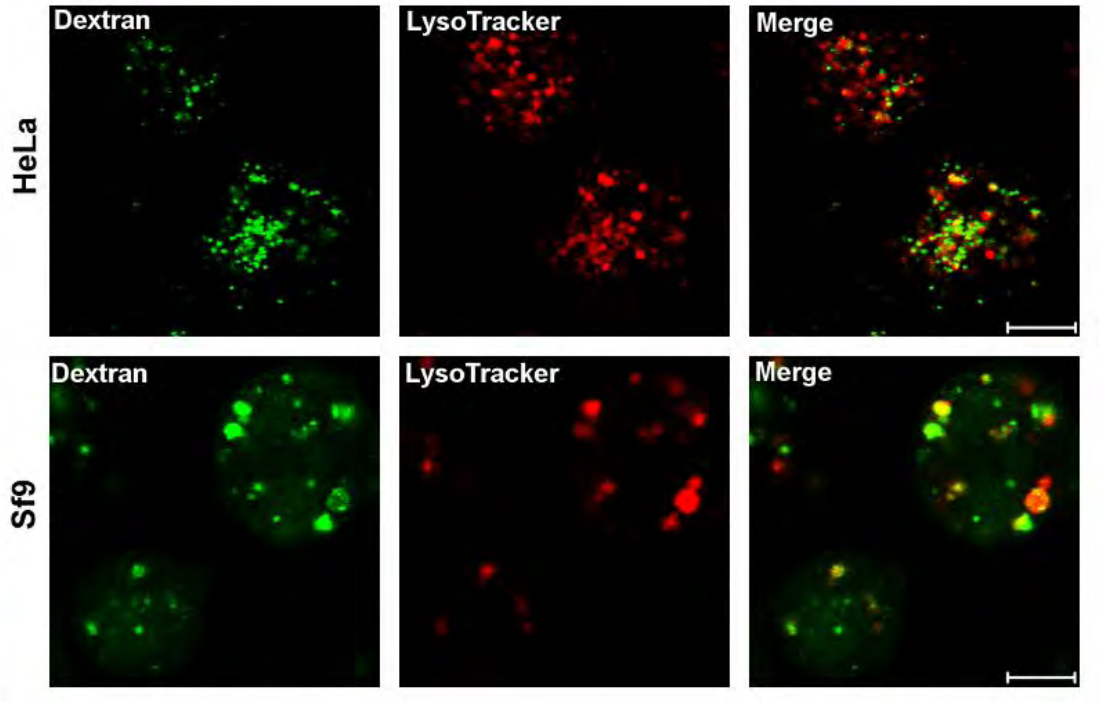

Figure 3.5: Comparison of the distribution of Cascade Blue®-conjugated dextran and LysoTracker®. Live HeLa (top) and Sf9 (bottom) were stained first with Cascade Blue®-conjugated dextran (for 23 hours) before LysoTracker® Red DND-99 was added for 30 minutes prior to imaging by confocal fluorescence microscopy. Yellow areas in the merged images (right) indicate areas of overlap. Scale bars represent 10 µm.

$REP_{1\text{-}1704}$-EGFP-associated punctate structures were highly dynamic (Supplementary data, videos S1a and S1b) and varied significantly in size, with the majority of the structures detected measuring between 0.2 and 4.0 µm in diameter. The rate and type of movement associated with each structure was generally size dependent with smaller vesicles (< 0.8 µm) being more mobile than the larger ones (> 2 µm) and in the majority of cases,

the movements appeared to be random. Interestingly, a number of structures moved large distances across the cell at speeds significantly higher than the random movements (> 2 μm.s^{-1}). Furthermore, in these cases the structures moved in a more directed manner, possibly along defined cellular pathways (Figure 3.6, Panel A). In one case, two vesicles were observed to traverse a similar region of the cell in the same direction and within a short space of time (Supplementary data, Video 2). Both of these structures dissociated at a similar position, at which point they again displayed random movements. Taken together, these data suggested that the REP$_{1\text{-}1704}$-EGFP-associated punctate structures might be transported within cells along defined pathways, most likely along the microtubule network, as is the case for endocytic vesicles between the early and late endosomes (Gruenberg *et al.*, 1989).

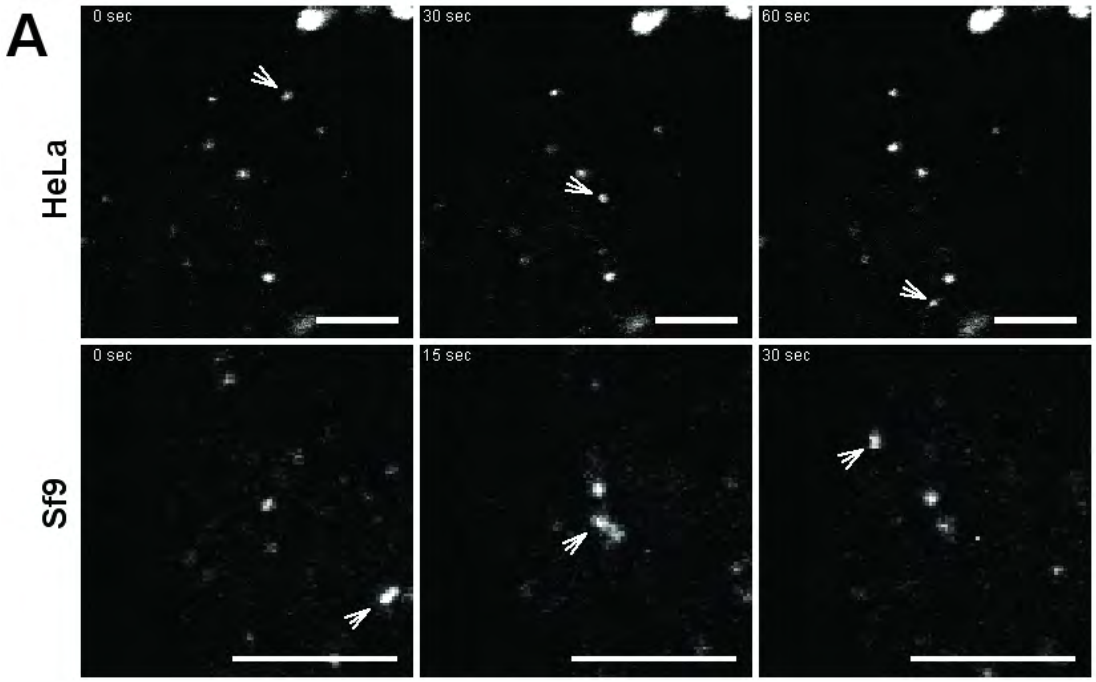

Figure 3.6 (Here and page 71): Transport, fusion and fission of REP$_{1\text{-}1704}$-EGFP containing structures in live HeLa and Sf9 cells. HeLa and Sf9 cells expressing REP$_{1\text{-}1704}$-EGFP were imaged between 16 and 24 hours after transfection using time-lapse confocal fluorescence microscopy. Analysis of time-lapse image series' from both cell types revealed structures associated with EGFP fluorescence that were transported along defined pathways (Panel A) and capable of fusion (Panel B) and fission (Panel C). All images represent 1 μm optical slices and scale bars represent 5 μm. (Additional data showing the transport of vesicles is available on the supplementary data CD as video S2.)

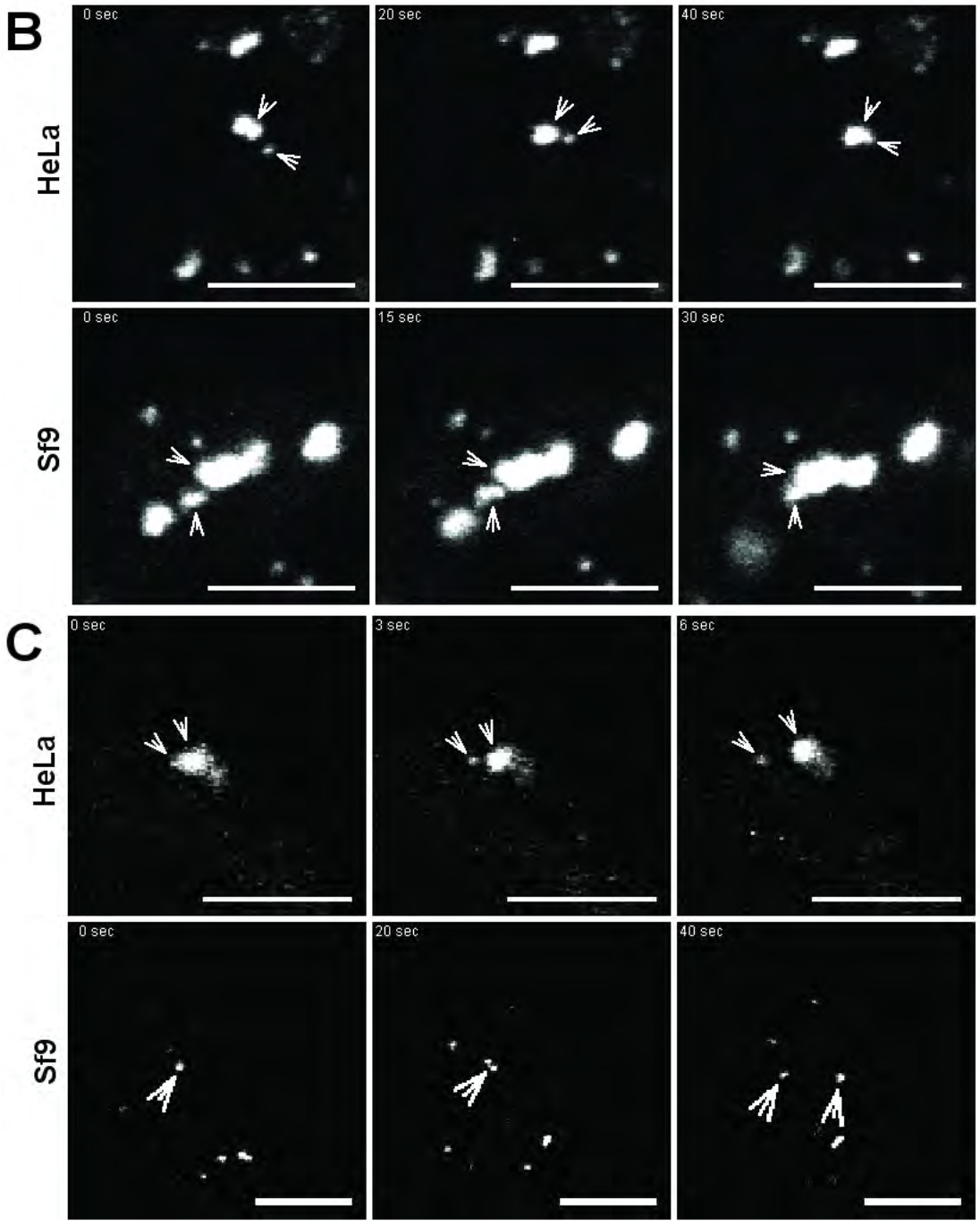

Figure 3.6: Figure legend on page 70.

Further analysis of “t-stacks” also revealed other interesting characteristics. In addition to transport along defined pathways, some EGFP-containing structures appeared to undergo both fusion (Figure 3.6, Panel B) and fission

(Figure 3.6, Panel C) reactions as well as a few instances of a combination of the two, called “kiss-and-run” events. Fusion was observed more frequently than fission and appeared to occur more readily between smaller structures, with vesicles less than 1 µm in diameter more likely to undergo fusion events than their larger counterparts. This fusion activity is likely to give rise to the higher proportion of larger structures (> 2 to 5 µm) at later time points (20 to 24 hours). Fission events, although less frequently observed, were noted for vesicles regardless of size. These characteristics are, as was the case with transport along cellular pathways, consistent with an association of $REP_{1\text{-}1704}$-EGFP with endocytic organelles (Bright *et al.*, 2005).

3.4 DISCUSSION

The aim of the experiments described in this chapter was to determine the subcellular localisation of replicase-EGFP fusion proteins in mammalian and insect tissue culture cells. The data represent the first experimental evidence of the targeting of a tetravirus replicase to a subcellular location and was obtained by studying the subcellular localisation of the HaSV replicase fused to EGFP in tissue culture cells. This system offered several advantages: first, EGFP fluorescence could be used to detect the presence and location of the replicase and second, EGFP provided the additional advantage of being detectable in live cells without the requirements of cell fixation and detection by immunofluorescence or the use of expensive substrates, as is the case for tetra-cysteine tags. Similar use of EGFP as a tag, fused to either the replicase or the capsid genes, has been employed in the generation of genetically stable and infectious recombinant SFV, Hepatitis E virus and Equine arteritis virus (Thakral *et al.*, 2005; Tamberg *et al*, 2007; Van den Born *et al.*, 2007) and in the analysis of various aspects of Hepatitis C virus, Rabies virus and Vesicular stomatitis virus life cycles in live cells (Kien *et al.*, 2003; Finke *et al.*, 2004; Das *et al*., 2006).

Initial analysis of full-length HaSV replicase-EGFP fusion proteins revealed that both N- and C-terminal fusions to EGFP resulted in a subcellular distribution of fluorescence that was different from cells expressing the untagged marker protein. Most significant was the observation that small punctate structures were produced when cells expressed REP_{1-1704}-EGFP. The cytosolic distribution of EGFP-REP_{1-1704} suggested that the N-terminus of the replicase may be important in the development of these structures. The absence of other viral proteins also suggested that the localisation was likely to be solely dependent on factors present within the viral replicase and host factors present within both HeLa and Sf9 cells. Comparison of these structures with those of cellular organelles demonstrated a possible association with endocytic organelles, although overlap was only observed with the late endosomal marker protein, CD63, and only at certain time points was this overlap significant. Unexpectedly, no overlap was observed with endocytosed dextran as it traversed the classical endocytic pathway into the lysosomes. Possible reasons for this include the active exclusion of certain host proteins from REP_{1-1704}-EGFP-containing vesicles, the permeabilisation of REP_{1-1704}-EGFP-containing vesicles in a replicase-dependent manner or the association of the HaSV replicase with non-clathrin-dependent endocytic pathways that do not incorporate dextran and intersect with the classical pathway at the late endosomes. These data suggested an atypical association with endocytic organelles, most likely those directly or closely associated with the late endosomes.

To further characterise this association, time-lapse imaging of cells expressing REP_{1-1704}-EGFP was conducted. Analysis of the resulting “t-stacks” also showed similarities to endocytic organelles, with both being capable of cellular transport, fusion and fission, strengthening the argument for the localisation of REP_{1-1704}-EGFP to the endocytic pathway in transfected tissue culture cells. Furthermore, these data suggest that continued

accumulation of replicase-associated structures within the cell through continued protein production and fusion reactions gradually sequesters increasing amounts of cellular membrane that must either be replaced by increased lipid production or adversely affect cellular processes, especially those reliant on the organelles targeted by the replicase. Similar punctate structures have also been observed in PrV-infected MG8 cells stained with anti-p40 antibodies (Walter, 2008). This suggests the possibility of a common cellular location of vRNA production among tetraviruses, even though the replicases differ significantly in amino acid sequence.

CHAPTER 4

RECOMBINANT EXPRESSION AND MEMBRANE ASSOCIATION OF NATIVE HaSV REPLICASE IN Sf9 CELLS

4.1 INTRODUCTION

Proteins that associate with cellular membranes are grouped into three major classes according to the type and strength of the interaction involved. (1) Transmembrane proteins may be strongly associated with membranes through one or more hydrophobic domains that span the entire width of the lipid bilayer resulting in a protein with regions present on both membrane surfaces; (2) Integral membrane proteins may interact with membranes through amphipathic helices that are embedded into a single leaflet of the lipid bilayer and/or covalent lipid attachments, both of which produce interactions that are generally weaker than that of transmembrane proteins; (3) Electrostatic and hydrophobic protein-protein interactions with other membrane-associated proteins result in the relatively weak interactions of peripheral membrane proteins (Alberts *et al.*, 2002).

Confocal fluorescence microscopy studies to determine the subcellular localisation of replicase-EGFP fusion proteins provided evidence for an association between the HaSV replicase and the endocytic organelles of mammalian (HeLa) and insect (Sf9) cells (Chapter 3). Biochemical fractionation of cellular membranes and associated proteins is frequently used to confirm protein-membrane interactions and to characterise the type of association involved. This chapter describes the use of such fractionation to characterise the interaction between the HaSV replicase and cellular membranes. Anti-$REP_{1\text{-}218}$(b) and anti-EGFP antisera were unable to detect the expression of replicase-EGFP fusion proteins in tissue culture cells due to the low transfection efficiencies associated with the full length replicase

expression vectors. Consequently, a recombinant baculovirus was developed for high level expression of the full-length HaSV replicase with an N-terminal 6xHis tag and a C-terminal V5 epitope tag, to facilitate detection of the recombinant protein. Subcellular fractionation of baculovirus-infected cells suggests that the HaSV replicase associates with cellular DRMs.

4.2 MATERIALS AND METHODS

All SDS-PAGE analyses were conducted using discontinuous glycine/polyacrylamide gels with 4% stacking gels. Analysis of His-REP-V5 was done using 7.5% resolving gels and the separation of the transmembrane protein control, voltage-dependent anion channel (VDAC), was done using 15% resolving gels. Western analysis was carried out as described in Section 2.2.5 using monoclonal mouse anti-His (Roche Applied Biosciences), rabbit anti-$REP_{1\text{-}218}$(b), monocolonal mouse anti-V5 (obtained from Richard Randall, School of Biology, University of St. Andrews, St. Andrews, Scotland, UK) or monocolonal mouse anti-VDAC (Santa-Cruz Biotechnology).

4.2.1. Construction of recombinant baculovirus JRS BV1 expressing recombinant HaSV replicase

The recombinant baculovirus for the expression of the full length HaSV replicase with N-terminal 6xHis and C-terminal V5 epitope tags (His-REP-V5) was generated using the Bac-to-Bac® Baculovirus Expression System (Invitrogen). The plasmid pJRS42 was constructed as described in Appendix A.7 and consists of the commercial vector, pFastBac™ Dual (Invitrogen), with the His-REP-V5 CDS inserted for expression under the control of the polyhedrin (PolH) promoter (Figure 4.1). The recombinant bacmid was generated by transforming pJRS42 into competent *E. coli* DH10Bac cells (*F– mcrA Δ*(*mrr-hsdRMS-mcrBC*) *Φ80lacZΔM15 ΔlacX74 recA1 endA1* ara*D139 Δ(ara leu) 7697 galU galK λ– rpsL nupG/ pMON14272/pMON7124*)

(Invitrogen). Bacmid DNA was purified and screened by polymerase chain reaction (PCR) amplification using the insert- (JRS2 and JRS13R) and bacmid-specific (M13F and M13R) primers as per manufacturer's recommendations (primer sequences are shown in Appendix B). Recombinant bacmid DNA was then transfected into Sf9 cells as follows. Sf9 cells were seeded at a density of 8 x 10^5 cells per well of a 6 well plate and allowed to settle for 30 to 60 minutes. During that time the transfection mixture consisting of approximately 800 ng purified bacmid DNA, 12 µl Fugene® HD and serum-free Grace's insect medium (200 µl total volume) was prepared, mixed and incubated at room temperature for 30 minutes. The medium was then aspirated and the DNA-lipid complex was added drop-wise with an additional 200 µl serum-free medium. Following incubation at 28 °C for 2 hours, 1 ml complete Grace's insect medium was added to each well and the cells incubated at 28 °C for four days before the supernatant was harvested as a passage 1 virus stock. This stock was then propagated and plaque-purified.

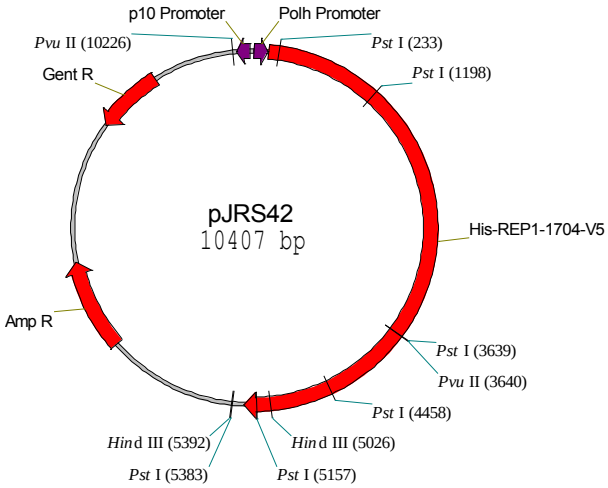

Figure 4.1: Plasmid map of the recombinant plasmid used in the production of JRS BV1, the recombinant baculovirus for the expression of His-REP-V5. Amp R: *β*-lactamase, Gent R: gentamicin acetyl transferase , PohH Promoter: AcMNPV polyhedrin promoter.

4.2.2. Plaque-purification of recombinant baculoviruses

Plaque-purification was conducted using 6 well tissue culture dishes. Each well was seeded with 8.5 x 10^5 Sf9 cells, which were allowed to settle for 30 to 60 minutes at 28 °C in complete Grace's insect medium. The medium was aspirated from the cells and each well infected with 500 µl of a 10-fold serial dilution of the passage 1 virus stock (10^{-1} to 10^{-6}) in complete Grace's insect medium. Cells were then incubated at 28 °C for 1 hour with very gentle agitation.

Tissue culture grade agarose (Sigma), at a concentration of 2 % (w/v), was dispersed in chilled sterile double distilled water before being heated to just below boiling point and shaken until the agarose was dissolved. Both the 2 % agarose and an equivalent volume of 2 x complete Grace's insect medium were then incubated in a water bath at 40 °C until needed. Following infection, the medium was aspirated from the cells and a 1:1 mixture of 2 % agarose and 2 x Grace's insect medium was prepared before 2 ml was added to each well. The agarose was allowed to set at room temperature for 10 to 20 minutes and the cells were then incubated at 28 °C for 6 days. After 5 days, 500 µl thiazolyl blue tetrazolium bromide (0.1 % (w/v) in PBS, pH 7.4) was added to each well to stain live cells and incubated at 28 °C overnight. Individual plaques visible after staining were then “picked” using sterilised disposable P1000 pipette tips and resuspended in 500 µl complete Grace's insect medium. Plaques purified in this manner were used to infect each of the wells of the freshly seeded 6 well plate as detailed below.

Each well of a fresh 6 well plate was seeded with 2 x 10^6 cells per well and allowed to settle for 30 to 60 minutes in complete Grace's medium at 28 °C. Each well was infected with 500 µl of the resuspended virus at 28 °C with very gentle agitation before a further 3 ml complete medium was added. Cells were incubated at 28 °C for 4 days before harvesting at which point the

cells were resuspended in the spent medium and pelleted by centrifugation at 5 000 x *g* for 5 minutes. The supernatant was retained as the passage 3 JRS BV1 virus stock while the cells were resuspended in 100 µl 1 x sample buffer and the crude protein extracts resolved by SDS-PAGE. Western analysis was used to confirm recombinant protein expression.

4.2.3. Calculation of virus infectivity

In order to determine the concentration of infectious virus particles in a particular virus stock, 8.5 x 10^5 Sf9 cells were seeded into each well of a 6 well plate and allowed to settle for 30 to 60 minutes in complete Grace's insect medium. Each well was then infected with 10-fold serial dilutions of each respective virus passage stock as described in Section 4.2.2. Agarose overlays were prepared and, after staining, the concentration of infectious virus particles (plaque-forming units (pfu).ml^{-1}) was calculated using the following formula provided by the manufacturer:

$pfu.ml^{-1}$ = (1/dilution factor) x no. plaques x (1/ml inoculum)

where the “dilution factor” is associated with the well in which between 2 and 20 plaques were observed and the “ml inoculum” is the volume of the dilution used in the infection.

4.2.4. Optimisation of His-REP-V5 expression

Once the expression of His-REP-V5 had been confirmed by SDS-PAGE analysis, a baculovirus stock (JRS BV1 (3), referred to as JRS BV1 hereafter) was selected for further use. The expression levels of His-REP-V5 were then optimised with respect to multiplicity of infection (MOI) (in pfu.$cell^{-1}$) and length of time for maximum expression. First, the optimal MOI for protein expression was determined by infecting 2 x 10^6 cells in each well of a 6 well plate with MOI's of 0.1, 1, 2, 5 and 10. After 4 days cells were harvested in

the spent medium and pelleted by centrifuging at 13 000 x *g* for 2 minutes before being resuspended in 100 µl 1 x sample buffer. Crude protein extracts were then resolved by SDS-PAGE and the proteins visualised by coomassie staining. Once the optimal MOI for protein expression had been determined, 4 wells of a 6 well plate were infected with JRS BV1 at an MOI of 5 and the cells harvested after 24, 48, 72 and 96 hours respectively. Cells were pelleted, resuspended in 1 x sample buffer, resolved by SDS-PAGE and the proteins visualised by coomassie staining.

4.2.5. Solubility of His-REP-V5

T25 (25 cm^2) and T75 (75 cm^2) flasks (Corning) were seeded with 4.5 x 10^6 or 1.4 x 10^7 cells, respectively, before being infected at an MOI of 5 for 72 hours. Once the expression of His-REP-V5 had been confirmed using SDS-PAGE followed by coomassie staining, the solubility of the recombinant HaSV replicase was determined. JRS BV1-infected cells from a T75 flask were harvested by centrifugation at 5 000 x *g* for 5 minutes. These cells were resuspended in 750 µl lysis buffer (50 mM Tris, 300 mM NaCl, 10 mM Imidazole, 1 % (v/v) Nonidet P40, pH 8.0, containing EDTA-free protease inhibitor cocktail, set III (Calbiochem)) and incubated on ice for 10 minutes in preparation for Ni-affinity chromatography. The lysate was then centrifuged at 10 000 x *g* for 10 minutes at 4 °C to obtain soluble (supernatant) and insoluble (pellet) protein fractions for analysis by SDS-PAGE.

The insolubility of His-REP-V5 produced in cells grown in Grace's insect medium led to the investigation of other insect growth media, including serum-free ExCell 420 medium (Sigma). Cells grown in either complete TC-100 (Lonza), Grace's or ExCell 420 insect media were infected with recombinant baculovirus at an MOI of 5 as before, and incubated in the respective media before being harvested after 4 days. Soluble and insoluble fractions were subjected to SDS-PAGE analysis and coomassie staining, as described above.

4.2.6. Subcellular fractionation of baculovirus-infected Sf9 cells

Subcellular fractionation of virus-infected cells was carried out according to a modified protocol originally provided by Prof. Tom Wileman (School of Medicine, Health Policy and Practice, University of East Anglia, UK). Virus-infected cells from a T75 tissue culture flask were harvested, pelleted at 5 000 x *g* for 5 minutes and resuspended in 800 µl chilled fractionation buffer (50 mM Tris, 1 mM Na_2EDTA, 8 % sucrose (w/v), pH 7.5, containing EDTA-free protease inhibitor cocktail, set III). Cells were lysed by 20 passes through a 25 gauge syringe needle and lysates were centrifuged at 3 300 x *g* for 2 minutes at 4 °C to pellet large cell debris, nuclei and whole cells. The supernatant was retained and the pellet re-extracted in 400 µl fractionation buffer, followed by pelleting of cell debris and nuclei as described above. The supernatants were pooled as the "post nuclear supernatant" (PNS) (used to generate the subsequence fractions) and 200 µl was retained for further analysis.

The remaining PNS was divided equally between three 1.5 ml centrifuge tubes (approximately 330 µl in each) and the membrane fraction pelleted at 17 000 x *g* for 20 minutes at 4 °C. The resulting supernatants were pooled as the soluble fraction while the pellets were resuspended in 330 µl of 100 mM $NaCO_3$ (pH 11.1) in distilled water or fractionation buffer containing either 1 M NaCl or 1 % Triton X-100 and incubated on ice for 15 minutes. These fractions were again centrifuged at 17 000 x *g* for 20 minutes at 4 °C. The soluble fractions were retained and diluted 4:1 with 5 x sample buffer, while the pellets were resuspended in 410 µl 1 x sample buffer. Equivalent volumes of each sample were resolved using SDS-PAGE and protein detected by western analysis.

4.3 RESULTS

4.3.1. The expression of His-REP-V5 in JRS BV1-infected Sf9 cells

The recombinant baculovirus JRS BV1 encodes the full length HaSV replicase with 6xHis (N-terminal) and V5 epitope (C-terminal) tags. Passage 1 virus was plaque-purified and cells infected, with each of six isolates analysed for His-REP-V5 expression. Cells infected with recombinant JRS BV1 isolated expressed a dominant protein band with a molecular mass of between 150 and 200 kDa, which correlated to the predicted molecular mass of 190 kDa for His-REP-V5 (Figure 4.2, Lanes 1 to 6). This band was not present in cells infected with wild-type baculovirus (Figure 4.2, Lanes 7 and 8) or mock infected cells (Figure 4.2, Lane 9).

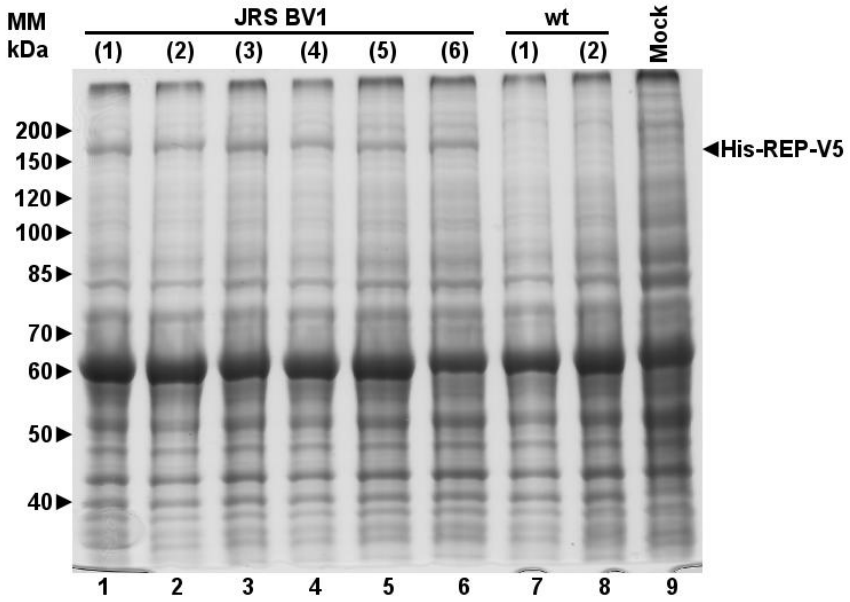

Figure 4.2: The expression of His-REP-V5 in Sf9 cells infected with various JRS BV1 isolates. SDS-PAGE analysis of crude extracts of Sf9 cells infected with six plaque-purified JRS BV1 isolates for the expression of His-REP-V5 (Lanes 1 to 6), two plaque-purified wild-type ("wt") baculovirus isolates (Lanes 7 and 8) and mock-infected Sf9 cells (Lane 9). Molecular mass standards are indicated on the left of the gel in kDa and His-REP-V5 is indicated on the right.

To confirm that the JRS BV1-specific protein band was His-REP-V5, cell-free extracts obtained from each of the sets of virus-infected cells were subjected to western analysis using anti-His, anti-REP_{1-218}(b) and anti-V5 epitope antisera to conclusively identify His-REP-V5. All three western blots confirmed the identity of the recombinant HaSV replicase with a distinct band being detected at the expected molecular mass (190 kDa) in cells infected with the JRS BV1 (Figure 4.3, Panels A, B and C).

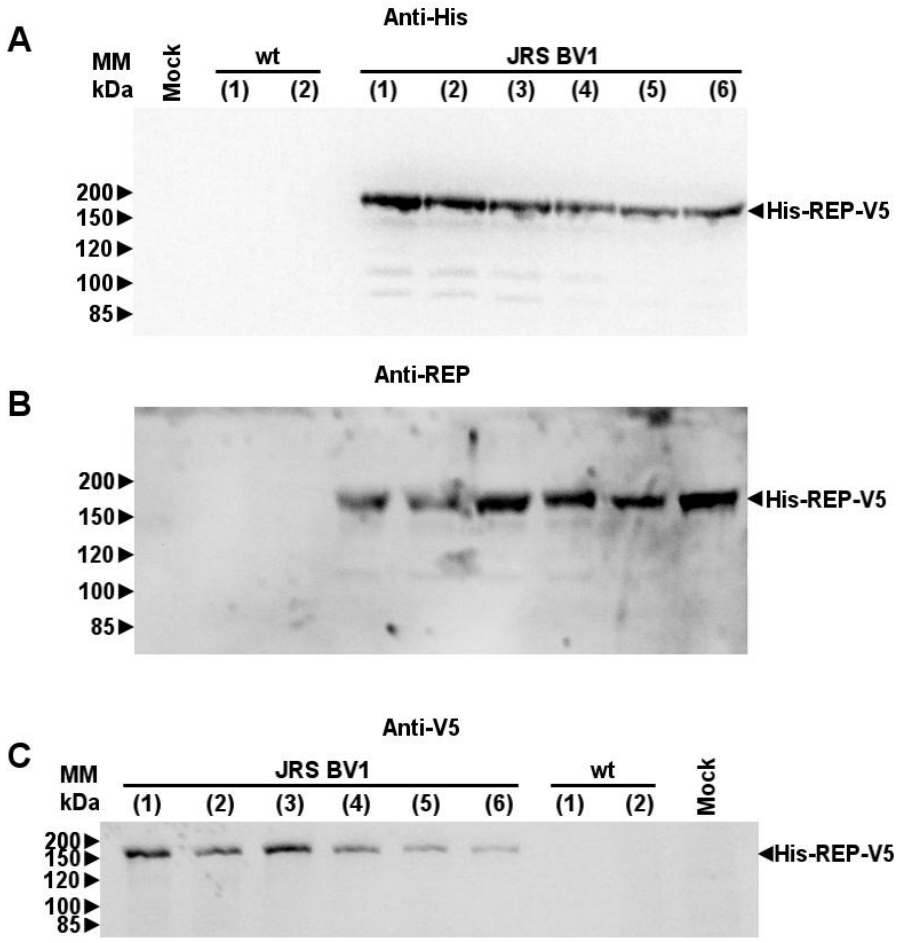

Figure 4.3: Specific detection of His-REP-V5 in Sf9 cells infected with JRS BV1 isolates. His-REP-V5 detected in crude extracts obtained from mock-infected Sf9 cells ("Mock") or Sf9 cells infected with six recombinant baculovirus isolates for the production of His-REP-V5 ("JRS BV1") or wild-type baculovirus ("wt") as detected by western analysis. Membranes were probed using anti-His (Panel A), anti-REP_{1-218}(b) (Panel B) or anti-V5 (Panel C) antisera at dilutions of 1:500, 1:15 000 and 1:1 000 respectively. Molecular mass standards are indicated on the left of the gel in kDa and His-REP-V5 is indicated on the right.

4.3.2. Optimisation of His-REP-V5 expression

The optimal MOI for the expression of His-REP-V5 was determined by infecting Sf9 cells with JRS BV1 at MOIs of 0.1, 1, 2, 5 or 10. SDS-PAGE analysis of crude protein extracts showed that His-REP-V5 production was maximal when cells were infected at an MOI of 5 pfu.cell^{-1} (Figure 4.4, Lane 7). A small increase in His-REP-V5 expression was observed when the MOI was increased from 1 to 2 and again from 2 to 5 (Figure 4.4, Lanes 5 to 7). However, a further increase in virus load (MOI = 10) resulted in a decrease in His-REP-V5 expression (Figure 4.4, Lane 8) as well as a decrease of approximately 25 % in the overall biomass harvested.

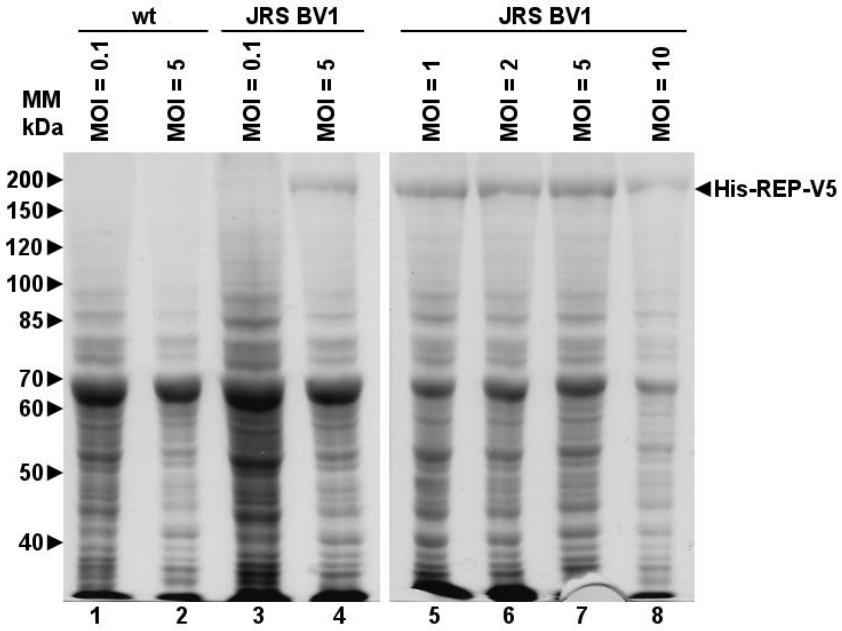

Figure 4.4: Optimisation of infection of Sf9 cells with the recombinant baculovirus, JRS BV1, expressing His-REP-V5. SDS-PAGE analysis of crude extracts of Sf9 cells harvested 4 days after infection with different multiplicities of infection (MOI's) of wild-type ("wt") baculovirus (Lanes 1 and 2) or JRS BV1 (Lanes 3 to 8). The MOI used in each infection (in pfu.cell^{-1}) is indicated above each lane. Molecular mass standards are indicated on the left in kDa and the recombinant HaSV replicase, His-REP-V5, is indicated on the right.

The effect of incubation time on protein expression was also investigated. Cells infected at the optimal MOI of 5 were harvested after 24, 48, 72 or 96 hours and crude protein extracts analysed by SDS-PAGE. No His-REP-V5

was observed after 24 hours, but only after 48 hours (Figure 4.5, Lanes 1 and 2). A significant increase in His-REP-V5 expression levels was observed after 72 hours (Figure 4.5, Lane 3) and although expression levels were relatively stable after this point, maximum production was observed when cells were harvested after 96 hours (Figure 4.5, Lane 4).

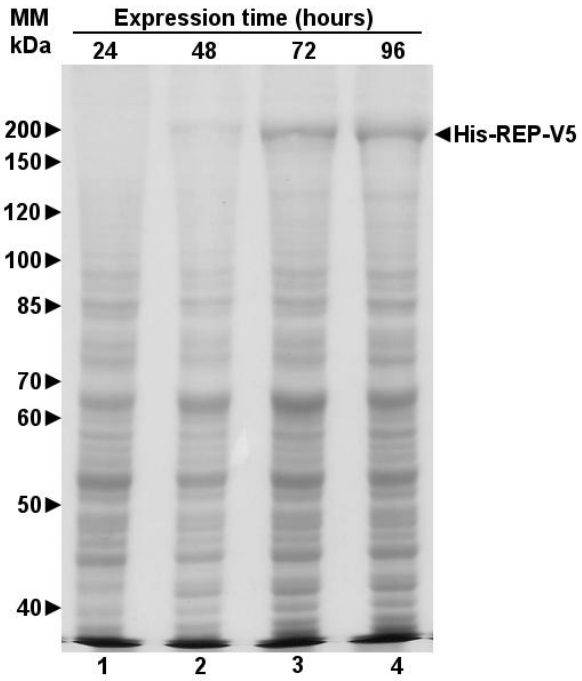

Figure 4.5: Optimisation of time for expression of His-REP-V5 following infection of Sf9 cells with JRS BV1. SDS-PAGE analysis of crude extracts of Sf9 cells infected with the recombinant baculovirus, JRS BV1, to determine the time following infection at which the maximum expression of His-REP-V5 was achieved. Cells were infected at the optimal MOI of 5 and harvested after 24, 48, 72 or 96 hours (Lanes 1 to 4 respectively). Molecular mass standards are indicated on the left and His-REP-V5 is shown on the right.

4.3.3. Solubility of His-REP-V5

Differential centrifugation was used to separate soluble and insoluble/membrane-associated protein fractions. A significant amount of His-REP-V5 was observed in the pellet fraction obtained from JRS BV1-infected cells (Figure 4.6, Lane 4), but none was detected in the supernatant fraction (Figure 4.6, Lane 3). This indicated that the recombinant HaSV replicase was present in the baculovirus-infected cells either as a membrane-associated protein or in insoluble aggregates. Sf9 cells grown in

TC-100 and serum-free ExCell 420 media were also infected with JRS BV1 in order to determine whether the growth medium and/or foetal calf serum could have an effect on solubility of the recombinant protein, However, the analysis of soluble and insoluble protein fractions by SDS-PAGE showed no change in the solubility of His-REP-V5 in either medium (Figure 4.7, Lanes 1 to 3 vs Lanes 4 to 6). Attempts at solubilisation and purification of His-REP-V5 using denaturing Ni-affinity purification (in the presence of 8 M urea) were equally unsuccessful (data not shown).

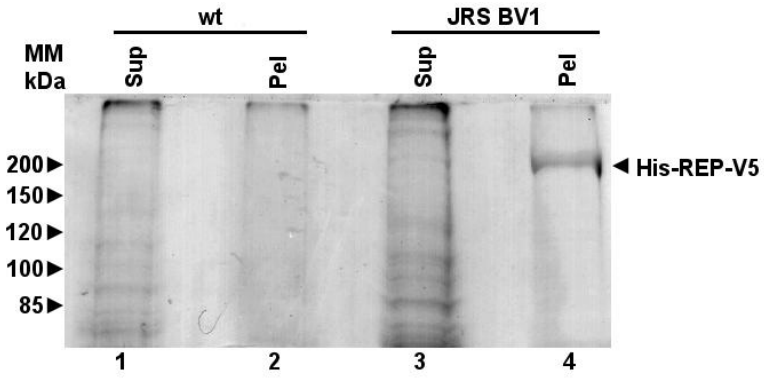

Figure 4.6: The solubility of His-REP-V5 expressed in Sf9 cells infected with JRS BV1. SDS-PAGE analysis of soluble ("Sup", Lanes 1 and 3) and insoluble ("Pel", Lanes 2 and 4) protein fractions from Sf9 cells infected with wild-type ("wt") baculovirus (Lanes 1 and 2) or the recombinant JRS BV1 (Lanes 3 and 4). Molecular mass standards are indicated on the left while His-REP-V5 is indicated on the right.

4.3.4. Subcellular fractionation of His-REP-V5

To determine whether His-REP-V5 was associated with cellular membranes, a subcellular fractionation protocol able to distinguish between the major groups of membrane-associated proteins was used. Validation of the fractionation protocol was done using VDAC, a ubiquitous transmembrane, pore-forming protein present in all eukaryotic mitochondria (Blachly-Dyson *et al.*, 1993). Small amounts of VDAC were detected in soluble/cytosolic fractions but the protein was mostly present in membrane-associated fractions (Figure 4.8, Panel A, Lanes 4 and 6). As expected, incubation of membrane-associated fractions in solutions of high ionic strength buffer (1 M

NaCl) or alkaline pH (11.1) did not release VDAC from membrane fractions, where it remained in the pellet fractions representing unliberated membrane proteins and insoluble aggregates (Figure 4.8, Panel A, Lanes 4 and 6). By contrast, the presence of the non-ionic detergent Triton X-100 resulted in the complete solubilisation of VDAC from the membrane-associated fraction (Figure 4.8, Panel A, Lane 7).

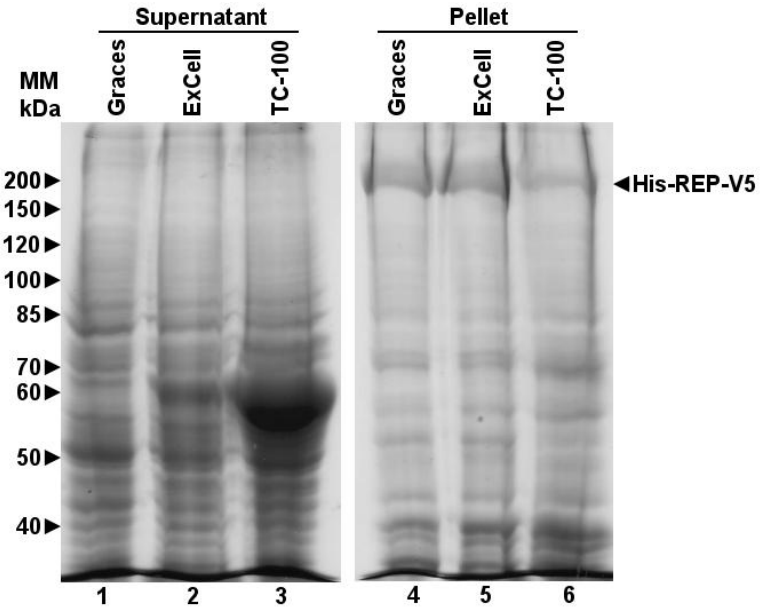

Figure 4.7: The effect of growth medium on the solubility of His-REP-V5 in Sf9 cells infected with JRS BV1. SDS-PAGE analysis of the soluble (Lanes 1 to 3) and insoluble (Lanes 4 to 6) protein fractions of Sf9 cells infected with JRS BV1 and grown in complete Grace's (Lanes 1 and 4), complete TC-100 (Lanes 3 and 6) or serum free ExCell 420 (Lanes 2 and 5) insect tissue culture media. Molecular mass standards are indicated on the left and His-REP-V5 is indicated on the right.

Western analysis of JRS BV1-infected cells showed that the full length His-REP-V5 pelleted with membrane-associated/insoluble proteins when incubated at an alkaline pH (11.1) (Figure 4.8, Panel B, Lane 6). Similar results were also obtained following incubation in buffer containing 1 M NaCl or 1 % Triton X-100 (Figure 4.8, Panel B, Lanes 4 and 8). In addition to the full length His-REP-V5, three degradation products of approximately 90, 110 and 150 kDa in size were detected (Figure 4.8, Panel B). While His-REP-V5 and the largest degradation product (150 kDa) were exclusively present in the respective pellet fractions, a small amount of the 90 and 110 kDa

polypeptides were detected in the soluble fraction (Figure 4.8, Panel B, Lane 2). The remainder were present with membrane-associated/insoluble protein fractions and remained in the pellet fractions (Figure 4.8, Panel B, Lanes 4, 6 and 8), with the exception of the smallest degradation product (90 kDa), the majority of which was detected in the fraction of membrane proteins solubilised by Triton X-100 (Figure 4.8, Panel B, Lane 7). This suggests that the proteolytic degradation of C-terminal region of His-REP-V5 affects the association of the polypeptide with the membrane-associated/insoluble protein fractions, implying that sequences within the C-terminal region could be involved in protein-membrane or protein-protein interactions. The proteolytic degradation of His-REP-V5 at 4 °C and in the presence of protease inhibitors also suggests that the recombinant protein is not likely to be present in insoluble aggregates, since aggregated proteins tend to be protected, to some degree, from proteolytic degradation (Kane and Hartley, 1988).

4.4 DISCUSSION

Previous attempts at detecting the replicase expressed in transfected tissue culture cells in western blots had been unsuccessful, primarily due to low transfection efficiencies of the plasmids encoding the full length HaSV replicase-EGFP fusion proteins, especially in mammalian cells. As a result, the expression of sufficient replicase for biochemical fractionation studies was achieved using baculovirus-mediated expression of His-REP-V5 in Sf9 cells. This system allowed for the expression of the recombinant HaSV replicase in a much higher proportion of cells, increasing the overall levels of production and enabling detection by western blot using anti-His, anti-V5 epitope and anti-$REP_{1\text{-}218}$(b) antisera.

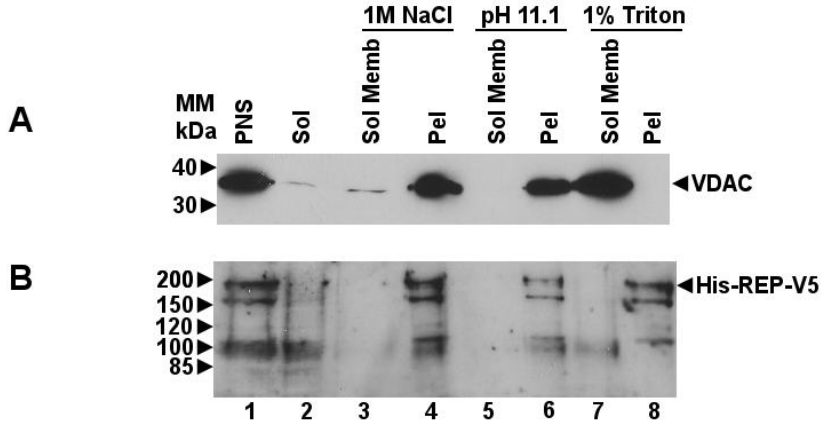

Figure 4.8: The subcellular fractionation of His-REP-V5 in Sf9 cells infected with the recombinant baculovirus, JRS BV1. Sf9 cells infected with JRS BV1 were fractionated to isolate subcellular protein fractions and subjected to western analysis using anti-VDAC (Panel A) or anti-REP_{1-218}(b) (Panel B) antisera at dilutions of 1:500 or 1:15 000, respectively. Cells were fractionated into "post nuclear supernatant" ("PNS", Lane 1), soluble ("Sol", Lane 2) and membrane-associated/insoluble protein fractions. The membrane-associated/insoluble protein fraction was further fractionated according to differential solubility in 100 mM $NaCO_3$ ("pH 11.1", Lanes 5 and 6) or buffers containing 1 M NaCl (Lanes 4 and 5) or 1 % Triton X-100 (Lanes 7 and 8). Proteins released from membranes by each treatment were present in the solubilised membrane ("Sol Memb") fractions (Lanes 3, 5 and 7) while the remaining membrane-associated and insoluble proteins were present in the pellet ("Pel") fractions (Lanes 4, 6 and 8). Molecular mass standards are shown on the left of each blot in kDa while VDAC and His-REP-V5 are indicated on the right.

Initial solubility studies showed that His-REP-V5 was predominantly insoluble. Repeated attempts at solubilisation in the presence of 8M urea were unsuccessful and the purification of the replicase using Ni-affinity purification was equally ineffective (data not shown). The frequent use of high concentrations of urea in the solubilisation of misfolded and aggregated proteins through the stabilisation of non-native polypeptide conformations (Bennion and Daggett, 2003) implies that the insolubility of His-REP-V5 is probably due to a strong, membrane-association rather than misfolding or aggregation.

Subcellular fractionation of cells expressing the HaSV replicase was conducted with the aim of demonstrating the membrane-association of the HaSV replicase and identifying the type of interaction involved. The full length His-REP-V5 remained in the membrane-associated/insoluble protein

fractions following treatment with high salt, alkaline pH and non-ionic detergent. The fractionation protocol was always performed at 4 °C in an attempt to prevent the proteolytic degradation of His-REP-V5 that was consistently observed, even in the presence of protease inhibitors. This meant that the protein fractions that pelleted in the presence of Triton X-100 would also include DRMs, naturally occurring cellular membranes that, at 4 °C, retain their protein content even in the presence of high concentrations of non-ionic detergents (reviewed in Anderson and Jacobson, 2002; Zheng and Foster, 2009). Attempts at further purification of DRMs by membrane floatation were unsuccessful and His-REP-V5 was not detected, largely due to the poor sensitivity of the anti-REP_{1-218}(b) antibodies (data not shown).

Analysis of the C-terminal degradation products detected by anti-REP_{1-218}(b) antiserum, generated against the N-terminal 218 amino acids of the HaSV replicase, showed a propensity to fractionate differently to the full length His-REP-V5. Notably, a significant proportion of the 110 and 90 kDa fragments were detected in the soluble fraction, with the remaining 90 kDa fragment being soluble in the presence of 1 % Triton X-100. Analysis of the HaSV replicase sequence reveals that protein fragments spanning from the N-terminus to either side of the RdRp domain would have theoretical molecular masses of approximately 97 and 152 kDa respectively. These data suggest that a region within the RdRp domain may be involved in the association of His-REP-V5 with membrane-associated/insoluble protein fractions.

While the solubility and membrane association of both His-REP-V5 could not be conclusively established in the experiments described in this chapter, there is evidence that these proteins are not present in insoluble aggregates. Firstly, the precipitation of His-REP-V5 continues unaffected by incubation with 8 M urea, which can be successfully used in the solubilisation of most insoluble aggregates. In addition, proteins present in insoluble aggregates and inclusion bodies tend to be protected to some degree from proteolytic

degradation, while His-REP-V5 shows significant and relatively rapid degradation during purification, even at 4 °C and in the presence of protease inhibitors. Finally, His-REP-V5 degradation products were detected in soluble and solubilised membrane-associated fractions, meaning that C-terminal degradation of the replicase beyond the RdRp domain resulted in liberation of those polypeptides from membrane-associated/insoluble fractions.

While the high levels of protein produced through the baculovirus-mediated expression of the HaSV replicase is necessary for the detection of the replicase using western analysis, the system inherently has significant shortcomings. Most notably, the overexpression of the replicase could hamper proper folding and/or trafficking by overloading cellular chaperone and transport machinery. The lack of any *in vivo* studies on the membrane-association of the HaSV replicase and the expression of His-REP-V5 in the absence of any other HaSV proteins makes it difficult to determine whether the apparent membrane-association of the recombinant replicase is representative of the natural replicase-host interactions or an artefact generated by the experimental system. The following chapter addresses this question by comparison of these results with similar data obtained from PrV-infected MG8 cells, the only available tissue culture system for studying *in vivo* tetravirus replication, and deletion mutants expressed in both experimental systems.

CHAPTER 5

CHARACTERISATION OF THE HaSV REPLICASE LOCALISATION DOMAINS

5.1 INTRODUCTION

The association of vRNA replication complexes with host-derived membranes is usually driven either by the replicase or one or more of its cleavage products. In the case of HaSV, the 187 kDa replicase appears to be the only viral replication protein and, as a result, is thought to carry sufficient information for the generation and targeting of vRNA replication factories. This hypothesis was investigated (Chapter 3; Short *et al*., 2010) with the expression of $REP_{1\text{-}1704}$-EGFP producing punctate structures in HeLa and Sf9 cells in the absence of other viral proteins and vRNA. Data already presented in this thesis imply that at least two regions may be involved in the localisation of the HaSV replicase. In the first instance, the suppression of localisation when EGFP was fused to the N-terminus of the replicase (Section 3.3.1) suggested that sequences at or near the N-terminus may be important in localisation. Secondly, the differential fractionation of His-REP-V5 degradation products implied that sequences within the RdRp domain were responsible for directing membrane association (Section 4.3.4).

This chapter describes the characterisation of two localisation domains by expressing a series of EGFP-fused replicase deletion mutants in HeLa and BHK-21 cells. In addition, a fluorescence microscopy-based method for the analysis of the membrane association of proteins in whole cells was developed and used to analyse the membrane interactions of a subset of replicase-EGFP fusion proteins in HeLa and Sf9 tissue culture cells. Finally, these results were compared to data obtained from the fractionation of PrV-infected MG8 cells, the only available *in vivo* tetravirus replication system.

5.2 MATERIALS AND METHODS

5.2.1. Recombinant plasmids for the expression of replicase-EGFP deletion mutants

Restriction maps of the recombinant plasmids used in the experiments described in this chapter are shown in Figure 5.1 and the cloning strategies used to construct each plasmid are outlined in Appendix A. A list of the constructs including the coordinates of HaSV replicase fragments can be found in Table 5.1. Recombinant plasmid DNA was transfected into cells on 13 mm glass coverslips as described in Section 3.2.2 and fixed within 24 hours of transfection using 4 % paraformaldehyde (w/v) in PBS for 15 minutes before being mounted on glass slides using Fluorescent Mounting Medium.

5.2.2. Statistical analysis of N- and C-terminal HaSV replicase-EGFP deletion mutants

At least 100 fields of view were imaged using a Zeiss LSM 510 META laser scanning confocal microscope with a 63x objective lens and a standard configuration for the detection of EGFP fluorescence in cells expressing replicase-EGFP fusion proteins. Cells were scored according to the distribution of the EGFP fluorescence into one of the three dominant distributions: “Cytosolic + Nuc”, a cytosolic distribution of EGFP fluorescence, with EGFP also present in the nucleus; “Cytosolic – Nuc”, cytosolic EGFP fluorescence excluded from the nucleus; and “Punctate”, a punctate cytosolic pattern with little to no cytosolic EGFP fluorescence. This analysis was repeated in duplicate by two “double-blind” analysts, who had no knowledge of which dataset represented which deletion mutant. The percentage of cells falling into each distribution from all three analyses over three repeats were summed, averaged and the standard deviation calculated.

Table 5.1: Plasmids used for the expression of HaSV replicase-EGFP fusion proteins.

Plasmid	Promoter	EGFP Fusion	Expressed Protein	Description of Construction
pEGFP-N1	CMV	-	EGFP	ClonTech
pJRS7	CMV	C-terminal	REP_{1-1704}-EGFP	A.5
pJRS7 N44Δ	CMV	C-terminal	$REP_{45-1704}$-EGFP	A.9
pJRS12	CMV	C-terminal	REP_{1-100}-EGFP	A.10
pJRS15	CMV	C-terminal	REP_{1-1368}-EGFP	A.11
pJRS34	CMV	C-terminal	REP_{1-1304}-EGFP	A.14
pJRS32	CMV	C-terminal	REP_{1-1241}-EGFP	A.13
pJRS16	CMV	C-terminal	REP_{1-1159}-EGFP	A.12
pJRS8	CMV	N-terminal	EGFP-REP_{1-1704}	A.6
pJRS4	CMV	N-terminal	EGFP-REP_{1-541}	A.6
pCW56	hr/AcMNPV (insect)	-	EGFP	Walter, 2008
pJRS26	hr/AcMNPV (insect)	C-terminal	REP_{1-1704}-EGFP	A.7
pJRS26 2A	hr/AcMNPV (insect)	C-terminal*	REP_{1-1704}-2A-EGFP	A.15

EGFP fusions are N- or C-terminal in relation to the replicase. "" indicates that the EGFP fusion is preceded by the 2A-like cleavage site from equine rhinitis A virus (ERAV).*

5.2.3. Bioinformatic and deletion analysis of the HaSV replicase N-terminus

The N-terminal 100 amino acids of the alpha-like tetravirus replicases, namely HaSV, DpTV and NβV (GenBank accession numbers EU345431, NP_048059 and YP_025094, respectively), were aligned using T-COFFEE (www.tcoffee.org, accessed 27 February 2010) with all parameters set at their default values. The same sequences were also subjected to secondary structure prediction using J-pred 3 (www.compbio.dundee.ac.uk/www-jpred/, accessed 27 February 2010). The results from the secondary structure prediction were superimposed onto the primary sequence alignment to produce an alignment of the predicted secondary structures.

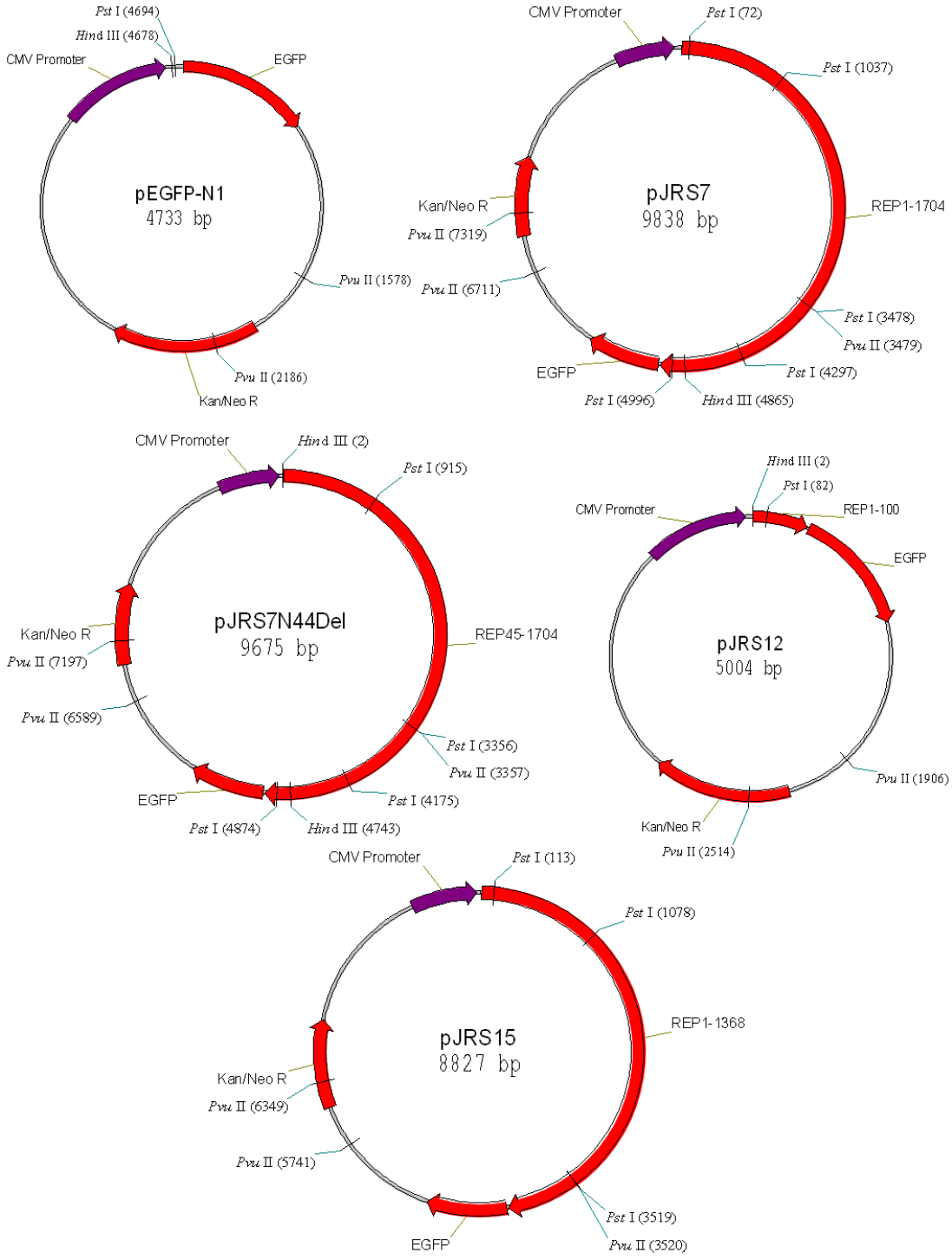

Figure 5.1 (Here and pages 96 and 97): Plasmid maps of the recombinant expression vectors for the expression of HaSV replicase-EGFP deletion mutants in tissue culture cells. Amp R: *β*-lactamase, CMV Promoter: Human cytomegalovirus immediate early promoter, EGFP: enhanced green fluorescent protein, ERAV 2A-like sequence: "2A-like" co-translational processing site derived from equine rhinitis A virus (ERAV), hr/AcMNPV Promoter: hybrid insect promoter, Kan/Neo R: neomycin phosphotransferase.

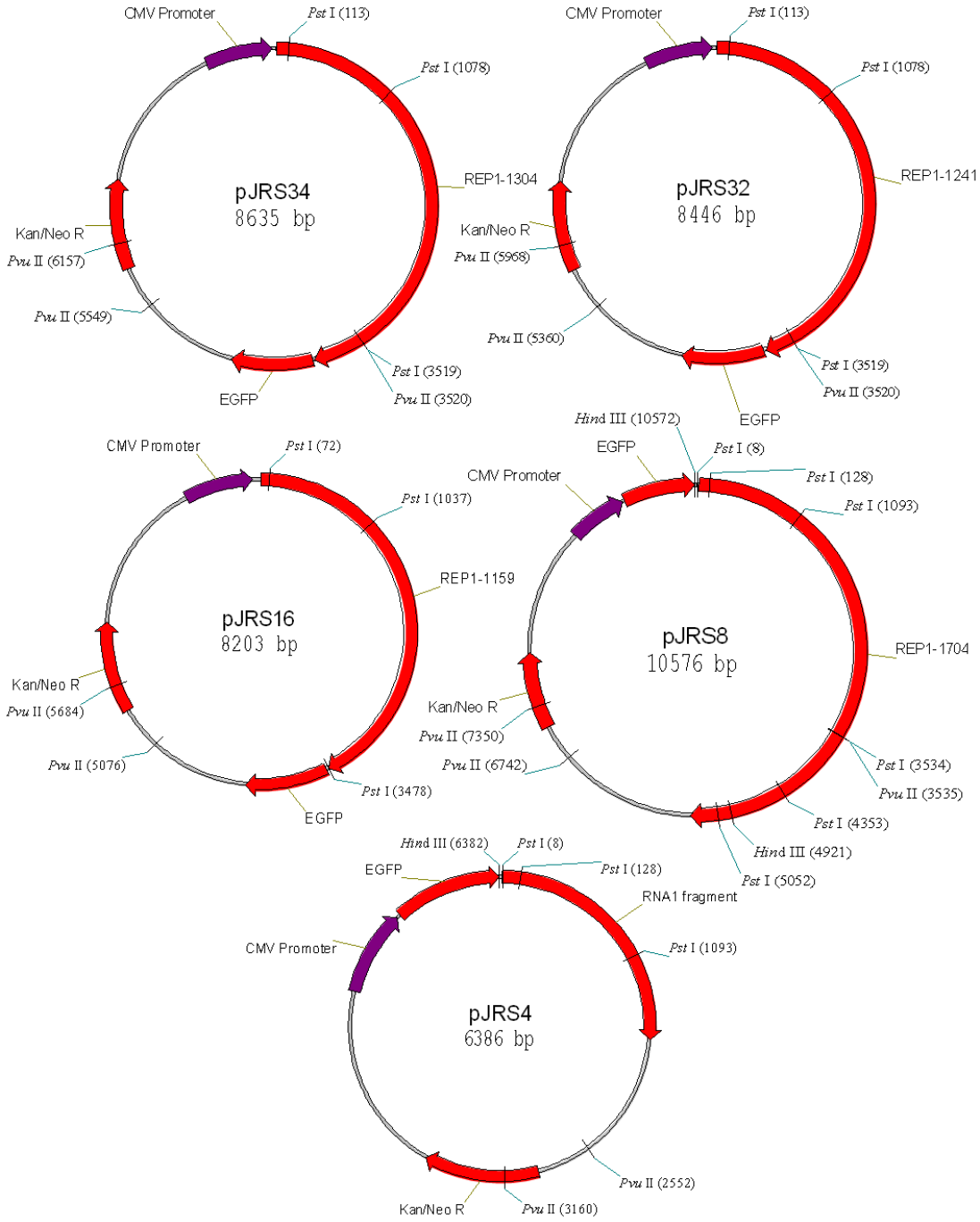

Figure 5.1 Continued: Figure legend on page 95.

A series of N-terminal deletion mutants, each having various predicted secondary structure elements disrupted or deleted, were produced by reverse PCR as described in Appendix A.16. An additional N-terminal domain-swap, replacing the HaSV N-terminus with the corresponding

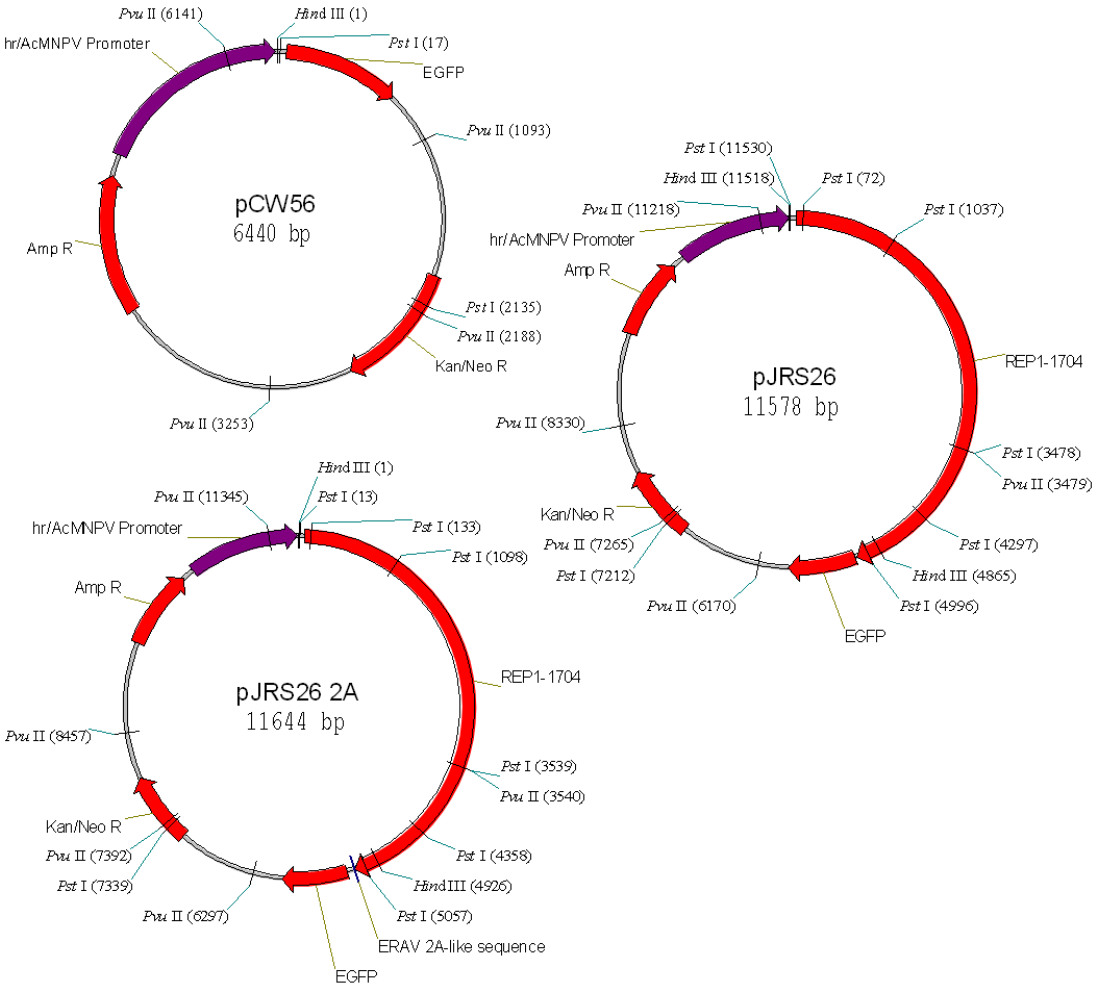

Figure 5.1 Continued: Figure legend on page 95.

sequence from NβV (pJRS7 N-NBV), was also produced (Appendix A.17). The analysis of cells transfected with each of these plasmids was performed using 50 images of transfected cells, representative of at least three experiments. Cells were scored according to three dominant distributions. Both “Cytosolic – Nuc” and “Punctate” were as defined in Section 5.2.2 while the third grouping was called “Mixed” and comprised cells displaying an incomplete localisation of EGFP fluorescence to the punctate structures (i.e. a noticeable punctate distribution with residual cytosolic EGFP fluorescence). The images were analysed by one “double-blind” analyst and the average percentages for the dominant distribution calculated.

5.2.4. Subcellular fractionation and western analysis

Transfected HeLa and baculovirus-infected Sf9 cells were fractionated as outlined in Section 4.2.6. The membrane-associated pellet obtained from transfected HeLa cells was treated with 1 % Triton X-100 to produce solubilised membrane (supernatant) and insoluble (pellet) fractions. In the western analyses, EGFP was detected using monoclonal mouse anti-EGFP antibodies (Sigma, G6539) and PrV p40 was detected in fractionated MG8 cells using polyclonal rabbit anti-p40 antiserum (Walter, 2008). In an attempt to determine whether the replicase was associated with DRMs when the fractionation was carried out at 4 °C, the purification protocol was also carried out at room temperature.

5.2.5. Subcellular fractionation using laser scanning confocal microscopy

HeLa and Sf9 cells were transfected with the purified plasmid DNA as indicated in Section 3.2.2 while PrV-infected MG8 cells were seeded onto coverslips. Approximately 20 hours after transfection cells were incubated in PBS (pH 7.4), 1 M NaCl (in PBS), 100 mM $NaCO_3$ (pH 11.1) or 1 % Triton X-100 (in PBS) for 15 minutes with gentle agitation before fixation using 4 % paraformaldehyde. Samples were subjected to immunofluorescence staining for the detection of CD63 or PrV p40 (Section 3.2.3) before mounting onto glass slides with Fluorescent Mounting Medium.

5.2.6. Construction of the recombinant baculovirus JRS BV2 for the production of His-ΔREP-V5

The plasmid pJRS42 N83Δ, which is derived from the pFastBac^{TM} Dual vector, was constructed as described in Appendix A.18 and is identical to pJRS42 except that the sequence encoding the N-terminal 83 amino acids of

the HaSV replicase are deleted for the production of the replicase deletion mutant, His-ΔREP-V5. The recombinant baculovirus for the expression of His-ΔREP-V5, JRS BV2, was generated, purified and optimised as described in Sections 4.2.1 to 4.2.4.

5.3 RESULTS

5.3.1. The role of N- and C-terminal regions on the localisation of replicase-EGFP fusion proteins

In order to determine which regions of the HaSV replicase were responsible for the development of the punctate structures observed in cells expressing REP_{1-1704}-EGFP, N- and C-terminal deletions were introduced into the replicase sequence and the truncated proteins expressed as EGFP fusions in HeLa and BHK-21 cells (Figure 5.2). The expression of the deletion mutants revealed three distinct distributions of EGFP fluorescence within cells from both cell lines (Figure 5.2, Panel A). Firstly, fluorescence from untagged EGFP was distributed throughout the cytoplasm and appeared to concentrate within the nucleus (labelled “Cytosolic + Nuc”). A cytosolic, extra-nuclear distribution was observed for a number of the deletion mutants (designated “Cytosolic – Nuc”) as was the “Punctate” localised distribution, previously observed for REP_{1-1704}-EGFP. The proportion of cells displaying each dominant distribution, expressed as a percentage of the total number of cells counted, is shown in Figure 5.2 (Panel B).

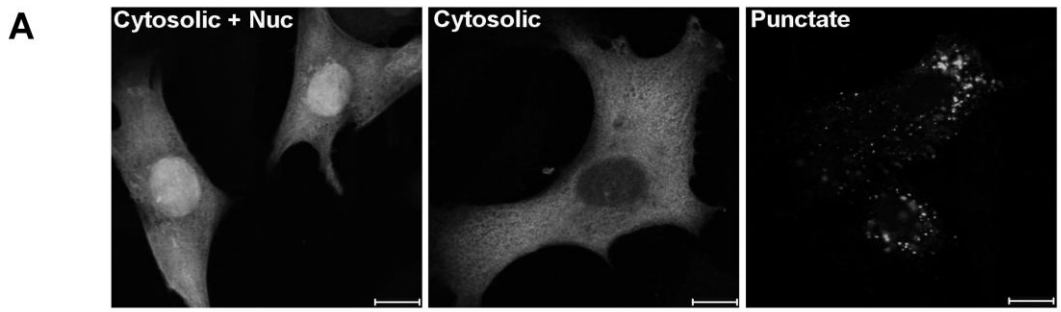

B

		Dominant distribution	% (+/- SD) * HeLa	BHK
HaSV Rep	MT Hel RdRp			
EGFP		Cytosolic + Nuc	97 (+/-5)	98 (+/-2)
REP_{1-1704} EGFP	1 1704	Punctate	94 (+/-2)	97 (+/-2)
$REP_{45-1704}$ EGFP	45 1704	Cytosolic - Nuc	97 (+/-1)	95 (+/-3)
REP_{1-100} EGFP	1 100	Cytosolic + Nuc	97 (+/-2)	ND
REP_{1-1368} EGFP	1 1368	Punctate	86 (+/-19)	90 (+/-11)
REP_{1-1304} EGFP	1 1304	Cytosolic - Nuc	99 (+/-1)	ND
REP_{1-1241} EGFP	1 1241	Cytosolic - Nuc	98 (+/-2)	ND
REP_{1-1159} EGFP	1 1159	Cytosolic - Nuc	98 (+/-3)	89 (+/-6)
EGFP REP_{1-1704}	1 1704	Cytosolic - Nuc	87 (+/-13)	92 (+/-5)
EGFP REP_{1-541}	1 541	Cytosolic - Nuc	97 (+/-2)	ND

Figure 5.2: Distribution of HaSV replicase deletion mutants fused to EGFP. The dominant distributions of EGFP fluorescence observed are shown in Panel A (HeLa cells) with “Cytosolic + Nuc” referring to a cellular distribution similar to that observed for EGFP. The distributions indicated by “Cytosolic – Nuc” and “Punctate” represent cytosolic EGFP fluorescence that is excluded from the nucleus and small localised structures distributed throughout the cytosol respectively. Panel B contains schematic diagrams of the HaSV replicase deletion mutants with the positioning of their respective EGFP fusions (left) as well as the dominant distribution observed for each (centre) and the percentage of cells counted with the dominant distribution (right). MT: methyltransferase, Hel: helicase, RdRp: RNA-dependent RNA polymerase, ND: not determined. Scale bar = 10 µm.

As expected, native EGFP displayed a “Cytosolic + Nuc” distribution in over 97% of the cells scored, while the distribution of REP_{1-1704}-EGFP fluorescence was predominantly “Punctate” as observed before (Section 3.3.1). Deletion of the N-terminal 44 amino acids ($REP_{45-1704}$-EGFP) resulted in a “Cytosolic – Nuc” distribution, similar to that observed for EGFP-REP_{1-1704}, indicating that the N-terminus of the protein may be required for localisation. The observation that the N-terminal 100 amino acids alone were insufficient for localisation (REP_{1-100}-EGFP), suggested that there were other regions involved in replicase targeting. In an attempt to identify these regions, a series of C-terminal deletions were expressed and analysed as above. When 336 amino acids were removed (REP_{1-1368}-EGFP), the distribution of the protein was still predominantly “Punctate”, indicating that all the requirements for targeting were still present. However, deletion of a further 64 amino acids from the C-terminus of the replicase (REP_{1-1304}-EGFP) resulted in a “Cytosolic – Nuc” pattern in the majority of cells scored (similar results were also obtained for REP_{1-1241}-EGFP and REP_{1-1159}-EGFP). These data strongly imply the presence of at least two regions, one at the N-terminus and the other at the C-terminus of the RdRp domain, between residues K^{1304} and P^{1368}, that may be responsible for the targeting of the HaSV replicase. Similar results were observed in BHK-21 cells (Figure 5.2, Panel B). It is unclear whether the loss of localisation in the C-terminal deletion mutants was due to the deletion/disruption of the targeting domain or the disturbance of secondary, tertiary or even quaternary structures.

5.3.2. Identification of potential targeting domains in the HaSV replicase N-terminus

A further analysis of the N-terminal region immediately upstream of the MT domain was undertaken to identify potential domains that might function in localisation of the HaSV replicase. Two α-helices, separated by a conserved

LDF tripeptide motif in a well conserved “linker region”, were predicted within the first 45 amino acids of all three replicase sequences (HaSV, DpTV and NβV) (Figure 5.3). In addition, 20 amino acid positions showed conservation of charge. These consisted of eight charged (DERKH), two aromatic (YFW) and ten non-polar (AGVLIPMC) amino acids and were evenly spread across the three regions with eight present in “Helix I” and six in each the “linker region” and “Helix II”. The conservation of charge across the N-terminal region and the significant similarity between the predicted secondary structures suggest the possibility of a common localisation mechanism for the alpha-like tetravirus replicases, which may require functions associated with this helix-linker-helix region.

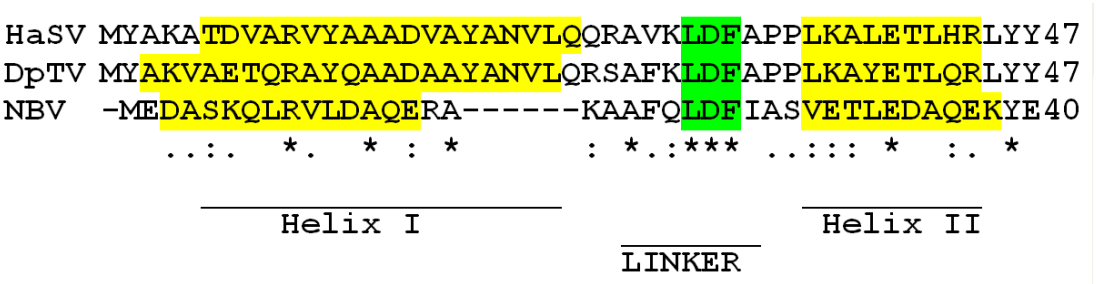

Figure 5.3: Primary amino acid sequence alignment of the alpha-like tetravirus replicases displaying predicted secondary structures. Predicted α-helices are highlighted in yellow with the conserved tripeptide (LDF) within the “linker region” in green. “*”: exact match of aligned amino acids, “:”: conserved amino acids, “.”: semi-conserved amino acids, HaSV: *Helicoverpa armigera* stunt virus, DpTV: *Dendrolimus punctatus* tetravirus, NβV: *Nudaurelia capensis* β virus.

5.3.3. The effects of the disruption of predicted N-terminal secondary structures on localisation

In order to further assess the role of each of the putative N-terminal structural elements on the targeting of the replicase to the punctate structures, a series of five deletion mutants was generated. The requirement of a free N-terminus was analysed through the addition of an N-terminal 6xHis tag. In

addition, a “domain-swap” chimeric protein was produced in which the N-terminal region from HaSV was substituted with the corresponding region from NβV (pJRS7 N-NBV) (Figure 5.4, Panel A).

HeLa cells expressing the EGFP-fused N-terminal deletion mutants displayed both the “Cytosolic – Nuc” distribution (Section 5.3.1) and a “Mixed” distribution where punctate structures were obvious but a significant amount of cytosolic fluorescence was also detected (Figure 5.4, Panel B, right). All of the N-terminal deletion mutants exhibited a decrease in localisation efficiency, displaying either the “Mixed” or “Cytosolic – Nuc” distributions. The first N-terminal deletion mutant (pJRS7 RPCR1) had helix I removed (Figure 5.4, Panel A) and displayed a “Mixed” EGFP fluorescence distribution in 60 % of the cells scored (Figure 5.4, Panel B). A partial helix I deletion was generated in the replicase CDS of pJRS7 RPCR2 (Figure 5.4, Panel A). HeLa cells expressing this N-terminal deletion mutant exhibited “Cytosolic – Nuc” EGFP fluorescence in 84 % of cells (Figure 5.4, Panel B). Similar results were obtained for the other three N-terminal deletion mutants. In 88 % of the cells expressing the EGFP fusion proteins expressed from pJRS7 RPCR3 and pJRS7 RPCR4, which encoded full or partial helix I deletions respectively in addition to the deletion of the full linker region and part of helix II (Figure 5.4, Panel A), the “Cytosolic – Nuc” distribution was observed (Figure 5.4, Panel B). Finally, the deletion mutant in which only the linker region and part of helix II was deleted (pJRS7 RPCR5) (Figure 5.4, Panel A) showed cytosolic EGFP fluorescence that was excluded from the nucleus (Cytosolic – Nuc) in 92 % of the cells counted (Figure 5.4, Panel B).

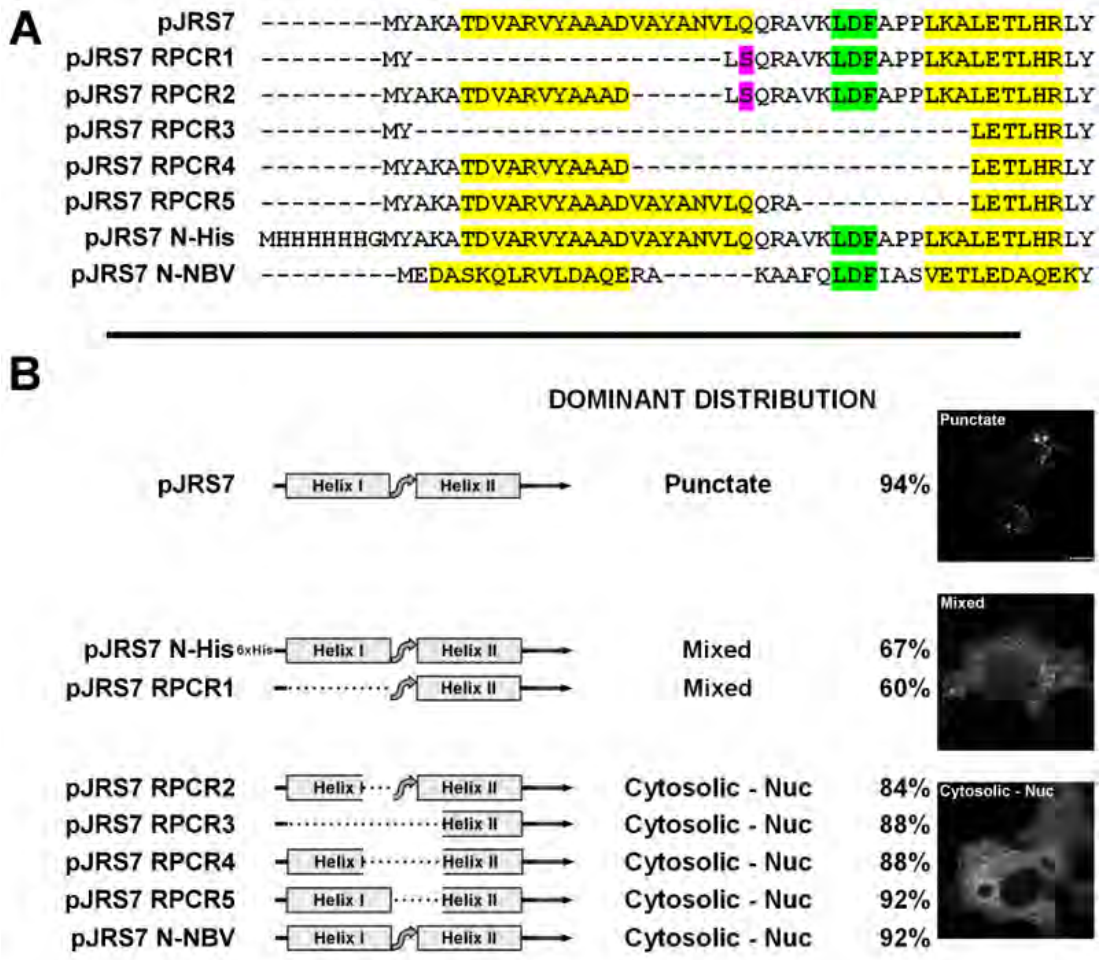

Figure 5.4: Distribution of N-terminal HaSV replicase mutants fused to EGFP. Panel A contains an alignment of the various N-terminal mutants generated while Panel B shows schematic representations of the respective mutants (left), the dominant distribution observed for each mutant (centre) along with the percentages of cells exhibiting each of the dominant distributions (right). Amino acids within the predicted α-helices of the alpha-like tetravirus replicases are highlighted in yellow and the conserved "linker region" tripeptide is highlighted in green. The single Q to S point mutation introduced in the cloning process is highlighted in purple. In Panel B the predicted helices are represented by grey boxes while the "linker region" is represented by the bent arrow between the helices. Scale bar = 10 μm.

The fusion of a 6xHis tag to the N-terminus of the HaSV replicase CDS (pJRS7 N-His) (Figure 5.4, Panel A) also resulted in a decrease in localisation of efficiency and produced a "Mixed" distribution in 67 % of the cells scored (Figure 5.4, Panel B). Interestingly, even though the predicted secondary structure elements were consistent between the HaSV and NβV sequences, the NβV sequence was not able to direct the targeting of the chimeric replicase, with the chimeric NβV/HaSV replicase sequence

(pJRS7 N-NBV) (Figure 5.4, Panel A) producing “Cytosolic – Nuc” EGFP fluorescence in 92 % of the cells counted (Figure 5.4, Panel B). It is worth noting that the two proteins displaying the “Mixed” distribution produced significantly lower percentages of their dominant distribution (60 and 67 % as compared to 84 to 92 % for the other mutants). This was interpreted as a decrease in localisation efficiency in these proteins rather than the complete abrogation of targeting as in the other mutants. Another interesting observation was that the partial removal of helix I (pJRS7 RPCR2) resulted in a “Cytosolic – Nuc” distribution while the complete removal of the same helix (an additional 14 amino acids) resulted in an apparent increase in targeting efficiency, possibly due to poor presentation of the remaining structural elements caused by the partial helix I.

The linker region appears to be required for the localisation of the replicase to the punctate structures although the partial deletion of helix I seems to inhibit its function, possibly through steric hindrances produced by the modification of the predicted secondary structure. The relative importance of the secondary structures, and the specific sequences contained within each of them, remains unclear and requires further investigation, although helix I may be dispensable. The data related to the importance of a free N-terminus are inconclusive and the effect of the small 6xHis tag may be indicative of a minor, complementary role although the decrease in targeting efficiency could simply be due to the introduction of charge into the region.

5.3.4. The subcellular distribution of replicase-EGFP fusion proteins in transfected tissue culture cells

Initial attempts at determining the type and degree of membrane association of the deletion mutants were made using the biochemical fractionation protocol described in Chapter 4. However, both anti-$REP_{1\text{-}218}$(b) and monoclonal anti-EGFP antibodies were unable to detect $REP_{1\text{-}1704}$-EGFP in

transfected HeLa cells (Figure 5.5, data not shown). The most likely reason for this was the low transfection efficiencies associated with the large plasmids used for the expression of the replicase-EGFP fusion proteins, especially in HeLa cells (Section 3.3.1).

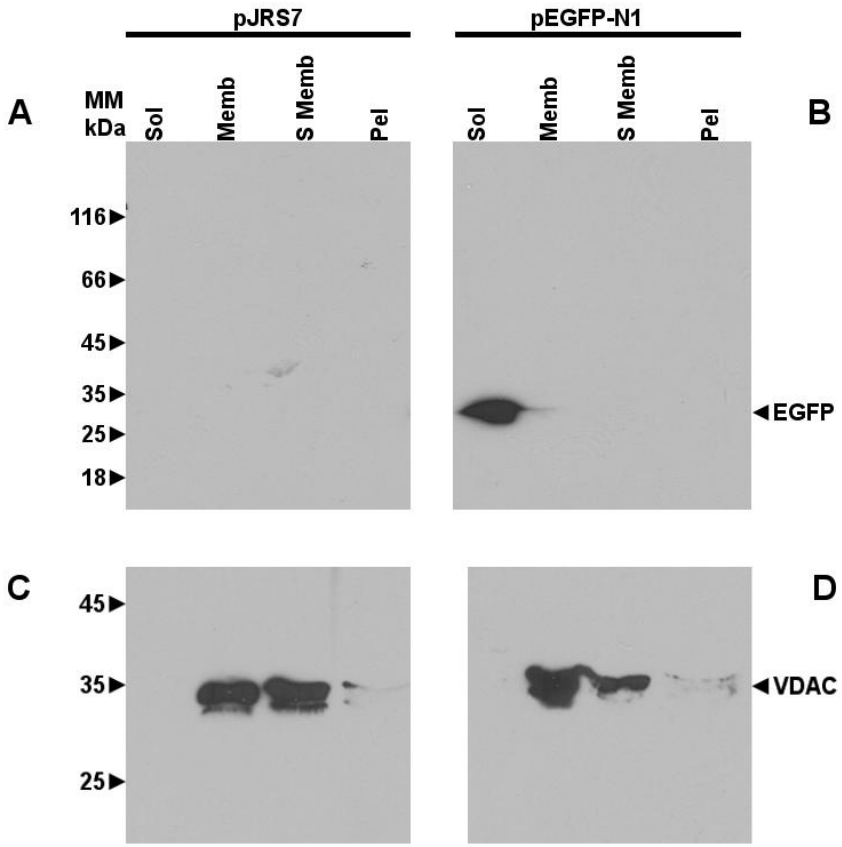

Figure 5.5: Distribution of EGFP in subcellular fractions of transfected HeLa cells. Western analysis of soluble ("Sol"), membrane associated ("Memb"), solubilised membrane ("S Memb") and insoluble ("Pel") fractions of HeLa cells transfected with either pJRS7 (Panels A and C) or pEGFP-N1 (Panels B and D). EGFP and VDAC were detected using anti-EGFP (Panels A and B) or anti-VDAC (Panels C and D) respectively, both at dilutions of 1:500. Molecular mass standards are indicated on the left in kDa while EGFP and VDAC are indicated on the right.

Therefore, it was decided to characterise the membrane association of the deletion mutants using a fluorescence microscopy-based protocol modified and expanded from Matthews *et al.* (2009). Transfected HeLa cells were incubated in the presence of buffer containing high salt (1 M NaCl), alkaline pH (11.1) or 1 % Triton X-100 (Figure 5.6). The cellular membrane-associated protein CD63 (Metzelaar *et al.*, 1991), the fluorescent tagged

mitochondrial marker DsRed2-Mito (carrying the mitochondrial targeting signal from subunit VIII of human cytochrome c oxidase) (ClonTech) and cytosolic EGFP were used for validation of the fractionation system (Figure 5.6, Images a to j). The cytosolic control (EGFP) showed that incubation of cells in high salt and high pH buffers was insufficient for the disruption of the plasma membrane and therefore did not result in the release of the cytosolic content into the extracellular environment (Figure 5.6, Images i and j). The addition of Triton X-100 however, resulted in disruption of the plasma membrane and the release of EGFP. Neither the high salt nor alkaline pH buffers had any effect on the distribution of the membrane-associated controls, CD63 or DsRed2-Mito (Figure 5.6, Images b, c, f and g). However, following the addition of Triton X-100, DsRed2-Mito was no longer detectable and the amount of CD63 present in the punctate structures was significantly, but not entirely diminished (Figure 5.6, Image d). This result is consistent with reports that CD63 is a member of the tetraspannins, a group of proteins that are often detected in DRMs (Section 1.5.2; Metzellar *et al.*, 1991; Maeker *et al.*, 1997; Berditchevski, 2001; Claas *et al.*, 2001; Levy and Shoham, 2005; Zheng and Foster, 2009).

The fractionation profile of REP_{1-1704}-EGFP resembled that of CD63, with the distribution remaining unchanged in the presence of high salt or alkaline pH but being diminished in the presence of Triton X-100 (Figure 5.6, Images k to n). For both CD63 and REP_{1-1704}-EGFP, treatment with the non-ionic detergents resulted in a concentration of the remaining fluorescence in regions close to the nucleus in all the cells in which fluorescence was detected (Figure 5.6, Images d and n), indicating that REP_{1-1704}-EGFP may be associating with DRMs similar to those associated with CD63. The loss of cell volume due to the permeabilisation of the plasma membrane could also account for the apparent condensation of fluorescence-labelled structures.

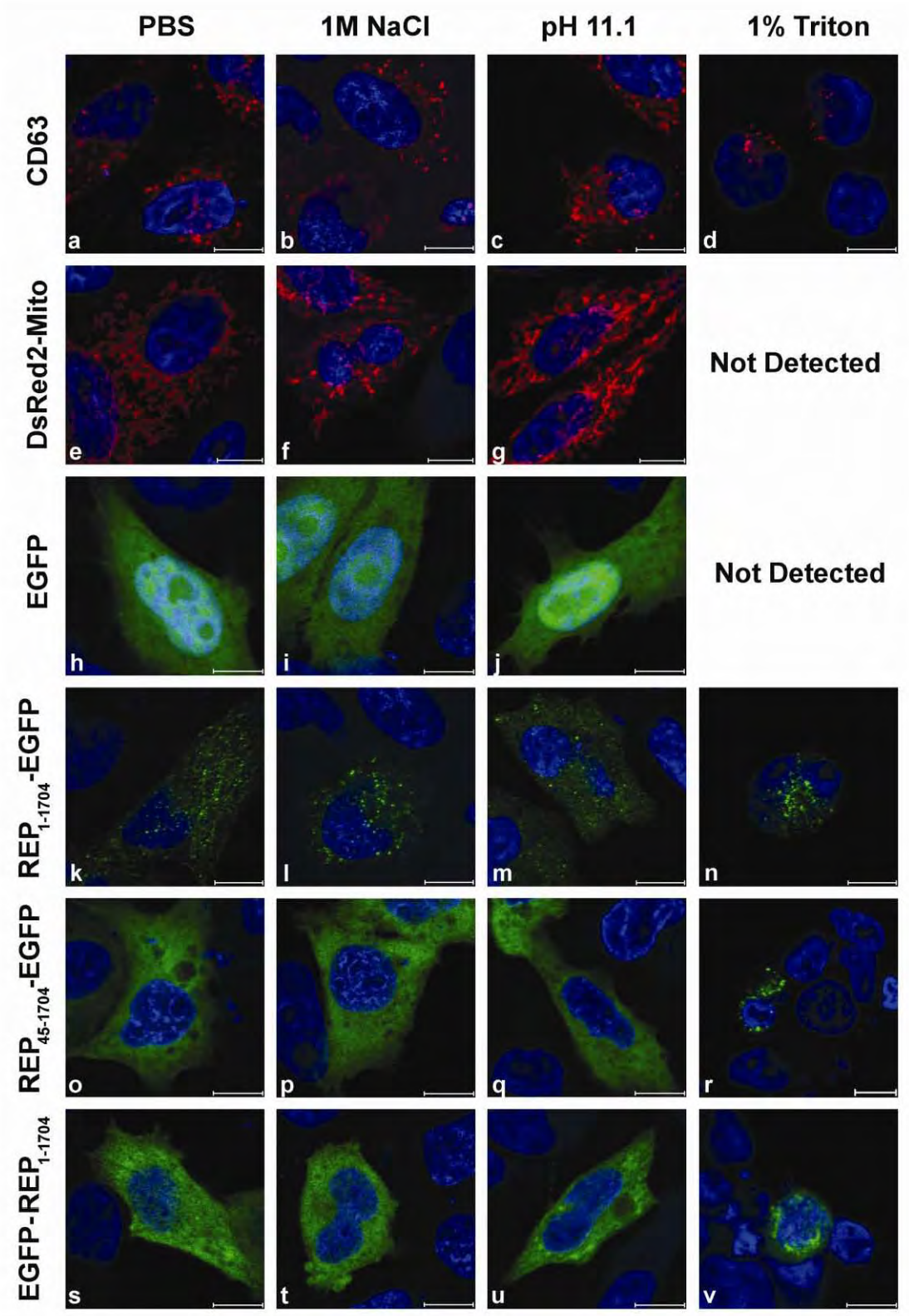

Figure 5.6: Figure legend on pg 109.

Figure 5.6 (pg 108): Differential solubilisation of proteins from transfected HeLa cells using high salt, alkaline pH or Triton X-100. HeLa cells were transfected with plasmids encoding EGFP (h to j), REP_{1-1704}-EGFP (k to n), EGFP-REP_{1-1704} (s to v), $REP_{45-1704}$-EGFP (o to r) or a mitochondrial-targeted DsRed variant (DsRed 2-Mito) (e to g) before being fractionated and prepared for imaging using confocal fluorescence microscopy. The late endosome marker protein CD63 was detected by immunofluorescence microscopy using monoclonal mouse anti-CD63 antibodies (a to d), which were visualised using Alexa Fluor 546-conjugated goat anti-mouse secondary antibodies. PBS: phosphate buffered saline, 1 M NaCl: PBS + 1 M NaCl, pH 11.1: 100 mM $NaCO_3$ (pH 11.1), 1% Triton: PBS + 1 % Triton X-100. "Not Detected" indicates samples where no fluorescence signal associated with the appropriate fluorophore was observed across an entire coverslip in both experiments. Scale bars = 10 µm.

Both the deletion mutant and the N-terminal EGFP fusion that were tested ($REP_{45-1704}$-EGFP and EGFP-REP_{1-1704}) displayed the typical "Cytosolic – Nuc" distribution, which was unaffected by the presence of high salt or alkaline pH, consistent with a soluble cytosolic distribution similar to that of EGFP (Figure 5.6, Images o to q and s to u). Treatment with 1 % Triton X-100 resulted in the loss of the cytosolic fluorescence (Figure 5.6, Images r and v) suggesting that the majority of each deletion mutant was present in the cell as a soluble cytoplasmic protein, released from the cell when the plasma membrane was permeabilised. However, a small amount of fluorescence was detected in punctate structures similar to those observed for REP_{1-1704}-EGFP and CD63 (Figure 5.6, Images d, n, r and v). While interpretation of this data is limited because the percentage of transfected cells in which this phenotype was observed could not be determined, the data does indicate that deletion mutants previously thought of as cytosolic ("Cytosolic – Nuc") may, in fact, be able to localise to the punctate structures, albeit either at a far slower rate or with a significantly lower affinity.

This experiment was repeated using Sf9 cells, but the lack of suitable antibodies directed against cellular membrane-associated protein markers meant that validation of the protocol as was done for HeLa cells, was not possible. As was the case for HeLa cells, EGFP was liberated in Sf9 cells transfected with pCW56 only after treatment with Triton X-100 (Figure 5.7, Images a to c). Similarly, REP_{1-1704}-EGFP behaved as in HeLa cells and

remained unaffected by both the high salt and alkaline pH treatments only to be partially released by treatment with Triton X-100 (Figure 5.7, Images d to g). Cells expressing REP_{1-1704}-2A-EGFP were also analysed. REP_{1-1704}-2A-EGFP consists of the HaSV replicase and EGFP sequences separated by the "2A-like" processing site from Equine rhinitis A virus (ERAV). This consensus sequence has been shown to cleave with an efficiency of >99 % in a reporter-based system and to produce very low levels of the full length product (<5 %) (Donnelly *et al.*, 2001a, 2001b). The processed EGFP, which would thus be expected to represent approximately 99 % of the expressed EGFP, behaved similarly to untagged EGFP and was released in the presence of 1 % Triton X-100. The remaining, uncleaved EGFP was detectable in some cells in a similar distribution to that observed for REP_{1-1704}-EGFP (Figure 5.7, Images g and k).

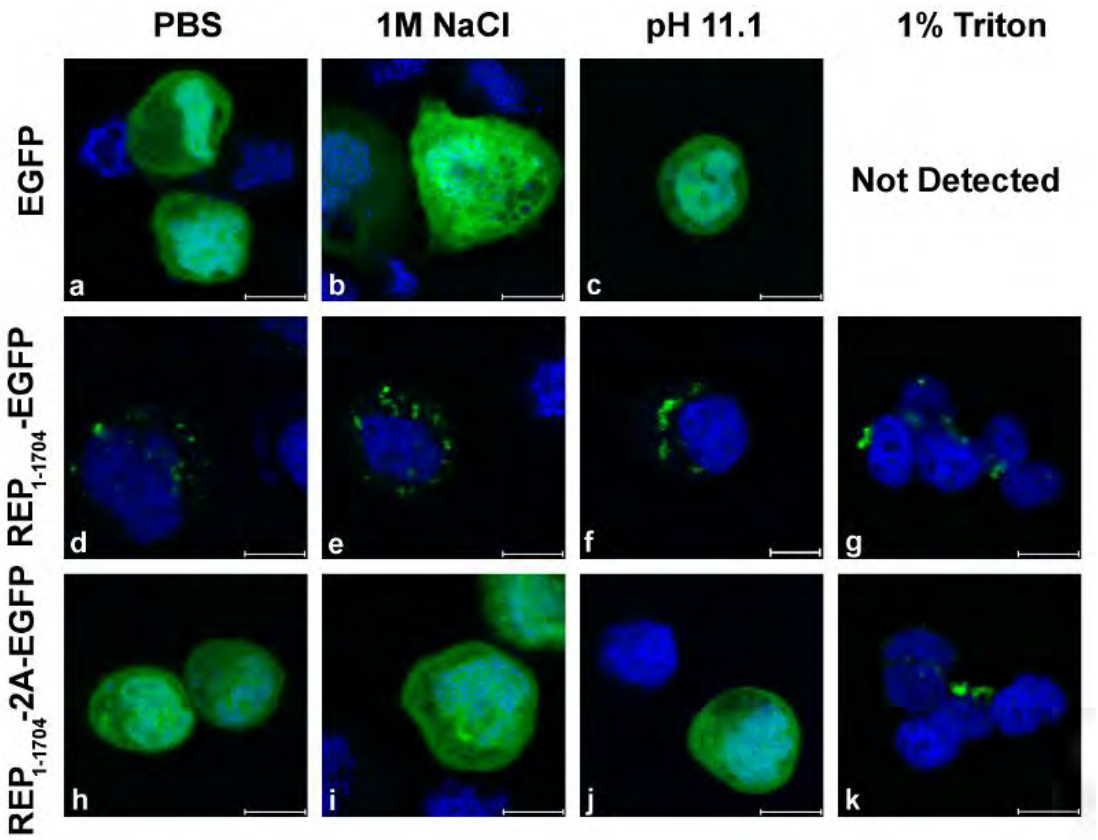

Figure 5.7: Legend on pg 111.

Figure 5.7 (pg110): Differential solubilisation of proteins from transfected Sf9 cells using salt, alkaline pH or Triton X-100. Sf9 cells were transfected with plasmids encoding EGFP (a to c), REP_{1-1704}-EGFP (d to g) or REP_{1-1704}-2A-EGFP (h to k) before being fractionated and prepared for imaging using confocal fluorescence microscopy. PBS: phosphate buffered saline, 1 M NaCl: PBS + 1 M NaCl, pH 11.1: 100 mM $NaCO_3$ (pH 11.1), 1% Triton: PBS + 1 % Triton X-100. "Not Detected" indicates samples were no EGFP fluorescence was observed across an entire coverslip in both experiments. Scale bars = 10 µm.

5.3.5. Subcellular fractionation of Sf9 cells infected with the recombinant baculovirus JRS BV2

The data presented in Section 5.3.1 showed that deletion of the N-terminus of the replicase resulted in loss of targeting ability in HeLa cells expressing replicase-EGFP fusion proteins, i.e. the removal of the N-terminal 44 amino acids from the replicase resulted in abrogation of the punctate distribution of EGFP fluorescence (Figure 5.2, Panel B). This raised the possibility that an N-terminal replicase deletion mutant might result in a soluble recombinant polypeptide that could be used for antibody production. Accordingly, the recombinant baculovirus, JRS BV2, expressing a replicase CDS with the N-terminal 83 amino acids replaced with a 6xHis tag and a V5 epitope tag fused to the C-terminus (His-ΔREP-V5), was constructed. The expression of the recombinant replicase deletion mutant was confirmed and optimised as for JRS BV1 (Sections 4.2.1 and 4.2.2) and was found to behave similarly, with maximum protein production occurring when cells were infected at an MOI of 5 for a period of four days (data not shown).

Western analysis of fractions generated from Sf9 cells infected with JRS BV2, using anti-REP_{1-218}(b) antiserum, revealed that the subcellular distribution of His-ΔREP-V5 was similar to that of the wild-type protein His-REP-V5 (compare Figure 5.8, Panel B with Figure 4.8, Panel B in Section 4.3.4). In addition, a similar degradation product profile was observed for both His-ΔREP-V5 and His-REP-V5 although additional minor degradation products were detected at approximately 150 and 120 kDa (Figure 5.8,

Panel B). The majority of His-ΔREP-V5 was present in pellet fractions following the treatment of membrane-associated/insoluble fractions with high salt or alkaline pH and in the presence of Triton X-100, which was unexpected (Figure 5.8, Panel B, Lanes 4, 6 and 8). The anti-REP_{1-218}(b) antibodies were only able to detect small amounts of the His-ΔREP-V5 degradation products in both the post nuclear supernatant and soluble protein fractions, likely due to a greater degree of proteolytic degradation of the deletion mutant (Figure 5.8, Panel B, Lanes 1 and 2). Interestingly, the full length His-ΔREP-V5 was not the major protein band detected in any of the fractions, with the 150 and 90 kDa degradation products appearing in greater abundance.

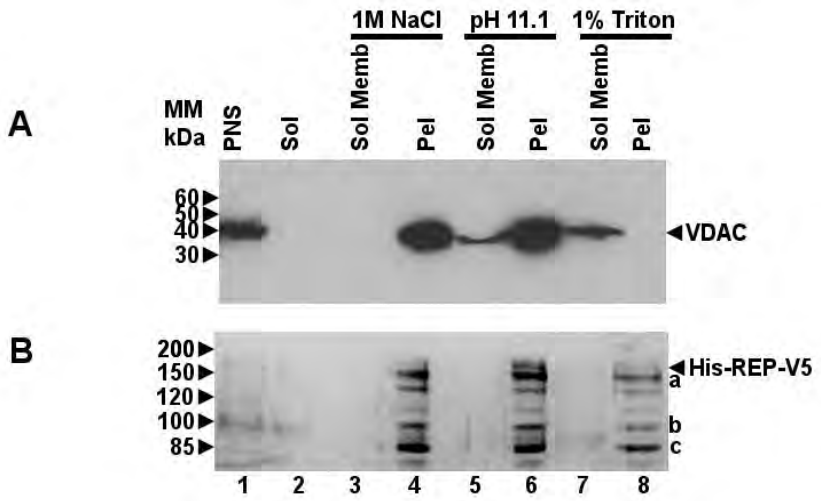

Figure 5.8: Subcellular fractionation of His-ΔREP-V5 performed at 4 °C. Western analysis of fractionated Sf9 cells expressing His-ΔREP-V5 using anti-VDAC (Panel A) or anti-REP_{1-218}(b) (Panel B) antiserum at dilutions of 1:500 and 1:15 000 respectively. Cells were fractionated into "post nuclear supernatant" ("PNS", Lane 1), soluble ("Sol", Lane 2) and membrane-associated/insoluble protein fractions. The latter was further fractionated according to differential solubility in 100 mM $NaCO_3$ ("pH 11.1", Lanes 5 and 6) or buffers containing 1 M NaCl (Lanes 4 and 5) or 1 % Triton X-100 (Lanes 7 and 8). Proteins released from membranes by each treatment were present in the solubilised membrane ("Sol Memb") fractions (Lanes 3, 5 and 7) while the remaining membrane-associated and insoluble proteins were present in the pellet ("Pel") fractions (Lanes 4, 6 and 8). Molecular mass standards are shown on the left of each blot in kDa while VDAC and His-ΔREP-V5 are indicated on the right.

Since the fractionation procedure was performed at 4 °C and would therefore facilitate the purification of DRMs, it was decided to repeat the fractionation experiments at room temperature to determine whether an increase in temperature might have an effect on solubilisation of His-ΔREP-V5 by Triton X-100. There was no change in the fractionation profile of His-ΔREP-V5, although the 90 kDa degradation product was detected in the detergent-solubilised fraction (Figure 5.9, Panel B, Lane 7). The 90 kDa polypeptide was the major protein detected, suggesting increased proteolytic degradation of the recombinant protein at the higher temperature.

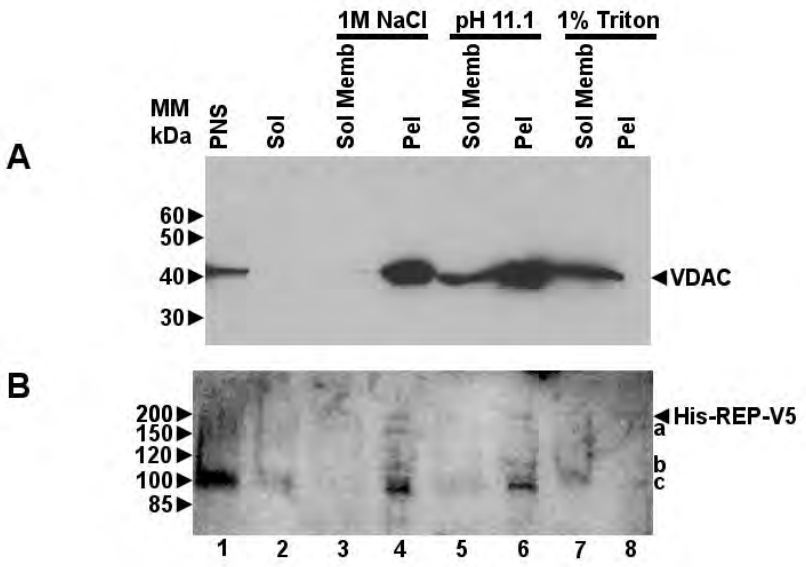

Figure 5.9: Subcellular fractionation of His-ΔREP-V5 performed at room temperature. Western analysis of fractionated Sf9 cells expressing His-ΔREP-V5 using anti-VDAC (Panel A) or anti-REP_{1-218}(b) (Panel B) antiserum at dilutions of 1:500 and 1:15 000 respectively. Cells were fractionated into "post nuclear supernatant" ("PNS", Lane 1), soluble ("Sol", Lane 2) and membrane-associated/insoluble protein fractions. The latter was further fractionated according to differential solubility in 100 mM $NaCO_3$ ("pH 11.1", Lanes 5 and 6) or buffers containing 1 M NaCl (Lanes 4 and 5) or 1 % Triton X-100 (Lanes 7 and 8). Proteins released from membranes by each treatment were present in the solubilised membrane ("Sol Memb") fractions (Lanes 3, 5 and 7) while the remaining membrane-associated and insoluble proteins were present in the pellet ("Pel") fractions (Lanes 4, 6 and 8). Molecular mass standards are shown on the left of each blot in kDa while VDAC and His-ΔREP-V5 are indicated on the right.

5.3.6. Subcellular localisation of the PrV replicase

Given that HaSV does not replicate in tissue culture, it was not possible to correlate data obtained using the recombinant HaSV replicase with the localisation of native replicase in HaSV-infected cells. Currently the only tetravirus known to replicate in tissue culture is PrV (Pringle *et al.*, 2003), but as discussed in Section 1.3.5, there are significant differences between PrV and HaSV. Most important is the fact that the PrV encodes a carmo-like replicase and is expressed as a major (p40) and minor (p104) translation product via the activity of a read-through stop codon.

For the purposes of this study, an important question was whether the PrV replicase was also associated with DRMs in infected cells. MG8 cells, which are persistently infected with PrV, were subjected to the same subcellular fractionation procedures as had been used for the recombinant HaSV replicase (Sections 4.2.6 and 5.2.5) and the PrV replicase (p40/p104) was detected using anti-p40 rabbit polyclonal antiserum. As was the case for His-REP-V5, PrV p40 remained in membrane-associated/insoluble fractions even in the presence of 1 % Triton X-100 (Figure 5.10, Panel B, Lane 8). Differential fractionation of the various degradation products (approximately 25 to 37 kDa in size) was also observed with the largest product being predominanty solubilised by the non-ionic detergent and partially soluble at alkaline pH (Figure 5.10, Panel B, Lanes 5 and 7). The large (minor) translation product (p104) was not detected.

Interestingly, a significant size difference was noted between the VDAC encoded by the Sf9 and MG8 cells (compare Figure 5.9, Panel A and Figure 5.10, Panel A). While the mammalian anti-VDAC antibodies detected a protein co-migrating at approximately 35 kDa in Sf9 cells, the corresponding protein in MG8 cells was present at approximately 20 kDa. This is not unexpected since VDAC homologues in various organisms range

significantly in size from rat VDAC at 30 kDa in size to some human isoforms as small as 16 kDa (Genbank accession numbers: AAH60558 and EAW66284.1 respectively).

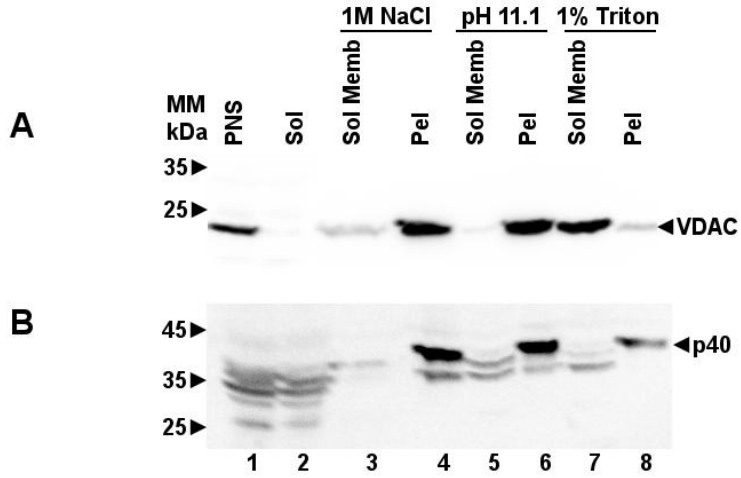

Figure 5.10: Subcellular fractionation of PrV-infected MG8 cells. Western analysis of fractionated MG8 cells using anti-VDAC (A) or anti-p40 (B) antiserum at dilutions of 1:500 and 1:75 000 respectively. Cells were fractionated into "post nuclear supernatant" ("PNS", Lane 1), soluble ("Sol", Lane 2) and membrane-associated/insoluble protein fractions. The latter was further fractionated according to differential solubility in 100 mM $NaCO_3$ ("pH 11.1", Lanes 5 and 6) or buffers containing 1 M NaCl (Lanes 4 and 5) or 1 % Triton X-100 (Lanes 7 and 8). Proteins released from membranes by each treatment were present in the solubilised membrane ("Sol Memb") fractions (Lanes 3, 5 and 7) while the remaining membrane-associated and insoluble proteins were present in the pellet ("Pel") fractions (Lanes 4, 6 and 8). Molecular mass standards are shown on the left of each blot in kDa while VDAC and PrV p40 are indicated on the right.

Finally, the subcellular distribution of p40 in PrV-infected MG8 cells was analysed using the fluorescence microscopy-based fractionation protocol using anti-p40 antiserum for the detection of wild-type p40. This antiserum would also detect the full length PrV replicase, p104, although p40 is hypothesised to be produced in 10-fold excess in infected MG8 cells (Walter *et al.*, 2010). The effects of high salt concentrations and alkaline pH could not be determined since immunofluorescence using the anti-p40 antibodies was inhibited by these treatments. However, as was the case for Sf9 cells expressing $REP_{1\text{-}1704}$-EGFP, incubation of MG8 cells in buffer containing 1 %

Triton X-100 did not completely liberate p40 (Figure 5.11), indicating like the HaSV replicase, the PrV replicase-associated structures were robust and also likely be associated with DRMs.

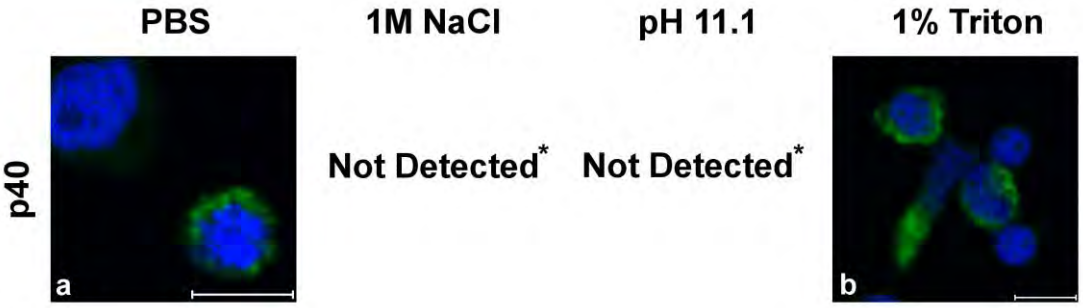

Figure 5.11: Differential solubilisation of p40 from MG8 cells infected with PrV using high salt, alkaline pH or Triton X-100. Persistently infected MG8 cells were fractionated and prepared for imaging using confocal fluorescence microscopy. PrV p40 was detected by immunofluorescence microscopy using rabbit anti-p40 antiserum, in turn detected using FITC-conjugated goat anti-rabbit secondary antibodies. PBS: phosphate buffered saline, 1 M NaCl: PBS + 1 M NaCl, pH 11.1: 100 mM $NaCO_3$ (pH 11.1), 1% Triton: PBS + 1 % Triton X-100. "Not Detected*" indicates where p40 was not detectable, possibly due to disturbance of the antibody-p40 interactions following incubation in the high salt and high pH buffers. Scale bars = 10 µm.

5.4 DISCUSSION

The primary aim of the experiments described in this chapter was to characterise the regions of the HaSV replicase required for the punctate distribution observed in $REP_{1\text{-}1704}$-EGFP-expressing cells. As such, a set of deletion mutants was used to identify two regions, one at the amino terminus and a second within the C-terminal region of the RdRp domain, both of which are required for efficient targeting of the replicase, in the absence of other viral proteins.

Several lines of evidence support a role for the N-terminus in subcellular localisation of the HaSV replicase to punctate structures. First, the addition of EGFP to the N-terminus of the replicase results in a loss of localisation,

while the addition of a 6xHis tag results in a decrease in targeting efficiency. Although the loss of localisation might be simply due to interference resulting from the large size (EGFP) or the positive charge (6xHis tag) of the fusion peptides, a free N-terminus could play a minor role in localisation but is most likely not an absolute requirement for localisation. Second, deletion of the N-terminal 44 amino acids of the replicase results in a largely soluble cytosolic fusion protein when expressed in HeLa cells. However, the N-terminal region is insufficient for the localisation. This is evidenced by the fact that the N-terminal 100 replicase amino acid residues are unable to target EGFP to the punctate structures.

Bioinformatic analysis of the putative N-terminal targeting domain revealed two predicted α-helices separated by eleven amino acids. Analysis of the N-termini of the other two available alpha-like tetravirus replicases, together with multiple alignment of the respective sequences, identified similar predicted secondary structures and charge distribution in the N-termini of both DpTV and NβV. In all three replicases, the two putative helices are separated by 11 to 13 amino acids, with each “linker region” containing an invariant LDF tripeptide. Deletion analysis of the three structural elements (the two helices and the “linker region”) suggested that the entire sequence was important for efficient localisation. Although further investigation is still needed, helix I may only contribute to targeting efficiency and is probably not an absolute requirement for localisation in HeLa cells. Despite the notable similarities between the N-terminal sequences the NβV N-terminal domain was unable to substitute for the equivalent HaSV region, suggesting that structural elements alone are insufficient for targeting and that HaSV-specific sequences are required. Further analysis would be required to determine the role of specific amino acids in targeting efficiency and the importance of the predicted secondary structures.

A series of C-terminal deletion mutants demonstrated that a second region within the RdRp domain was also required for punctate distribution of the replicase. This was supported by the observation that the degradation products of the recombinant replicase expressed in Sf9 cells infected with recombinant baculoviruses JRS BV1 or JRS BV2 were present in different fractions depending on whether the polypeptide contained the RdRp domain. The 90 kDa degradation product consistently detected by the anti-REP_{1-218}(b) antiserum (directed against the replicase N-terminus), is predicted to include the N-terminal half of the replicase, excluding the RdRp domain. While the exact location and sequence of the targeting domain remains to be determined, it appears that this internal localisation region is responsible for the strong association with detergent resistant structures in both transfected and infected tissue culture cells.

Further insight into the role of the replicase localisation domains was gained through the subcellular fractionation of cells expressing replicase-EGFP fusion proteins. Both the control proteins, CD63 and DsRed2-Mito, are integral membrane proteins, with CD63 being a member of the multiple pass tetraspannin family often associated with DRMs (Section 1.5.2). Both CD63 and DsRed2-Mito retained their normal cellular distribution following incubation in high salt and alkaline pH buffers and were released only by treatment with 1 % Triton X-100. A proportion of CD63 remained after detergent treatment, which is consistent with the reported association of a sub-population of CD63 with DRMs. The REP_{1-1704}-EGFP fusion protein exhibited a similar fractionation pattern as CD63, with a proportion of the EGFP fluorescence remaining associated with punctate structures even in the presence of Triton X-100. Strikingly, the deletion mutant $REP_{45-1704}$-EGFP and EGFP-REP_{1-1704}, that appeared to be cytosolic and soluble in previous experiments (Sections 3.3.1), were found to include a sub-population of protein that was associated with similar detergent-resistant structures. These data suggest that the “Cytosolic – Nuc” distributions observed for many of the

deletion mutants do not necessarily represent a complete loss of targeting ability, but rather a significant decrease in the efficiency with which the localisation to the punctate structures occurs. Since both the N-terminal fusion protein (EGFP-REP_{1-1704}) and the N-terminal deletion mutant ($REP_{45-1704}$-EGFP) displayed this phenotype, the implication is that the localisation domain present within the C-terminal region of the RdRp domain (or another as yet unidentified region) is sufficient for localisation to detergent-resistant structures similar to those associated with CD63. The absence of the N-terminal domain results in localisation that is less efficient, either due to a lower rate of association or because of a decrease in affinity for the structures. The N-terminal domain could then function either in the stabilisation of the interaction or as an activator, increasing the rate of association.

This hypothesis is supported by data from baculoviral expression of His-ΔREP-V5 in Sf9 cells. Here, deletion of the N-terminal localisation domain appeared to have little effect on the association of the protein with DRMs. The strong association with detergent-resistant fractions of the baculovirus-expressed His-ΔREP-V5 could also be due to the long period of time allowed for expression (96 hours as opposed 24 hours in transfected cells). HeLa and BHK-21 cells were harvested 20 hours after transfection and observations made in live cells (Section 3.3.4) suggest that prolonged expression results in an increased accumulation of the punctate structures (through homotypic fusion) into larger structures that are less mobile. The increased time required for baculovirus expression in Sf9 cells may result in the development of similar aggregated structures that could represent misfolded protein but are more likely to be replicase-induced structures that are resistant to detergent solubilisation. Alternatively the replicase could have a higher affinity for protein and/or membrane host factors present in insect cells or that host factors involved in the stabilisation of the replicase-membrane association in HaSV-infected cells are present in Sf9

cells and absent in mammalian cells. These factors could strengthen the interaction to the point that the N-terminal domain is unnecessary in insect cells.

The heterologous expression of the HaSV replicase in the absence of other viral proteins raised the possibility that the membrane-association and subcellular distribution were experimental artefacts. In the absence of experimental systems for the analysis of wild-type HaSV replication complexes, the subcellular fractionation data was compared with data similarly obtained from tissue culture cells persistently infected with PrV. The consistency with which both the recombinant HaSV replicase and the wild-type PrV p40 were present in detergent-resistant fractions suggests that both associate with DRMs *in vivo* and that the punctate structures observed in cells expressing $REP_{1\text{-}1704}$-EGFP are most likely the result of replicase-directed membrane-association rather than the aggregation of misfolded proteins. Since the interaction of the HaSV replicase with membranes occurs in the absence of other viral proteins, the targeting signals present within the replicase CDS appear to be sufficient for localisation. In addition, even though the PrV and HaSV replicases differ significantly in terms of amino acid sequence, similarities observed in the distribution and membrane-association suggest that the subcellular location of tetravirus replication complexes may be consistent throughout the family.

CHAPTER 6
GENERAL DISCUSSION AND CONCLUSIONS

While there is a significant body of literature on the assembly and maturation of tetravirus particles, very little progress has been made towards a fundamental understanding of the molecular mechanisms of tetravirus replication. The study of virus-host interactions among the tetraviruses has been hampered by the absence of suitable *in vivo* (tissue culture) replication systems. The overall aim of this study was to develop experimental systems for the study of the replication biology of the omegatetravirus, HaSV, which is the only tetravirus for which the cDNAs have been shown to be infectious (Gordon *et al.*, 2001). The focus of the research was on the subcellular location of recombinant HaSV replicase in mammalian and insect tissue culture cells.

6.1 PRODUCTION OF ANTI-REPLICASE ANTIBODIES

The first objective was to generate antibodies that could be used to detect the replicase in cell-free extracts (by western analysis) and in whole cells (by immunofluorescence microscopy). During the course of this study, two sets of polyclonal antibodies were produced using an N-terminal replicase polypeptide fragment expressed in *E. coli* (Chapter 2). There were problems with the solubility of all the polypeptides used, probably due to misfolding of the recombinant protein. Both antisera generated had poor sensitivity and were unable to detect the replicase in HaSV-infected midgut extracts by western analysis or in transfected tissue culture cells by immunofluorescence microscopy. The increased expression levels via recombinant baculoviruses (See Section 6.2 below) did however produce sufficient replicase for detection using the anti-replicase antibodies.

The poor sensitivity of the anti-replicase antiserum when used in the detection of the native replicase was likely due to a combination of low antigenicity, possibly due to misfolding, and the relatively small size of the recombinant polypeptide (25 kDa) as compared to the full length replicase (180 kDa). While every attempt was made to select the region of the replicase sequence with the highest degree of hydrophilicity, the polypeptide fragments were consistently present as insoluble aggregates in the *E. coli* expression system used for their production. The low sensitivity of the antiserum was further compounded by the difficulties of working with HaSV-infected larvae. Since HaSV preferentially infects early instar *H. armigera* and stunting is induced in infected insects, the isolation of sufficient quantities of infected larval midgut cells is prohibitive due to their small size and flaccidity. As the midgut cannot be readily separated from the body wall, this essentially results in the dilution of infected cells with the uninfected tissue, which makes up the vast majority of each larva. These observations suggest that the sensitivity of the anti-replicase antiserum would be increased by the expression of larger replicase fragments with a greater number of potential antigenic sites and the expression of such polypeptides in experimental systems capable of overexpressing larger protein such as Sf9 cells, derived from *S. frugiperda* (Order: *Lepidoptera*, Family: *Noctuidae*), which is closely related to *H. armigera*.

The observation that the N-terminal deletion mutant $REP_{45\text{-}1704}$-EGFP produced a cytosolic distribution in transfected mammalian cells (Section 5.3.1) suggested that a similar deletion mutant expressed in Sf9 cells would generate a polypeptide well suited to the generation of anti-replicase antiserum with enhanced sensitivity. Further analysis of localisation mechanisms of the replicase in both mammalian and Sf9 cells (Sections 5.3.4 and 5.3.5) however, demonstrated that the localisation domain within the C-terminal region of the RdRp domain was likely to be responsible for the tight membrane association of the replicase with host cellular membranes.

The expression of a replicase fragment containing the full N-terminus of the replicase up to and including the full HEL domain, similar to the 90 kDa degradation product observed in Sf9 cells expressing both His-REP-V5 and His-ΔREP-V5, would therefore represent a good candidate for the production of anti-replicase antiserum in the future.

6.2 THE SUBCELLULAR LOCALISATION OF THE HaSV REPLICASE

6.2.1. Experimental systems

Two different approaches were used to study the subcellular localisation of the HaSV replicase, namely fluorescence microscopy on fixed and live cells and biochemical fractionation of cell-free extracts. In the absence of replicase-specific antibodies suitable for immunofluorescence microscopy, the replicase was expressed as an EGFP fusion protein. This system allowed for the detection of the protein of interest expressed in mammalian and insect cells by confocal fluorescence microscopy as live or fixed cells and subcellular localisation by live cell staining and immunofluorescence microscopy. An added advantage was the potential of analysing the membrane association of proteins through biochemical fractionation of whole cells with proteins being detected by fluorescence microscopy. A disadvantage of the experimental system, however, was the low transfection frequencies leading to low levels of overall protein expression preventing the detection of the replicase by western analysis using anti-replicase or anti-EGFP antibodies. As a result, a second experimental system based on the baculovirus-mediated expression of replicase fusion proteins was also developed. The infection of Sf9 cells with recombinant baculoviruses led to an increase in the number of cells expressing the replicase and an overall increase in recombinant protein production that allowed for the detection of the replicase by western analysis using anti-replicase, anti-His or anti-V5

epitope antisera. This allowed for further biochemical analysis of the intracellular membrane interactions of recombinant HaSV replicase.

One of the major questions that remains unanswered is what factors are responsible for the narrow host range and tissue tropism exhibited among the tetraviruses. In addition to the further analysis of the association of the HaSV replicase with DRMs, the expression of the replicase-fusion proteins in Sf9 cells presents the possibility of identifying host factors associated with viral replication complexes in Sf9 cells. The recombinant replicase could be purified either by the Ni-affinity chromatography or by co-immunoprecipitation – if suitable antiserum can be generated. Stable transfectants generated in both mammalian and insect tissue culture cells could be used to identify and analyse the elements required for vRNA replication. Transfection of cells expressing the viral replicase with vRNA or vRNA:protein complexes could help to identify the function of structural proteins or RNA sequence elements in the initiation of vRNA replication.

6.2.2. The HaSV replicase is targeted to membranes derived from endocytic compartments

Transient expression of the C-terminal HaSV replicase-EGFP fusion protein (REP_{1-1704}-EGFP) in mammalian and insect tissue culture cells resulted in the localisation of EGFP fluorescence to small punctate structures distributed throughout the cytoplasm. Immunofluorescence co-localisation studies showed a partial overlap between the replicase-EGFP fusion protein and the late endosome marker CD63 16 to 18 hours after transfection, but no overlap had been observed with endocytosed dextran used as a marker for the classical endocytic pathway (Sections 3.3.2 and 3.3.3). Time-lapse confocal microscopy of live cells showed that the punctate structures underwent fusion, fission and “kiss-and-run” events as well as what appeared to be directed transport, all of which are characteristics of endocytic organelles

(Gruenberg *et al.*, 1989; Bright *et al.*, 2005). These data suggests that the punctate structures are either derived from organelles that are similar to (but not part of) the classical endocytic pathway or that the accumulating replicase possesses a mechanism for excluding soluble, luminal endocytic contents (such as dextran) and/or membrane associated marker proteins (like CD63).

6.2.3. Association of the HaSV replicase with DRMs derived from non-classical endocytic organelles

Biochemical fractionation of mammalian and insect cells showed that REP_{1-1704}-EGFP-containing punctate structures displayed characteristics typical of an association with DRMs (Section 5.3.4). Interestingly, the late endosomal marker, CD63, also appeared to interact with similar membranes in HeLa cells, further evidence supporting the hypothesis that the HaSV replicase is targeted to membranes derived from endocytic organelles. This data presents three possible mechanisms for the subcellular localisation of the replicase. First, the replicase may be targeted to a subset of late endosomes with fluid phase endocytic contents and host marker proteins being excluded by an unknown replicase-dependent mechanism. Second, the replicase might associate with a subset of CD63-positive organelles that do not necessarily form part of the classical endocytic pathway. Although CD63 accumulates primarily in multivesicular late endosomes, it has been shown to cycle between endocytic and secretory pathways in some cell types (Kobayashi *et al.*, 2000). Finally, the punctate structures could represent an unidentified structure that interacts, through fusion or “kiss-and-run” events, with CD63-positive late endosomes. The partial overlap between CD63 immunofluorescence and REP-EGFP fluorescence 16 to 18 hours after transfection could therefore represent hybrid organelles generated by the mixing of membranes between these structures. In this case, the lack of

overlap at later time points would imply that the accumulation of the HaSV replicase resulted either in an inhibition of fusion and membrane cycling or an active exclusion of at least some host proteins, such as CD63. Comparison of the data obtained from transfected Sf9 and HeLa cells demonstrates that the endocytic organelles targeted by the replicase are common to both cell types.

A further survey of the available literature has highlighted the relatively recent discovery of alternate endocytic pathways (reviewed in Nichols and Lippincott-Schwartz, 2001; Johannes and Lamaze, 2002; Pelkmans and Helenius, 2003; Mayor and Pagano, 2007). The HaSV replicase may be associated with membranes derived from one of these pathways. This hypothesis is especially tempting since DRMs appear to be important constituents of a number of these alternative pathways (See Section 1.5.2). In addition, endocytic organelles that function in parallel to the classical endosomes have been identified. These alternate endocytic organelles can be identical to classical endocytic organelles in terms of subcellular distribution, transport and maturation, differing only in protein content, with some being devoid of typical endosomal markers such as EEA1, Rab4 and Rab5 (Kalia *et al.*, 2006). Although the majority of endocytosed material is ultimately delivered to classical early endosomes (Hansen *et al.*, 1993; Mayor and Pagano, 2007), the partial overlap of the punctate structures with late endosomes could represent the merging of an alternate endocytic pathway with classical late endosomes.

The complete lack of overlap between endocytosed dextran and replicase-associated punctate structures, even at the earlier time points (16 to 18 hours), suggests that the replicase is not associating with classical late endosomes. A more likely hypothesis is that the temporary overlap with CD63-positive organelles demonstrates that the punctate structures fuse with late endosomes until this reaction is inhibited by a replicase-dependent

mechanism. Although further investigation is necessary, the most likely site for the localisation of the HaSV replicase is therefore alternate endocytic organelles that usually merge with classical endosomes.

These data are strikingly similar to recent studies on the subcellular interactions of the RV replication complex in infected cells (Matthews *et al.*, 2009, 2010) suggesting that these viruses may share a common site for vRNA replication and that they may make use of a similar mechanism for membrane association. The authors noted that the both replicating vRNA and viral replication complexes only partially overlapped with the late endosome/lysosomal marker protein LAMP2, even though the distributions appeared to be similar especially during the early stages of infection. The vast majority of the RV replication protein, P150, was also found to remain associated with detergent-resistant fractions both during infection and when expressed alone in transfected cells, leading the authors to suggest a strong association between P150 and membranes. Subsequently, Matthews *et al.* (2010) showed that the RV replication proteins associate with microtubules during the formation of unique intracellular fibres and although neither the fibres nor microtubules are required for vRNA replication, they may facilitate the cell-to-cell spread of RV without the need for infectious virus particles.

DRMs are thought to be present in distinct membrane microdomains in a number, if not all, cellular membranes and are likely to function in the concentration of cellular factors (proteins, co-factors, etc.) to specific areas in order to generate localised reaction sites (discussed in detail in Section 1.5.2). It is possible that the association of the viral replicase to such sites could aid in the concentration of vRNA replication factories and the assembly of vRNA replication complexes. This could parallel or further enhance the function of replicase-induced spherules analogous to those observed for many other viruses. The similarities exhibited by these viruses

could be indicative of common viral replication strategies that, with further study, could further the understanding (+ve) RNA virus replication in general.

6.3 Localisation of the HaSV replicase is directed by two targeting domains

Since HaSV (and the other known alpha-like tetraviruses) carries a single replication protein, the information required for the development of *in vivo* replication complexes, and the punctate structures observed in transfected cells, is likely to be encoded by the replicase CDS. In addition to the analysis of the subcellular location of the HaSV replicase, this study provided an opportunity to identify and characterise the targeting domains.

Bioinformatic analysis of the HaSV replicase amino acid sequence did not detect any similarities to any known targeting motifs and, as a result, deletion mutagenesis was used to identify the regions required for targeting. This analysis revealed two putative targeting regions. Deletion mutants lacking either the N-terminal 44 amino acids or the C-terminus of the replicase up to P^{1368} in the RdRp domain displayed cytosolic distributions suggesting that both were essential for the localisation of the replicase.

The role of these domains was investigated by biochemical fractionation of Sf9 cells expressing either full length (His-REP-V5) or N-terminal deletion mutant (His-ΔREP-V5) replicase fusion proteins. The replicase was strongly associated with DRM fractions in both cases. Analysis of the degradation products detected by antiserum directed against the N-terminus of the replicase demonstrated that degradation products missing the C-terminal region of the replicase including the RdRp domain were either soluble or released from DRM fractions in the presence of Triton X-100 (Sections 4.3.4 and 5.3.5). This implied that the N-terminal region was not required for membrane association in insect tissue culture cells and that the sole region

required for efficient targeting in this system was present within the RdRp domain. Interestingly, incubation of cells expressing $REP_{45-1704}$-EGFP in the presence of Triton X-100 resulted in a significant proportion of EGFP fluorescence remaining in structures similar to those observed for both the full length replicase-EGFP fusion and CD63. This suggested that, while the majority of this polypeptide was present within the cell as a cytosolic protein, a significant proportion was associated with cellular DRMs.

Time-lapse imaging of live cells suggest that prolonged expression of REP_{1-1704}-EGFP in HeLa and Sf9 cells results in the accumulation of punctate structures into larger and less mobile structures. It is possible that the prolonged expression of the replicase in the baculovirus-mediated expression system results in the association of a greater proportion of the replicase with DRM fractions. Alternatively, the difference could be due to host factors that influence the membrane association of the replicase, either positively in Sf9 cells or negatively in HeLa cells. Although further investigation is required, it is more likely to be the presence of activating host factors in Sf9 cells since they are relatively closely related to *H. armigera*, the natural host for HaSV. Replicase-host interactions could therefore result in an increase in targeting efficiency meaning that the single, internal domain is sufficient for localisation. While the N-terminal domain is not capable of targeting EGFP in mammalian cells, it could stimulate membrane-association of the replicase by other regions, giving the impression that it is required for localisation when it is rather increasing the rate of association or stabilising the interaction.

In an attempt to further understand the role of the N-terminal region in the membrane association of the viral replicase, bioinformatic analysis was done on the N-terminal regions of all three of the alpha-like tetravirus replicases sequenced to date (HaSV, DpTV and NβV). The presence of conserved predicted secondary structural elements in this region, along with the distribution of a series of N-terminal deletion mutants, suggested that the

structure was important in localisation. However, the lack of complementation between the two N-terminal regions demonstrates that the function of the N-terminal domain in the activation of replicase localisation is most likely due to a combination of structural and virus-specific sequence elements.

6.4 Tetravirus replicases-host interactions: a comparison between HaSV and PrV

Although the PrV and HaSV replicases differ significantly in terms of their functional organisation, their RdRp domains and the expression strategies used, two interesting similarities have been highlighted during the course of this study. First, while the subcellular location of PrV replication proteins has not been thoroughly analysed, the distribution of p40 in persistently infected MG8 cells is remarkably similar to the distribution of HaSV replicase-EGFP fusion proteins expressed in both HeLa and Sf9 cells, indicating that a common subcellular location may be targeted as vRNA replication sites by both viruses. This may be due to the fact that both infect similar host tissues i.e. the midgut cells with specialised endocytic functions. Secondly, both the HaSV replicase and PrV p40 displayed a similar association with DRMs suggesting that the strength and type of association could be consistent between the replicases. It is possible that even though the replicases are classified into different superfamilies in terms of their amino acid sequence, there could be a common mechanism for the localisation of replication.

6.5 The role of the viral replicase in the induction of apoptosis in tetravirus-infected cells

The association of the HaSV replicase with acidic organelles, such as lysosomes, was originally hypothesised by Tomasicchio *et al*. (2007). *In vitro* maturation of VLPs is induced under acidic pH (<5.5) conditions (Canady *et*

al., 2000, 2001; Taylor *et al.*, 2002) and the induction of apoptosis in yeast cells expressing the HaSV capsid protein precursor results in the spontaneous maturation of VLPs (Tomasicchio *et al.*, 2007). The cytosolic acidification that occurs as a result of apoptosis is therefore thought to be important in the maturation of infectious tetravirus particles *in vivo* (Tomasicchio *et al.*, 2007). This hypothesis was further supported by the increased incidence of apoptosis observed in HaSV-infected *H. armigera* midgut cells (Brooks *et al.*, 2002).

The data presented in this thesis suggest that the HaSV replicase (and perhaps the PrV replicase) associates with organelles from an alternate endocytic pathway that overlaps in part with the classical endocytic pathway through the late endosomes. At no point was there any indication that the HaSV replicase expressed in either experimental system resulted in an increase in the incidence of apoptosis, suggesting that the association with endocytic organelles was not the source of the apoptosis observed by Brooks *et al.* (2002). While the role of the replicase in the induction of apoptosis in infected cells cannot be discounted since these data were obtained in cells expressing the replicase in isolation of other viral proteins and vRNA, a more likely hypothesis is that apoptosis is induced by the host in response to viral infection and may be exploited by tetraviruses for capsid maturation.

6.6 A model for the association of HaSV replicase with host endosome-derived membranes and the viral life cycle

As hypothesised by Munshi *et al.* (1996), HaSV is thought to bind to the surface of cells containing permissive surface receptors and enter the cell via endocytosis. As is the case with a number of viruses, including the structurally-related FHV, the low pH of the endosomal lumen would then induce the translocation of vRNA in a reaction dependent on the pentameric bundles generated by the autoproteolytic cleavage of the capsid precursor

protein upon particle maturation. Once within the cytosol, expression of the viral replicase would be initiated by host ribosomes and the replicase targeted to endosomes by an unknown localisation signal. Here it associates with DRMs through the localisation domain present within the C-terminus of the RdRp domain. The rate at which the replicase associates with host membranes and generation of vRNA replication factories is likely to be enhanced by the N-terminal domain in a sequence- and structure-dependent manner, probably through inter- and/or intra-replicase as well as replicase-host interactions. Once replication complexes are established, the replication of vRNA proceeds with RNA1 being preferentially reproduced during the initial stages of infection (Bawden *et al.*, 1999). Once sufficient RNA1 and/or viral replicase has been generated, a switch is made and the production of RNA2 (Bawden *et al.*, 1999) and the viral structural proteins is prioritised with the resulting assembly of HaSV provirions containing both RNAs and uncleaved capsid protein precursors. Whether cytosolic acidification is required for the maturation of virus particles *in vivo* remains to be determined, but the maturation of virus particles could be induced as a result of apoptosis that is directed either by the host cell itself or by an unknown virus-dependent mechanism.

6.7 Concluding remarks

The absence of suitable experimental systems has severely hindered the study of tetravirus replication biology. In an attempt to gain insight into this area of the tetravirus lifecycle, two experimental systems were developed and used to analyse the subcellular localisation and membrane association of the HaSV replicase, the first study of its kind on a tetravirus. The exact subcellular location of the replicase remains to be conclusively demonstrated and the role that DRMs play in the viral life cycle is still unclear. The generation of suitable antiserum for the detection of the replicase in infected insects remains a significant challenge, but replicase-specific antibodies will

provide an opportunity to compare the data obtained here with the virus-host interactions *in vivo*. While the observations made using the experimental systems developed during the course of this research are limited by the absence of other virus proteins and vRNA, they do present an important opportunity to investigate the role of other viral proteins in vRNA replication and to identify the factors required for the generation of *ex vivo* tetravirus replication systems.

REFERENCES

Aboulaich, N., Vainonen, J. P., Strålfors, P. and Vener, A. V. (2004). Vectorial proteomics reveal targeting, phosphorylation and specific fragmentation of polymerase I and transcript release factor (PTRF) at the surface of caveolae in human adipocytes. *Biochem. J.* **383,**237-248.

Ahlquist, P. (2002). RNA-dependent RNA polymerases, viruses, and RNA Silencing. *Science* **296,**1270-1273.

Ajioka, R. A. and Kaplan, J. (1986). Intracellular pools of transferrin receptors result from constitutive internalization of unoccupied receptors. *Proc. Natl. Acad. Sci. U.S.A.* **83,**6445-6449.

Alberts, B., Johnson, A., Lewis, J., Raff, M., Roberts, K. and Walter, P. (2002). Chapter 10: Membrane Structure, pp 583-614 In: Molecular Biology of the Cell (4th Edition) (Garland Science).

Alder, M. N., Dames, S., Gaudet, J. and Mango, S. E. (2003). Gene silencing in *Caenorhabditis elegans* by transitive RNA interference. *RNA* **9,**25-32.

Ambrose, R. L., Lander, G. C., Maaty, W. S., Bothner, B., Johnson, J. E. and Johnson, K. N. (2009). Drosophila A virus is an unusual RNA virus with a *T* = 3 icosahedral core and permuted RNA-dependant RNA polymerase. *J. Gen. Virol.* **90,**2191-2200.

Anderson, R. G. W. and Jacobson, K. (2002). A role for lipid shells in targeting proteins to caveolae, rafts, and other lipid domains. *Science* **296,**1821-1825.

Aniento, F., Emans, N., Griffiths, G. and Gruenberg, J. (1993). Cytoplasmic dynein-dependent vesicular transport from early to late endosomes. *J. Cell Biol.* **123,**1373-1388.

Argos, P. (1988). A sequence motif in many polymerases. *Nucleic Acids Res.* **16,**9909-9916.

Aumiller, J. J., Hollister, J. R. and Jarvis, D. L. (2006). Molecular cloning and functional characterisation of β-*N*- acetylglucosaminidase genes from Sf9 cells. *Prot. Exp. Purif.* **47,**571-590.

Ball, L. A. (1995). Requirements for the self-directed replication of Flock House virus RNA1. *J. Virol.***69,**720-727.

Ball, L. A. and Li, Y. (1993). *cis*-acting requirements for the replication of Flock House virus RNA2. *J. Virol.* **67,**3544-3551.

Bananis, E., Nath, S., Satir, P., Stockert, R. J., Murray, J. W., Wolkoff, A. W. (2004). Microtubule-dependent movement of late endocytic vesicles *in vitro*: requirements for dynein and kinesin. *Mol. Biol. Cell* **8,**3688-3697.

Bawden, A. L., Gordon, K. H. J. and Hanzlik, T. N. (1999). The specificity of *Helicoverpa armigera* stunt virus infectivity. *J. Inv. Pathol.* **74,**156-163.

Bennion, B. J. and Daggett, V. (2003). The molecular basis for the chemical denaturation of proteins by urea. *Proc. Natl. Acad. Sci. U.S.A.* **100,**5142-5147.

Berditchevski, F. (2001). Complexes of tetraspanins with integrins: more than meets the eye. *J. Cell Sci.* **114,**4143-4151.

Bienz, K., Egger, D. and Pasamontes, L. (1987). Association of polioviral proteins of the P2 genomic region with the viral replication complex and virus-induced membrane synthesis as visualised by electron microscopic immunocytochemistry and autoradiography. *Virol.* **160,**220-226.

Blachly-Dyson, E., Zambronicz, E. B., Yu, W. H., Adams, V., McCabe, E. R., B., Adelman, J., Colombini, M. and Forte, M. (1993). Cloning and functional expression in yeast of two human isoforms of the outer mitochondrial membrane channel, the voltage-dependant anion channel. *J. Biol. Chem.* **268,**1835-1841.

Bolten, R., Egger, D., Gosert, R., Schaub, G., Landmann, L. and Bienz, K. (1998). Intracellular localisation of Poliovirus plus- and minus- strand RNA visualised by strand-specific fluorescent in situ hybridisation. *J. Virol.* **72,**8578-8585.

Bomsel, M., Parton, R., Kuznetsov, S. A., Schroer, T. A. and Gruenberg, J. (1990). Microtubule- and motor-dependent fusion *in vitro* between apical and basolateral endocytic vesicles from MDCK cells. *Cell* **62,**719-731.

Botto, L., Masserini, M., Cassetti, A. and Palestini, P. (2004). Immunoseparation of prion protein-enriched domains from other detergent-resistant membrane fractions, isolated from neuronal cells. *FEBS Letters* **557,**143-147.

Bright, N. A., Reaves, B. J., Mullock, B. M. and Luzio, J. P. (1997). Dense core lysosomes can fuse with late endosomes and are reformed from the resultant hybrid organelles. *J. Cell Sci.* **110,**2027–2040.

Bright, N. A., Gratian, M. J. and Luzio, J. P. (2005). Endocytic delivery to lysosomes mediated by concurrent fusion and kissing events in living cells. *Curr. Biol.* **15,**360-365.

Brooks, E. M., Gordon, K. H. J., Dorrian, S. J., Hines, E. R. and Hanzlik, T. N. (2002). Infection of its lepidopteran host by the *Helicoverpa* armigera stunt virus (*Tetraviridae*). *J. Invertebr. Pathol.* **80,**97–111.

Bucci, C., Parton, R. G., Mather, I. H., Stunnenberg, H., Simons, K., Hoflack, B. and Zerial, M. (1992). The small GTPase rab5 functions as a regulatory factor in the early endocytic pathway. *Cell*. **70,**715-728.

Bucci, C., Thomsen, P., Nicoziani, P., McCarthy, J., Van Deurs, B. (2000). Rab7: a key to lysosome biogenesis. *Mol. Biol. Cell* **11,**467-480.

Buck, K. W. (1996). Comparison of the replication of positive-stranded RNA viruses of plants and animals. *Adv. Vir. Res.* **47,**159-251.

Canady, M. A., Tihova, M., Hanzlik, T. N., Johnson, J. E. and Yeager, M. (2000). Large conformational changes in the maturation of a simple RNA virus, *Nudaurelia capensis* ω virus (NωV). *J. Mol. Biol.* **299,**573-584.

Canady, M. A., Tsuruta, H. and Johnson, J. E. (2001). Analysis of rapid, large-scale protein quaternary structural changes: time-resolved X-ray solution scattering of *Nudaurelia capensis* ω virus (NωV) maturation. *J. Mol. Biol.***311,**803-814.

Carpenter, G. and Cohen, S. (1979). Epidermal growth factor. *Ann. Rev. Biochem.* **48,**193-216.

Carroll, K. S., Hanna, J., Simon, I., Krise, J., Barbero, P. and Pfeffer, S. R. (2001). Role of Rab9 GTPase in facilitating receptor recruitment by TIP47. *Science* **292,**1373-1376.

Chen, C. S., Bach, G. and Pagano, R. E. (1998). Abnormal transport along the lysosomal pathway in mucolipidosis, type IV disease. *Proc. Natl. Acad. Sci. U.S.A.* **95,**6373-6378.

Cheng, Z., Singh, R. D., Sharma, D. K., Holicky, E. L., Hanada, K., Marks, D. L. and Pagano, R. E. (2006). Distinct mechanisms of clathrin-independent endocytosis have unique sphingolipid requirements. *Mol. Biol. Cell* **17,**3197-3210.

Chow, K. M., Gakh, O., Payne, I. C., Juliano, M. A., Juliano, L., Isaya, G. and Hersh, L. B. (2009). Mammalian pitrilysin: substrate specificity and mitochondrial targeting. *Biochemistry* **48,**2868-2877.

Claas, C., Stipp, C. S. and Hemler, M. E. (2001). Evaluation of prototype transmembrane 4 superfamily protein complexes and their relation to lipid rafts. *J. Biol. Chem.* **276,**7974-7984.

Clague, M. J. (1999). Membrane transport: take your fusion partners. *Curr. Biol.* **9,**R258-260.

Das, S. C., Nayak, D., Zhou, Y and Pattnaik, A. K. (2006). Visualisation of intracellular transport of Vesicular stomatitis virus nucleocapsids in living cells. *J. Gen. Virol.* **80,**6369-6377.

Dautry-Varsat, A., Ciechanover, C. and Lodish, H.F. (1983). pH and the recycling of transferrin during receptor-mediated endocytosis. *Proc. Natl. Acad. Sci. U.S.A.* **80,**2258-2262.

Den Boon, J. A., Chen, J. and Ahlquist, P. (2001). Identification of sequences in Brome mosaic virus replicase protein 1a that mediate association with endoplasmic reticulum membranes. *J. Virol.* **75,**12370-12381.

Díez, J., Ishikawa, M., Kaido, M. and Ahlquist, P. (2000). Identification and characterisation of a host protein required for efficient template selection in viral RNA replication. *Proc. Natl. Acad. Sci. U.S.A.* **97,**3913-3918.

Donnelly, M. L. L., Luke, G., Mehrotra, A., Li, X., Hughes, L. E., Gani, D. and Ryan, M. D. (2001a). Analysis of the aphthovirus 2A/2B polyprotein „cleavage" mechanism indicates not a proteolytic reaction, but a novel translational effect: a putative ribosomal „skip". *J. Gen. Virol.* **82,**1013-1025.

Donnelly, M. L. L., Hughes, L. E., Luke, G., Mendoza, H., Ten Dam, E., Gani, D. and Ryan, M. D. (2001b). The „cleavage" activities of Foot-and-mouth disease virus 2A site-directed mutants and naturally occurring „2A-like" sequences. *J. Gen. Virol.* **82,**1027-1041.

Dorrington, R. A. and Short, J. R. (2010). The tetraviruses. In "Insect virology". Johnson, K. and Asqari, S (eds). (Horizon Scientific Press). In print.

Dunn, K. W. and Maxfield, F. R. (1992). Delivery of ligands from sorting endosomes to late endosomes occurs by maturation of sorting endosomes. *J. Cell Biol.* **117,**301-310.

Dunn, K. W., McGraw, T. E. and Maxfield, F. R. (1989). Iterative fractionation of recycling receptors from lysosomally destined ligands in an early sorting endosome. *J. Cell Biol.* **109,**3303-3314.

Du Plessis, L., Hendry, D. A., Dorrington, R. A., Hanzlik, T. N., Johnson, J. E. and Appel, M. (2005). Revised RNA2 sequence of the tetravirus, *Nudaurelia capensis* ω virus (NωV). *Arch. Virol.* **150,**2397–2402.

Dye, B. T., Miller, D. J. and Ahlquist, P. (2005). In vivo self-interaction of nodavirus RNA replicase protein A revealed by fluorescence resonance energy transfer. *J. Virol.* **79,**8909-8919.

Emans, N., Gorval, J. P., Walter, C., Gerke, V., Kellner, R., Griffiths, G. and Gruenberg, J. (1993). Annexin II is a major component of fusogenic endosomal vesicles. *J. Cell Biol.* **120,**1357-1370.

Entchev, E. V., Schwabedissen, A. and González-Gaitán, M. (2000). Gradient Formation of the TGF-β Homolog Dpp. *Cell* **103,**981-991.

Feng, Y., Press, B. and Wanginger-Ness, A. (1995). Rab 7: An important regulator of late endocytic membrane traffic. *J. Cell Biol.* **131,**1435-1452.

Ferrer-Orta, C., Arias, A., Excarmis, C. and Verdauguer, N. (2006). A comparison of viral RNA-dependant RNA polymerases. *Curr. Opin. Struct. Biol.* **16,**27-34.

Fielding, C. J. and Fielding, P. E. (1997). Intracellular cholesterol transport. *J. Lipid Res.* **38,**1503-1521.

Finch, J. T., Crowther, R. A., Hendry, D. A. and Struthers, J. K. (1974). The structure of *Nudaurelia capensis* β virus: the first example of a capsid with icosahedral surface symmetry *T* = 4. *J. Gen. Virol.* **24,**191-200.

Finke, S., Brzózka, K. and Conzelmann, K-K. (2004). Tracking fluorescence-labelled Rabies virus: enhanced green fluorescent protein-tagged phosphoprotein P supports virus gene expression and formation of infectious particles. *J. Virol.* **78,**12333-12343.

Fisher, A.J. and Johnson, J.E. (1993). Ordered duplex RNA controls capsid architecture in an icosahedral animal virus. *Nature* **361,**176-179

Foster, L. J., De Hoog, C. L. and Mann, M. (2003). Unbiased quantitative proteomics of lipid rafts reveals high specificity for signalling factors. *Proc. Natl. Acad. Sci. U.S.A.* **100,**5813-5818.

Froshauer, S., Kartenbeck, J. and Helenius, A. (1988). Alphavirus RNA replicase is located on the cytoplasmic surface of endosomes and lysosomes. *J. Cell Biol.* **107,**2075-2086.

Garzon, S., Strykowski, H. and Charpentier, G. (1990). Implication of mitochondria in the replication of Nodamura virus in larvae of the Lepidoptera, Galleria mellonella (L.) and in suckling mice. *Arch. Virol.* **113,**165-176.

Gasteiger, E., Hoogland, C., Gattiker, A., Duvaud, S., Wilkins, M. R., Appel, R. D. and Bairoch, A. (2005). Protein identification and analysis tools on the ExPASy server. pp 571-607. In: The proteomics protocols handbook, J. M. Walker (ed). (Humana Press inc.).

Gagescu, R., Demaurex, N., Parton, R. G., Hunziker, W., Huber, L. A. and Gruenberg, J. (2000). The recycling endosome of Madin-Darby canine kidney cells is a mildly acidic compartment rich in raft components. *Mol. Biol. Cell.* **11,**2775-2791.

Gauthier, N. C., Monzo, P., Kaddai, V., Doye, A., Ricci, V. and Boquet, P. (2005). *Helicobacter pylori* VacA cytotoxin: a probe for a clathrin-independent and Cdc42-dependent pinocytic pathway routed to late endosomes. *Mol. Biol. Cell* **16,**4852-4866.

Geuze, H. J., Stoorvogel, W., Strous, G. J., Slot, J. W., Bleekemolen, J. E. and Mellman, I. (1988). Sorting of mannose-6-phosphate receptors and lysosomal membrane proteins in endocytic vesicles. *J. Cell Biol.* **107,**2491-2501.

Ghosh, R. N., Mallet, W. G., Soe, T. T., McGraw, T. E. and Maxfield, F. R (1998). An endocytosed TGN38 chimeric protein is delivered to the TGN after trafficking through the endocytic recycling compartment in CHO cells. *J. Cell Biol.* **142,**923-936.

Goldstein, J.L. Anderson, R. G. W. and Brown, M. S. (1979). Coated pits, coated vesicles and receptor-mediated endocytosis. *Nature (Lond.).* **279,**679-685.

Gorbalenya, A. E., Koonin, E. V., Donchenko, A. P. and Blinov, V. M. (1988). A novel superfamily of nucleoside triphosphate binding motif containing proteins which are probably involved in duplex unwinding in DNA and RNA replication and recombination. *FEBS Lett.* **235,**16-24.

Gorbalenya, A. E., Koonin, E. V., Donchenko, A. P. and Blinov, V. M. (1989). Two related superfamilies of putative helicases involved in replication, recombination, repair and expression of DNA and RNA genomes. *Nucleic Acids Res.* **17,**4713-4730.

Gorbalenya, A. E., Koonin, E. V. and Wolf, Y. I. (1990). A new superfamily of putative NTP-binding domains encoded by genomes of small DNA and RNA viruses. *FEBS Lett*. **262,**145-148.

Gorbalenya, A. E., Pringle, F. M., Zeddam, J-L., Luke, B. T., Cameron, C. E., Kalmakoff, J., Hanzlik, T. N. Gordon, K. H. J. and Ward, V. K. (2002). The palm subdomain-base active site is internally permuted in viral RNA-dependent RNA polymerases of an ancient lineage. *J. Mol. Biol.* **324,**47-62.

Gordon, K. H. J., Johnson, K. N. and Hanzlik, T. N. (1995). The larger genomic RNA of *Helicoverpa armigera* stunt virus encodes the viral RNA polymerase and has a novel 3'-terminal tRNA-like structure. *Virol.* **208,**84-98.

Gordon, K. H. J., Williams, M. R., Hendry, D. A. and Hanzlik, T. N. (1999). Sequence of the genomic RNA of *Nudaurelia* β virus (Tetraviridae) defines a novel genome organization. *Virol.* **258,**42-53.

Gordon, K. H. J., Williams, M. R., Baker, J. S., Gibson, J. M., Bawden, A. L., Millgate, A. G., Larkin, P. J. and Hanzlik, T. N. (2001). Replication-independent assembly of an insect virus (*Tetraviridae*) in plant cells. *Virol.* **288,**36-50.

Gorvel, J. P., Chavrier, P., Zerial, M. and Gruenberg, J. (1991). Rab5 controls early endosome fusion *in vitro*. *Cell*. **64,**915-925.

Greenwood, L. K. and Moore, N. F. (1984). Determination of the location of an infection in *Trichoplusia ni* larvae by a small RNA-containing virus using enzyme-linked immunosorbent assay and electron microscopy. *Microbiologica* **7,**97-102.

Griffiths, G., Hoflack, B., Simons, K., Mellman, I. and Kornfeld, S. (1988). The mannose 6-phosphate receptor and the biogenesis of lysosomes. *Cell* **52,**329-341.

Grimley, P. M., Berezesky, I. K. and Friedman, R. M. (1968). Cytoplasmic stuctures associated with an arbovirus infection: loci of viral ribonucleic acid synthesis. *J. Virol.* **2,**1326-1338.

Gruenberg, J. and Maxfield, F. R. (1995). Membrane transport in the endocytic pathway. *Curr. Opin. Cell Biol.* **7,**552-563.

Gruenberg, J., Griffiths, G. and Howell, K. E. (1989). Characterisation of the early endosome and putative endocytic carrier vesicles *in vivo* with an assay of vesicle fusion *in vitro*. *J. Cell Biol.* **108,**1301-1316.

Gu, F. and Gruenberg, J. (1999). Biogenesis of transport intermediates in the endocytic pathway. *FEBS Lett.* **452,**61-66.

Han, S. and Sanfaçon, H. (2003). Tomato ringspot virus proteins containing the nucleoside triphosphate binding domain are transmembrane proteins that associate with the endoplasmic reticulum and cofractionate with replication complexes. *J. Virol.* **77,**523-534.

Hanahan, D. (1983). Studies on transformation of *Escherichia coli* with plasmids. *J. Mol. Biol.* **166,**557-580.

Hansen, J. L., Long, A. M. and Schultz, S. C. (1997). Structure of the RNA-dependent RNA polymerase of Poliovirus. *Structure* **5,**1109-1122.

Hanzlik, T. N., Dorrian, S. J., Gordon, K. H. J. and Christian, P. D. (1993). A novel small RNA virus isolated from the cotton bollworm, *Helicoverpa armigera*. *J. Gen. Virol.* **74,**1805-1810.

Hansen, S. H., Sandvig, K. and van Deurs, B. (1993). Molecules internalised by clathrin-independent endocytosis are delivered to endosomes containing transferrin receptors. *J. Cell Biol.* **123,**89-97.

Hanzlik, T. N., Dorrian, S. J., Gordon, K. H. J. and Christian, P. D. (1993). A novel small RNA virus isolated from the cotton bollworm, *Helicoverpa armigera. J. Gen. Virol.* **74,**1805-1810.

Hanzlik, T. N., Dorrian, S. J., Johnson, K. N., Brooks, E. M. and Gordon, K. H. J. (1995). Sequence of RNA 2 of the *Helicoverpa armigera* stunt virus (*Tetraviridae*) and bacterial expression of its genes. *J. Gen. Virol.* **76,**799-811.

Hanzlik, T. N., Gordon, K. H. J., Gorbalenya, A. E., Hendry, D. A., Pringle, F. M., Ward, V. K. and Zeddam, J. L. (2005). Family *Tetraviridae*. pp 877-883. In: Virus Taxonomy: Eighth Report of the International Committee on Taxonomy of Viruses. Fauquet, C. M., Mayo, M. A., Maniloff, J., Desselberger, U. and Ball, L. A. (eds) (Academic Press).

Hein, Z., Hooper, N. M. and Naim, H. Y. (2009). Association of a GPI-anchored protein with detergent-resistant membranes facilitates it's trafficking through the early secretory pathway. *Exp. Cell Res.* **315,**348-356.

Helenius, A., Kartenbeck, J., Simons, K. and Fries, E. (1980). On the entry of Semliki Forest virus into BHK-21 cells. *J. Cell Biol.* **84,**404-420.

Helgstrand, C., Munshi, S., Johnson, J. E. and Liljas, L. (2004). The refined structure of *Nudaurelia capensis* ω virus reveals control elements for a *T* = 4 capsid maturation. *Virol.* **318,**192-203.

Hendry, D. A., Becker M. F. and van Regenmortel M. H. V. (1968). A non inclusion virus of the pine emperor moth *Nudaurelia cytherea capensis* Stoll. *S. Afr. Med. J.* ***42,***117.

Hendry, D. A., Hodgson, V., Clark, R. and Newman, J. (1985). Small RNA viruses co-infecting the pine emperor moth (*Nudaurelia cytherea capensis*). *J. Gen. Virol.* **66,**627-632.

Henley, J. R., Krueger, E. W., Oswald, B. J. and McNiven, M. A. (1998). Dynamin-mediated internalisation of caveolae. *J. Cell Biol.* **141,**85-99.

Itin, C., Rancaño, C., Nakajima, Y. and Pfeffer, S. R. (1997). A novel assay reveals a role for soluble *N*-ethylmaleimide-sensitive fusion attachment protein in mannose-6-phosphate receptor transport from endosomes to the *trans* Golgi network. *J. Biol. Chem.* **272,**27737-27744.

Johannes, L. and Goud, B. (1998) Surfing on a retrograde wave: how does Shiga toxin reach the endoplasmic reticulum? *Trends Cell Biol.* **8,**158-162.

Johannes, L. and Lamaze, C. (2002). Clathrin-dependent or not: is it still the Question? *Traffic* **3,**443-451.

Johnson, J. E., Munshi, S., Liljas, L., Agrawal, D., Olson, N. H., Reddy, V., Fisher, A., McKinney, B., Schmidt, T. and Baker, T. S. (1994). Comparative studies of *T* = 3 and *T* = 4 icosahedral insect viruses. *Arch. Virol.* **9,**497-512.

Johnson, K. N., Johnson, K. L., Dasgupta, R., Gratsch, T. and Ball, L. A. (2001). Comparisons among the larger genome segments of six nodaviruses and their encoded RNA replicases. *J. Gen. Virol.***82,**1855-1866.

Jonczyk, M., Pathak, K. B., Sharma, M. and Naggy, P. D. (2007). Exploiting alternative subcellular localisation for replication: Tombusvirus replication switches to the endoplasmic reticulum in the absence of peroxisomes. *Virol.* **362,**320-330.

Jukes, I. R. M. (1970). Viruses of the Pine Emperor Moth. *Bull. S. Afr. Soc. Plant Pathol. Miocrobiol.* **4,**18.

Jukes, I. R. M. (1979). Comparison of some biophysical properties of the *Nudaurelia* β and ω viruses. *J. Gen. Virol.* **42,**89-94.

Kadre, G. and Haenni, A. L. (1997). Virus-encoded RNA helicases. *J. Virol.* **71,**2583-2590.

Kalia, M., Kumari, S., Chadda, R., Hill, M. M., Parton, R. G. and Mayor, S. (2006). Arf6-independent GPI-anchored protein-enriched early endosomal compartments fuse with sorting endosomes via a Rab5/Phosphatidylinositol-3'-kinase-dependent machinery. *Mol. Biol. Cell.* **17,**3689-3704.

Kamer, G. and Argos, P. (1984). Primary structural comparison of RNA-dependent polymerases from plant, animal and bacterial viruses. *Nucleic Acids Res.* **12,**7269-7282.

Kampmueller, K. M. and Miller, D. J. (2005). The cellular chaperone heat shock protein 90 facilitates Flock House virus RNA replication in *Drosophila* Cells. *J. Virol.* **79,**6827-6837.

Kane, J. F. and Hartley, D. L. (1988). Formation of recombinant protein inclusion bodies in *Escherichia coli*. *Trends. Biotech*. **6,**95-101.

Kartenbeck, J., Stukenbrok, H. and Helenius, A. (1989). Endocytosis of Simian virus 40 into the endoplasmic reticulum. *J. Cell Biol.* **109,**2721-2729.

Kawar, Z. and Jarvis, D. L. (2001). Biosynthesis and subcellular localization of a lepidopteran insect alpha 1,2-mannosidase. *Insect Biochem. Mol. Biol.* **31,**289-297.

Kawar, Z., Karaveg, K., Moremen, K. W. and Jarvis, D. L. (2001). Insect cells encode a class II *α*-mannosidase with unique properties. *J. Biol. Chem.* **276,**16335-16340.

Kien, F., Abraham, J-D., Schuster, C. and Kieny, M. P. (2003). Analysis of the subcellular localization of Hepatitis C virus E2 glycoprotein in live cells using EGFP fusion proteins. *J. Gen. Virol.* **84,**561-566.

Kirkegaard, T. and Jäättelä, M. (2009). Lysosomal involvement in cell death and cancer. *Biochem. Biophys. Acta* **1793,**746-754.

Kirkham, M., Fujita, A., Chadda, R., Nixon, S. J., Kurzchalia, T. V., Sharma, D. K., Pagano, R. E., Hancock, J. F., Mayor, S. and Parton, R. G. (2005). Ultrastructural identification of uncoated caveolin-independent endocytic vehicles. *J. Cell Biol.* **168,**465-476.

Klausner, R. D., Ashwell, G., Van Renswoude, J., Harford, J. B. and Bridges, K. R. (1983). Binding of apotransferrin to K562 cells: explanation of the transferrin cycle. *Proc. Natl. Acad. Sci. U.S.A.* **80,**2263-2266.

Knox, C., Moffat, K., Ali, S., Ryan, M. and Wileman, T. (2005). Foot-and-mouth disease virus replication sites form next to the nucleus and close to the Golgi apparatus, but exclude marker proteins associated with host membrane compartments. *J. Gen. Virol.* **86,**687-696.

Kobayashi, T., Vischer, U. M., Rosnoblet, C., Lebrand, C., Lindsay, M., Parton, R. G., Kruithof, E. K. O. and Gruenberg, J. (2000). The tetraspanin CD63/lamp3 cycles between endocytic and secretory compartments in human endothelial cells. *Mol. Biol. Cell* **11,**1829-1843.

Koonin, E. V. (1991). The phylogeny of RNA-dependant RNA polymerases of positive strand RNA viruses. *J. Gen. Virol.* **72,**2197-2206.

Kopek, B. G., Perkins, G., Miller, D. J., Ellisman, M. H. and Ahlquist, P. (2007). Three-dimensional analysis of a viral RNA replication complex reveals a virus-induced mini-organelle. *PLoS Biol.* **5,**e220

Koval, M. and Pagano, R. E. (1990). Sorting of an internalised plasma membrane lipid between recycling and degradative pathways in normal and Niemann-Pick, type A fibroblasts. *J. Cell Bio.* **111,**429-442.

Kujala, P., Ahola, T., Ehsani, N., Auvinen, P., Vihinen, H. and Kääriäinen, L. (1999). Intracellular distribution of Rubella virus nonstructural protein P150. *J. Virol.* **73,**7805-7811.

Kujala, P., Ikäheimonen, A., Ehsani, N., Vihinen, H., Auvinen, P. and Kääriäinen, L. (2001). Biogenesis of the Semliki Forest virus RNA replication complex. *J. Virol.* **75,**3873-3884.

Kurisu, M., Morita, M., Kashiwayama, Y., Yokota, S., Hayashi, H., Sakai, Y., Ohkuma, S., Nishimura, M. and Imanaka, T. (2003). Existence of catalase-less peroxisomes in Sf21 insect cells. *Biochem. Biophys. Res. Comm.* **306,**169-176.

Kurzchalia, T. V. and Parton, R. G. (1999). Membrane microdomains and caveolae. *Curr. Opin. Cell Biol.* **11,**424-431.

Kushner, D. B., Lindenbach, B. D., Grdzelishvili, V. Z., Noueiry, A. O., Paul, S. M., and Ahlquist, P. (2003). Systematic, genome-wide identification of host genes affecting replication of a positive-strand RNA virus. *Proc. Natl. Acad. Sci. U.S.A.* **100,**15764-15769.

Kyte, J. and Doolittle, R. F. (1982). A simple method for displaying the hydropathic character of a protein. *J. Mol. Biol.* **157,**105-132.

Lamaze, C., Dujeancourt, A., Baba, T., Lo, C. G., Benmerah, A. and Dautry-Varsat, A. (2001). Interleukin 2 receptors and detergent-resistant membrane domains define a clathrin-independent endocytic pathway. *Mol. Cell* **7,**661-671.

Laemmli, U. K. (1970). Cleavage of structural proteins during the assembly of the head of bacteriophage T4. *Nature* **227,**680-685.

Lawrence, P. and Rieder, E. (2009). Identification of RNA helicase A as a new host factor in the replication cycle of Foot-and-mouth disease virus. *J. Virol.* **83,**11356-11366.

Lee, W-M., Ishikawa, M. and Ahlquist, P. (2001). Mutation of host Δ9 fatty acid desaturase inhibits Brome mosaic virus replication between template recognition and RNA synthesis. *J. Virol.* **75,**2097-2106.

Levy, S. and Shoham, T. (2005). The tetraspanin web modulates immune-signalling complexes. *Nat. Rev. Imm.* **5,**136-148.

Li, N., Mak, A., Richards, D. P., Naber, C., Keller, B. O., Li, L. and Shaw, A. R. E. (2003). Monocyte lipid rafts contain proteins implicated in vesicular trafficking and phagosome formation. *Proteomics* **3,** 563-548.

Lichtenberg, D., Goni, F. M and Heerklotz, H. (2005). Detergent-resistant membranes should not be identified with membrane rafts. *Trends Biochem. Sci.* **30,** 430-436.

Liu, J., Oh, P., Horner, T., Rogers, R. A. and Schnitzer, J. E. (1997). Organlised endothelial cell surface signal transduction in caveolae distinct from glycosylphosphatidylinositol-anchored protein microdomains. *J. Biol. Chem.* **272,**7211-7222.

Lombardi, D., Soldati, T., Riederer, M. A., Goda, Y., Zerial, M. and Pfeffer, S. R. (1993). Rab9 functions in transport between late endosomes and the trans Golgi network. *EMBO J.* **12,**677-682.

Lord, J. M. and Roberts, L. M. (1998). Toxin entry: retrograde transport through the secretory pathway. *J. Cell Biol.* **140,**733-736.

Luke, G. J (2001). Assembly of full-length cDNA, and heterologous expression of, *Nudaurelia* β virus RNA. Rhodes University MSc thesis.

Luzio, J. P., Rous, B. A., Bright, N. A., Pryor, P. R., Mullock, B. M. and Piper, R. C. (2000). Lysosome-endosome fusion and lysosome biogenesis. *J. Cell Sci.* **113,**1515-1524.

Maecker, H. T., Todd, S. C. and Levy, S. (1997). The tetraspanin superfamily: molecular facilitators. *FASEB J.* **11,**428-442.

Magliano, D., Marshall, J. A., Bowden, D. S., Vardaxis, N., Meanger, J. and Lee, J-Y. (1998). Rubella virus replication complexes are virus-modified lysosomes. *Virol.* **240,**57-63.

Mallard, F., Antony, C., Tenza, D., Salamero, J., Goud, B. and Johannes, L. (1998). Direct pathway from early/recycling endosomes to the Golgi apparatus revealed through the study of shiga toxin B-fragment transport. *J. Cell Biol.* **143,**973-990.

Mallard, F., Tang, B. L., Galli, T., Tenza, D., Saint-Pol, A., Yue, X., Antony, C., Hong, W., Goud, B. and Johannes, L. (2002). Early/recycling endosomes-to-TGN transport involves two SNARE complexes and a Rab6 isoform. *J. Cell Biol.* **156,**653-664.

Mas, A., Alves-Rodrigues, I., Noueiry, A., Ahlquist, P. and Díez, J. (2006). Host deadenylation-dependant mRNA decapping factors are required for a key step in Brome mosaic virus RNA replication. *J. Virol.* **80,**246-251.

Matsui, W. and Kichhausen, T. (1990). Stabilization of clathrin coats by the core of the clathrin-associated protein complex AP-2. *Biochemistry* **29,**10791-10798.

Matsuyama, S. and Reed, J. C. (2000). Mitochondria-dependent apoptosis and cellular pH regulation. *Cell Death Diff.* **7,**1155-1165.

Matthews, J. D., Tzeng, W-P. and Frey, T. K. (2009). Determinants of subcellular localization of the Rubella virus nonstructural replicase proteins. *Virol.* **390,**315-323.

Matthews, J. D., Tzeng, W-P. and Frey, T. K. (2010). Analysis of the function of cytoplasmic fibers formed by the rubella virus nonstructural replicase proteins. *Virol.* **406,**212-217.

Matthews, R. E. F. (1982). Classification and nomenclature of viruses. Fourth report of the international committee on taxonomy of viruses. *Intervirology* **17,**1-160.

Mayor, S. and Pagano, R. E. (2007). Pathways of clathrin-independent endocytosis. *Nat. Rev. Mol. Cell Biol.* **8,**603-612.

McBride, H. M., Rybin, V., Murphy, C., Giner, A., Teasdale, R. and Zerial, M. (1999). Oligomeric complexes link Rab5 effectors with NSF and drive membrane fusion via interactions between EEA1 and syntaxin 13. *Cell* **98,**377-386.

Mellman, I., Fuches, R. and Helenius, A. (1986). Acidification of the endocytic and exocytic pathways. *Ann. Rev. Biochem.* **55,**663-700.

Metzelaar, M. J., Wijngaard, P. L. J., Peters, P. J., Sixma, J. J., Nieuwenhuis, H. K. and Clevers, H. C. (1991). CD63 antigen. *J. Biol. Chem.* **266,**3239-3245.

Mézeth, K. B., Nylund, S., Henriksen, Patel, S., Nerland, A. H. and Szilvay, A. M. (2007). RNA-dependant RNA polymerase from Atlantic halibut nodavirus contains two signals for localisation to the mitochondria. *Vir. Res.* **130,**43-52.

Miller, D. J. and Ahlquist, P. (2002). Flock House virus RNA polymerase is a transmembrane protein with amino-terminal sequences sufficient for mitochondrial localisation and membrane insertion. *J. Virol.* **76,**9856-9867.

Miller, D. J., Schwartz, M. D. and Ahlquist, P. (2001). Flock House virus RNA replicates on outer mitochondrial membranes in *Drosophila* cells. *J. Virol.* **75,**11664-11676.

Miller, D. J., Schwartz, M. D., Dye, B. T. and Ahlquist, P. (2003). Engineered retargeting of viral RNA replication complexes to an alternate intracellular membrane. *J. Virol.* **77,**12193-12202.

Moffat, K., Howell, G., Knox, C., Belsham, G. J., Monaghan, P., Ryan, M. D. and Wileman, T. (2005). Effects of Foot-and-mouth disease virus nonstructural proteins on the structure and function of the early secretory pathway: 2BC but not 3A blocks endoplasmic reticulum-to-Golgi transport. *J. Virol.* **79,**4382-4395.

Moore, N. F., Reavy, B. and King, L. A. (1985). General characteristics, gene organisation and expression of small RNA viruses of insects. *J. Gen. Virol.* **66,**647-559.

Mousavi, S. A., Malerød, L., Berg, T. and Kjeken, R. (2004). Clathrin-dependant endocytosis. *Biochem. J.* **377,**1-16.

Mullins, C. and Bonifacino, J. S. (2001). The molecular machinery for lysosome biogenesis. *Bioessays* **23,**333-343.

Mullock, B. M., Perex, J. H., Kuwana, T., Gray, S. R. and Luzio, J. P. (1994). Lysosomes can fuse with a late endosomal compartment in a cell-free system from rat liver. *J. Cell Biol.* **126,**1173-1182.

Mullock, B. M., Bright, N. A., Fearon, C. W., Gray, S. R. and Luzio, J. P. (1998). Fusion of lysosomes with late endosomes produces a hybrid organelle of intermediate density and is NSF dependent. *J. Cell Biol.* **140,**591-601.

Munshi, S., Liljas, L., Cavarelli, J., Bomu, W., McKinney, B., Reddy, V. and Johnson, J. E. (1996). The 2.8 Å structure of a T = 4 animal virus and its implications for membrane translocation of RNA. *J. Mol. Biol.* **261,**1-10.

Murphy, S. C., Samuel, B. U., Harrison, T., Speicher, K. D., Speicher, D. W., Reid, M. E., Prohaska, R., Low, P. S., Tanner, M. J and other authors (2003). Erythrocyte detergent-resistant membrane proteins: their characterisation and selective uptake during malarial infection. *Blood* **103,**1920-1928.

Naslavsky, N., Weigert, R. and Donaldson, J. G. (2003). Convergence of non-clathrin- and clathrin-derived endosomes involves ARF6 inactivation and changes in phosphoinosides. *Mol. Biol. Cell* **14,**417-431.

Netherton, C., Moffat, K., Brooks, E. and Wileman, T. (2007). A guide to viral inclusion, membrane rearrangements, factories, and viroplasm produced during virus replication. *Adv. Vir. Res.* **70,**101-182.

Nichols, B. J. and Lippincott-Schwartz, J. (2001). Endocytosis without clathrin coats. *Trends Cell Biol.* **11,**406-412.

Nilsson, C., Johansson, U., Johansson, A-C, Kågedal, K., Öllinger, K. (2006). Cytosolic acidification and lysosomal alkalinization during TNF-α induced apoptosis in U937 cells. *Apoptosis* **11,**1149-1159.

Nishi, K. and Saigo, K. (2007). Cellular internalisation of green fluorescent protein fused with Herpes simplex virus VP22 via a lipid raft-mediated endocytic pathway independent of caveolae and Rho family GTPases but dependent on dynamin and ARF6. *J. Biol. Chem.* **282,**27503-27517.

Norkin, L. C. (1999). Simian virus 40 infection via MHC class I molecules and caveolae. *Immunol. Rev.* **168,**13-22.

Ollis, D. L., Brick, P., Hamiln, R., Xuong, N. G. and Steitz, T. A. (1985). Structure of large fragment of *Escherichia coli* DNA polymerase I complexed with dTNP. *Nature* **313,**762-766.

Olson, N. H., Baker, T. S., Johnson, J. E. and Hendry, D. A. (1990). The three-dimensional structure of frozen-hydrated *Nudaurelia capensis* beta virus, a *T* = 4 insect virus. *J. Struct. Biol.* **105,**111-122.

O'Rielly, E. K., Wang, Z., French, R. and Kao, C. C. (1998). Interactions between the structural domains of the RNA replication proteins of plant-infecting RNA viruses. *J. Virol.* **72,**7160-7169.

Ortín, J. and Parra, F. (2006). Structure and function of RNA replication. *Ann. Rev. Microbiol.* **60,**305-326.

Pagno, R. E. (2003). Endocytic trafficking of glycosphingolipids in sphingolipid storage diseases. *Phil. Trans. R. Soc. Lond. B Biol. Sci.* **358,**885-891.

Pagano, R. E., Watanabe, R., Wheatley, C. and Chen, C. S. (1999). Use of *N*-[5-(5,7-dimethyl boron dipyrromethene difluoride-sphingomyelin to study membrane traffic along the endocytic pathway. *Chem. Phys. Lipids.* **102,**55-63.

Palade, G. E. (1953). Fine structure of blood capillaries. *J. Appl. Phys.* **24,** 1424.

Parton, R. G., Joggerst, B. and Simons, K. (1994). Regulated internalization of caveolae. *J. Cell Biol.* **127,**1199-1215.

Pata, J. D., Schultz, S. C. and Kirkegaard, K. (1995). Functional oligomerization of Poliovirus RNA-dependant RNA polymerase. *RNA* **1,**466-477.

Pelkmans, L. and Helenius, A. (2003). Insider information: what viruses tell us about endocytosis. *Curr. Opin. Cell Biol.* **15,**414-422.
Pelkmans, L., Kartenbeck, J. and Helenius, A. (2001). Caveolar endocytosis of Simian virus 40 reveals a new two-step vesicular pathway to the ER. *Nat. Cell Biol.* **3,**473-483.

Piper, R. C. and Luzio, J. P. (2001). Late endosomes: sorting and partitioning in multivesicular bodies. *Traffic* **2,**612-621.

Poch, O., Sauvaget, I., Delarue, M. and Tordo, N. (1989). Identification of four conserved motifs among the RNA-dependant polymerase encoding elements. *EMBO J.* **8,**3867-3874.

Pringle, F. M., Gordon, K. H. J., Hanzlik, T. N., Kalmakoff, J., Scotti, P. D. and Ward, V. (1999). A novel capsid expression strategy for *Thosea asigna* virus (*Tetraviridae*). *J. Gen. Virol.* **80,**1855-1863.

Pringle, F. M., Johnson, K. N., Goodman, C. L., McIntosh, A. H. and Ball, L. A. (2003). Providence virus: a new member of the *Tetraviridae* that infects cultured insect cells. *Virol.* **306,**359-370.

Puri, V., Watanabe, R., Singh, R. D., Dominguez, M., Brown, J. C., Wheatley, C. L., Marks. D. L. and Pagano, R. E. (2001). Clathrin-dependant and -independent internalization of plasma membrane sphingolipids initiates two Golgi targeting pathways. *J. Cell Biol.* **154,**535-547.

Radhakrishna, H. and Donaldson, J. G. (1997). ADP-ribosylation factor 6 regulates a novel plasma membrane recycling pathway. *J. Cell Biol.* **139,**49-61.

Reinganum, C., Robertson, J. S. and Tinsley, T. W. (1978). A new group of RNA viruses from insects. *J. Gen. Virol.* **40,**195-202.

Restrepo-Hartwig, M. A. and Ahlquist, P. (1996). Brome mosaic virus helicase- and polymerase-like proteins colocalize on the endoplasmic reticulum at sites of viral RNA synthesis. *J. Virol.* **70,**8908-8916.

Restrepo-Hartwig, M. A. and Ahlquist, P. (1999). Brome mosaic virus RNA replication proteins 1a and 2a colocalize and 1a independently localizes on the yeast endoplasmic reticulum. *J. Virol.* **73,**10303-10309.

Robinson, M. S. (1994). The role of clathrin, adaptors and dynamin in endocytosis. *Curr. Opin. Cell Biol.* **6,**538-544.

Rossmann, M. G. and Johnson, J. E. (1989). Icosahedral RNA virus structure. *Ann. Rev. Biochem.* **58,**553-573.

Rothberg, K. G., Heuser, J. E., Donzell, W. C., Ying, Y-S., Glenney, J. R. and Anderson, R. G. W. (1992). Caveolin, a protein component of caveolae membrane coats. *Cell* **68,** 673-682.

Rozanov, M. N., Koonin, E. V. and Gorbalenya, A. E. (1992). Conservation of the putative methyltransferase domain: a hallmark of the 'Sindbis-like' supergroup of positive-strand RNA viruses. *J. Gen. Virol.* **73,**2129-2134.

Rust, R. C., Landmann, L., Gosert, R., Tang, B. L., Hong, W., Hauri, H-P., Egger, D. and Bienz, K. (2001). Cellular COPII proteins are involved in production of the vesicles that form the Poliovirus replication complex. *J. Virol.* **75,**9808-9818.

Sabanadzovic, A., Ghanem-Sabanadzovic, N. A. and Gorbalenya, A. E. (2009). Permutation of the active site of putative RNA-dependant RNA polymerase in a newly identified species of plant alpha-like virus. *Virol.***394,** 1-7.

Sabharanjak, S., Sharma, P., Parton, R. G. and Mayor, S. (2002). GPI-anchored proteins are delivered to recycling endosomes via a distinct CDC42-regulated, clathrin-independant pinocytic pathway. *Dev. Cell* **2,**411-423.

Sambrook, J., Fritsche, E. F. and Maniatis, T. (1989). Molecular cloning, a laboratory manual. 2nd Ed. Cold Spring Harbor Press, New York.

Sandvig, K., Torgersen, M. L., Raa., A. H. and Van Deurs, B. (2008). Clathrin-independent endocytosis: from nonexisting to an extreme degree of complexity. *Histochem. Cell Biol.* **129,**267-276.

Sasamura, T., Ishikawa, H. O., Sasaki, N., Higashi, S., Kanai, M., Nakao, S., Ayukawa, T., Aigaki, T., Noda, K. and other authors (2007). The *O*-fucosyltransferase O-fut1 is an extracellular component that is essential for the constitutive endocytic trafficking of Notch in *Drosophila*. *Development* **134,**1347-1356.

Sbalzarini, I. F. and Koumoutsakos, P. (2005). Feature point tracking and trajectory analysis for video imaging in cell biology. *J. Struct. Biol.* **151,**182-195.

Schiebel, W., Haas, B.,Marincović, S., Klanner, A. and Sänger, H. L. (1993). RNA-directed RNA polymerase from tomato leaves I: purification and physical properties. *J. Biol. Chem.* **268,**11851-11857.

Schiebel, W., Pélissier, T., Riedel, L., Thalmeir, S., Schiebel, R., Kempe, D., Lottspeich, F., Sänger, H. L. and Wassengger, M. (1998). Isolation of an RNA-directed RNA polymerase-specific cDNA clone from tomato. *Plant Cell* **10,**2087-2101.

Schlegel, A., Giddings, T. H. Jr., Ladinsky, M. S. and Kirkegaard, K. (1996). Cellular origin and ultrastructure of membranes induced during Poliovirus infection. *J. Virol.* **70,**6576-6588.

Schlesinger, S. and Schlesinger, M. J. (2001). *Togaviridae*: The viruses and their replication. pp 895-916. In *Fields' Virology* 4th Edition Knipe, D. M. and Howley, P. M. (eds). Lippincott, Williams and Wilkins (Philadelphia).

Schmid, S. L., McNiven, M. A. and De Camilli, P. (1998). Dynamin and its partners: a progress report. *Curr. Opin. Cell Biol.* **10,**504-512.

Sehnke, P. C., Harrington, M., Hosur, M. V., Li, Y., Usha, R., Tucker, R. C., Bomu, W., Stauffacher, C. V. and Johnson, J. E. (1988). Crystalization of viruses and virus proteins. *J. Cryst. Growth* **90,**222-230.

Shih, W., Gallusser, A. and Kirchhausen, T. (1995). A clathrin-binding site in the hinge of the β2 chain of mammalin AP-2 complexes. *J. Biol. Chem.* **270,**31083-31090.

Short, J. R., Knox, C. and Dorrington, R. A. (2010). Subcellular localisation and live-cell imaging of the *Helicoverpa armigera* stunt virus replicase in mammalian and *Spodoptera frugiperda* cells. *J. Gen. Virol.* **91,**1514-1523.

Sigismund, S., Woelk, T., Puri, C., Maspero, E., Tacchetti, C., Transidico, P., Di Fiore, P. P. and Polo, S. (2005). Clathrin-independent endocytosis of ubiquitinated cargos. *Proc. Natl. Acad. Sci. U.S.A.* **102,**2760-2765.

Sijen, T., Fleenor, J., Simmer, F., Thijssen, K. L., Parrish, S., Timmons, L., Plasterk, R. H. A. and Fire, A. (2001). On the role of RNA amplification in dsRNA-triggered gene silencing. *Cell* **107,**465-476.

Simons, K. and Ikonen, E. (1997). Functional rafts in cell membranes. *Nature* **387,** 569-572.

Sowa, G., Pypaert, M. and Sessa, W. C. (2001). Distinction between signalling mechanisms in lipid rafts vs. caveolae. *Proc. Natl. Acad. Sci. U.S.A.* **98,**14072-14077.

Speir, J. A. and Johnson, J. E. (2008). Tetraviruses. pp 27-37 In: Encyclopaedia of Virology. Mahy, B. W. J. and Van Regenmortel, M. H. V. (eds). (Elsevier).

Speir, J. A., Taylor, D. J., Natarajan, P., Pringle, F. M., Ball, L. A. and Johnson, J. E. (2010). Evolution in action: N and C termini of subunits in related *T* = 4 viruses exchange roles as molecular switches. *Structure* **18,**700-709.

Sprenger, R. R., Speijer, D., Back, J. W., De Koster, C. G., Pannekoek, H. and Horrevoets, A. J. G., (2004). Comparative proteomics of human endothelial cell caveolae and rafts using two-dimensional gel electrophoresis and mass spectrometry. *Electrophoresis* **25,**156-172.

Stan, R. V. (2005). Structure of caveolae. *Biochem. Biophys. Acta Mol. Cell Res.* **1746,**334-348.

Studier, F. W. and Moffatt, B. A. (1986). Use of bacteriophage T7 RNA polymerase to direct selective high-level expression of cloned genes. *J. Mol. Biol.* **189,**113-130.

Studier, F. W., Rosenberg, A. H., Dunn, J. J. and Dubendorf, J. W. (1990). Use of T7 RNA polymerase to direct expression of cloned genes. *Methods Enzymol.* **185,**60-85.

Tamberg, N., Lulla, V., Fragkoudis, R., Lulla, A., Frazakerley, J. K. and Merits, A. (2007). Insertion of EGFP into the replicase gene of Semliki Forest virus results in a novel, genetically stable marker virus. *J. Gen. Virol.* **88,**1225-1230.

Tang, J., Lee, K. K., Bothner, B., Baker, T. S., Yeager, M. and Johnson, J. E. (2009). Dynamics and stability in maturation of a T = 4 virus. *J. Mol. Biol.* **392,**803-812.

Taylor, D. J. and Johnson, J. E. (2005). Folding and particle assembly are disrupted by single-point mutations near the autocatalytic cleavage site of *Nudaurelia capensis* ω virus capsid protein. *Prot. Sci.* **14,**401-408.

Taylor, D. J., Krishna, N. K., Canady, M. A., Schneemann, A. and Johnson, J. E. (2002). Large-scale, pH-dependant, quaternary structure changes in an RNA virus capsid are reversible in the absence of subunit autoproteolysis. *J. Virol.* **76,**9972-9980.

Thakral, D., Nayak, B., Rehman, S., Durgapal, H. and Panda, S. K. (2005). Replication of a recombinant Hepatitis E virus genome tagged with reporter genes and generation of a short-term cell line producing viral RNA and proteins. *J. Gen. Virol.* **86,**1189-1200.

Thilo, L., Stroud. E. and Haylett, T. (1995). Maturation of early endosomes and vesicular traffic to lysosomes in relation to membrane recycling. *J. Cell Sci.* **108,** 1791-1803.

Thompsen, P., Roepstorff, K., Stahlhut, M. and Van Deurs, B. (2002). Caveolae are highly immobile plasma membrane microdomains, which are not involved in constitutive endocytic trafficking. *Mol. Biol. Cell* **13,**238-250.

Tomasicchio, M., Venter, P. A., Gordon, K. H. J., Hanzlik, T. N. and Dorrington, R. A. (2007). Induction of apoptosis in *Saccharomyces cerevisiae* results in the spontaneous maturation of tetravirus procapsids *in vivo*. *J. Gen. Virol.* **88,**1576-1582.

Tran, D., Carpentier, J-L., Sawano, F., Gorden, P. and Orci, L. (1987). Ligands internalised through coated and noncoated invaginations follow a common intracellular pathway. *Proc. Natl. Acad. Sci. U.S.A.* **84,**7957-7961.

Traub, L. M. (2009). Tickets to ride: selecting cargo for clathrin-regulated internalization. *Nat. Rev. Mol. Cell Biol.* **10,**583-596.

Trowbridge, I. S., Collawn, J. F. and Hopkins, C. R. (1993). Signal-dependent membrane protein trafficking in the endocytic pathway. *Ann. Rev. Cell Biol.* **9,**129-161.

Van den Born, E., Posthuma, C. C., Knoops, K. and Snijder, E. J. (2007). An infectious recombinant Equine arteritis virus expressing green fluorescent protein from its replicase gene. *J. Gen. Virol.* **88,**1196-1205.

Van der Heijden, M. W. and Bol, J. F. (2002). Composition of alphavirus-like replication complexes: involvement of virus and host encoded protein. *Arch. Virol.* **147,**875-898.

Van der Sluijs, P., Hull, M., Webster, P., Mâle, P., Goud, B. and Mellman, I. (1992). The small GTP-binding protein rab4 controls an early sorting event in the endocytic pathway. *Cell* **70,**729-740.

Vastij, F. E., Jones, L. and Baulcombe, D. C. (2002). Spreading of RNA targeting and DNA methylation in RNA silencing requires transcription of the target gene and a putative RNA-dependent RNA polymerase. *Plant Cell* **14,**857-867.

Venter, P. A. (2001). Non-host production of the *Helicoverpa armigera* stunt virus in *Saccharomyces cerevisiae*. Rhodes University PhD thesis.

Walter, C. T. (2008). Establishment of experimental systems for studying the replication biology of Providence virus. Rhodes University PhD thesis.
Walter, C. T., Tomasicchio, M., Hodgson, V., Hendry, D. A., Hill, M. P. and Dorrington, R. A. (2008). Characterisation of a succession of small insect viruses in a wild South African population of *Nudaurelia cytherea capensis*. *S. Afr. J. Sci.* **104,**147-152.

Walter, C. T., Pringle, F. M., Nakayinga, R., De Felipe, P., Ryan, M. D., Ball, L. A. and Dorrington, R. A. (2010). Genome organisation and translation products of Providence virus: insight into a unique tetravirus. *J. Gen. Virol.* Accepted.

Wang, A. Han, S. and Sanfaçon, H. (2004). Topogenesis in membranes of the NTB-VPg protein of Tomato ringspot nepovirus: definition of the C-terminal transmembrane domain. *J. Gen. Virol.* **85,**799-809.

Ward, D. M., Hackenyos, D. P. and Kaplan, J. (1990). Fusion of sequentially internalized vesicles in alveolar macrophages. *J. Cell Biol.* **110,**1013-1022.

Wileman, T. (2006). Aggresomes and autophagy generate sites for virus replication. *Science* **312,**875-878.

Wimmer, E., Hellen, C. U. T. and Cao, X. (1993). Genetics of Poliovirus. *Ann. Rev. Genet.* **27,**353-436

Woodman, P. G., Mundy, D. I., Cohen, P. and Warren, G. (1992). Cell-free fusion of endocytic vesicles is regulated by phosphorylation. *J. Cell Biol.* **116,**331-338.

Wu, S-X., Ahlquist, P. and Kaesberg, P. (1992). Active complete *in vitro* replication of nodavirus RNA requires glycerophospholipid. *Proc. Natl. Acad. Sci. U.S.A.* **89,**11136-11140.

Yi, F., Zhang, J., Yu, H., Liu, C., Wang, J. and Hu, Y. (2005). Isolation and identification of a new tetravirus from *Dendrolimus punctatus* larvae collected from Yunnan province, China. *J. Gen. Virol.* **86,**789-796.

Zaremba, S. and Keen, J. H. (1983). Assembly polypeptides from coated vesicles mediate reassembly of unique clathrin coats. *J. Cell Biol.* **97,**1339-1347.

Zeddam, J-L., Gordon, K. H. J., Lauber, C., Felipe Alves, C. A., Luke, B. T., Hanzlik, T. N., Ward, V. K. and Gorbalenya, A. E. (2010). *Euprosterna elaeasa* virus genome sequence and evolution of the *Tetraviridae* family:

Emergence of bipartite genomes and conservation of the VPg signal with the dsRNA *Birnaviridae* family. *Virol.* **397,**145-154.

Zhang, G and Sanfaçon, H. (2006). Characterization of membrane association domains within the Tomato ringspot nepovirus X2 protein, an endoplasmic reticulum-targeted polytopic membrane protein. *J. Virol.* **80,**10847-10857.

Zhang, S. C., Zhang, G., Yang, L., Chisholm, J. and Sanfaçon, H. (2005). Evidence that insertion of Tomato ringspot nepovirus NTB-VPg protein in endoplasmic reticulum membranes is directed by two domains: a C-terminal transmembrane helix and an N-terminal amphipathic helix. *J. Virol.* **79,**11752-11765.

Zheng, Y. Z. and Foster, L. J. (2009). Biochemical and proteomic approaches for the study of membrane microdomains. *J. Proteomics* **72,** 12-22.

Zhou, L., Zhang, J., Wang, X., Jiang, H., Yi, F. and Hu, Y. (2006). Expression and characterisation of RNA-dependent RNA polymerase of Dendrolimus punctatus tetravirus. *J. Biochem. Mol. Biol.* **39,**571-577.

Zhou, L., Zheng, Y., Jiang, H., Zhou, W., Lin, M., Han, Y., Cao, X., Zhang, J. and Hu, Y. (2008). RNA-binding properties of *Dendrolimus punctatus* tetravirus p17 protein. *Virus Res.* **138,**1-6.

APPENDIX A

CONSTRUCTION OF RECOMBINANT PLASMIDS

All PCR reactions were performed using the Expand High Fidelity PCR system (Roche Applied Biosystems) and reverse PCR (RPCR) reactions were carried out using *Pfu* DNA Polymerase (Promega), both in accordance with manufacturers' instructions. HaSV replicase RNA1-derived sequences were either PCR amplified or sub-cloned from pAV13HC G+ (called pAV13 throughout the text) or pMLY1 (Venter, 2001) both of which were generated using the HaSV RNA1 sequence from pDVHStuR1HC (GenBank Acc. No. EU345431) obtained from T. Hanzlik and K. Gordon (CSIRO). Finally, PCR products were all ligated into pGEM T-easy (Promega) according to the manufacturer's instructions using 25 ng pGEM T-easy per reaction. Ligations were done using 3 U T4 DNA ligase (Promega) in a final volume of 10 µl, at 4 °C overnight or for 3 hours at room temperature. Characteristics of the plasmids used in this study are summarised in Table A.1 below and their construction is described in detail below.

Table A.1: Plasmids used in this study (Key on pg 156)

Plasmid	Vector Backbone	Antibiotic resistance	Host(s)	Comments	Chapter	Appendix	Reference
pCW56	N/A	Kan/Amp	B, I	EGFP-fusion expression vector	3		Walter, 2008
pEGFP-C1	N/A	Kan	B, M	EGFP-fusion expression vector	N/A		ClonTech
pEGFP-N1	N/A	Kan	B, M	EGFP-fusion expression vector	3		ClonTech
pFastBac™ DUAL	N/A	Amp/ Gent	B, I (Bac)	Recombinant bacmid shuttle vector	4		Invitrogen
pGEX-4T-2	N/A	Amp	B	*E. coli* expression vector	N/A		GE Healthcare
pJRS4	pEGFP-C1	Kan	B, M	REP_{1-541}-EGFP expression vector	5	A.5	Constructed in this study
pJRS7	pEGFP-N1	Kan	B, M	REP_{1-1704}-EGFP expression vector	3	A.4	Constructed in this study
pJRS7 N44Δ	pEGFP-N1	Kan	B, M	$REP_{45-1704}$-EGFP expression vector	5	A.8	Constructed in this study
pJRS7 N-His	pEGFP-N1	Kan	B, M	His-REP_{1-1704}-EGFP expression vector	5	A.15	Constructed in this study
pJRS7 N-NBV	pEGFP-N1	Kan	B, M	Replicase N-terminal domain swap expression vector	5	A.17	Constructed in this study
pJRS7 RPCR1	pEGFP-N1	Kan	B, M	Replicase N-terminal deletion mutant expression vector	5	A.16	Constructed in this study
pJRS7 RPCR2	pEGFP-N1	Kan	B, M	Replicase N-terminal deletion mutant expression vector	5	A.16	Constructed in this study
pJRS7 RPCR3	pEGFP-N1	Kan	B, M	Replicase N-terminal deletion mutant expression vector	5	A.16	Constructed in this study
pJRS7 RPCR4	pEGFP-N1	Kan	B, M	Replicase N-terminal deletion mutant expression vector	5	A.16	Constructed in this study
pJRS7 RPCR5	pEGFP-N1	Kan	B, M	Replicase N-terminal deletion mutant expression vector	5	A.16	Constructed in this study
pJRS8	pEGFP-C1	Kan	B, M	EGFP-REP_{1-1704} expression vector	3	A.4	Constructed in this study
pJRS12	pEGFP-N1	Kan	B, M	REP_{1-100}-EGFP expression vector	5	A.9	Constructed in this study
pJRS15	pEGFP-N1	Kan	B, M	REP_{1-1368}-EGFP expression vector	5	A.10	Constructed in this study
pJRS16	pEGFP-N1	Kan	B, M	REP_{1-1159}-EGFP expression vector	5	A.11	Constructed in this study
pJRS17	pT7-7_6xHis	Amp	B	His-REP_{1-150} expression vector	2	A.1	Constructed in this study
pJRS19	pT7-7_6xHis	Amp	B	His-REP_{1-218} expression vector	2	A.2	Constructed in this study
pJRS23	pGEX-4T-2	Amp	B	GST-$REP_{1140-1704}$ expression vector	2	A.3	Constructed in this study
pJRS26	pCW56	Kan/Amp	B, I	REP_{1-1704}-EGFP expression vector	3	A.6	Constructed in this study
pJRS26 2A	pCW56	Kan/Amp	B, I	REP_{1-1704}-2A-EGFP expression vector	5	A.14	Constructed in this study
pJRS32	pEGFP-N1	Kan	B, M	REP_{1-1241}-EGFP expression vector	5	A.12	Constructed in this study
pJRS34	pEGFP-N1	Kan	B, M	REP_{1-1304}-EGFP expression vector	5	A.13	Constructed in this study
pJRS42	pFastBac™ DUAL	Amp/ Gent	B, I (Bac)	Recombinant shuttle vector for generating JRS BV1 (His-REP-V5)	4	A.7	Constructed in this study
pJRS42 N83Δ	pFastBac™ DUAL	Amp/ Gent	B, I (Bac)	Recombinant shuttle vector for generating JRS BV1 (His-ΔREP-V5)	5	A.18	Constructed in this study
pT7-7_6xHis	pT7-7	Amp	B	*E. coli* expression vector	2		Constructed in this study

Key to Table A.1: Antibiotic Resistance – Amp: Ampicillin, Kan: Kanamycin, Gent: Gentamicin. Hosts – B: Bacteria (*E. coli*), I: Insect (Sf9), I (Bac): Insect (Baculovirus mediated expression), M: Mammalian (HeLa, BHK-21). "Chapter" – chapter in which the respective plasmid is first mentioned. "Appendix" – Appendix entry describing construction of the plasmid.

A.1 pJRS17

Firstly, the 5' region of the HaSV replicase CDS, up to and including the wild-type *Kpn*I site, was PCR amplified, using the primers JRS6F and JRS5R, which included an additional 5' *Nde*I site. The PCR product was ligated into pGEM T-easy to produce pJRS11F. To allow for the restriction of the *Xba*I site, pJRS11F was transformed into *E. coli* JM110 (*rpsL* (Str^r) *thr leu thi-1 lacY galK galT ara tonA tsx dam dcm supE44* Δ(*lac-proAB*) [F´ *traD36 proAB* $lacI^qZ\Delta M15$]) cells (Stratagene). The sequence coding for the amino-terminal 150 amino acids of the HaSV replicase was removed from pJRS11F using *Nde*I and *Xba*I. The production of pJRS17 was completed by ligating this fragment into the similarly restricted expression vector pT7-7 6xHis, which contains an inducible T7 RNA polymerase promoter, ribosome binding site (RBS) and a hexahistidine (6xHis) sequence followed by a multiple cloning cassette for the overexpression of N-terminal 6xHis-tagged proteins (Figure A.1).

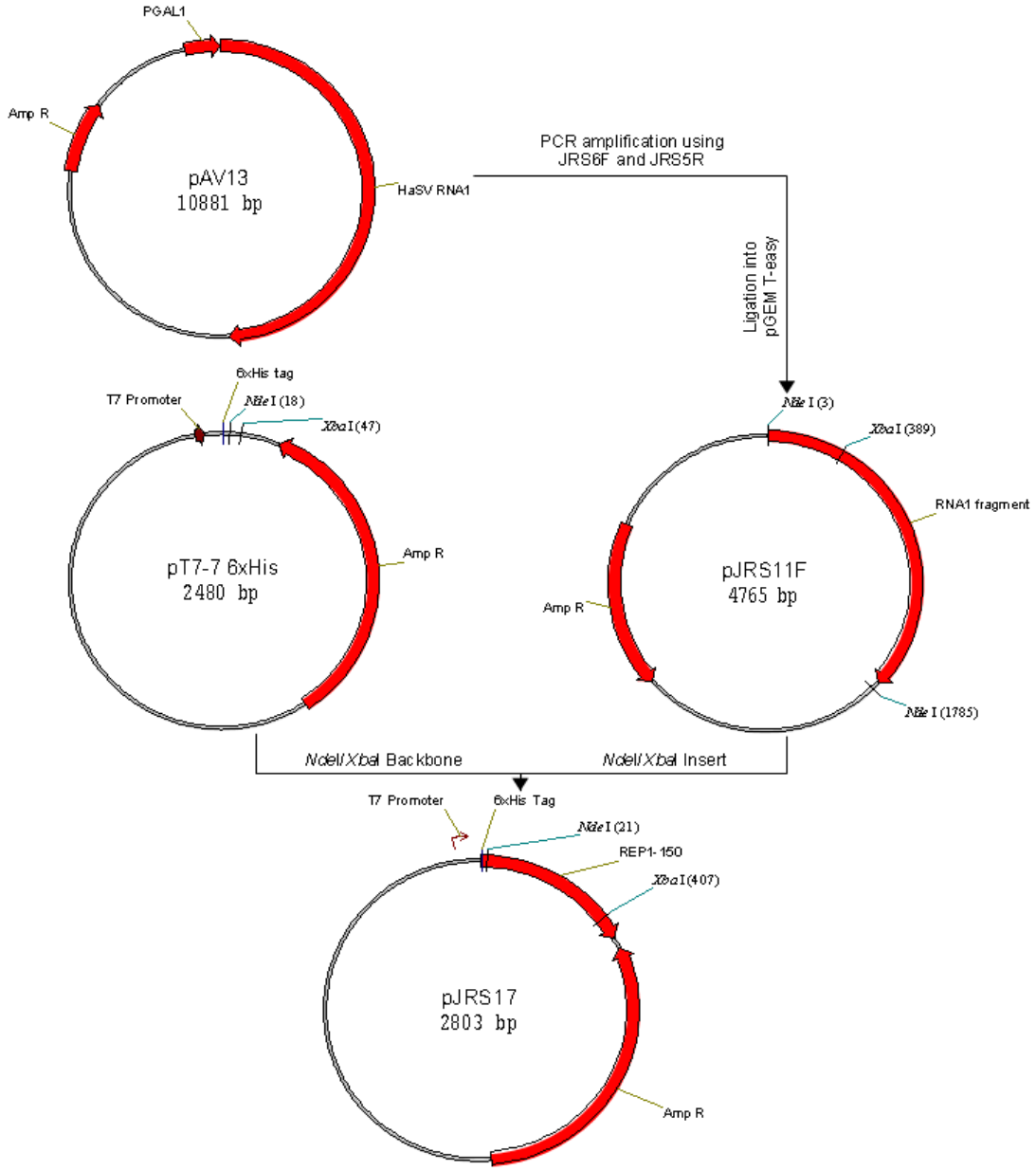

Figure A.1: The construction of pJRS17. Amp R: *β*-lactamase, T7 Promoter: T7 bacteriophage RNA polymerase promoter.

A.2 pJRS19

Approximately 660 bp from the 5’ end of the HaSV replicase CDS was PCR amplified from pJRS8 (Section A.5) using the primers JRS6F and JRS18R, introducing 5' *Nde*I and 3' *Hind*III sites to the PCR product, before it was ligated into pGEM T-easy to produce pJRS18F. The smaller *Nde*I and *Hind*III fragment from pJRS18F was then ligated into pT7-7 6xHis, also restricted with *Nde*I and *Hind*III to create pJRS19 (Figure A.2).

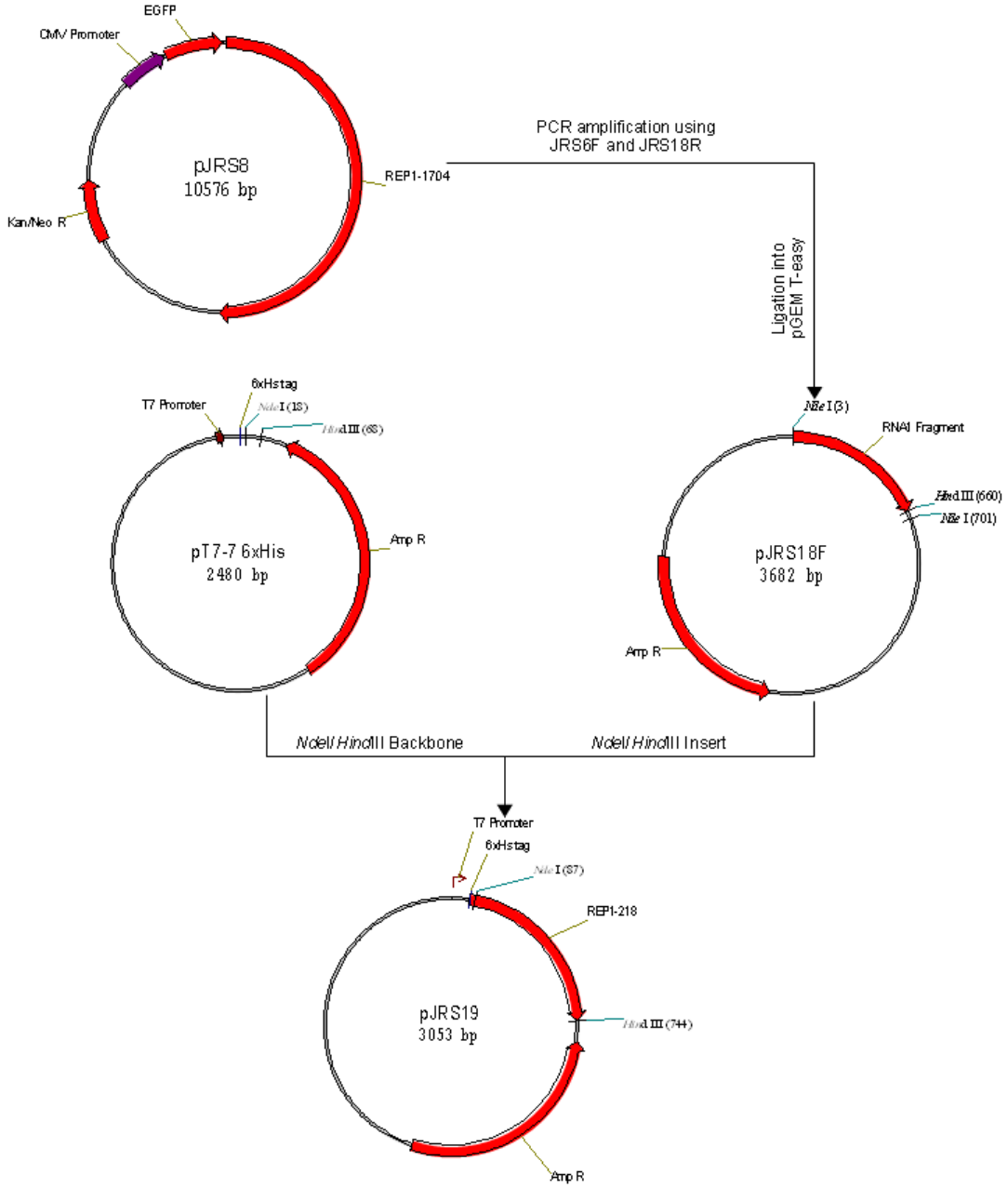

Figure A.2: The construction of pJRS19. Amp R: *β*-lactamase, CMV Promoter: *Human Cytomegalovirus* immediate early promoter, Kan/Neo R: neomycin phosphotransferase, T7 Promoter: T7 bacteriophage RNA polymerase promoter.

A.3 pJRS23

pJRS8 (Section A.5) was used as the template in the PCR amplification of approximately 1750 bp from the 3' of the HaSV replicase CDS using the primers JRS21F and JRS22R, introducing a 5' *Bam*HI and a 3' *Cla*I site into the PCR product. The PCR product was then ligated into pGEM T-easy to create pJRS21 (BamHI-ClaI) R, which was subsequently restricted with *Bam*HI and *Not*I. The resulting insert was ligated into pGEX-4T-2 (GE Healthcare) also digested with *Bam*HI and *Not*I, producing pJRS23 (Figure A.3).

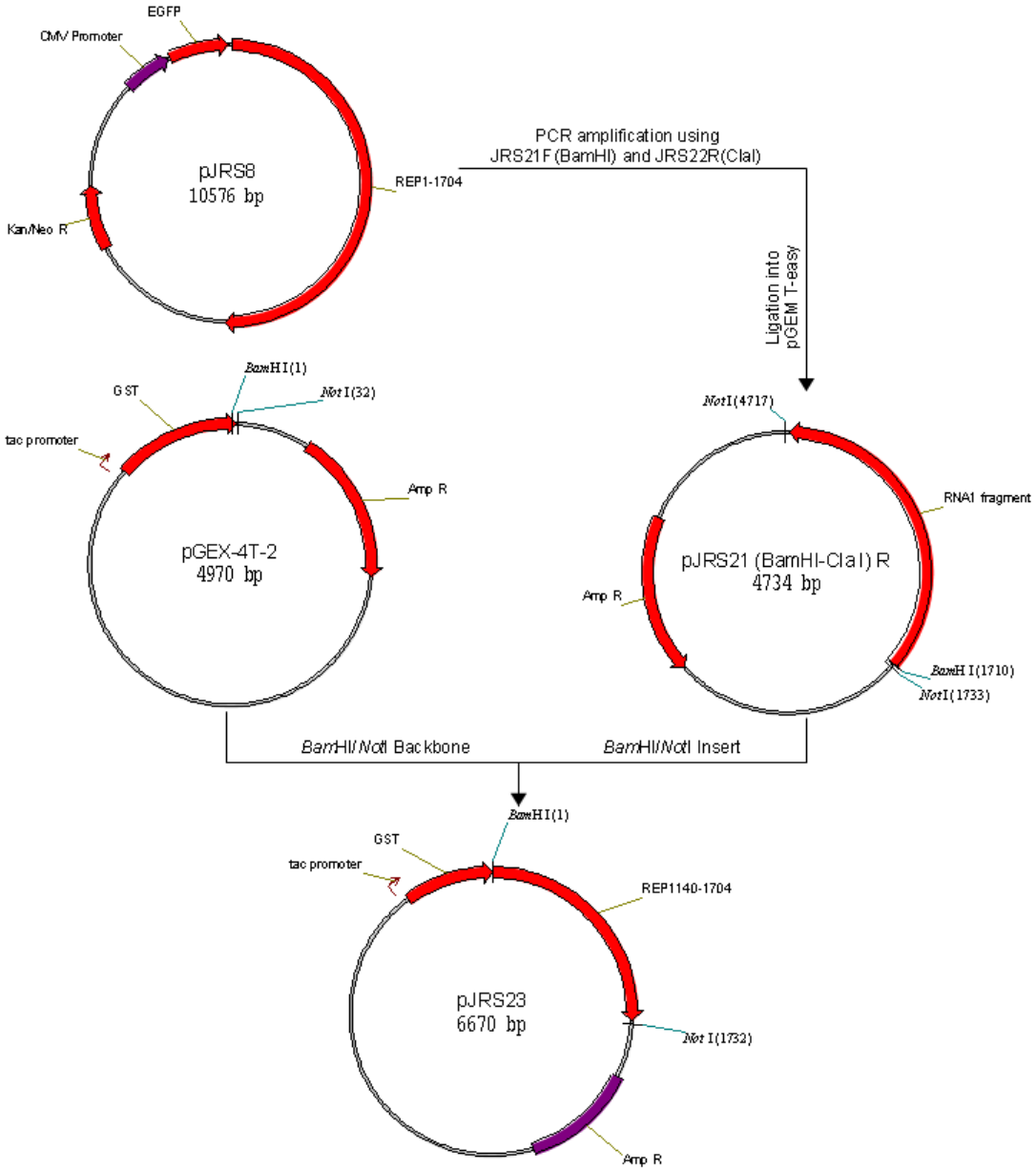

Figure A.3: The construction of pJRS23. Amp R: *β*-lactamase, CMV Promoter: *Human Cytomegalovirus* immediate early promoter, EGFP: enhanced green fluorescent protein, GST: glutathione S-transferase, Kan/Neo R: neomycin phosphotransferase, tac Promoter: hybrid bacterial promoter.

A.4 pJRS7

The REP_{1-1704}-EGFP expression vector was constructed in a two step process starting with the restriction of pMLY1 with *Bam*HI and *Hind*III and ligation of the resulting fragment into pEGFP-N1 restricted with *Bgl*II and *Hind*III, producing pJRS5. The remaining 3' 251 bp of the HaSV replicase CDS was PCR amplified using the primers JRS2 and LMR2 (designed by Lindsay Murray) and ligated into pGEM-T easy, generating pJRS6. The PCR product included the internal *Hind*III site and an engineered 3' *Bam*HI site downstream of the mutated opal stop codon that produced an in-frame fusion with the EGFP coding sequence in pEGFP-N1. Finally, both pJRS5 and pJRS6 were digested with *Hind*III and *Bam*HI and the respective fragments ligated (Figure A.4).

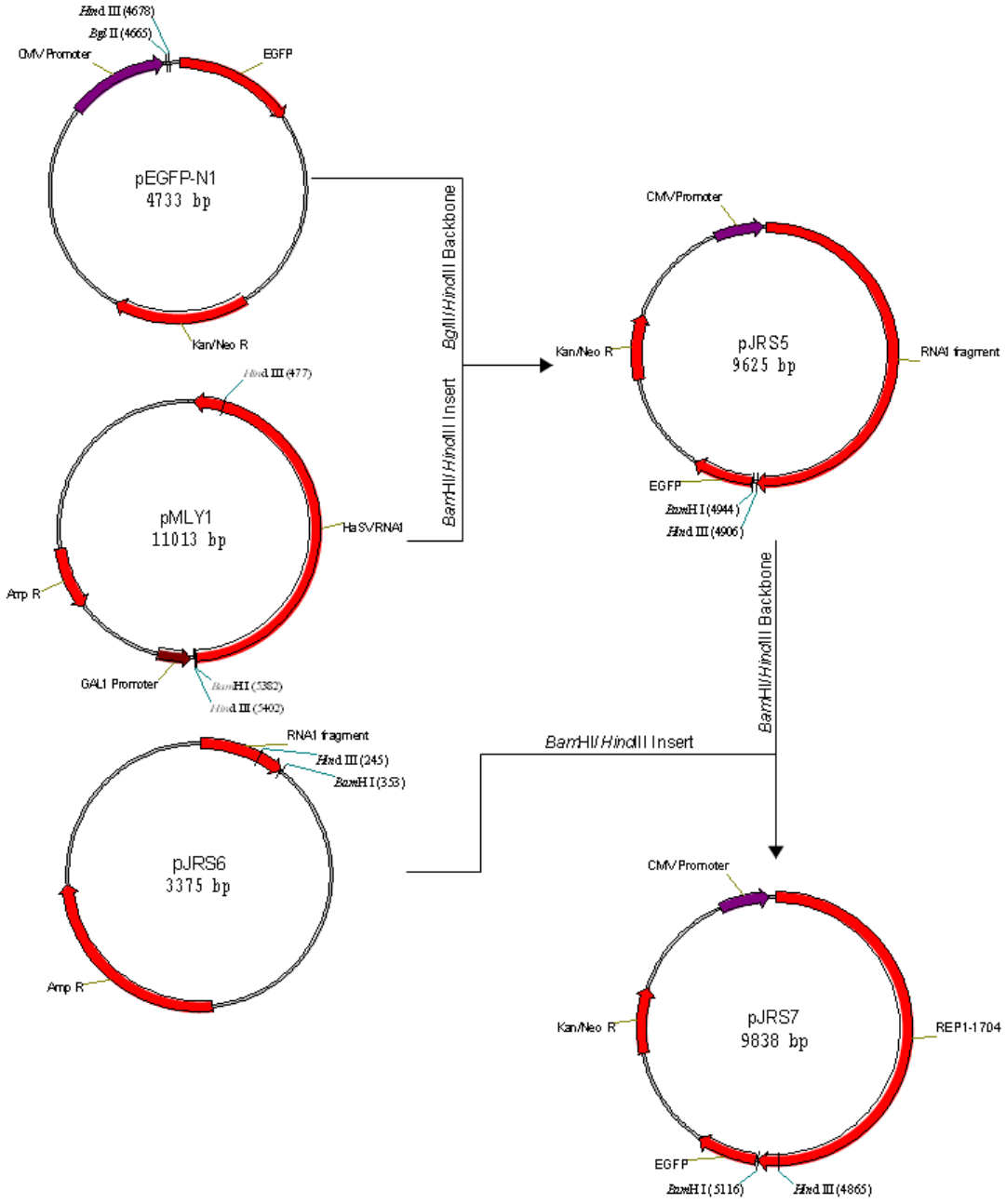

Figure A.4: The construction of pJRS7. Amp R: *β*-lactamase, CMV Promoter: *Human Cytomegalovirus* immediate early promoter, EGFP: enhanced green fluorescent protein, Kan/Neo R: neomycin phosphotransferase.

A.5 pJRS8

pMLY1 was restricted with *Hind*III and *Kpn*I and the 1682 bp fragment gel purified before ligating it into pEGFP-C1, also restricted with *Hind*III and *Kpn*I to produce pJRS4. The remaining fragment of the HaSV replicase CDS was obtained by the restriction of pMLY1 with *Kpn*I and ligated into *Kpn*I-digested pJRS4 (Figure A.5).

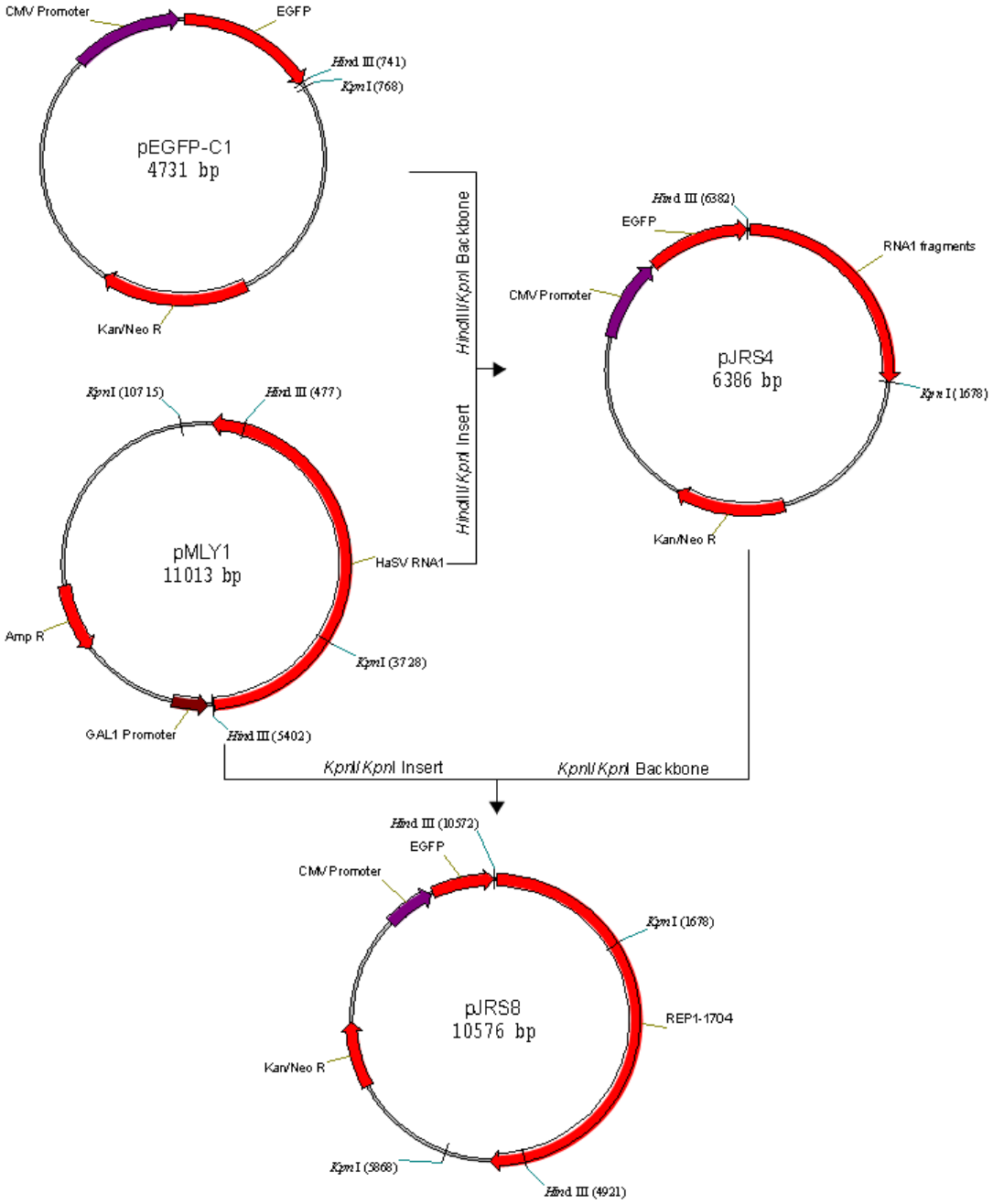

Figure A.5: The construction of pJRS8. Amp R: *β*-lactamase, CMV Promoter: *Human Cytomegalovirus* immediate early promoter, EGFP: enhanced green fluorescent protein, Kan/Neo R: neomycin phosphotransferase.

A.6 pJRS26

The restriction of pJRS6 with *Bam*HI and *Hind*III produced a fragment containing the 3' 251 bp of the HaSV replicase cDNA. This was ligated into pCW56 also digested with *Bam*HI and *Hind*III to create pJRS25. The remaining portion of the HaSV replicase CDS was added to pJRS25 by restricting pMLY1 with *Hind*III (cutting at two sites) and ligating the resulting fragment into *Hind*III digested pJRS26 (Figure A.6).

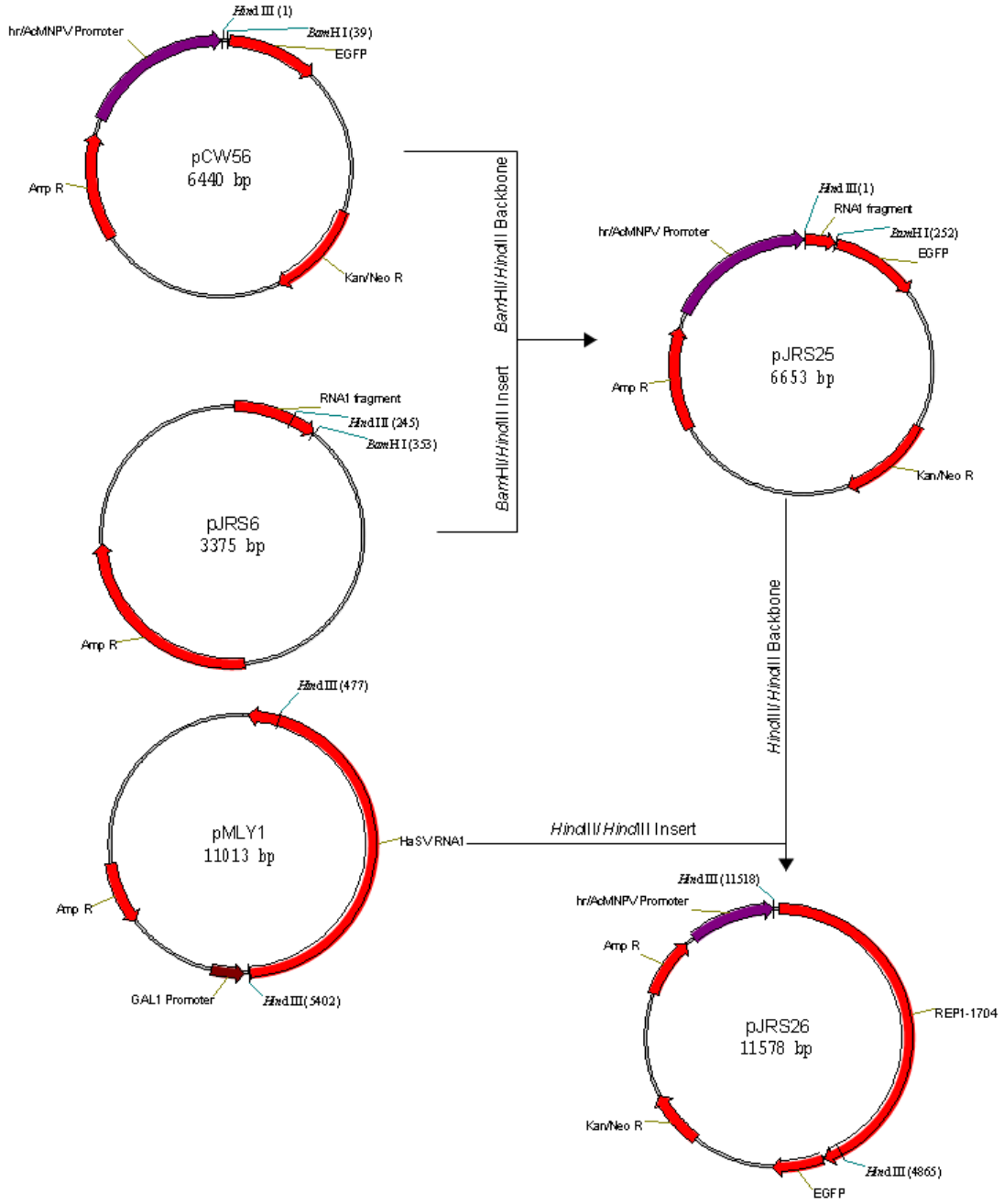

Figure A.6: The construction of pJRS26. Amp R: *β*-lactamase, EGFP: enhanced green fluorescent protein, hr/AcMNPV Promoter: hybrid insect promoter, Kan/Neo R: neomycin phosphotransferase.

A.7 pJRS 42

The V5 epitope (derived from Simian virus 5) CDS was PCR amplified using the primers JRS30F and JRS31R and ligated into pGEM T-easy to create pJRS40F. This vector was digested with *Bam*HI and *Not*I to produce an insert containing the V5 epitope CDS that was ligated into similarly restricted pJRS7. This produced the mammalian expression vector pJRS7 C-V5, which contained the sequence coding for the expression of a C-terminal full-length HaSV replicase-V5 fusion protein. Both pJRS7 C-V5 and pJRS39 (Section A.15), were restricted with *Nde*I and *Kpn*I and the resulting fragments were gel purified and ligated to create pJRS41. The sequence coding for the full-length HaSV replicase with N-terminal 6xHis and C-terminal V5 epitope tags was removed from pJRS41 by restriction with *Bgl*II and *Not*I and ligated into pFastBac^{TM} DUAL (Invitrogen), also digested with these enzymes, producing the baculovirus expression vector pJRS42 (Figure A.7).

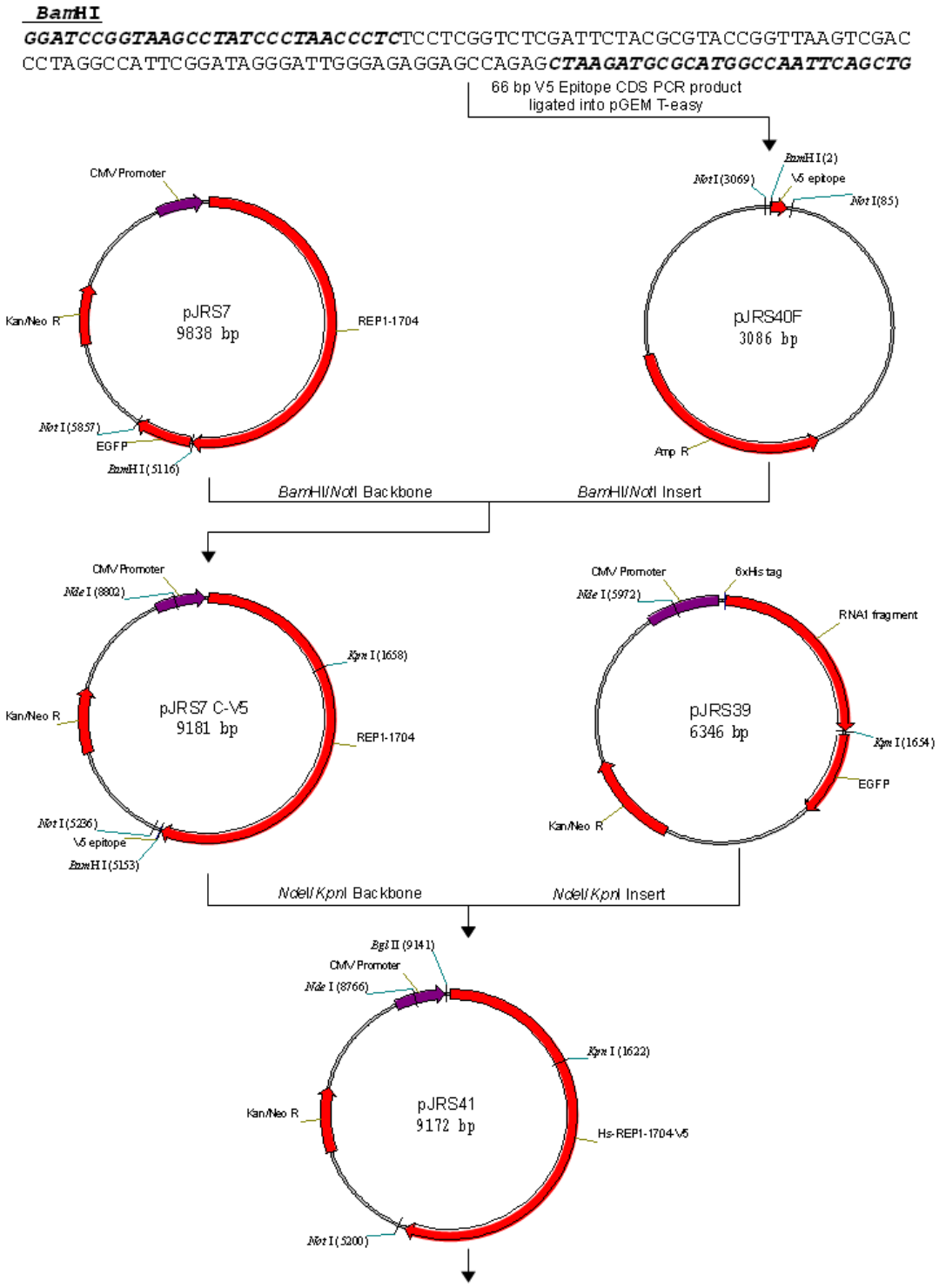

Figure A.7 (Here and page 170): The construction of pJRS42. The PCR product of the V5 epitope CDS is indicated at the top of the image with the primer sequences in bold and italics. The introduced *Bam*HI site is displayed above the sequence. Amp R: *β*-lactamase, CMV Promoter: *Human Cytomegalovirus* immediate early promoter, EGFP: enhanced green fluorescent protein, Gent R: gentamicin acetyl transferase, Kan/Neo R: neomycin phosphotransferase, PohH Promoter: AcMNPV polyhedrin promoter.

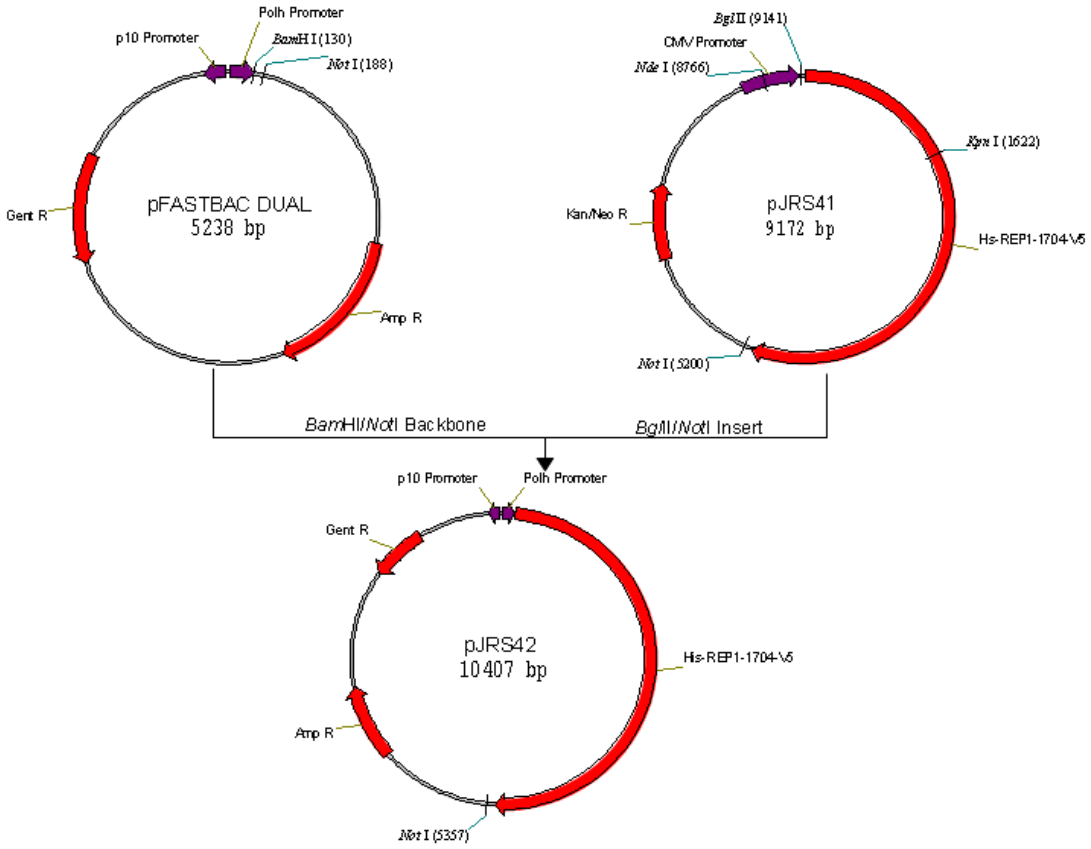

Figure A.7: Figure legend on page 169

A.8 pJRS7 N44Δ

The HaSV replicase CDS nts 134 to 1658 were PCR amplified using the primers JRS4F and JRS5R, which introduced a *Hind*III site, an engineered start codon at the 5' end and included the internal HaSV replicase *Kpn*I site at the 3' end. This product was ligated into pGEM T-easy to create pJRS9F. This was restricted with *Hind*III and *Kpn*I and the resulting fragment inserted into pEGFP-N1, also restricted with the same restriction enzymes, producing pJRS10. Both pJRS10 and pJRS7 were then digested with *Bam*HI and *Kpn*I and the resulting fragments ligated together to make pJRS7 N44Δ (Figure A.8).

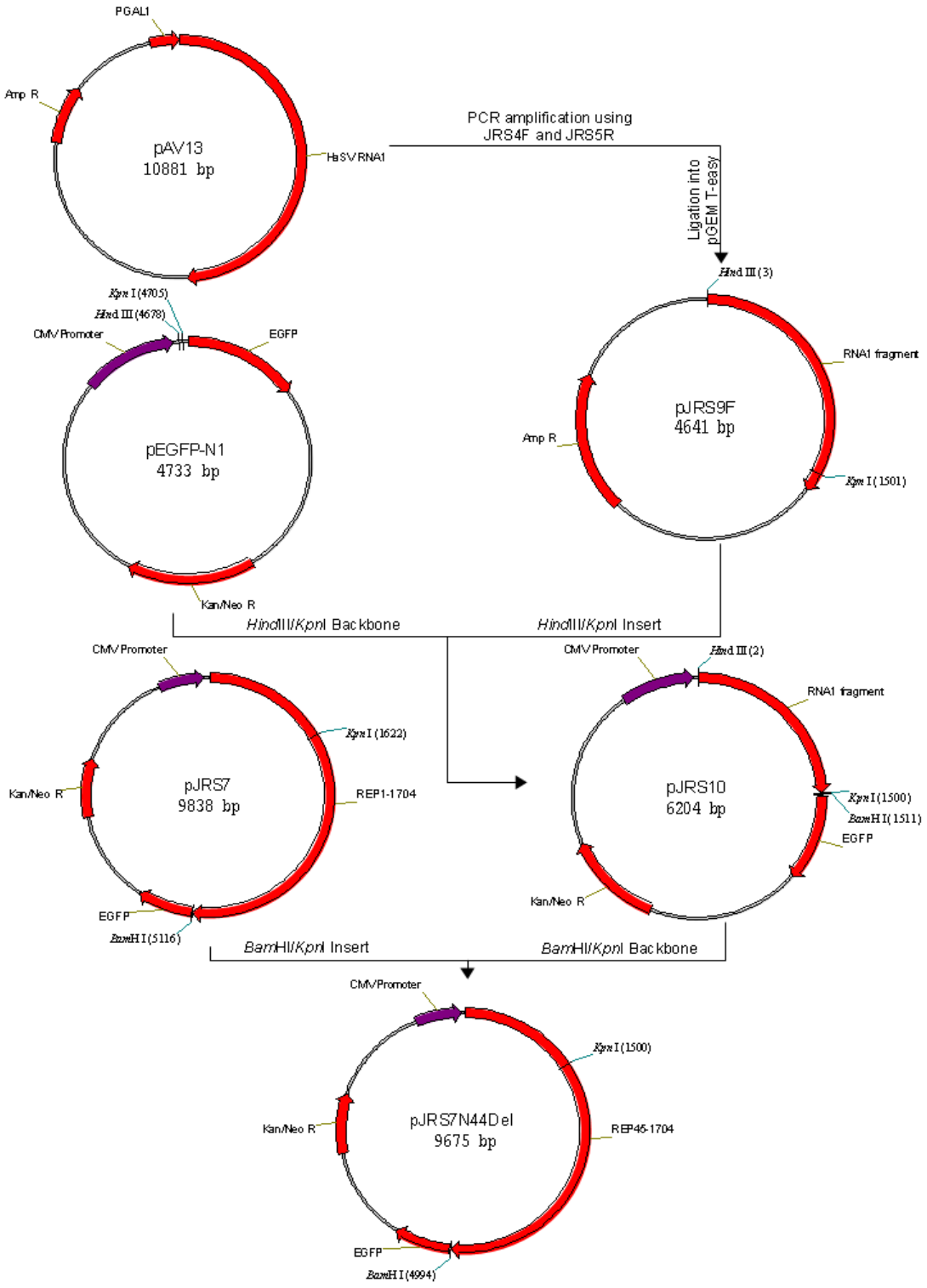

Figure A.8: The construction of pJRS7N44Δ. Amp R: *β*-lactamase, CMV Promoter: *Human Cytomegalovirus* immediate early promoter, EGFP: enhanced green fluorescent protein, Kan/Neo R: neomycin phosphotransferase.

A.9 pJRS12

Approximately 300 nts of the 5’ of the HaSV replicase were PCR amplified using JRS14F and JRS13R, which introduced 5' *Hind*III and 3' *Bam*HI sites into the PCR product, and ligated into pGEM T-easy to created pJRS13F. The 5' replicase amplicon was then removed from pJRS13F by restriction using *Hind*III and *Bam*HI and ligated into similarly digested pEGFP-N1 (Figure A.9).

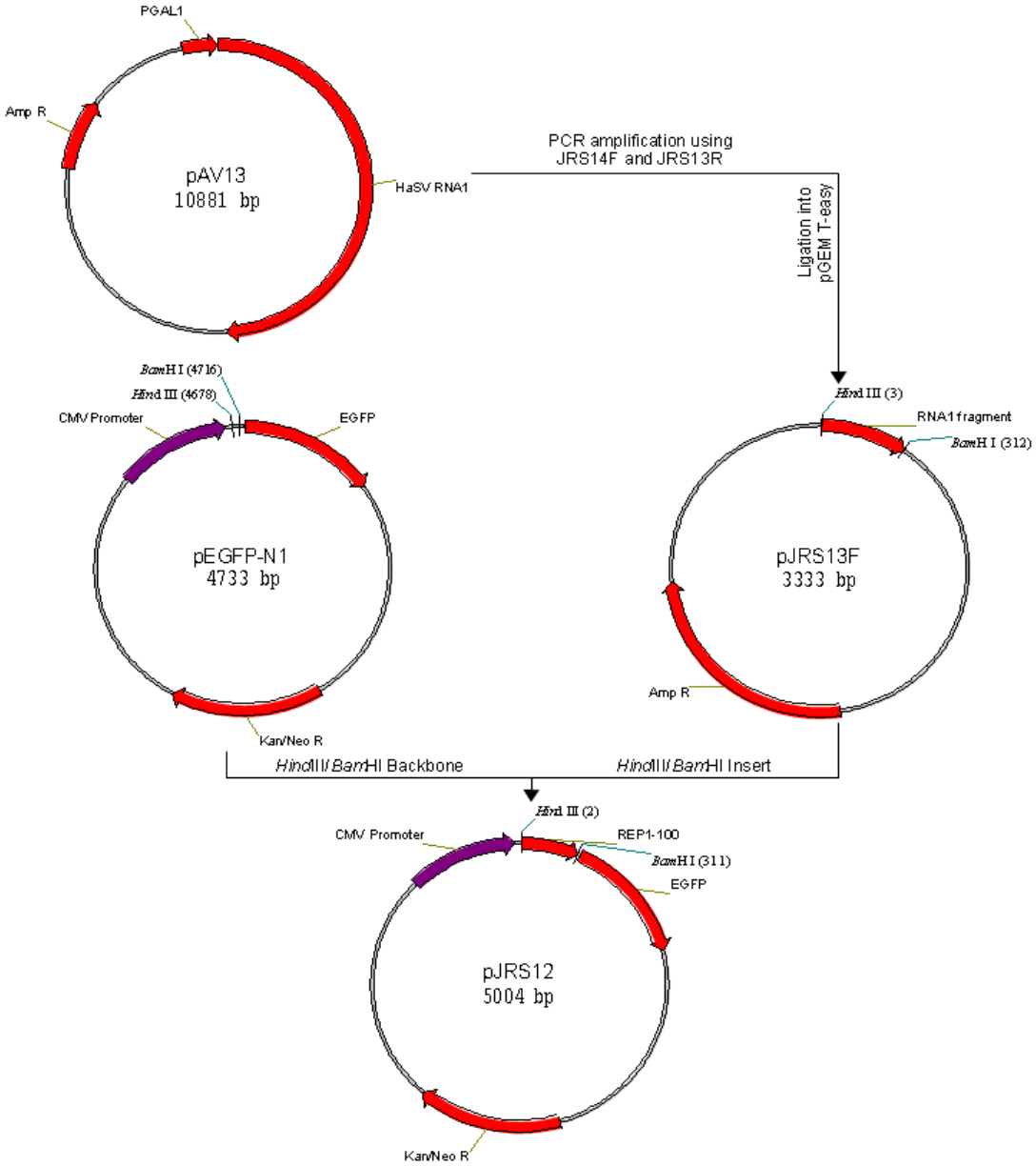

Figure A.9: The construction of pJRS12. Amp R: *β*-lactamase, CMV Promoter: *Human Cytomegalovirus* immediate early promoter, EGFP: enhanced green fluorescent protein, Kan/Neo R: neomycin phosphotransferase.

A.10 pJRS15

The region of the replicase CDS from the internal *Kpn*I site up to the 5' end of the sequence encoding the RdRp domain were PCR amplified using the primers JRS7F and JRS17R. This PCR product was ligated into pGEM T-easy to produce pJRS14R. Both pJRS14R and pJRS7 were in turn digested with *Kpn*I and *Bam*HI and the respective fragments ligated together to generate pJRS15 (Figure A.10).

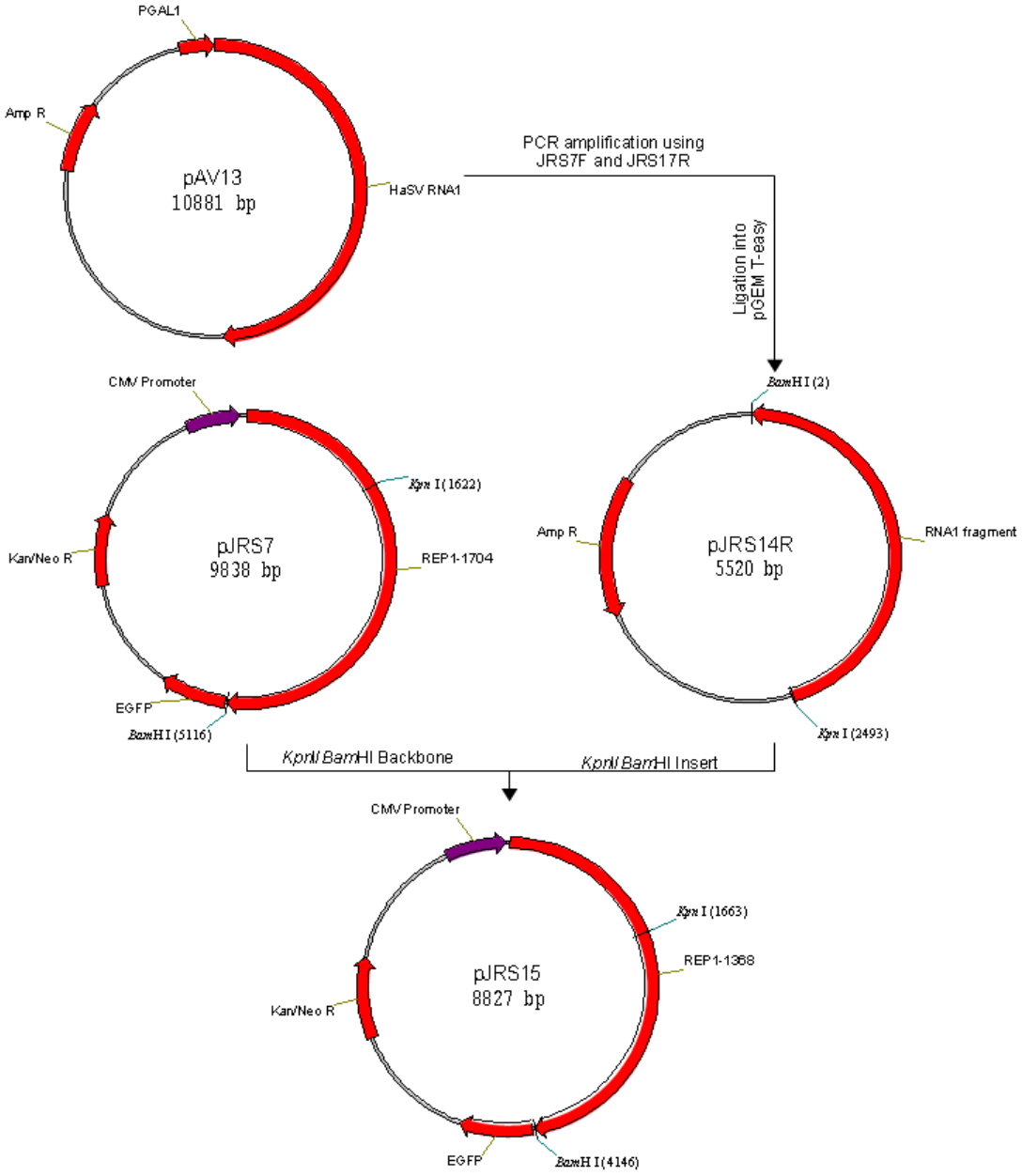

Figure A.10: The construction of pJRS15. Amp R: *β*-lactamase, CMV Promoter: *Human Cytomegalovirus* immediate early promoter, EGFP: enhanced green fluorescent protein, Kan/Neo R: neomycin phosphotransferase.

A.11 pJRS16

pEGFP-N1 was digested with *Bgl*II and *Sma*I and the HaSV replicase CDS fragment, obtained from pMLY1 restricted with *Bam*HI and *Pvu*II, was ligated into the pEGFP-N1 backbone to produce pJRS16 (Figure A.11).

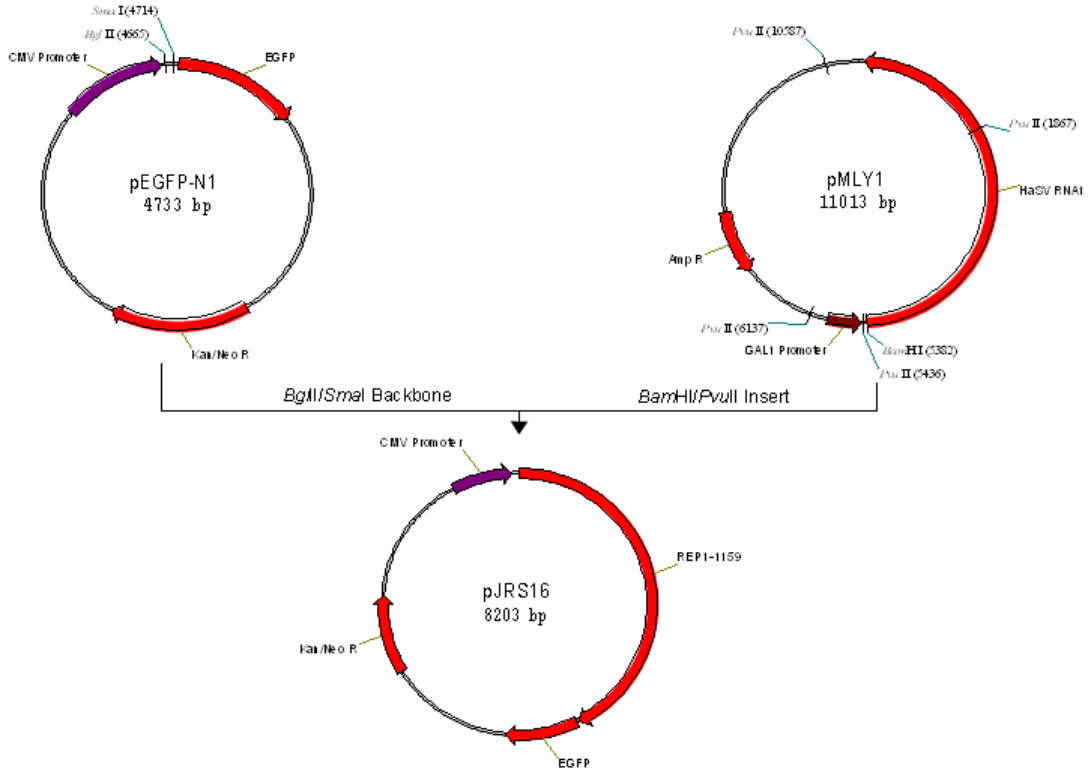

Figure A.11: The construction of pJRS16. Amp R: *β*-lactamase, CMV Promoter: *Human Cytomegalovirus* immediate early promoter, EGFP: enhanced green fluorescent protein, Kan/Neo R: neomycin phosphotransferase.

A.12 pJRS32

A fragment of the HaSV replicase spanning from the internal *Sma*I site to a region within the RdRp domain of the CDS was PCR amplified using the primers JRS23F and JRS24R, which introduced a *Bam*HI site at the 3' end of the amplicon. The PCR product was ligated into pGEM T-easy to generate pJRS31F. Both pJRS16 and pJRS31F were digested with *Sma*I and *Bam*HI and the respective fragments gel-purified and ligated together to form pJRS32 (Figure A.12).

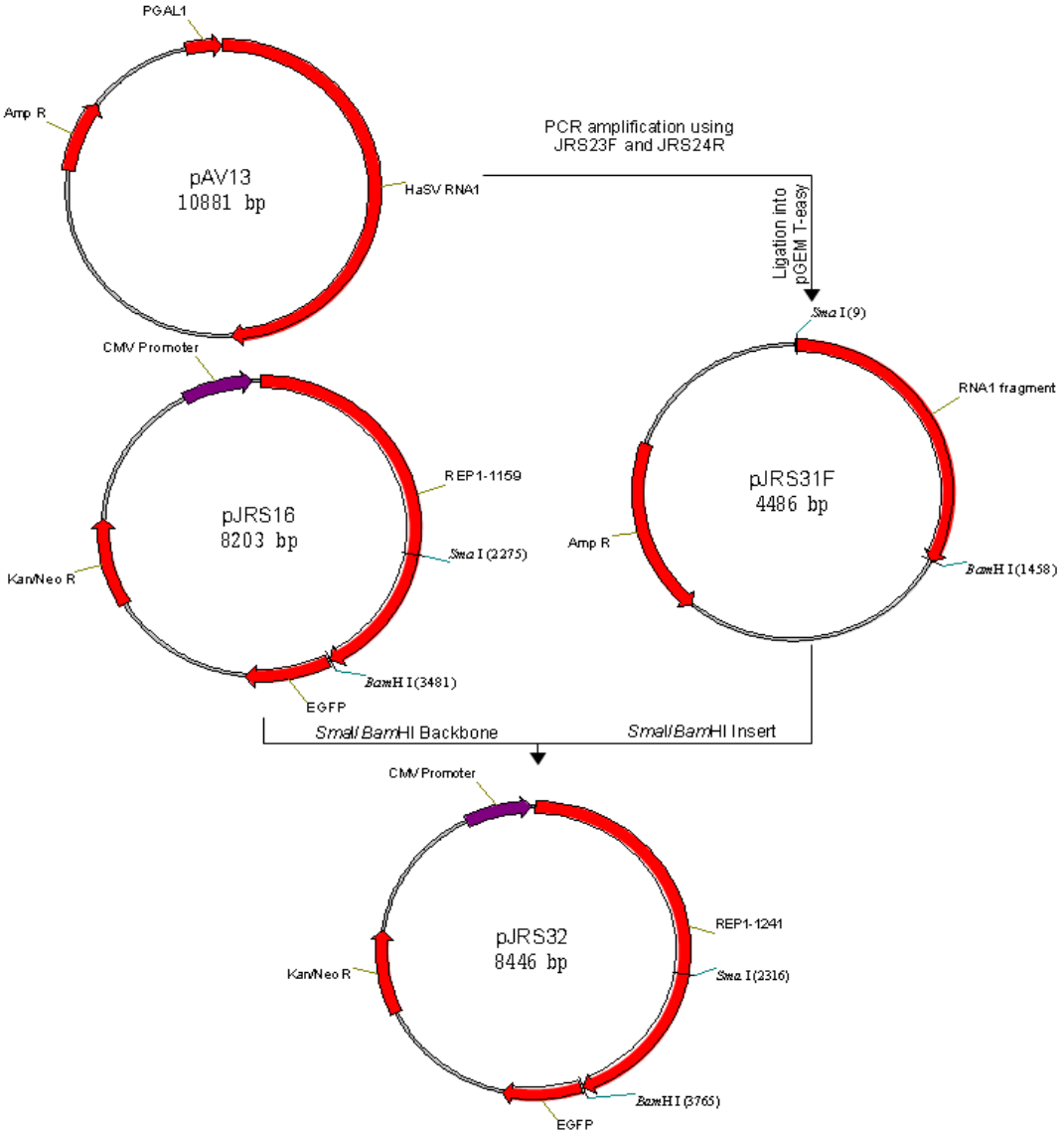

Figure A.12: The construction of pJRS32. Amp R: *β*-lactamase, CMV Promoter: *Human Cytomegalovirus* immediate early promoter, EGFP: enhanced green fluorescent protein, Kan/Neo R: neomycin phosphotransferase.

A.13 pJRS34

A replicase fragment from the internal *Sma*I site of the replicase CDS to a region within the RdRp domain was PCR amplified using the primers JRS23F and JRS25R, introducing a *Bam*HI site at the 3' end of the PCR product. This was ligated into pGEM T-easy to generate pJRS33F. pJRS34 was then generated by digesting pJRS33F and pJRS16 with *Sma*I and *Bam*HI and ligating the gel-purified products together (Figure A.13).

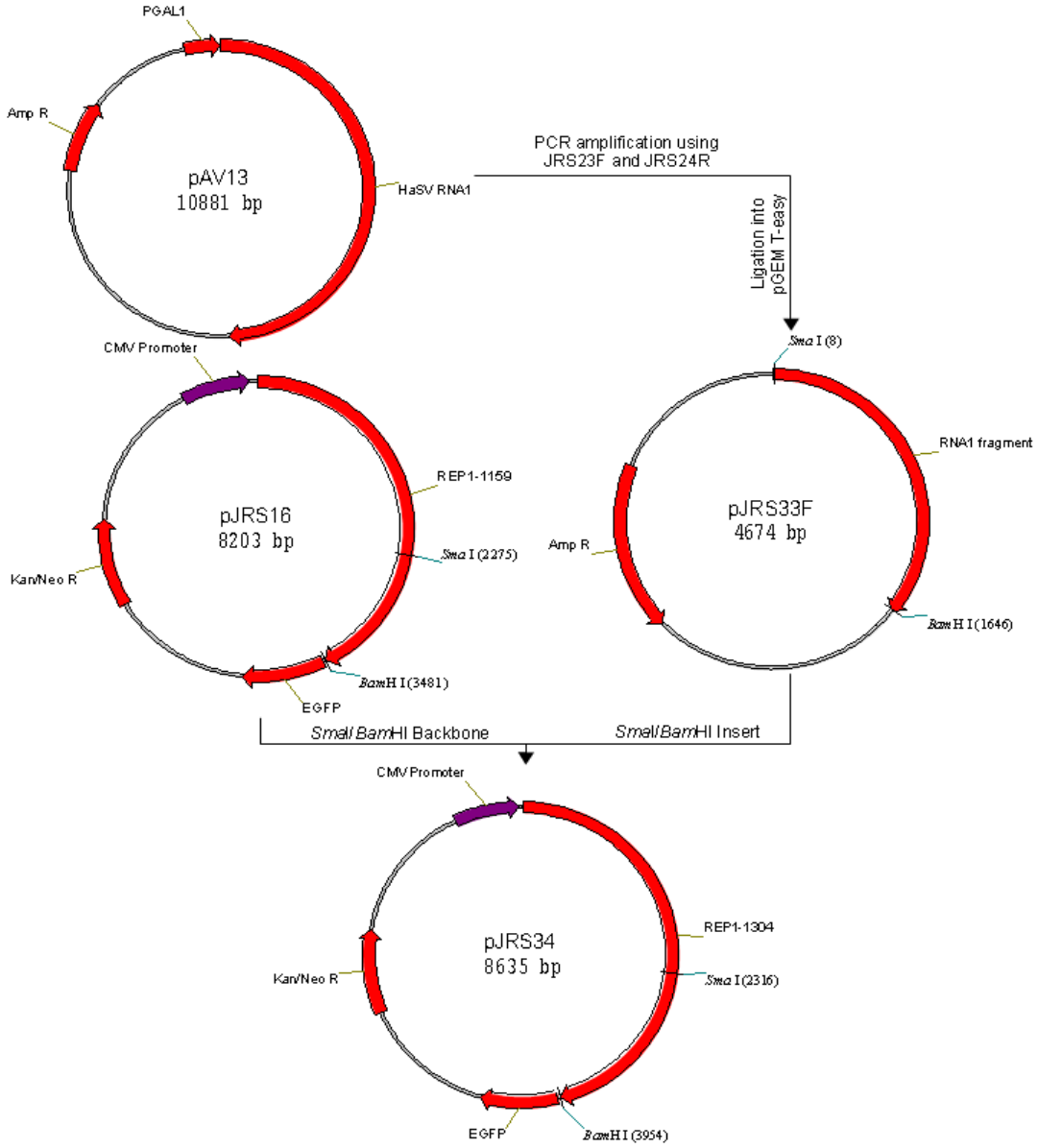

Figure A.13: The construction of pJRS34. Amp R: *β*-lactamase, CMV Promoter: *Human Cytomegalovirus* immediate early promoter, EGFP: enhanced green fluorescent protein, Kan/Neo R: neomycin phosphotransferase.

A.14 pJRS26 2A

A ds oligonucleotide containing partial *Bam*HI sites and the entire CDS of the ERAV 2A-like sequence was produced as follows. Forward and reverse primers (JRS33F and JRS34R) (50 nmol of each) were phosphorylated in the presence of 1.875 mM ATP, 1 x polynucleotide kinase buffer and 7.5 U T4 polynucleotide kinase (Promega) (in a total of 20 µl) at 37 °C for 30 minutes. The phosphorylated primers were then purified by adding 130 µl phenol:chloroform:isoamyl alcohol (25:24:1) (PCI), mixing vigorously and centrifuging at 14 000 rpm in a benchtop microcentrifuge at 4 °C for 2 minutes. The aqueous phase was then re-extracted under the same conditions. To the retained aqueous phase, 15 µl 3 M NaAc and 300 µl 96 % ethanol was added and the sample placed at -80 °C for 1 hour. The precipitated DNA was collected by centrifugation at 14 000 rpm at 4 °C for 5 minutes and air dried after the excess ethanol was removed. The pellet was resuspended in 35 µl ddH_2O, 5 µl 1 M $MgCl_2$ and 10 µl 1 M Tris (pH 7.6) and the primers annealed by incubation in boiling water for 2 minutes and slow cooling to room temperature. The ds oligonucleotide was then ligated into pJRS25 (Section A.6) restricted with *Bam*HI to generate pJRS25 2A. The remaining HaSV replicase CDS was removed from pJRS26 (Section A.6) using *Hind*III, gel purified and ligated into pJRS25 2A, also digested with *Hind*III, to produce pJRS26 2A (Figure A.14).

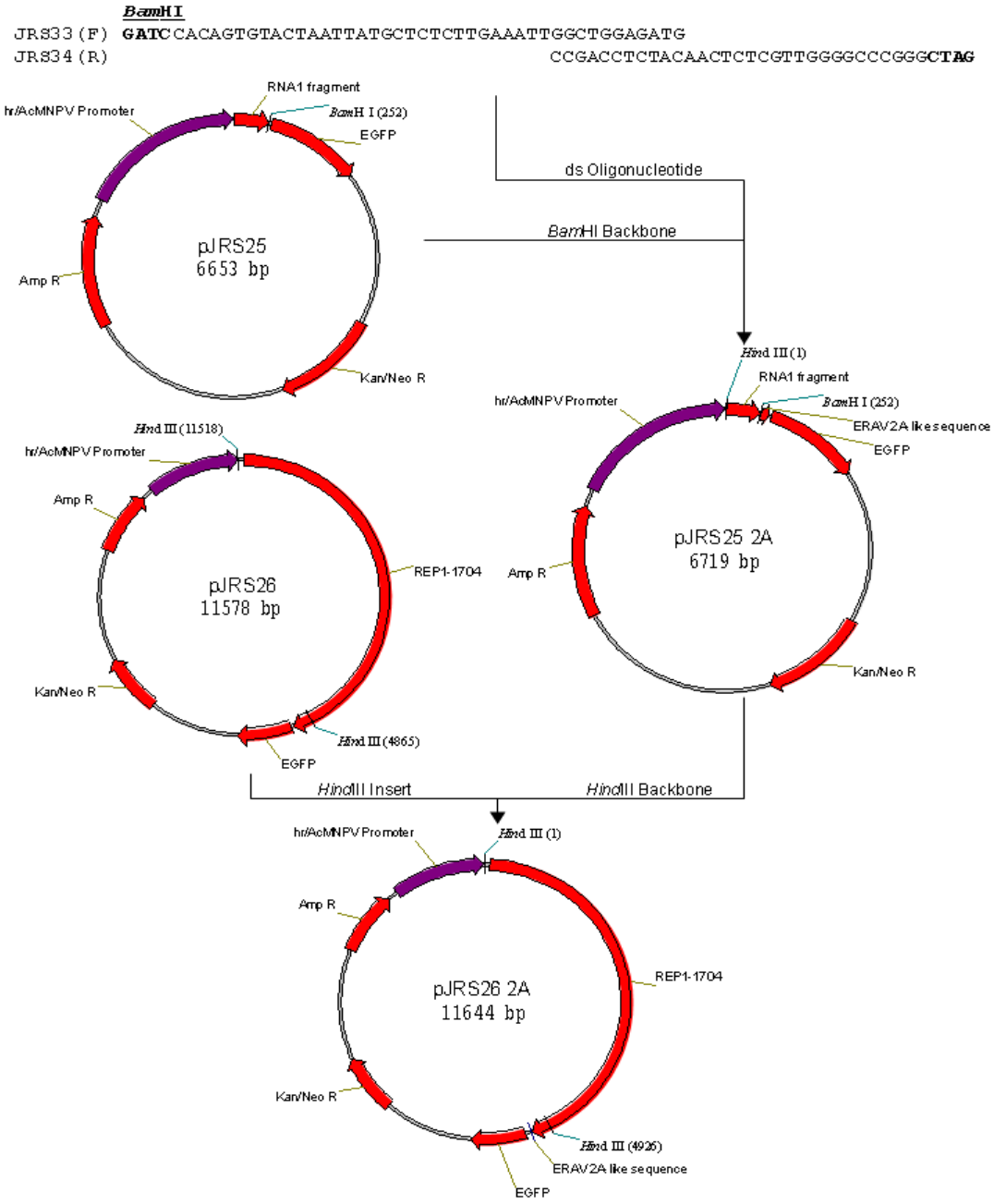

Figure A.14: The construction of pJRS26 2A. The ds oligonucleotide generated by annealing JRS33F and JRS34R is displayed at the top of the image. *Bam*HI-complimentary overhangs are indicated in bold while the sequence for recreating the *Bam*HI site is designated above the sequence. Amp R: *β*-lactamase, EGFP: enhanced green fluorescent protein, hr/AcMNPV Promoter: hybrid insect promoter, Kan/Neo R: neomycin phosphotransferase.

A.15 pJRS7 N-His

A ds oligonucleotide including 5' *Hind*III and *Bam*HI sites, the CDS for a 6xHis tag and partial *Kpn*I and *Nde*I sites at the 5' and 3' ends respectively, was produced from the primers JRS28F and JRS29R as described in section A.14. This was inserted into pJRS17 (Section A.1) digested with *Kpn*I and *Nde*I to produce pJRS37. The 5' end of the 6xHis tagged replicase CDS fragment was then removed from pJRS37, using *Hind*III and *Xho*I, and ligated into pJRS9F (Section A.8), also digested with these enzymes, generating pJRS38. *Bgl*II and *Kpn*I digestion of pJRS38 produced an N-terminal 6xHis tagged replicase CDS fragment that was inserted into the similarly digested pEGFP-N1 backbone (pJRS39). Finally, pJRS7 N-His was generated by digesting both pJRS7 (Section A.4) and pJRS39 with *Bam*HI and *Kpn*I and ligating the 3' end of the replicase CDS into pJRS39 (Figure A.15).

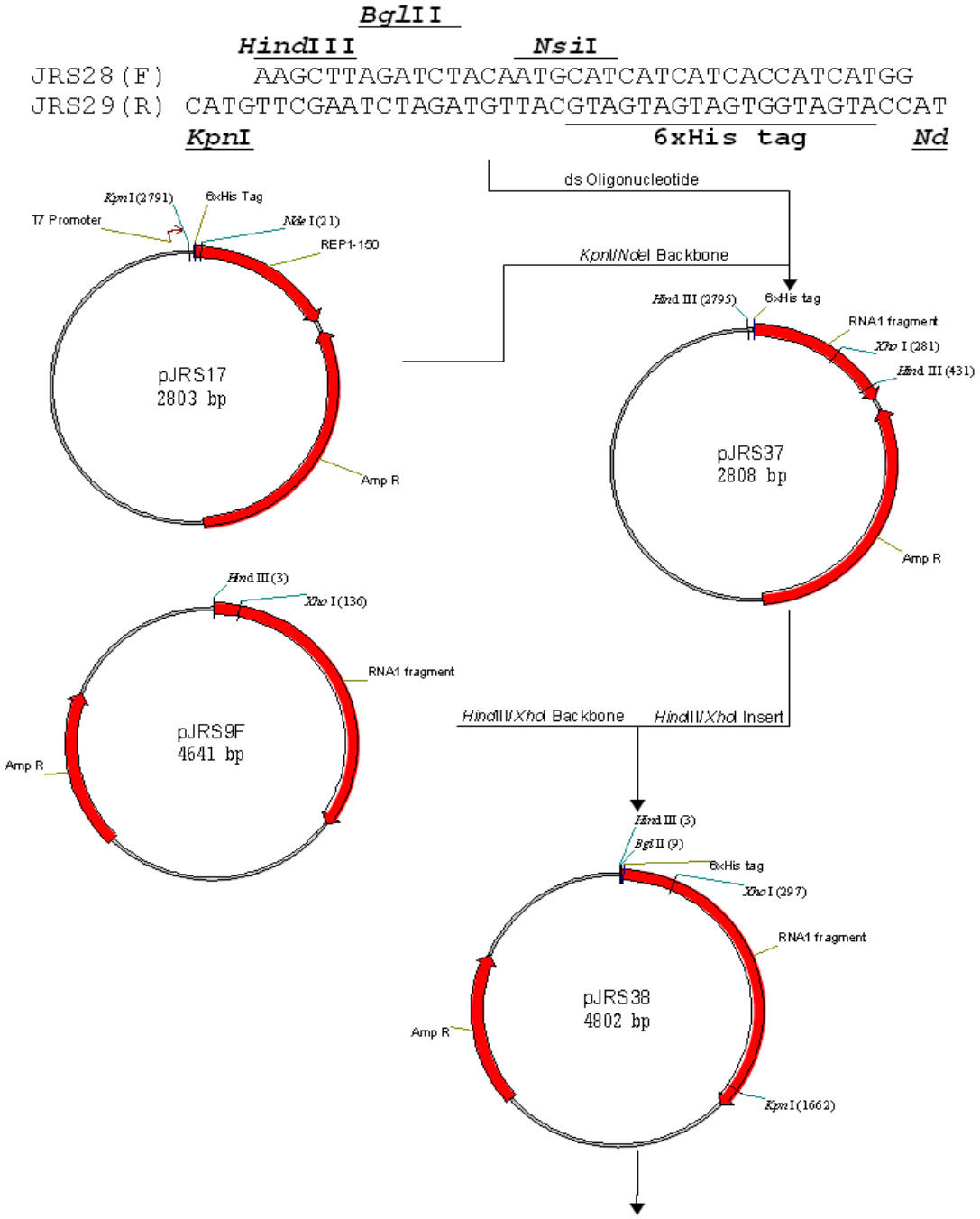

Figure A.15 (Here and pg 186): The construction of pJRS7 N-His. The ds oligonucleotide generated by annealing JRS28F and JRS29R is displayed at the top of the image. Full restriction sites are shown above the sequence while sequences complimentary to, but not capable of reforming *Kpn*I and *Nde*I sites are shown below the sequence. The 6xHis tag CDS is also displayed below the sequence. Amp R: *β*-lactamase, CMV Promoter: *Human Cytomegalovirus* immediate early promoter, EGFP: enhanced green fluorescent protein, Kan/Neo R: neomycin phosphotransferase, T7 Promoter: T7 bacteriophage RNA polymerase promoter.

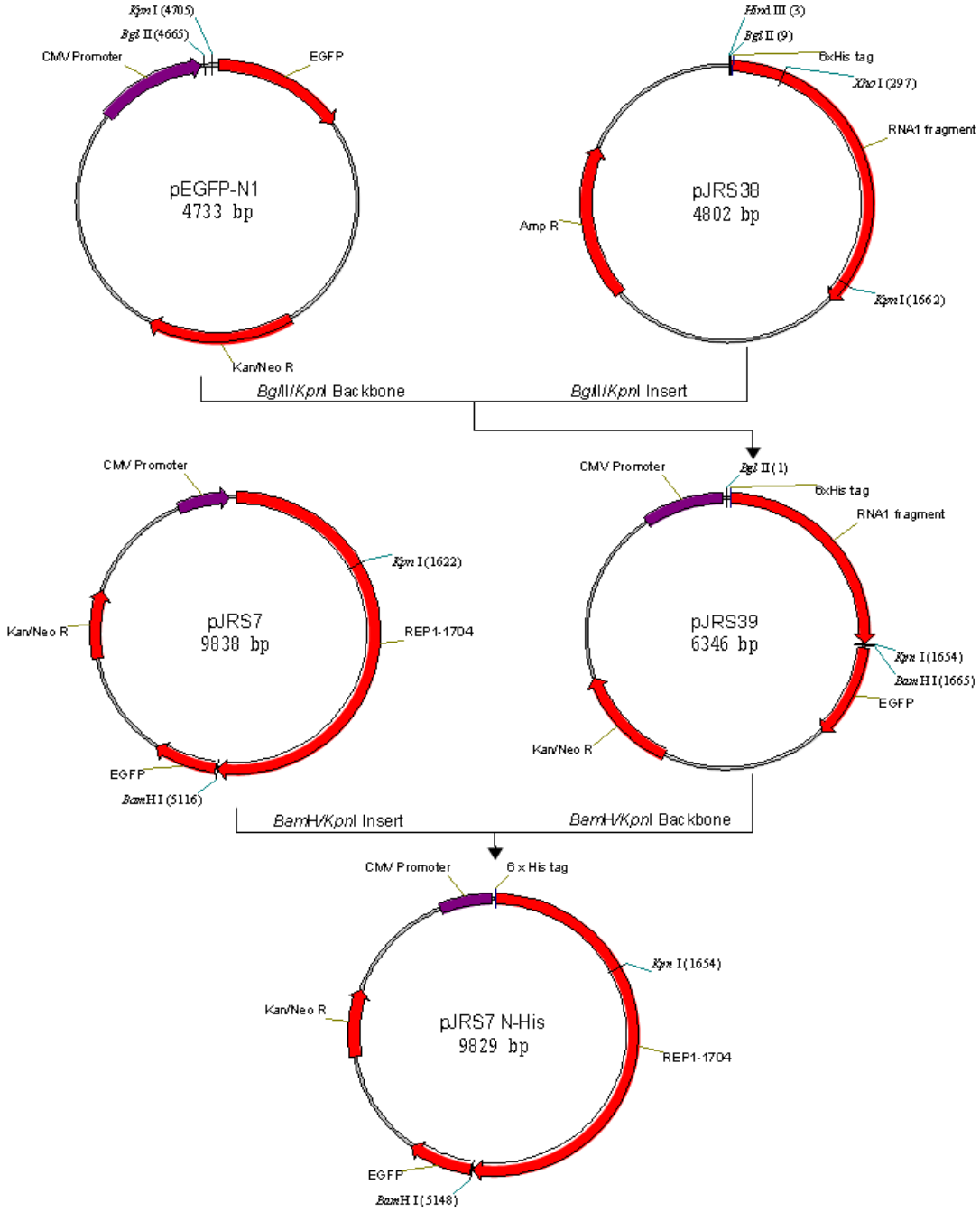

Figure A.15: Figure legend on pg 185

A.16 pJRS7 RPCR1-5

The 5' end of the HaSV replicase CDS, including the wild-type HaSV replicase Kozak sequence, was PCR amplified using the primers JRS45F and JRS5R, introducing a 5' *Bgl*II site and including the native *Kpn*I site. This PCR product was ligated into pGEM T-easy to generate pJRS48F. Five different primer sets (JRS49R and JRS52F, JRS50R and JRS52F, JRS49R and JRS53F, JRS50R and JRS53F, JRS51R and JRS53F) were then used in RPCR reactions, using pJRS48F as a template. The RPCR products were then phosphorylated with polynucleotide kinase (Promega) (as described in Section A.14) and re-ligated to produce pJRS48 RPCR1-5 (Figure A.16a). Four of the RPCR products (1, 2, 3 and 5) were then restricted with *Bgl*II and *Spe*I and the resulting inserts ligated into pJRS7 N-His (Section A.15), also digested with *Bgl*II and *Spe*I resulting in pJRS7 RPCR1, -2, -3 and -5, respectively (Figure A.16b). Due to the presence of a second internal *Bgl*II site in the 5' of the HaSV replicase sequence of pJRS48 RPCR4, an alternate process for the production of pJRS7 RPCR4 was necessary. pJRS7 N-His and pJRS48 RPCR4 were restricted with *Bgl*II and *Nco*I, respectively, before being “filled in” using Klenow DNA polymerase (Promega). Thereafter they were digested with *Spe*I and the resulting fragments ligated together to form pJRS7 RPCR4 (Figure A.16c).

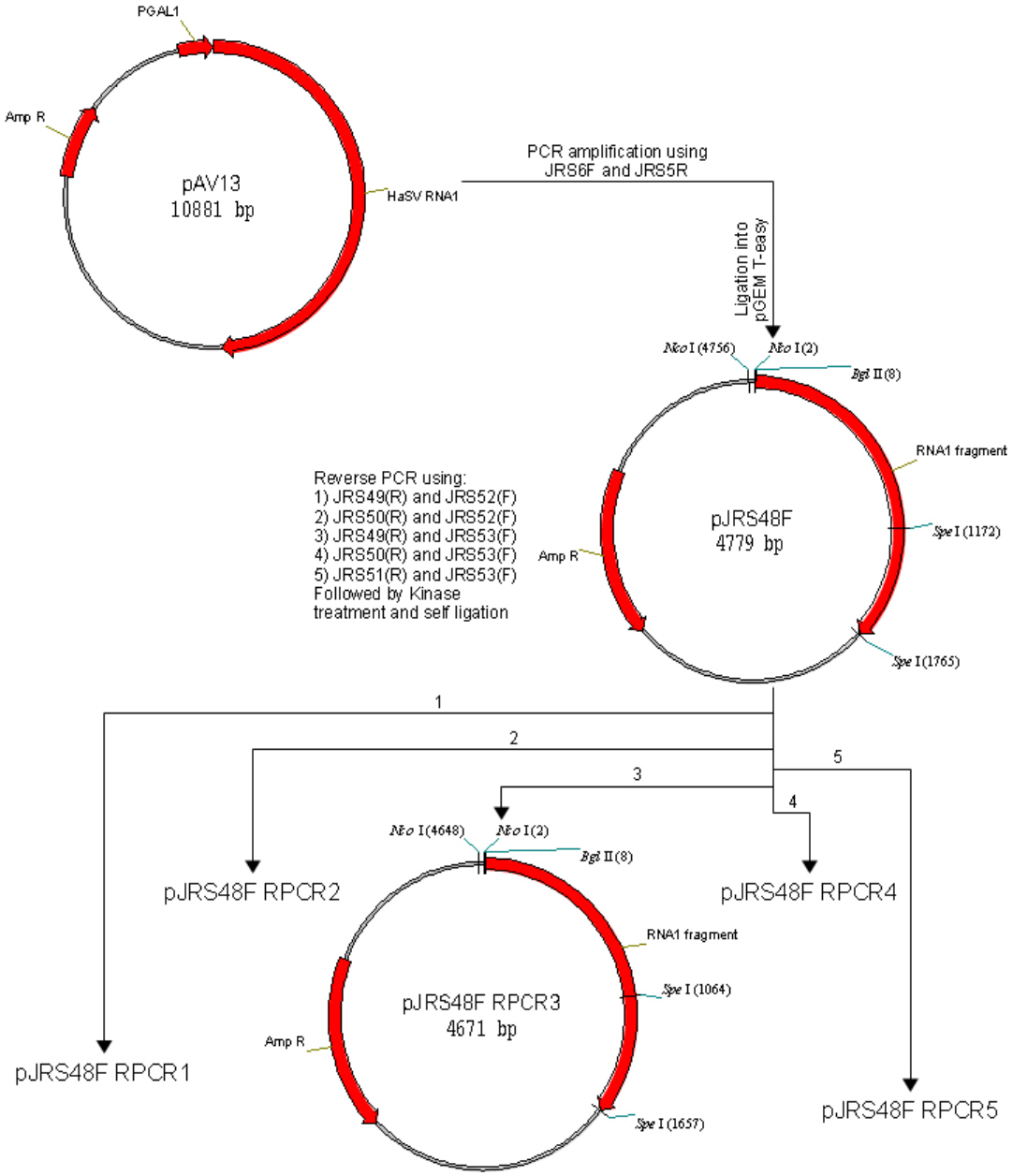

Figure A.16a: The construction of pJRS48F RPCR1-5. Amp R: *β*-lactamase, T7 Promoter: T7 bacteriophage RNA polymerase promoter.

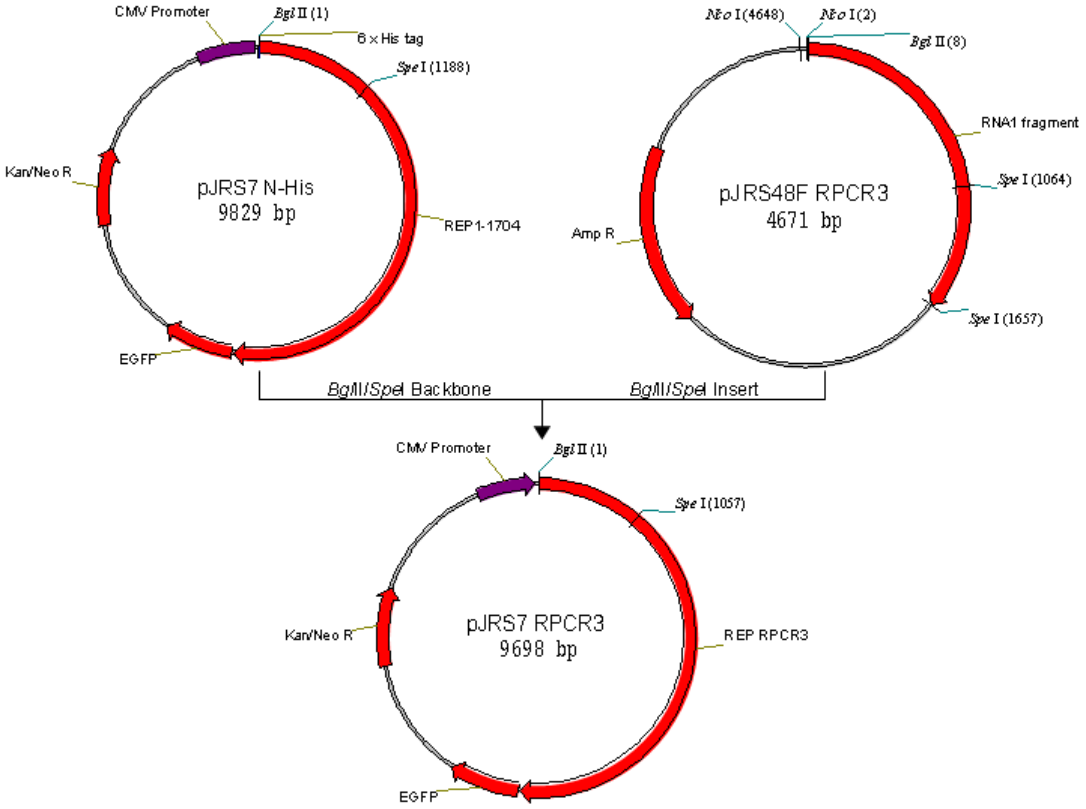

Figure A.16b: The construction of pJRS7 RPCR3. Amp R: *β*-lactamase, CMV Promoter: *Human Cytomegalovirus* immediate early promoter, EGFP: enhanced green fluorescent protein, Kan/Neo R: neomycin phosphotransferase.

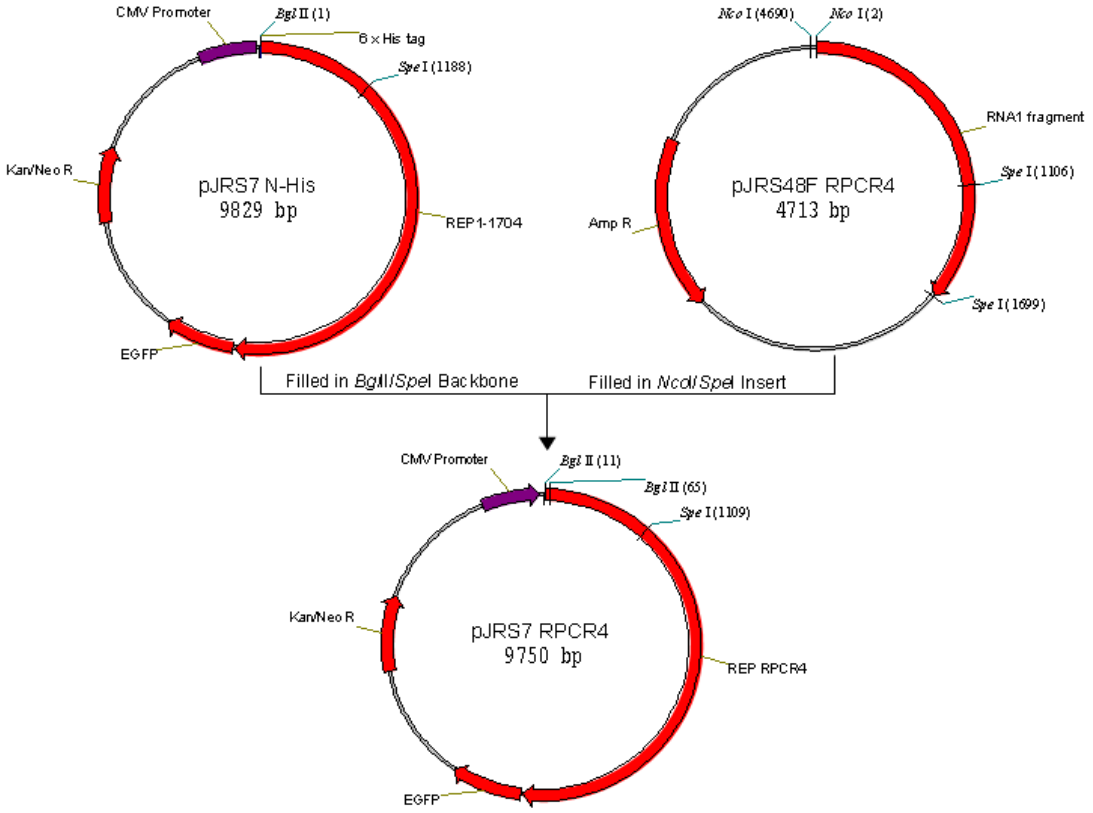

Figure A.16c: The construction of pJRS7 RPCR4. Amp R: *β*-lactamase, CMV Promoter: *Human Cytomegalovirus* immediate early promoter, EGFP: enhanced green fluorescent protein, Kan/Neo R: neomycin phosphotransferase.

A.17 pJRS7 N-NBV

The 5' region of the NβV replicase CDS was PCR amplified from pGEM6625 (Luke, 2001) using JRS47F and JRS48R and ligated into pGEM T-easy to generate pJRS49. The HaSV replicase 5' sequence was replaced by the 235 nts encoding the NβV replicase N-terminus by digesting both pJRS48F and pJRS49 with *Nco*I and *Xho*I and ligating the products together to form pJRS48 NBV. The NβV/HaSV replicase chimeric 5' sequence (removed from pJRS48 NBV using *Bam*HI and *Spe*I) was then used to replace the existing 5' sequence of the HaSV replicase in pJRS7 N-His (section A.15) (digested with *Bgl*II and *Spe*I), resulting in pJRS7 N-NBV (Figure A.17).

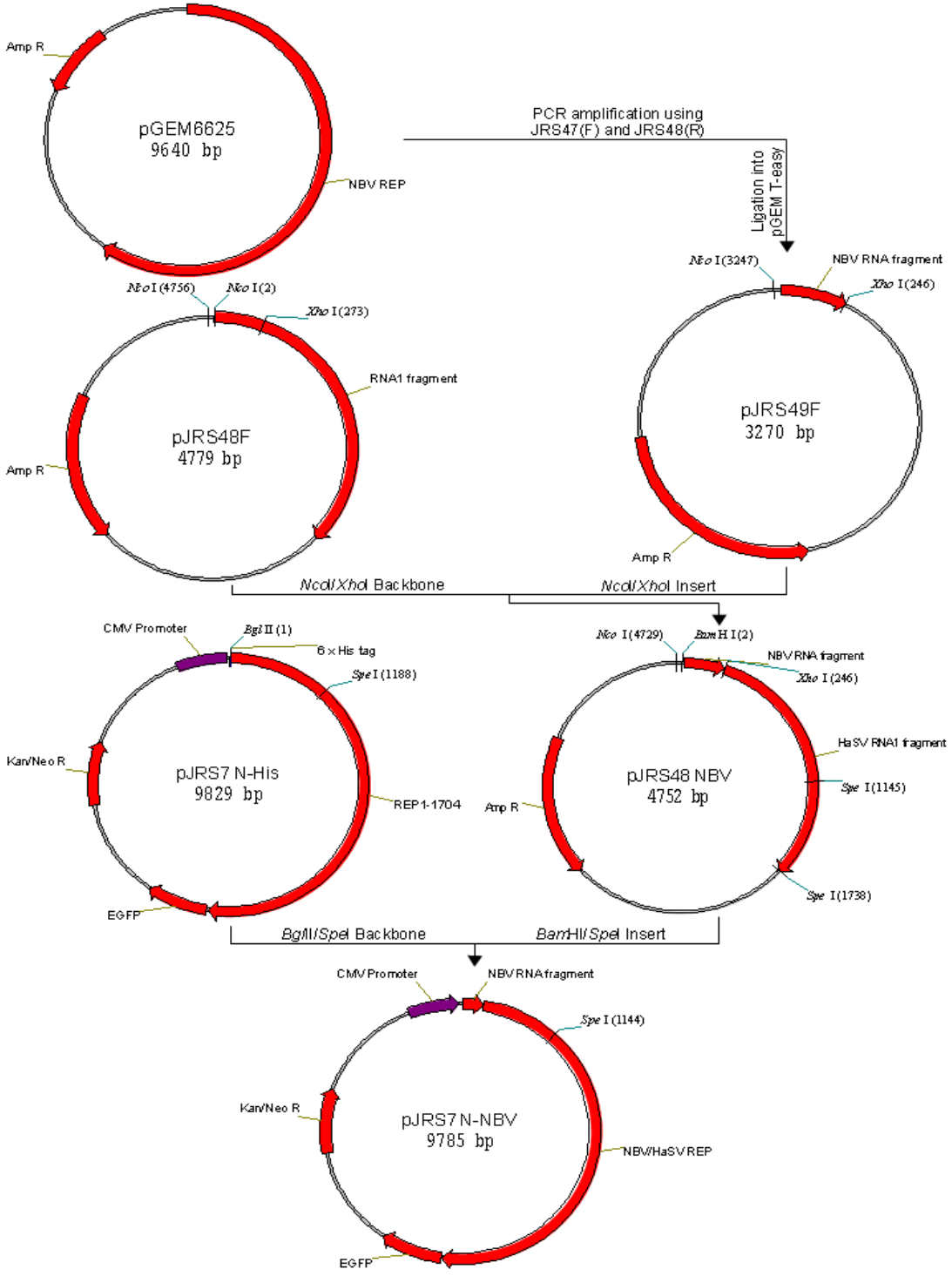

Figure A.17: The construction of pJRS7 N-NβV. Amp R: *β*-lactamase, CMV Promoter: *Human Cytomegalovirus* immediate early promoter, EGFP: enhanced green fluorescent protein, Kan/Neo R: neomycin phosphotransferase.

A.18 pJRS42 N83Δ

Primers JRS43F and JRS44R were used to generate a ds oligonucleotide containing the CDS for a 6xHis tag and partial *Bgl*II and *Xho*I sites (5' and 3' respectively) as described in section A.14. This ds oligonucleotide was then ligated into pJRS10 (section A.8) digested first with *Bgl*II and then *Xho*I, generating a 256 nt deletion of the HaSV replicase CDS with an N-terminal 6xHis tag (pJRS46). The truncated 5' sequence was then transferred to pJRS41 by digesting both plasmids with *Bgl*II and *Kpn*I and ligating the resulting fragments to create pJRS41 N83Δ. The replicase CDS was then inserted into pFastBac^{TM} DUAL (Invitrogen) by restricting both with *Bam*HI and *Not*I and subsequently ligating the appropriate fragments to produce pJRS42 N83Δ (Figure A.18).

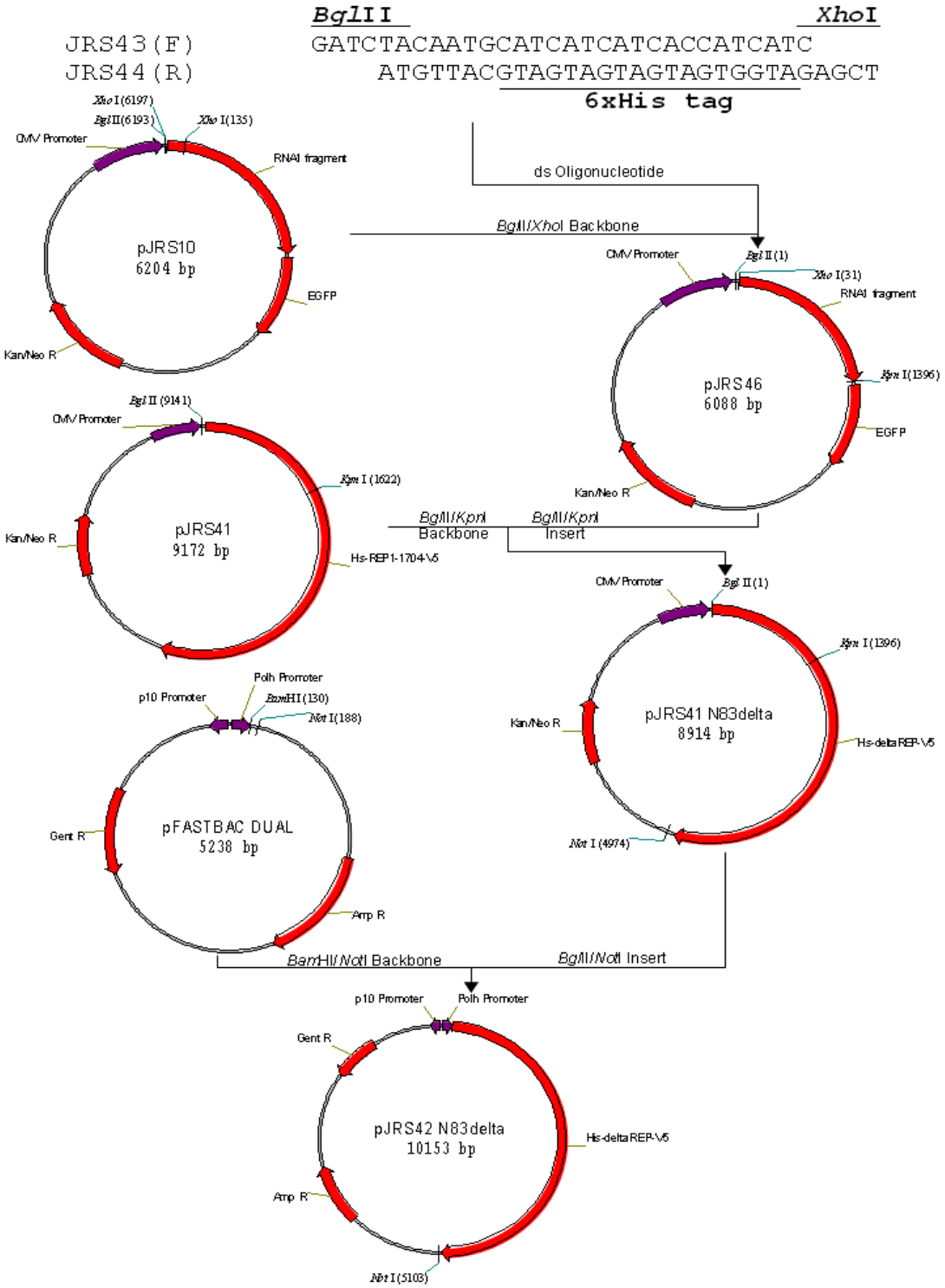

Figure A.18: The construction of pJRS42N83Δ. The ds oligonucleotide generated by annealing JRS43F and JRS44R is displayed above. Also shown are the *Bgl*II and *Xho*I half-sites and the 6xHis CDS. Amp R: *β*-lactamase, CMV Promoter: *Human Cytomegalovirus* immediate early promoter, EGFP: enhanced green fluorescent protein, Gent R: gentamicin acetyl transferase, hr/AcMNPV Promoter: hybrid insect promoter, Kan/Neo R: neomycin phosphotransferase, PohH Promoter: AcMNPV polyhedrin promoter.

APPENDIX B

PRIMERS USED IN THIS STUDY

Name	Sequence	Description	Ref.
JRS2	5'GTGGAAGGGCGTGACCGG'3		A.4
JRS4F	5'G**AAGCTT**GAACATGTACTATCCGCTGCGCTTC'3	*Hind*III	A.8
JRS5R	5'GCTGCTTGACGTCGGTGTTGAGACC'3		A.1, A.8, A.16
JRS6F	5'**CATATG**TACGCGAAAGCGACAGACG'3	*Nde*I	A.1, A.2
JRS7F	5'CGAACGTCC**GGTACC**TTCCACTCC'3	*Kpn*I	A.10
JRS13R	5'**GGATCC**CCATGTAGCTTAAGTGCG'3	*Bam*HI	A.9
JRS14F	5'G**AAGCTT**AACAATGTACGCGAAAGCG'3	*Hind*III	A.9
JRS17R	5'**GGATCC**GGATACGTGCTGCTGTAAGC'3	*Bam*HI	A.10
JRS18R	5'**AAGCTT**AGCCGAGCTCGGCATTAACCACG'3	*Hind*III	A.2
JRS21F	5'**GGATCC**CACAATAACACGAGTGAGCTG'3	*Bam*HI	A.3
JRS22R	5'C**ATCGAT**CCTTCATGCGCTCTTGCTGATC'3	*Cla*I	A.3
JRS23F	5'GTAC**CCCGGG**TGCACAACCAC'3	*Sma*I	A.12, A.13
JRS24R	5'CTAT**GGATCC**ATGTGAAGGCGGCTAGCG'3	*Bam*HI	A.12
JRS25R	5'CTAT**GGATCC**TTGGTGATGTCTCTCACAGCC'3	*Bam*HI	A.13
JRS28F JRS29R	5'**AAGCTTAGATCT**ACA**ATGCAT**CATCATCACCATCATGG'3 3'***CATG*****TTCGAATCTAGA**TGT**TACGTA**GTAGTAGTGGTAGTACC***AT***'5	ds oligonucleotide *Kpn*I, *Nde*I, *Hind*III, *Bgl*II, *Nsi*I, 6xHis tag	A.15
JRS30F	5'**GGATCC**GGTAAGCCTATCCCTAACCCTC'3	*Bam*HI	A.7
JRS31R	5'GTCGACTTAACCGGTACGCGTAGAATC'3		A.7
JRS33F JRS34R	5'**GATCC**ACAGTGTACTAATTATGCTCTCTTGAAATTGGCTGGAGATG'3 3'CCGACCTCTAC AACTCTCGTTGGGGCCCGGG***CTAG***'5	ds oligonucleotide *Hind*III, ERAV 2A-like sequence	A.14
JRS43F JRS44R	5'**GATCT**ACAATGCATCATCATCACCATCAT**C**'3 3'**A**TGTTACGTAGTAGTAGTAGTGGTA**GAGCT**'5	ds oligonucleotide *Bgl*II, *Xho*I, 6xHis tag	A.18
JRS45F	5'CCATGG**AGATCT**AACAATGTACGCGAAAGCG'3	*Bgl*II	A.16
JRS47F	5'**GGATCC**AACAATGGAAGACGCAAGCAAG'3	*Bam*HI	A.17
JRS48R	5'**CTCGAG**CACTGTCGGTACATTCTTAACGTGC'3	*Xho*I	A.17
JRS49R	5'TACATTGTT**AGATCT**CCATGGAATCGAATTC'3	*Bgl*II	A.16
JRS50R	5'TCTGCCGCGGCGTAGACAC'3		A.16
JRS51R	5'GCTCTCTG**CTGCAG**TACGTTCGC'3	*Pst*I	A.16
JRS52F	5'**CCTGAGC**CAGAGAGCAGTCAAGTTG'3	*Bpu*10I	A.16
JRS53F	5'**TCTAGA**AACCCTCCACAGACTGTACTATCC'3	*Xba*I	A.16
LMR2	5'CCC**GGATCC**CCGGGTGCAGGGATGTCTGTAAAC'3	*Bam*HI	A.4
M13F	5′CCCAGTCACGACGTTGTAAAACG′3		Section 4.2.1
M13R	5′AGCGGATAACAATTTCACACAGG′3		Section 4.2.1

Key: Complete restriction sites are in bold and underlined, partial restriction sites are in bold and ds oligonucleotide sequences complimentary to overhangs generated by restriction with specific enzymes but do not regenerate the recognition sequence are in bold and italics.

APPENDIX C

MAINTENANCE OF TISSUE CULTURE CELL LINES

HeLa S3 immortalised human cervical cancer cell line ECACC 93021013 (HeLa cells) (Gey *et al.*, 1952) and Baby Hamster Kidney cell line IZSBS BS CL21 (BHK-21 cells) (Macpherson and Stoker, 1962) were maintained in buffered Dulbecco's modified Eagle medium (Lonza) supplemented with 10 % heat-inactivated foetal calf serum (Invitrogen), 100 U ml^{-1} penicillin, 10 mg ml^{-1} streptomycin and 25 µg ml^{-1} Fungizone^{TM} (Lonza) at 37 °C in 10% CO_2.

Spodoptera frugiperda pupal ovarian (Sf9) cells (cell line 9 CRL 1711) (Vaughn *et al.*, 1977) were maintained in TC100 insect medium (Lonza) or Grace's insect medium supplemented with 10 % foetal calf serum (Invitrogen), 100 U ml^{-1} penicillin and 10 mg ml^{-1} streptomycin (Lonza) at 28 °C without CO_2. *H. zea* midgut cells (cell line BCIRL-HZ-MG8, referred to as MG8 cells in text) (Pringle *et al.*, 2003), were grown in ExCell 420 complete insect medium containing 100 U ml^{-1} penicillin and 10 mg ml^{-1} streptomycin at 28 °C without CO_2 or foetal calf serum.